The metabolic context for virulence in *Pseudomonas syringae*

A thesis submitted for the degree of Doctor of Philosophy at

the University of Oxford

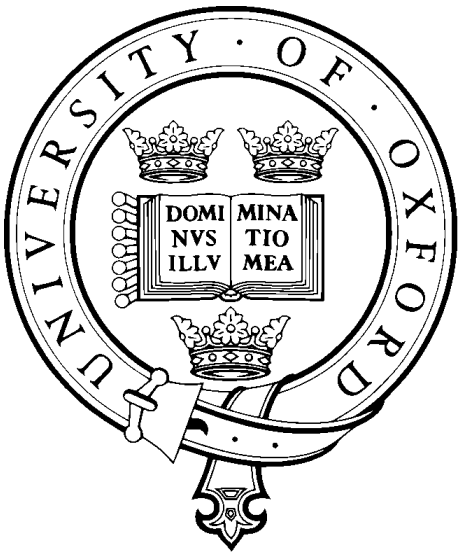

Sarah L McCraw

Magdalen College

Michaelmas Term, 2013

The metabolic context for virulence in *Pseudomonas syringae*

SARAH L McCRAW
MAGDALEN COLLEGE

A thesis submitted for the degree of Doctor of Philosophy
at the University of Oxford, Michaelmas Term 2013

Abstract

The apoplast is the site of infection for many important bacterial crop pathogens, including the model pathogen *Pseudomonas syringae* pv. tomato DC3000 (Pst DC3000). The chemical environment within the plant apoplast can determine the outcome of bacterial infection and the composition of this compartment is known to change in response to the presence of invading organisms. However, this metabolically dynamic environment has received little attention in the literature, and even less is known about how metabolites in the apoplast influence the expression of virulence genes.

In this study, several aspects of the metabolic context of virulence were assessed. First, a broad-scale analysis of the tomato apoplast was undertaken, which identified metal ions, sugars, organic acids and amino acids, the most abundant of which was the non-protein amino acid γ-aminobutyric acid (GABA). The impact these components had on the expression of virulence genes and metabolism in Pst DC3000 were then tested. Components such as fructose and aspartate caused high levels of virulence gene expression which correlated with the accumulation of intracellular glutamate, whereas repressive components, such as GABA and threonine, resulted in lower glutamate levels. Second, metabolic flux analysis showed that Pst DC3000 underwent major changes in central carbon metabolism in response to virulence gene inducing conditions. The identification of altered internal metabolism in Pst DC3000 cells expressing virulence genes led to the conclusion that Pst DC3000 may understand its external environment by sensing intracellular metabolites or metabolic fluxes. Third, the role of GABA assimilation in virulence was explored, and it was found that high internal GABA levels resulted in virulence gene repression. In addition, previously unidentified mechanisms for GABA uptake and transport were detected by the use of a novel 'unlabelling' experiment.

Acknowledgements

My first thanks are to Magdalen College, for the generous Tavella Stewart scholarship that enabled this research, and also for giving me a beautiful, stimulating and inspiring place to work and rest for the past seven years.

Secondly, my deepest thanks go to my supervisors, Gail Preston, Nick Kruger and George Ratcliffe, for their unfailing enthusiasm, for their kind patience, and for their wise guidance. Many thanks also go to Andrew Smith and Sarah Gurr for providing invaluable mentorship throughout my research, and to Lee Sweetlove and Dawn Arnold for their insightful comments and suggestions for my thesis.

Thirdly, my thanks go to Shyam Masakapalli, for introducing me so well to the wonders and quirks of metabolic flux analysis, for being an excellent teacher and always being willing to help, however bizarre the problem. Thanks are also due to Pedro Bota, whose technical expertise aided and rescued many an experiment.

I consider myself very fortunate to have worked in the Preston lab, which is a lively, friendly and engaging environment. Thanks in particular go to Helen, Astrid, Michael, Pete, Sarena, Liz, Anja, Brendan, Marketa, Ivey, Jasper, Monica, Niloufer and Charlotte, for celebrating and commiserating with me in the ups and downs of lab working, for always being ready for tea, cake and a natter, and for their friendship to me. Souvik, Javier, Marina, Irene, Qi Qin, Vincenzo, Merja, Andy and Ian also offered me help and advice for which I am very grateful. Thanks go to Arantza Rico and Rachel Jones, whose research gave rise to mine, and to Sarah and Caroline for all their technical help in the lab. I am thankful more generally to the Department of Plant Sciences for making me feel so welcome throughout my studies.

In addition, thanks are due to those who helped with various elements of the lab research itself or who provided materials and analysis. Thanks go to Phil Holdship, Jane Ward, Mike Beale, Duck-Hwan Park, Bryan Swingle, John Baker, Michael Bentley and Khalid Al-Qahtani for giving their time and effort to this work.

I would like to thank my family, my Mum, Dad and Katie, as well as my Oxford housemates and friends, for all their support and encouragement, and for keeping me laughing.

And finally, my most heartfelt thanks are to Dan, who is the champion of this work, and to whom it is dedicated.

Abbreviations

2OG	2-Oxoglutarate
DHAP	Dihydroxyacetone phosphate
dH_2O	Distilled water
E4P	Erythrose-4-phosphate
ED	Entner-Doudoroff
F6P	Fructose-6-phosphate
FBP	Fructose-1,6-phosphate
Frc	Fructose
G6P	Glucose-6-phosphate
GABA	γ-Aminobutyric acid
GAD	Glutamate decarboxylase
GAP	Glyceraldehyde-3-phosphate
GC-MS	Gas chromatography-mass spectrometry
Glc	Glucose
KDPG	2-keto-3-deoxy-6-phosphogluconate
LC-MS	Liquid chromatography-mass spectrometry
MFA	Metabolic flux analysis
MSTFA	N-methyl-N-trimethylsilyl trifluroacetamide
MTHF	5,10-methylenetetrahydrofolate
NH_4	Ammonium
NMR	Nuclear magnetic resonance
OAA	Oxaloacetate
OD	Optical density
P5P	Pentose-5-phosphate
PCA	Principal component analysis
PEP	Phosphoenolpyruvate
Pfl	*Pseudomonas fluorescens*
PPP	Pentose phosphate pathway
Pst	*Pseudomonas syringae* pv. tomato
qRT-PCR	Quantitative real time polymerase chain reaction
S7P	Sedoheptulose-7-phosphate
T3SS	Type III secretion system
TBDMS	N-methyl-N-t-butyl dimethylsilyl
TCA	Tricarboxylic acid

Contents

Chapter 1

Introduction

To a pathogenic bacterium, the host environment is its growth medium [1]. Upon entry into the host, a bacterium must be able to readily assimilate those nutrients present in the host [2] and thus an intimate metabolic association is created between host and pathogen early in the stages of infection [3]. Interestingly, whilst bacterial plant pathogens have been well characterised in terms of their genetic interaction with their hosts, that is, the identification of genes involved in virulence and defence responses, information about bacterial metabolism during infection is lacking [3]. Metabolic and transcriptional changes experienced by plant hosts in response to the invasion of bacteria have been documented in some species [4–9] and transcriptional changes have been monitored in some pathogens in response to their host environment [10]. However, very little attention has been given to the study of the composition of the host environment and the metabolic response of plant-pathogenic bacteria to that environment and the metabolic components within it.

Virulence gene expression is known to be altered by the metabolic composition of the environment plant pathogens inhabit, therefore, in order to truly understand bacterial pathogenesis, metabolic changes during infection must be addressed [11]. In the last couple of decades, the methods required to analyse bacterial and plant metabolomes have greatly improved and now it is possible to detect thousands of metabolites and monitor changes in abundance over time [12].

This work seeks to address how the metabolic environment experienced by the important model plant pathogen *Pseudomonas syringae* pv. tomato DC3000 influences the expression of its virulence genes. The following sections provide an introduction to the *Pseudomonas* genus and *Pseudomonas syringae* more specifically, the importance of studying the *P. syringae*-plant interaction, changes known to occur in the expression of virulence determinants in *P. syringae* in response to environmental stimuli, the metabolic capabilities of *P. syringae*, plant metabolic changes associated with *P. syringae* infection, and finally, tools for studying metabolism in bacteria.

1.1 *Pseudomonas*: evolution, diversity and importance

The *Pseudomonas* genus is a highly versatile subgroup within the γ-Proteobacteria. Over 100 species have been identified and these include strains which are medically and agriculturally important [13]. Pseudomonads have long been noted for their

abundance in natural environments and in particular for their metabolic and genetic diversity. Indeed, less than 35 % of each pseudomonad's genome is conserved across the whole genus [14].

Well known and well characterised *Pseudomonas* species include *P. aeruginosa*, the opportunistic human pathogen, *P. putida*, a commonly used species in biotechnology ventures, *P. fluorescens*, a large group of diverse plant commensals, and *P. syringae*, a group of important plant pathogens [14]. Interactions with plants presents a common theme among the pseudomonads, and these interactions vary from those species which promote the growth of their plant hosts and protect them from other pathogenic species, to those which cause serious, economically important diseases.

The availability of genome sequences, the ease of culturing individual strains, and the huge variety of environmental niches and metabolic capabilities of this genus make these bacteria particularly attractive research organisms [15].

1.2 The plant-*Pseudomonas syringae* model system

Up to 10 % of all crops grown globally are lost each year to damage caused by plant pathogens [16] and so research into the key pathogens involved is of high importance in order to develop sucessful control strategies. *P. syringae* pathovars are known to

cause disease in many different plant species. Attention to *P. syringae*-plant interactions has naturally been focused on important crop species, and *P. syringae* has been found to infect bean, kiwi, soybean, rice, cherry, olive, tomato, tobacco and barley plants, in addition to larger species such as chestnut, hazelnut and maple trees [17]. Recent significant outbreaks of *P. syringae* include *P. syringae* pv. actinidae which infects kiwi and *P. syringae* pv. aesuli which infects horse chestnut trees [18, 19]. Each pathovar of *P. syringae* tends to be host species-specific, though some pathovars are able to infect multiple host species [20, 21].

P. syringae is not an obligate pathogen and so is able to survive in the environment outwith the host and has been found in soil, rivers, lakes, snowfall and clouds [22]. Bacteria can arrive on a plant via rain drops or from infected seeds [23] and can live epiphytically on the surface of the aerial parts of the host plant [21]. Indeed, wet weather conditions and cool temperatures appear to increase the colonisation of hosts by *P. syringae* [21].

P. syringae can enter host plant tissues by several methods. First, bacteria can gain access to the intercellular spaces (apoplast) of leaves through stomata or hydrathodes, which allow diffusion of gas and water respectively [24]. Second, wounds can present a site of entry for the bacteria, and wounding can be caused by the bacterial cells themselves under cold conditions. Certain strains of *P. syringae* can produce ice nucleating proteins which stimulate freezing of host tissues, and thus frost damage, at higher temperatures than would occur normally [25]. *P. syringae*

cells are then able to enter into the apoplast through the resulting surface wounds. *P. syringae* cells upregulate genes involved in nutrient acquisition, metabolism and virulence upon arrival on the surface of the host, indicating they have mechanisms to detect they have arrived on a suitable host plant [26].

The apoplastic compartment within plants is the site of infection for *P. syringae* bacteria and is shown in Figure 1.1. The known composition of the apoplast and the attack and defence responses from pathogen and host are discussed below (Sections 1.4 and 1.3 respectively).

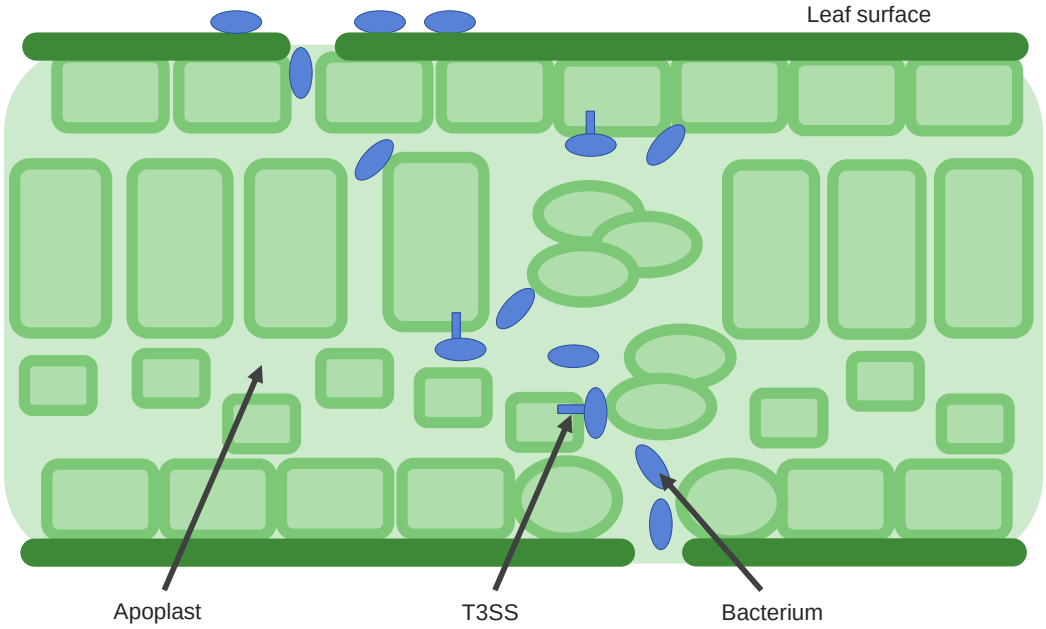

Figure 1.1: The apoplast is the site of infection for Pst DC3000 and many other plant-pathogenic bacteria. Bacterial cells enter leaves of host plants through stomata or surface wounds, where they proliferate within the apoplastic compartment. Bacteria will upregulate their type III secretion systems (T3SS) in order to subdue the host's defence response.

P. syringae has become a model pathogen in the study of plant-bacteria interactions and much of our knowledge of bacterial plant pathogens in general and their mode

of infection has come from the study of *P. syringae* [27].

1.2.1 *Pseudomonas syringae* pv. tomato DC3000

One *P. syringae* strain in particular has been used extensively in the characterisation of host defence responses and the genetic interactions involved during the infection process. It is an easily cultured strain which is amenable to genetic manipulation and its host plant, tomato (*Solanum lycopersicum*), is similarly suitable for genetic transformation [21]. *P. syringae* pv. tomato DC3000 (Pst DC3000) was first isolated in 1961 in the United Kingdom and causes bacterial speck disease of tomato plants [28]. The discovery that Pst DC3000 is able to infect the model plant *Arabidopsis thaliana* as well as tomato plants, in addition to detailed genetic characterisation, has led to the *A. thaliana*-Pst DC3000 pathosystem becoming the best-studied of all plant-pathogen interactions [27, 29, 30].

The genome of Pst DC3000 was fully sequenced by Buell *et al* (2003) [30] and was the first *P. syringae* strain to be genome sequenced. The Pst DC3000 genome is comprised of one circular chromosome and two plasmids, shows high levels of gene duplication and its largest gene category is predicted to be for substrate transport and binding [30].

Along with a closely related strain, *P. syringae* pv. maculicola, which can also infect *A. thaliana*, Pst DC3000 has been fundamental in the discovery of plant-pathogen perception, defence response signalling and genetic determinants of virulence [23].

The mechanisms by which Pst DC3000 infects its plant hosts are discussed below and the important contributions this pathogen has made to our understanding of plant-pathogen interactions more broadly are explored.

1.3 Infection of the host: virulence determinants, the type III secretion system and plant defence responses

The primary aim of bacterial pathogens is to gain nutrition from their hosts [3, 31]. For bacterial plant pathogens, including Pst DC3000, this nutrition is obtained from the host apoplast and the manipulation of host cells to release particular metabolites [32]. However, upon entering the host apoplast, bacteria are detected as foreign cells by the plant and the plant subsequently begins to mount its defence responses. This defence is two-stranded, and both strategies are discussed in the following section in relation to the responses of tomato and *A. thaliana* to Pst DC3000. Whilst specific examples are given, the principles of these interactions apply more broadly to plant-pathogenic bacterial interactions in general.

1.3.1 Detection of invading bacteria by the plant host

In order for a plant to produce a successful defence response against invading bacterial cells, it must first be able to identify the presence of pathogenic organisms. Pattern recognition receptors (PRRs), which are located on the plasma membrane

of plant cells, recognise the extracellular presence of invading bacteria by their pathogen-associated molecular patterns (PAMPs) [33]. One of the key characteristics of PAMPs is their high level of conservation across large groups of microbes. PAMPs incorporate a wide range of molecules, such as flagellin, elongation factor (EF-Tu), lipopolysaccharides and peptidoglycan [33]. Two types of PRR have been characterised in plants, receptor kinases and receptor-like proteins, and these PRRs each interact with specific PAMPs. A well-documented example of PAMP-PRR interaction is the recognition of the flg22 epitope in the N-terminus of bacterial flagellin by the leucine-rich repeat receptor kinase PRR FLS2 (FLAGELLIN SENSITIVE 2) [34, 35]. A few bacterial species are known to mutate the recognised elements of their PAMPs, and thus remain undetected, though not many examples of this kind of immune evasion have been described [34].

1.3.2 PAMP-triggered immunity

The identification of bacterial PAMPs triggers a regulatory cascade which stimulates the first level of plant defence, PAMP-triggered immunity (PTI). Almost immediately post-recognition there is a localised ion-flux across the plasma membrane of the detecting cell, which is accompanied by an oxidative burst, increased intracellular Ca^{2+} and the activation of MAP kinases [36]. Large-scale transcriptional changes can then be observed as defence responses are upregulated, and many of these are stimulated by salicylic acid accumulation [37]. Several hours after the initial detection depositions of callose, ethylene biosynthesis and stomatal closure can occur which prevent both movement of bacterial cells within the plant and more bacterial

cells entering the plant [36]. A hypersensitive response (HR) - localised cell death triggered by the oxidative burst - can occur as a result of PTI, though it has most commonly been associated with the second branch of the plant immune response, effector-triggered immunity (Section 1.3.5).

PTI is sufficient to halt the progression of bacterial pathogens through plant tissues unless it is suppressed, which bacterial pathogens can achieve by the production of effector molecules [38]. Effectors suppress PTI by binding to or modifying PRRs or mimicking negative host regulators of PTI [36]. These effector molecules are delivered via a type III secretion system (T3SS) and their primary function is the suppression of this first layer of plant immunity [39].

1.3.3 The type III secretion system

The T3SS is a needle-like injection structure which certain bacterial pathogens can use to directly insert effector molecules into host cells, and which consists of inner and outer membrane rings as well as the injection pilus [40]. The T3SS in Pst DC3000 is encoded by a set of *hrp*/*hrc* genes (hypersensitive reaction and pathogenicity genes, and *hrp* genes that are conserved) and effector molecules are encoded by *hop* (Hrp outer protein) and *avr* (avirulence) genes [41]. The *hrp*/*hrc* genes are arranged in a gene cluster over several operons along with certain effectors (with other effector genes scattered throughout the genome) [40]. Pst DC3000 is currently thought to be able to produce 28 different effector proteins and of these, eight have been shown to be core effectors that are required for successful pathogenesis [42]. Effectors are

diverse molecules [33] and play many different roles during pathogenesis, of which some of the best characterised include blocking RNA pathways and vesicle trafficking, altering organelle functions and interfering with signalling receptors involved in the plant immune response [43].

The genes involved in pathogenesis in Pst DC3000 are very well characterised, and this is also true of the regulatory genes that control *hrp*/*hrc* and effector gene expression. The T3SS is regulated at the most basic level by *hrpL*, which encodes an alternative sigma factor that belongs to the extracytoplasmic function (ECF) family [40]. Alternative sigma factors are proteins which confer promoter selectivity to the initiation of transcription by binding to RNA polymerase [44]. HrpL is a positive regulator of the suite of T3SS and effector genes (known as T3 effectors), and *hrpL* itself is positively regulated by the dual action of the HrpR and HrpS proteins. *hrp*R and *hrpS* are located on an operon which is controlled by a promoter region upstream of *hrpR* [40]. These regulatory proteins are members of the NtrC (nitrogen regulatory) family of two-component regulators and are thought to bind to form a heterodimer that can interact with the *rpoN*-RNA polymerase holoenzyme, thus stimulating the transcription of *hrpL* [40]. Both *hrpS* and *hrpRS* are regulated by HrpV and HrpG: HrpV can bind and inhibit the action of *hrpS* or *hrpRS*, and this inactivation can then be reversed by the action of HrpG suppressing HrpV [45]. In addition, the expression of *rpoN* and *hrpRS* in various *P. syringae* strains is known to be regulated by the global regulators GacS and GacA [46, 47], and in Pst DC3000, a *gacA* mutant was found to have reduced levels of the expression of both

alternative sigma factors *hrpL* and *rpoN*, as well as the stress-response regulator alternative sigma factor *rpoS* [48]. *gac*S encodes a sensor kinase and *gacA* encodes a response regulator which is activated by the autophosphorylation of GacS [49]. The GacS-GacA system is also involved in the regulation of quorum sensing and in the production of the phytotoxin coronatine [48]. An additional *hrp* gene, *hrpA*, which encodes a major subunit of the T3SS pilus [50], has also been implicated in the regulation of T3SS genes [46, 51]. Finally, the Lon protease is a negative regulator of *hrp* genes by the post-transcriptional regulation of HrpR [50], and is thought to be important for long-term systemic disease [52, 53]. The known regulators of the T3SS in Pst DC3000 are displayed in Figure 1.2.

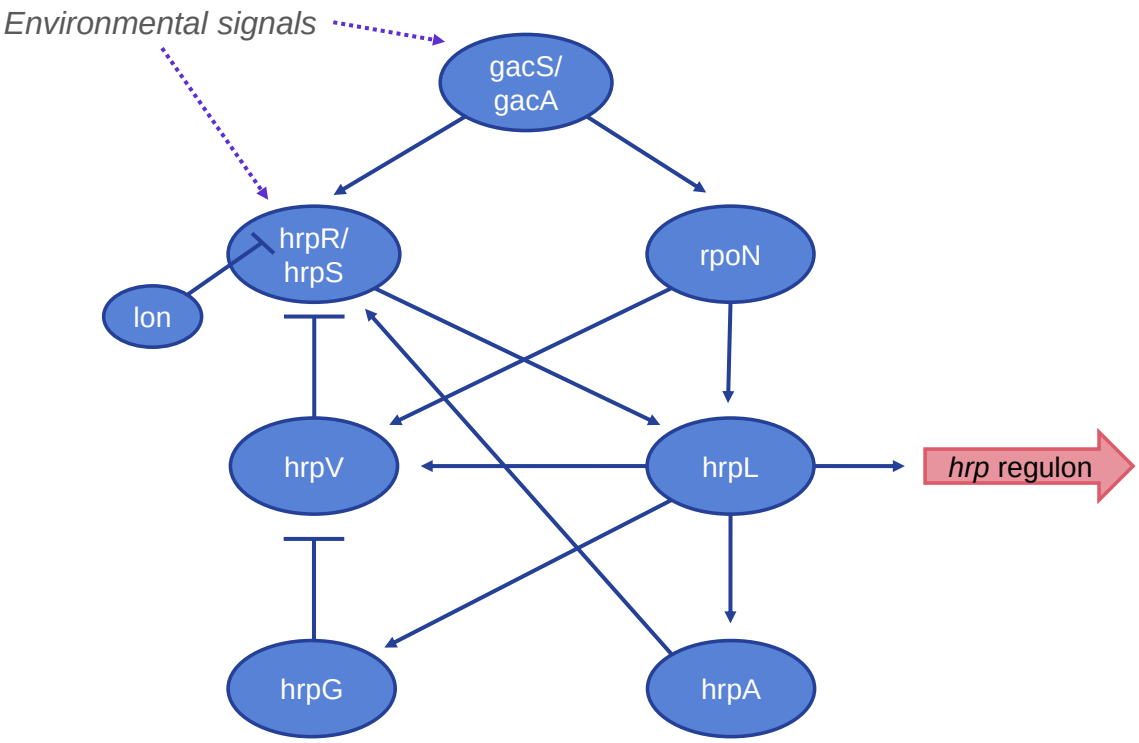

Figure 1.2: Type III secretion system regulation in *Pseudomonas syringae*. The global regulators GacS and GacA respond to environmental stimuli and induce the expression of *hrpR*, *hrpS* and *rpoN* genes. The *hrpR* and *hrpS* genes are also upregulated in under the same environmental conditions as GacS and GacA (for example, low pH and nitrogen limitation [40]). HrpR and HrpS form a heterodimer that interacts with RpoN which results in the transcription of *hrpL*. HrpL is the regulator of a suite of genes known as the '*hrp* regulon' which includes *hrpV*, *hrpG*, T3SS structural genes and T3 effector genes [54]. HrpV and HrpG are known to regulate the *hrpRS* genes: HrpV negatively regulates *hrpRS* and the action of HrpG alleviates this suppression by negatively regulating *hrpV*. HrpA, a *hrp* regulon protein and which encodes a major subunit of the T3SS pilus, positively regulates *hrpRS* [46, 51]. Finally, the Lon protease has been shown to negatively regulate the system by the post-translational regulation of *hrpR* [50]. Arrow headed lines indicate induction and bar headed lines indicate repression. Figure based on MacLean & Studholme (2010) [45].

The *hrp* genes of *P. syringae* are rapidly induced upon introduction into the plant environment (as early as one hour post inoculation) and continued high level induction has been observed for over six hours [50]. Environmental and metabolic factors have long been known to act as signals for the induction of the various components of the T3SS and its regulators, and these are discussed in Section 1.5.

1.3.4 Additional virulence determinants

In addition to the production of the T3SS and T3 effectors, Pst DC3000 is also known to have several other offensive molecules, which play important roles in disease progression and the suppression of host immunity.

One of the best known toxins produced by Pst DC3000 is the phytotoxin coronatine, which is unique to certain *P. syringae* pathovars [55]. The production of coronatine by Pst DC3000 cells appears to serve several functions: coronatine mimics the plant hormone jasmonic acid, thus suppressing the production of salicylic acid, which is required for both PAMP and effector-triggered immunity; it also stimulates stomatal opening to allow other bacterial cells to gain entry to the apoplast; and, in addition, contributes to the disease symptom chlorosis, which is a deprivation of chlorophyll, by the induction of chlorophyllase genes in the host [56, 57]. A reduction in photosynthetic activity due to chlorosis has been shown to have a major impact on plant metabolism, particularly on free amino acid abundances [58]. The expression of coronatine biosynthesis genes is regulated by HrpL [59] and, interestingly, *corR*, the response regulator of the coronatine gene cluster, has also been shown to be involved in the regulation of the *hrp* regulon in Pst DC3000 [59].

The production of extracellular polysaccharides, such as alginate, are also associated with Pst DC3000 virulence. Alginate is produced in response to both susceptible and resistant host plants and is involved in the protection of bacterial cells from

oxidative stress [60]. In a related strain of *P. syringae*, *P. syringae* pv. syringae B728a, GacS and GacA control alginate production [61], however, this has not been found to be the case in Pst DC3000 [48].

In addition to alginate and coronatine, Pst DC3000 has been shown to manipulate host defence responses by the production of auxin indole-3-acetic acid [62]. Auxin increases plants' susceptibility to invading bacteria, and in addition to producing their own auxin, *P. syringae* strains actively alter host auxin physiology by the action of the type III effector protein AvrRpt2 [63].

1.3.5 Effector-triggered immunity

The second layer of plant defence is triggered by the products of virulence gene expression and is known as effector-triggered immunity (ETI). Whilst PAMPs present plants with a static target for recognition, owing to the conserved nature of these molecules, effectors are highly variable and thus effector-triggered immune receptors must be more flexible in their responses [33].

Plants are able to recognise bacterial effectors by several mechanisms, each of which is based around nucleotide-binding - leucine rich repeats (NB-LRR) protein receptors, often called R (resistance) proteins, which are located in the plant cell cytoplasm. Two different types of NB-LRR have been described: those with an N-terminal coiled-coil (CC) domain and those with a TIR (Toll, Interleukin and 1R resistance) domain [33].

Broadly, the recognition of effectors by R proteins can be direct or indirect, but these interactions are highly molecule specific, with one R protein usually recognising one effector protein. Thus, the name 'gene-for-gene' hypothesis was given to describe this system of detection. The gene-for-gene hypothesis was first described by Flor in the 1940s as a result of his observations of immunity to the rust fungus *Melampsora lini* by flax plants, and the interactions between R proteins and effectors were assumed to be by direct contact [64]. Other examples of this type of direct recognition have subsequently been described in bacterial pathogens, including the recognition of PopP2, an effector produced by *Ralstonia solanacearum* (the causal agent of bacterial wilt), by the R protein RRS1-R, which was detected by yeast two-hybrid analysis [65].

The more common method of recognition, however, appears to be by indirect systems, particularly in *P. syringae*. Three indirect recognition mechanisms have been proposed: the Guard Hypothesis, the Decoy Model and the Bait-and-Switch Model [33]. The Guard Hypothesis, proposed by Van der Biezen and Jones (1998) [66], arose from the discovery of the mechanism by which the tomato proteins Pto and Prf recognise the *P. syringae* effector AvrPto (which blocks receptor-like kinases involved in PAMP-triggered immunity [67]). The Pfr NB-LRR protein is proposed to guard the Pto protein kinase and detects any interaction between AvrPto and Pto [68]. More recently, van der Hoorn and Kamoun (2008) [67] proposed the Decoy Model to deal with recognition events which did not fit with the Guard

Model Hypothesis. The Decoy Model proposes that effectors bind to decoy targets - molecules that the effector recognises as the target - but which are just highly similar molecules. The key difference between the Guard Hypothesis and the Decoy Model is that instead of a guardee, which if not associated with an R protein (the case in a susceptible host) leads to increased pathogen fitness, the decoy, which if not associated with an R protein does not lead to increased pathogen fitness, is the target molecule. Finally, the Bait-and-Switch Model, proposed by Collier and Moffat (2009) [69], describes a 'bait' molecule that brings an effector protein to the NB-LRR protein, which is subsequently 'switched on'.

Thus, effector-triggered immunity is a sophisticated set of recognition events which arose as result of an evolutionary arms race between plant and pathogen. The importance of rapidly evolving unrecognisable effector proteins and their successful injection into the host is of primary importance if a pathogen is to successfully colonise the host apoplast.

1.4 The metabolic environment within the host apoplast

Whilst the genetic interactions of effector and detector molecules involved in PTI and ETI are well established (both in the plant and in Pst DC3000), less attention has been given to the environment in which the initial interactions take place - the apoplast [3]. The apoplast has long been known to be the site of many bacterial

infections, and thus has been a source of interest to plant pathologists for some time. The apoplastic compartment comprises around 5 % or less of total plant tissue [70] and it facilitates the transport of many compounds around the plant and between tissues. For example, sugars are able to move through the apoplast from photosynthetic sources to sink organs as a result of differences in osmotic potential [32]. The apoplast is also known to contain enzymes, to be involved in the transmission of signalling molecules and in the movement and storage of mineral nutrients [70]. The apoplastic fluid of leaves can be extracted by vacuum-infiltrating excised leaves with water or a buffer and then centrifuging the infiltrated leaves to collect the apoplastic fluid [71]. In this way, the composition of the apoplast can be assessed. In the following section, studies which have identified compositional elements of apoplast extracts from tomato plants, the main host of Pst DC3000, are discussed.

The apoplasts of many different plants have been reported to be acidic, with pH values of between pH 4 and pH 7, most commonly between pH 5 and pH 6.5 [72]. For tomato plants, the main host of Pst DC3000, leaf pH has also been reported to be pH 5-6.5 [71, 73] and tomato fruits range from pH 6.7 for immature fruits to pH 4.4 for ripened fruits [74]. The acidity of the apoplast aids the action of proton pumps that move nutrients between different compartments, which is specifically important for proton symporters that transport sugars and amino acids into the cytoplast from the apoplast [32].

Healthy, uninfected apoplastic fluid is known to contain a mixture of sugars, or-

ganic acids and amino acids, though the composition of apoplast extract changes from species to species and can depend on the growing conditions the plant is subject to and the time of day samples are taken [2, 71]. The primary sugars found in the tomato leaf are fructose, glucose, sucrose and mannitol [3], though little work has been undertaken to understand their levels of abundance, or to detect the presence of less concentrated sugars. In terms of amino acids, all of these have been detected in tomato apoplast extract, except cysteine and tryptophan, the most abundant of which are aspartate and glutamate [71]. In addition to the canonical amino acids, γ-amino butyric acid (GABA) has been detected at very high concentrations within the tomato leaf apoplast, with estimates ranging from 0.6mM to 0.8mM [71, 75]. Organic acids, such as citrate and malate, have been shown to be present in tomato leaf apoplast [76] and fumarate and succinate are likely also to be present as they have been detected along with citrate and malate in the apoplast extracts of other plant species including tobacco [2] and sugar beet [70]. In addition to these primary metabolites, the plant cell wall is known to be rich in secondary metabolites and metal ions [77] which invading bacterial cells also potentially have access to. Rico *et al* (2008) [71] demonstrated that extracted tomato leaf apoplast supports a very high level of growth for Pst DC3000, as high as or higher than that observed with rich culture medium, and thus the apoplast provides a complete growth medium for this pathogen.

With the continuing improvements to metabolomics techniques for the detection and identification of lower abundance molecules, it is hoped that a comprehensive

inventory of components of the apoplastic environment will be developed. Apoplast extracts almost certainly do not contain all the chemical components bacteria are exposed to *in planta*, and so *in planta* visualisation techniques (such as those which have recently been used to visualise trace elements in rice plants [78]) will likely aid in understanding compositional and spacial elements of the apoplastic environment. The small size of the apoplastic compartment means that even slight changes in metabolite transport can radically change concentrations within the apoplast [70], thus being better able to quantify these changes will allow a much clearer picture of the dynamic environment invading bacteria are faced with.

1.5 Environmental factors causing changes in T3SS expression in Pst DC3000

The apoplastic environment acts as a signal for the upregulation of virulence genes in Pst DC3000, which has been demonstrated by monitoring the expression of both T3SS genes and coronatine biosynthesis genes in the presence of apoplast extracts [71, 76]. The apoplast, therefore, contains the major signals required by Pst DC3000 to discern the suitability of an environment for the expression of virulence genes. Understanding the composition of the apoplast thus remains an important task.

The expression of virulence genes in Pst DC3000 and other phytopathogenic bacteria, has long been known to be controlled by environmental stimuli. Low pH, nitrogen limitation and certain carbon sources (for example, fructose, sucrose and

mannitol) are all known to cause up-regulation of virulence gene expression in Pst DC3000 *in vitro* [3, 79, 80]. Conversely, the introduction of TCA cycle intermediates, amino acids and complex carbon and nitrogen sources generally cause the *in vitro* down-regulation of virulence determinants in Pst DC3000 [3, 32]. Specifically, medium with a pH of 5.5 and containing fructose or mannitol as the sole carbon source, such as the *hrp*-derepressing medium developed by Huyhn *et al* [79], cause the highest recorded levels of virulence gene expression *in vitro* for *P. syringae* strains [50, 81]. The strength of *hrp* gene induction observed in this medium has historically been interpreted as meaning the plant apoplast shares similar metabolic and ionic qualities [71]. However, it should be noted that synthetic *hrp*-inducing media typically cause a much higher level of virulence gene expression than that observed when Pst DC3000 cells are grown in extracted host apoplast [32, 71]. The reasons for this discrepancy are currently unclear, but may be a result of the rapid growth of Pst DC3000 in extracted apoplast as the expression of virulence genes are known to be inversely proportional to cell density [80]. An alternative hypothesis would be that some element of current apoplast extraction techniques alters the composition which results in reduced virulence gene expression in Pst DC3000.

At a regulatory level, not all genes in the *hrp* regulon in Pst DC3000 respond identically to the various known stimuli. Stauber *et al* (2012) [80] recently showed that whilst fructose optimally induced the expression of the *hrpRS* genes, other carbon sources which caused upregulation of downstream genes such as *hrpL* and *avrPto* (sucrose, glucose, mannitol, citrate and succinate) did not have the same effect on

the expression of *hrpRS*. Therefore, it appears that Pst DC3000 integrates signals in addition to that from *hrpRS* to stimulate the production of the T3SS. Perhaps unsurprisingly other genes required for the regulation of the T3SS also respond to environmental stimuli. *gacA* expression is induced under the same conditions as *hrpL*: low pH, fructose and sucrose, low osmolarity and the presence of non-complex carbon and nitrogen sources [48, 82]. Notably nitrogen sensing appears to be of great importance to the regulation of the T3SS as the *hrp* genes are regulated by RpoN, a nitrogen-responsive alternative sigma factor, and HrpRS, which is related to the NtrC nitrogen regulatory family of genes [83]. Thus, the perception of metabolic signals and the expression of virulence genes are tightly linked in Pst DC3000. Recently this relationship was found to be potentially cyclical in the phytopathogen *Xanthomonas axonopodis* pv. citri as the virulence genes *hrpX* and *hrpG* appear to have a role in the regulation of amino acid biosynthesis and sugar transport [84].

1.6 The metabolic capabilities of Pst DC3000

Whilst metabolism has been shown to play an important role in Pst DC3000's perception of its environment in the context of virulence gene regulation, it is also known to show metabolic characteristics which reveal its dependence on host nutrients.

The advent of genome sequencing has allowed for the putative identification of metabolic enzymes within the genomes of many different species. The genome se-

quence of Pst DC3000, published in 2003, has revealed a great deal about the nutritional specialisation this pathogen exhibits [30]. Unlike obligate pathogens, Pst DC3000 is able to survive outwith the host and thus must be metabolically flexible to survive in diverse natural environments. It possesses a full suite of genes for the traditional central carbon metabolic pathways identified in gram-negative bacteria: glycolysis, gluconeogenesis, the pentose phosphate pathway, the Entner Doudoroff pathway, the TCA cycle and recycling reactions such as the anaplerotic pathway from pyruvate to oxaloacetate. These features remain conserved among Pseudomonads for which genome sequences exist [30]. Where Pst DC3000 does show significant differences to other *Pseudomonas* strains lies in the uptake and assimilation of different carbon and nitrogen sources. Both *Pseudomonas putida* and *Pseudomonas aeruginosa* have four genes described as ABC (ATP-binding cassette) sugar transporters, whereas *P. syringae* has 15 genes which have been annotated as specific ABC sugar transporters for plant-derived sugars such as xylose and arabinose [30]. Interestingly this trend is reversed for APC (amino acid/polyamine/organocation)-family transporters of amino acids: Pst DC3000 is annotated as possessing four of these genes, whilst *P. putida* and *P. aeruginosa* have 21 [30]. The four APC family transporters that Pst DC3000 does have are predicted to encode proline, ethanolamine, GABA and aromatic amino acid permeases [85].

In addition to these differences, Pst DC3000 is also noted as lacking lactate dehydrogenase (for the conversion of pyruvate to lactate), arginine dihydrolase (for the conversion of arginine to citrulline) and the glycerate pathway (for the con-

version of glyoxylate to glycerate) which are present in other *Pseudomonas* species [30, 86].

One final metabolic difference that Buell *et al* (2003) [30] note in Pst DC3000's genome is the large number of genes related to the metabolism of GABA. GABA is the most abundant amino acid present in extracted tomato leaf apoplast [71], and is known to rapidly increase in concentration in *A. thaliana* leaves in response to biotic stress [87]. GABA is converted to succinic semialdehyde (SSA) by the action of GABA transaminase and SSA is subsequently converted to succinate by the action of succinic semialdehyde dehydrogenase (SSADH). Pst DC3000 possesses three genes annotated as GABA transaminases (and all demonstrated to have this function by Park *et al* (2010) [88]) and three putative SSADH genes [30]. Pst DC3000 has thus been postulated as having an exceptional ability to turn over GABA *in planta* [30].

Databases such as KEGG (http://www.genome.jp/kegg/) and MetaCyc [89] have greatly aided in the curation and accessibility of metabolic data from genomes and have provided useful platforms for analysing and comparing the abilities of different strains. One study which made specific use of the KEGG database compared the metabolic annotations and reaction path lengths in nine different strains of *Pseudomonas*, including Pst DC3000 and two further *P. syringae* strains. Mithani *et al* (2011) [86] found that Pst DC3000 had the highest number of species-specific features of all of the strain analysed, and that the majority of these were the absence

of certain metabolic reactions. A reduction in metabolic genes is a common feature of the genomes of bacterial pathogens in comparison with their non-pathogenic relatives [90]. Pst DC3000 was found to have fewer genes than other pseudomonads for the assimilation of nutrient sources and notably lacks the metabolic pathways required to assimilate amino acids that are found at a low abundance in tomato apoplast [71, 86]. Assimilation pathways for branched-chain amino acids (leucine, isoleucine and valine) and sulphur-containing amino acids (cysteine and methionine) were predicted to be absent in Pst DC3000 but present in *P. aeruginosa* and *P. fluorescens*. The two other *P. syringae* strains included in the analysis, *P. syringae* pv. syringae B728a and *P. syringae* pv. phaseolicola 1448A, were found to be very similar to Pst DC3000 in their metabolic capabilities, which emphasises the hypothesis that specialism at a metabolic level is a mark of the pathogenic lifestyle [86].

Across *Pseudomonas* strains more generally, Mithani *et al* (2011) [86] found that there is much variability in the presence or absence of genes associated with carbon and nitrogen metabolism. Seventy-one reactions involved in nitrogen metabolism were found in the nine strains analysed, however, only 11 of these were conserved across all of the strains [86]. It was therefore suggested that the ancestral pseudomonad would have been very metabolically versatile [86]. Finally, the authors noted that amino acids which are preferred carbon and nitrogen sources for *Pseudomonas* strains, for example asparagine, aspartate, glutamate and GABA, tend to have the shortest reaction path lengths from the substrate to either NH_3 or a TCA cycle intermediate [86].

Pst DC3000 has also been shown to be metabolically competent in fully exploiting its host's apoplastic environment. As noted previously, extracted tomato apoplast provides a complete growth medium for Pst DC3000: it grows more rapidly and to higher densities in apoplast extract than in rich synthetic media [71]. In addition, both Pst DC3000 and other *P. syringae* strains appears to be well adapted for growth in the apoplastic compartment as many of the metabolite utilisation capabilities detected by Rico *et al* (2008) matched metabolites which have previously been shown to be present within plant tissues [71].

1.7 Metabolic adaptation to, and manipulation of, the host apoplast

As well as being capable of metabolising all of the main components of the apoplast, Pst DC3000 is also known to adapt to the apoplast and to manipulate its composition [71]. Rico *et al* (2008) showed that Pst DC3000 cells have different carbon source utilisation profiles after two hours of incubation in apoplast extracts [71]. Utilisation pathways for both fructose and citrate were switched on in the presence of tomato apoplast, both of which are known to be abundant components of tomato apoplastic fluid [71]. Upon entry into the apoplast, Pst DC3000 cells are likely to go through a process of metabolic adaptation, upregulating their set of plant-adapted metabolite uptake pathways.

P. syringae, as with many other plant pathogens, is thought to modulate the composition of the apoplast for its own nutritional benefit [32], though the possibility exists that these pathogens have merely adapted to utilise compounds that the host produces specifically as defence molecules, or as part of a broader defence response. Examples include the alkalinsation of the apoplast, which is hypothesised to be beneficial for *P. syringae* growth and the export of asaparagine into the apoplast, an amino acid which is readily utilised by *P. syringae* [32]. Other changes which occur in the plant host in response to *P. syringae* are explored in the following section (Section 1.8).

1.8 Metabolic changes arising during infection

The effect of infection on the transcription of metabolic genes and on metabolite abundance in plant hosts

Metabolic changes associated with the progression of disease in plants have become a well documented aspect of the plant-pathogen interface over the last decade, with infection by bacteria causing changes to both primary and secondary host metabolism [3]. Studies have noted changes in transcriptional and protein abundances during the interaction between *P. syringae* and its host plants, which will be addressed briefly first, and also changes to the host metabolome, which will be explored in more depth.

Two key studies have investigated transcriptional changes in *A. thaliana* upon infection by Pst DC3000 [9, 91]. Thilmony *et al* (2006) [9] found that 944 genes were

involved in the plant's response to the phytotoxin coronatine and 791 genes were involved in the plant's response to *hrp*-encoded proteins. Truman *et al* (2006) [91] found that a similarly large number of genes changed in expression in response to Pst DC3000: 880 genes had altered expression at 12 hours post-infection. Both studies reported a significant reduction in genes involved with photosynthetic pathways, which would be likely to have a impact on primary metabolism [9, 91]. Truman *et al* (2006) [91] found a striking reduction in the expression of genes associated with the biosynthesis of the phenylpropanoids. Lignin is the most common plant phenylpropanoid and the authors postulate that Pst DC3000 T3 effectors actively suppress the deposition of lignin, which is a normal part of the plant's defence response, to limit pathogen access to nutrients [91]. Other studies have found significant changes in nitrogen metabolism-associated genes: asparagine synthetase and glutamine synthetase genes show a high level of induction in response to the presence of *P. syringae* cells [4, 92]. A coordinated mobilisation of nitrogen in the form of asparagine away from diseased tissues has been hypothesised as the reason for these transcriptional changes [4].

Changes in protein expression induced by *P. syringae* infection have been noted in several investigations [93–95]. Jones *et al* (2006) [94] detected specific changes in abundance of ten enzymes which are involved with central carbon metabolism, such as a decrease in enzymes involved in glycolysis and in the pentose phosphate pathway in *A. thaliana*. A more recent study by Parker *et al* (2013) [95] was able to monitor changes in a much larger group of proteins and could show that of the

2,369 proteins they were able to identify in tomato plants, 477 were involved in the response to inoculation with Pst DC3000. Several metabolic proteins were found to change in abundance, including glutamate dehydrogenase, which converts glutamate to the TCA cycle intermediate 2-oxoglutarate, and is known to be involved in nitrogen metabolism and leaf senescence [95].

Whilst changes in gene transcript and protein abundances can give an indication of the plant host's general response to the presence of *P. syringae* cells, they cannot reliably inform on specific changes in metabolite abundance occurring in the apoplast [96]. A metabolomics approach is required to fully understand compositional changes, and this has been undertaken in a number of studies. Ward *et al* (2010) monitored changes in *A. thaliana* leaves after inoculation with Pst DC3000 and a Pst DC3000 *hrpA* mutant by using a combination of metabolomics technologies [7]. This study found that many amino acids increased in abundance after treatment with both Pst DC3000 and Pst DC3000 *hrpA*-, specifically, alanine, glutamine, isoleucine, leucine, phenylalanine, threonine, tyrosine and valine became more abundant relative to control plants. Aromatic amino acids (phenylalanine, tyrosine and tryptophan) are known to be precursors for defence compounds such as lignin and salicylic acid [97] and in increase in these amino acids may therefore be part of the plant's defence response. Some metabolites showed different levels of change depending on whether they were Pst DC3000- or Pst DC3000 *hrpA*- treated: alanine, GABA, isoleucine and methionine were all higher in Pst DC3000-inoculated leaves, but not in Pst DC3000 *hrpA*- treated leaves. Levels of aspartate and gluta-

mate were significantly lower in Pst DC3000 and Pst DC3000 *hrpA*- treated plants after 18 hours in comparison with control plants [7]. In addition to changes in amino acids, differences were also observed in betaine, which was elevated in response to Pst DC3000, and citrate, which showed a reduction in Pst DC3000 *hrpA*- treated leaves [7]. Lopez-Gresa *et al* (2009) also reported a general increase in amino acids and organic acids in association with bacterial infection, though in tomato leaves, and with the changes occurring after a longer time period [8]. Tomato plant responses to pathogen invasion can also be pathogen-specific: sugar levels do not appear to be radically altered in response to *P. syringae* in tomato leaves, though tomato leaves show a decrease in sugar levels if inoculated with the fungus *Botyritis cinerea* [98].

When taken all together, the transcriptomic, proteomic and metabolomic studies all point to large-scale metabolomic reprogramming of the host occurring during infection by *P. syringae*, though little is understood about why the abundances of certain metabolites change in response to this pathogen. Specifically, central carbon metabolism shows differential regulation, as well as amino acid biosynthesis. The degree to which these changes are occurring as part of the plant's defence response, or because of pathogen manipulation by effector proteins is debatable.

The general metabolic response to the presence of *P. syringae* cells operates not only at the level of primary metabolism, but also at the level of secondary metabolism. The most important group of metabolites that are synthesised through secondary metabolic pathways during the course of infection are defensive compounds. The

flavinoid rutin, chlorogenic acid, and the phytoalexin hydroxycinnamic acid amides (HCAAs) of noradrenaline and octopamine were detected by Lopez-Gresa *et al* (2011) in tomato plants infected with *P. syringae* [99]. Zacares *et al* (2007) also detected HCAAs in *P. syringae*-infected tomato plants, p-coumaroyldopamine and feruloyldopamine, both of which were previously unknown molecules [100].

Several studies have examined how the environmental conditions encountered by the plant host can alter the outcome of infection by phytopathogenic bacteria. Glutamine synthetase, which appears to have an important role in the plant's response to invading bacteria, was shown to decrease in activity in tomato leaves in response to the presence of *P. syringae* pv. tomato more markedly under photosynthetic conditions than under non-photosynthetic conditions [92]. Interestingly, the effect of light on Pst DC3000 virulence has recently been explored by Alvarez *et al* (2013) [101], where motility was found to be inhibited by light and leaf attachment was found to be promoted by light [101]. Thus, even the time of day can affect pathogen virulence and plant metabolic defence responses.

The form and abundance of nitrogen supplied to plants can also impact a plant's ability to defend itself from *P. syringae*. Increasing nitrogen concentration has been shown to increase tomato plants' susceptibility to *P. syringae* pv. tomato [102]. Resistance to *P. syringae* pv. phaseolicola, characterised by the HR, was found to be faster in tobacco plants which had been fed NO_3 than in plants which had been fed with NH_4 [2]. These different forms of nutrition also changed apoplastic

levels of sugars (fructose, glucose, sucrose) which were higher in NH_4-fed plants [2]. Amino and organic acid abundances were also altered: NO_3 resulted in elevated levels of polyamine biosynthesis, whilst in NH_4-treated plants, GABA biosynthesis was more prominent [2]. A plant's environment, particularly in an agricultural setting, can therefore significantly impact its apoplastic composition and also the result of bacterial infections.

Transcriptional changes observed in phytopathogenic bacteria *in planta*

Whilst much work has been done to establish changes in metabolic activities in host plants during plant-pathogen interactions, few studies have addressed the changes which occur in bacteria in response to contact with the host. The transcriptional responses of two *P. syringae* strains to extracts from *Phaseolus vulgaris*, the common bean plant, have been used to identify changes in metabolic genes which occur during the course of infection [10, 103]. In the first study, by Hernandez-Morales *et al* (2009) [10], transcripts were monitored for changes in response to leaf extract, apoplastic fluid and bean pod extract. In addition to the T3SS and toxin genes which were upregulated, metabolic gene transcripts were also found to change in abundance. Genes encoding phosphoenolpyruvate carboxylase, acetate CoA ligase, aldolase I-epimerase, transketolase, nitrate reductase, histidine-ammonia lyase and NADH-quinone oxireductase were found to increase in abundance in response to apoplast extract [10]. Several ABC transporters, 2-dehydro-3-deoxyphosphogluconase aldolase, glutathione S-transferase, isocitrate dehydrogenase and genes involved in iron accumulation were all downregulated in the presence of apoplast extract [10]. These

changes imply that *P. syringae* may be undergoing significant metabolic changes in response to the host plant. Interestingly, the authors also identified a downregulation of genes involved in iron uptake and metabolism, and suggested that this indicates that the plant environment is rich in iron [10]. In the second study, by Yu *et al* (2013) [103], transcript abundances were monitored in response to epiphytic and apoplastic environments. One of the main groups of genes identified as having a significant change in response to apoplastic extracts were for the metabolism and transport of GABA, which were on average upregulated 4-fold relative to the basal medium [103]. The study also examined transcriptional changes associated with environmental stresses and found the same set of genes upregulated in response to nitrogen limitation and osmotic stress, thus implying *P. syringae* cells encounter both nitrogen limitation and osmotic stress in the apoplastic compartment of bean plants [103].

In addition, Allwood *et al* (2010) [6] demonstrate in their 'dual metabolomics' study that Pst DC3000 cells show discrete metabolite changes in response to co-cultivation with *A. thaliana* cells. It appears, therefore, that *P. syringae* cells respond at a metabolic level to the plant host. However, whilst transcriptional changes can give an indication of areas of metabolism which are regulated in response to the plant environment, without measurements of metabolite abundances or metabolic fluxes, we still do not have a full picture of how important pathogens change and adapt to produce virulent responses.

1.9 A role for GABA in Pst DC3000-plant interactions?

As previously discussed, GABA is the most abundant metabolite detected in extracted tomato apoplastic fluid [71, 75], and has also been shown to increase in quantity in *A. thaliana* plants upon inoculation with Pst DC3000 cells [7]. GABA is therefore a highly abundant metabolite during Pst DC3000 infection of its two host species. Pst DC3000 is known to have retained a putative GABA permease, where many other amino acid permeases have been lost, and also has three GABA transaminase genes encoded in its genome, and these genomic features have been interpreted to indicate GABA is an important metabolite for Pst DC3000 in its host environment [30]. GABA uptake and metabolic genes have been shown to be upregulated in a related pathovar (*P. syringae* pv. phaseolicola NPS3121) in response to plant apoplastic extracts [10, 103]. In addition, Park *et al* (2010) [88] demonstrated that this metabolite causes virulence gene repression in Pst DC3000. All of these lines of evidence point to a significant role for GABA in Pst DC3000 infections, and the metabolic context of GABA-mediated virulence gene suppression is explored in this study.

1.10 Metabolomics and its application to bacteria-host interactions

The metabolic interactions between plants and their pathogens have been described as some of the most biochemically challenging questions being addressed by metabolomic approaches [12]. Allwood *et al* (2010) [6] describe the three different components which must be assessed in order to understand these interactions fully. First, the constitutive metabolism of the plant and the pathogen prior to the interaction and then second, the subsequent changes that arise within each organism in response to the interaction. Changes in metabolism may include the excretion and subsequent assimilation of metabolites by the different interactors, and thus must be included within this second aspect. The third set of metabolites which must be characterised are those that are produced and excreted by either of the organisms and which remain in the the extracellular space (in this case, the apoplast) [6]. Within the plant-Pst DC3000 interaction, both biochemical changes in the apoplast and in the surrounding plant cells should be taken into account and Pst DC3000 has the ability to manipulate both [32].

Three main challenges exist in the characterisation of these interactions. First, the detection and identification of metabolites present in both organisms. It is estimated that plants contain between 100,000-200,000 different metabolites [104], thus making it currently impossible to quantify all the metabolites which may be present in one organism, let alone in two interacting ones [12]. No single method exists which

can quantify all these metabolites and so constructing metabolic profiles can be very time consuming as multiple approaches must been used. Second, the interactions between organisms do not remain constant over time: plant-pathogen interactions are both dynamic and responsive in nature. Therefore, examining them experimentally requires assumptions to be made about key time points as techniques do not yet exist to measure metabolic changes in real time. Third, many metabolites are common to both plants and their pathogens, most notably those which are involved in central metabolic processes such as nitrogen assimilation, glycolysis and the TCA cycle. How to distinguish the origin of these metabolites, either from the plant or the pathogen, remains experimentally challenging, especially where these molecules may be freely swapped between both partners.

The aforementioned study by Allwood *et al* (2010) [6] sought to address some of the these issues, by developing a novel method of separating Pst DC3000 and *A. thaliana* cell suspension after incubation together in order to be able to assess the metabolome of the bacterial cells, plant cells and the extracellular culture medium. They were able to demonstrate significant metabolic changes took place in all three elements of the interaction by using Fourier-transform infrared spectroscopy, however no steps were taken in characterising the nature of these changes in terms of metabolite identification [6].

Two types of spectroscopy are most commonly used in the identification of plant and bacterial metabolites: nuclear magnetic resonance spectroscopy and mass spec-

troscopy. These established techniques allow for quantification of many metabolites and have been instrumental in furthering metabolic knowledge. Both have been employed in this study and are described in Chapter 2. In addition, metabolic flux analysis, the means by which metabolic fluxes (the flow of molecules though metabolic networks), can be assessed, has proven to be a useful tool in the characterisation of both bacterial and plant fluxes [105, 106] and is fully described in Section 4.3.4.

The tools required to analyse plant-pathogen interactions at a metabolomic level are now sufficiently sophisticated to make significant steps towards a more in-depth understanding of metabolic changes during infection. The task of mapping metabolic changes in both plant and pathogen is considerable, and so this study seeks to address the changes which occur in Pst DC3000 as a starting point for a fuller characterisation of the Pst DC3000-host relationship.

1.11 Major aims and hypotheses

A host is, ultimately, a source of nutrition for its pathogens [31]. Infections cannot proceed without pathogens making successful use of available host resources and using these to produce toxins, infection structures and, most importantly, to divide and multiply.

Current understanding of how available host metabolites affect the outcome of bac-

terial infections of plants remains limited, due in part to the complexities of monitoring metabolite abundances and changes, and, in part, to a recent emphasis on characterising genetic interactions over biochemical ones. The finding that virulence gene expression can be controlled *in vitro* by changing the chemical composition of growth media implies that Pst DC3000 uses metabolic signals to understand its environment and assess an environment's suitability for the upregulation of virulence genes. What currently remains unclear is precisely what those metabolic signals are and how Pst DC3000 responds to them, both at a genetic and metabolic level. This thesis therefore aims to characterise the metabolic context of virulence for Pst DC3000, specifically addressing the following aims:

1. The identification of constituents of the plant host apoplast and the effect these have on virulence gene expression in Pst DC3000

2. The use of metabolic flux analysis to examine the internal metabolic context of virulence gene expression

3. The exploration of the metabolic context of GABA-mediated virulence gene repression

Chapter 2

General Materials and Methods

This chapter describes the materials and methods which have been used in the following chapters.

2.1 Chemicals and antibiotics

All chemicals and antibiotics were obtained from Sigma-Aldrich Co. (Gillingham, UK), Thermo Fisher Scientific (Waltham, Massachusetts, USA) or VWR International (Lutterworth, UK) unless otherwise stated. The concentrations of antibiotics used in this study are given in Table 2.1.

Antibiotic	**Concentration**	**Solvent**
Gentamycin	10 µg/ml	dH_2O
Kanamycin	25 µg/ml	dH_2O
Rifampicin	50 µg/ml	DMSO

Table 2.1: Antibiotics and working concentrations used in this study

2.2 Bacterial strains and plasmids

The bacterial strains and plasmids used in this study are given in Table 2.2 along with their antibiotic resistances and literature references (where a literature reference is not available the contributor is given).

Strain/Plasmid	**Abbreviation**	**Reference**
P. syringae DC3000 Rif^R	Pst DC3000	Buell *et al* (2003) [30]
Pst DC3000 Δ*gabP* Rif^R	Δ*gabP*	Gift from D.H. Park
Pst DC3000 Δ*gabT2/T3/T1* Rif^R	Δ*gabT2/T3/T1*	Park *et al* 2010 [88]
P. fluorescens SBW25	Pfl SBW25	Silby *et al* (2009) [107]
Pfl SBW25 pRspR	Pfl SBW25 pRspR Gen^R	Jackson *et al* (2005) [108]
pBBR1MCS5 (pBS46::*gabP*) Gen^R	pBS46::*gabP*	Gift from D.H. Park
pUICP *hrpL::luxCDABE* Kan^R	pBS63	Gift from B. Swingle
pUICP *gap-1::luxCDABE* Kan^R	pBS70	Gift from B. Swingle
pUICP *avrPtoB::luxCDABE* Kan^R	pBS45	Gift from B. Swingle
pUICP empty*::luxCDABE* Kan^R	pBS44	Gift from B. Swingle

Table 2.2: Strains and plasmids used in this study

2.3 Bacterial growth conditions and media

All bacterial strains were stored at -80 °C in 20% glycerol and were cultured on Luria-Bertani (LB) agar, incubated at 28 °C (*Pseudomonas* strains) or 37 °C (*Escherichia coli*). 10 ml liquid cultures of LB (unless stated) were inoculated using single colonies from agar plates and were grown in 25 ml tubes (Sterilin, Newport, UK) at 28 °C or 37 °C and shaken at 200 rpm.

Bacteria were routinely cultured in LB medium (10 g tryptone, 10 g NaCl, 5 g yeast extract, 1 l dH_2O), M9 medium (0.1 mM $CaCl_2$, 2 mM $MgSO_4$, 6 g Na_2HPO_4, 3 g KH_2PO_4, 0.5 g NaCl, 1 g NH_4Cl, 22 mM D-glucose, 1 l dH_2O) [109] and *hrp-*

inducing medium (0.05 mM potassium phosphate (6.6 K_2HPO_4: 43.4 KH_2PO_4), 0.38 mM $(NH_4)_2SO_4$, 0.085 mM $MgCl_2$, 0.085 mM NaCl, 10 mM D-fructose in dH_2O) [79]. For agar plates, agar was added at a concentration of 30 g/l.

2.4 Spectrophotometric measurements: growth and luminescence

Bacterial luminescence and growth were measured using a Tecan Infinite M200 in either Microtext 96 well plates (BD Biosciences, San Jose, CA, USA) or Costar black-walled 96 well plates (Corning Incorporated, Corning, NY, USA). Black opaque-walled 96 well plates were used for measuring luminescence so as to reduce background light and cross-talk between wells. Bacteria were usually washed through twice in the experimental assay media at double the final concentration (both of cells and media) and 75 µl was added to each well (some control wells would also be included, containing media without bacteria). An additional 75 µl of, for example, an amino acid of interest, would then be added, again at double the required final concentration. Plates were incubated at 28 °C and shaken for 10 seconds prior to measurements, which were taken every 20 minutes for up to 48 hours. The optical density of bacterial cell cultures were also monitored using a Jenway Genova spectrophotometer (Bibby Scientific Limited, Staffordshire, UK) in 1.5 ml cuvettes (Plastibrand, Wertheim, Germany). Except where stated, bacterial culture densities were measured at OD_{600}.

2.4.1 Biolog GN2 phenoarrays

Biolog GN2 MicroPlates (Biolog, Hayward, CA, USA) were used to assess the carbon utilisation profiles of various strains of bacteria and these were inoculated according to Rico *et al* (2008) [71]. Bacteria were grown on LB agar plates for 48 hours after which colonies were scraped off and resuspended in inoculating fluid (Biolog, Hayward, CA, USA) to an OD_{620} of 0.28. The pH of the inoculating fluid was adjusted using concentrated HCl prior to inoculation. 10 µl of dH_2O was added to the contents of each well in the Biolog GN2 MicroPlate, this was pipetted up and down vigorously to resuspend the dried contents of the cell and then transferred to the corresponding well of a black-walled 96 well plate (Biolog plates have transparent sides and so are not suitable for luminescence measurements). 150 µl of bacterial suspension was added to each of the 96 wells of the black-walled plate. Plates were then incubated at 28°C for 36 hours and shaken every 20 minutes for 10 seconds. Spectrophotometric measurements (OD_{620} and luminescence) were also taken every 20 minutes. The Biolog GN2 MicroPlates contain a control well, where no carbon source is present. This well was used in the analysis to determine the level of growth which could be attributed to reserve carbon within the bacteria. Data from the Biolog GN2 phenoarrays was internally normalised to account for high variability in lag phase time and in the levels of gene expression. Metabolism data was corrected by subtracting the starting OD value of each well from all subsequent measurements to adjust for any coloured metabolites and the metabolic activity curves were then integrated for the first 36 hours of incubation. For each 96-well plate, the total sum

of all integrated measurements was used to normalise the plate in order to make replicate plates more easily comparable. Luminescence data was corrected against the optical density at every time point (luminescence/OD) and subsequent values were also integrated over the first 36 hours and normalised as done for optical density values.

2.5 Plant growth conditions, extractions and inoculations

2.5.1 Species and cultivation

Tobacco (*Nicotiana tabacum cv. Delgold*) seeds were stored at 4 °C and were germinated by immersion in 0.5 mg/ml giberellic acid overnight before planting in soil. Tomato (*Solanum lycopersicum* L. cv. Rio Grande) seeds were stored on dry filter paper (Whatman, Maidstone, UK) at room temperature and were germinated on wet filter paper for 3 days at 4 °C in darkness before planting in soil. Seedlings were grown in Erin Excel Multipurpose Compost (Erin Horticulture, Hinxworth, UK) at 21 °C with a 16 hour photoperiod and were watered three times a week. Six- to eight-week-old plants were used for apoplast extractions and bacterial inoculations.

2.5.2 Apoplast extractions

Apoplastic fluid was extracted from tomato leaflets and tobacco leaves as described by Rico *et al* (2008) [71] with minor modifications. Leaves were always harvested at the same time of day (early afternoon) and from plants that were the same age and which had been kept under identical light and watering regimes. Leaves were removed from plants with a scalpel and kept in moist paper until infiltration, and larger leaves were cut into small pieces (around 3-5 cm) in order to fit into the vacuum-infiltration apparatus. Leaves were placed in 200 ml of dH_2O in a 1 l vacuum flask attached to a vacuum pump (Welch Vacuum, Niles, Illinois, USA). Vacuum was applied for around 30 seconds and then released. This was done repeatedly until the the leaf sections were fully infiltrated with water. The leaves were blotted dry and then inserted, petiole downwards, into a 10 ml syringe with the plunger removed and additional holes drilled in the bottom. The syringes were placed in 50 ml tubes and centrifuged at 2000 rpm for 5 minutes at 4 °C. The fluid collected was transferred to a 1.5 ml tube and centrifuged again at 4 °C for 10 minutes at 14000 g to pellet any cytoplasmic components. The supernatant was then removed and stored at -80 °C. For use as a bacterial growth medium, the extracted apoplastic fluid was lyophilised overnight in a Christ Alpha 2-4 LD freeze dryer (SciQuip, Shrewsbury, UK) and, once dried, reconstituted to half its original volume in ultrapure dH_2O in accordance with the Rico *et al* (2008) [71] estimation of the degree of dilution caused by the infiltration protocol. Rifampicin was added to select for Pst DC3000.

2.5.3 Plant inoculations and symptom development

Bacteria from overnight LB cultures were resuspended into 10 mM $MgCl_2$ and adjusted to an optical density (OD_{600}) of 0.1 (around 10^7 colony-forming units/ml) and serially diluted to 10^6, 10^5, 10^4 colony-forming units/ml. Leaves were pierced on the adaxial surface and bacterial suspensions of all dilutions were introduced into the leaves in 1 ml syringes by applying pressure over the pierced hole. Once the bacterial suspension had spread through a leaf section (the area between the midrib and lateral veins), the inoculated area appeared dark in colour. Plants were typically left for 12-24 hours before symptoms were recorded. Alternatively, for leaf-disc excisions, samples were removed at regular intervals by core-borer and either homogenised in 10 mM $MgCl_2$ with a 12V minidrill (Radiotronics, Bulwell, UK) fitted with a micropestle (Eppendorf, Stevenage, UK) and serially diluted before being spread on selective agar plates. Plates were left to dry and then incubated at 28 °C until colonies were large enough to count. Three technical replicates were plated per sample and averages were calculated and from these values colony-forming units/cm^2 could be determined.

2.6 DNA and RNA manipulations

The genome sequences and gene locations for *Pseudomonas syringae* pv. tomato DC3000 and *Pseudomonas fluorescens* SBW25 were taken from pseudomonas.com [110].

2.6.1 Genomic DNA extraction

Genomic DNA was isolated from 5 ml of overnight LB bacterial culture (except for biomass measurements, see Section 2.14) as per the manufacturer's instructions (Wizard Genomic DNA purification Kit, Promega, Madison, USA).

2.6.2 Plasmid DNA extraction

Plasmid DNA was extracted from 5 ml of overnight LB bacterial culture as per the manufacturer's instructions (QIAprep Spin Miniprep kit, Qiagen, Crawley, UK). For plasmids such as pBS63, large plasmid adjustments were made (elution buffer was heated to 70 °C prior to elution).

2.6.3 Quantification of nucleic acids

DNA and RNA were both quantified using the ND-1000 Nanodrop spectrophotometer (Thermo Fisher Scientific, Waltham, Massachusetts, USA) with elution buffer or water used as blanking controls. Both DNA and RNA absorb light at 260nm and this wavelength was used for quantification. The purity of the samples was assessed by using the 260/280nm ratio (protein absorbs at 280nm and this ratio allows the level of protein contamination to be assessed). Pure DNA samples were expected to have a 260/280nm ratio of around 1.8 and for RNA the expected ratio was around 2.0. Samples with low levels of purity were discarded.

2.6.4 Ethanol precipitation

Extracted plasmid DNA was ethanol precipitated prior to electroporation. Three volumes of 100 % ethanol were added to eluted DNA, followed by 0.3 volumes of 0.3 M sodium acetate and the samples were then stored at -80 °C overnight. The following day the precipitation solution was centrifuged for 30 minutes at 13,000 rpm, after which the supernatant was removed and the DNA pellet resuspended at one third of the original elution volume in ultra pure dH_2O.

2.6.5 PCR methods

Polymerase chain reactions (PCRs) were performed using the the master mix specified in Table 2.3, in a PTC-200 Peltier Thermal Cycler (MJ Research, Waltham, Massachusetts, USA). Typically, the following reaction settings were used: 3 minutes at 95 °C, followed by 30 cycles of 30 seconds at 95 °C, 30 seconds at 60 °C and 2.5 - 3.5 minutes at 72 °C (depending on the length of the desired PCR product). After 30 cycles the samples were kept at 72 °C for 7 minutes before being stored at 4 °C until required for further analysis.

Chemical	**Concentration**	**Volume**
6X PCR buffer	As supplied	4 µl
dNTP mix	10 mM	0.4 µl
Go Taq polymerase	As supplied	0.2 µl
ultrapure dH_2O	N/A	12.4 µl
Forward primer	10 µM	1 µl
Reverse primer	10 µM	1 µl
DNA	100 ng/µl	1 µl

Table 2.3: PCR master mix, with total volume of 20 µl

2.6.6 Gel electrophoresis

PCR products were mixed with 6X loading buffer (0.21 % (w/v) xylene cyanol, 0.21 % (w/v) bromophenol blue, 50 % (w/v) glycerol in dH_2O) at a 5:1 ratio. Electrophoresis gels consisting of 1 % agarose in TAE buffer (40 mM Tris acetate and 1 mM EDTA in dH_2O at pH 8.3), and containing 0.2 mg/ml ethidium bromide, were immersed in TAE buffer in electrophoresis tanks (Geneflow, Elmhurst, UK) and the PCR products were loaded into the wells. A 1 kb DNA ladder (New England Biolabs, Ipswich, Massachusetts, USA) was also loaded on the gel to act as a reference for the size of the PCR product. A potential difference of 90 V (PowerPac 300, BioRad, Hemel Hempstead, UK) was used for between 30 minutes and 1 hour depending on the size of the gel. Gels were then visualised using a BioRad transilluminator with QuantityOne 4.1.0 software (BioRad, Hemel Hempstead, UK).

2.6.7 RNA extraction

RNA was extracted according to the manufacturer's instructions (RNeasy minikit, Qiagen, Crawley, UK), with, typically, 500 µl of culture used as the starting volume. An RNase-free working environment was maintained using RNaseZap (Ambion, Invitrogen, Paisley, UK). The extracted DNA was treated with DNase I (RNAse-Free DNase set, Qiagen, Crawley, UK) according to the manufacturer's instructions.

2.6.8 Quantitative reverse-transcription PCR

Extracted RNA samples were first adjusted to the concentration of the sample containing the least amount of RNA. Subsequently, RNA was converted to cDNA using a cDNA synthesis kit (Bioline, London, UK) according to the manufacturer's instructions along with non-reverse transcription controls. Samples were diluted to 200 µl with RNase-free ultra pure dH_2O and then a small volume of each sample was combined to give the starting concentration for a five-fold dilution series which was used to test the efficiency of the primers (the primers and their efficiencies are given in Table 2.4). Using the calculation,

$$E = 5^{(1/slope)} \tag{2.1}$$

(with the slope given by the Ct values plotted against dilution) the efficiency of the primers was determined [111]. Into a 96-well PCR plate (Thermo Fisher Scientific, Waltham, Massachusetts, USA) 7.5 µl of cDNA, water (acting as a no template control) or non-RT control was added into each well, followed by 2.5 µl of each of the forward and reverse primers and finally 12.5 µl of SYBRGreen master mix (Applied Biosystems, Foster City, California, USA). The plate was then sealed with adhesive PCR film (Thermo Fisher Scientific, Waltham, Massachusetts, USA) to prevent sample loss and evaporation. Plates were run in an Applied Biosystems 7300 RealTime PCR machine and data was collected in the 7300 System SDS Software (Applied Biosystems, Foster City, California, USA). The programme settings were as follows: 50 °C for 2 minutes, 95 °C for 10 minutes, then 40 cycles of 95 °C for

15 seconds followed by 60 °C for 1 minute. A dissociation step was added to assess the quality of the samples: this was programmed for 15 seconds at 95 °C, followed by 30 seconds at 60 °C and then 15 seconds at 95 °C.

The fold change (C) in gene expression was calculated using Ct values. Ct values denote the number of cycles required to pass an automated threshold level and so are inversely proportional to the concentration of target cDNA present in the reaction mixture. The following equation is used to calculate the fold change:

$$C = \frac{E_t^{(Ct_{control} - Ct_{treatment})}}{NF} \tag{2.2}$$

Where t is the gene of interest (target gene) and NF is explained as follows:

$$NF = geometricmean(E_{R1}^{(Ct_{control} - Ct_{treatment})}, E_{R2}^{(Ct_{control} - Ct_{treatment})}) \tag{2.3}$$

Where $R1$ and $R2$ are reference genes (in this study, *groEL* and *rpoD*) [112]. 'Control' and 'treatment' denote the different conditions that strains were exposed to prior to RNA extraction.

Gene	**Forward Primer**	**Reverse Primer**	**E**
avrPtoB	AATCCGACGGACACGTCGCAG	TCTGGTCATCGGATGCTCAGG	1.87
avrE	TGGTCGACAAGATCGATGAAGGCA	TGTGGAATACCACCAGACGCTTGA	1.99
groEL	TTTCGGCCAACTCTGATCACTCCA	TTTCCAGGCCCGAACCTTCTTCAA	1.93
hrcJ	GGGCTGCTGCTGTTGTGC	CGGCGCGGTTCATTTCGC	2.08
hrpL	TCAGGAAAGCTGGGAAGACGAAGT	ATGTTCGACGGCAGGCAATCAATG	1.93
rpoD	GTTTCGGTGCGGTTTCCGATCAAA	ATCGGCATGAACAATTCGGCAAGG	1.94
gabP	TAGCGTGAGTGGCGTCAGTCA	ACGATCTCGGTGCCCATGAACG	1.88
gabT2	GCCGTGAAGATCGCTCGTGCT	AAGGCACAACCTTACCGGTCA	1.92

Table 2.4: qRT-PCR primers and E-values (efficiencies)

2.7 Bacterial transformation by electroporation

Plasmid DNA (which had undergone ethanol precipitation, Section 2.6.4) was electroporated into competent cells using a BioRad Gene Pulser connected to a BioRad Pulse Controller (BioRad, Hemel Hempstead, UK) at 1.75 V (capacitance was set at 25 µFD and resistance at 200 Ω). Cells were prepared from 10 ml overnight LB cultures, washed through 3 times with ice-cold glycerol-HEPES solution (10 % glycerrol and 1 mM HEPES) and resuspended in 100 µl. 5 µl of between 50 and 250 ng/µl of plasmid DNA was added and the bacteria-DNA suspension was transferred to an electroporation cuvette (BioRad, Hemel Hempstead, UK). Cells were electroporated for 4 seconds and immediately 1 ml of 28 °C SOC medium (20 g tryptone, 5 g yeast extract, 0.5 g NaCl, 0.186 g KCl, 0.952 g $MgCl_2$ and 3.603 g glucose in 1 l dH_2O) was added to the cells. Cells were then incubated at either 28 °C or 37 °C for 2 hours before plating out onto selective agar plates.

2.8 Imaging: Digital photography and photon counting

Digital photographs were taken using a Lumix DMC-FZ18 camera (Panasonic, Bracknel, UK) and photon images were collecting using a photon counting camera (Photek, St Leonards-on-Sea, UK) and processed with Photek IFS32 software.

2.9 Bioinformatics

The *Pseudomonas* phylogeny and the identification of GABA permease and GABA transaminase genes was constructed by Mr. Michael Bentley (University of Oxford), using the following methods.

2.9.1 Construction of *Pseudomonas* phylogeny

All *Pseudomonas* genomes present in the NCBI database, both those that were fully and partially assembled, were included in the phylogenetic analysis. This list of genomes was assessed for the quality of each assembly (by the number of contigs, the assembly size and the identification of unfragmented housekeeping genes) and those of insufficient quality were discarded. Twelve housekeeping genes were chosen (*dsbA*, *fabD*, *fdxA*, *groEL*, *gyrB*, *proC*, *recA*, *rpoB*, *rpoC*, *rpoD*, *rpsG*, *rpsL*) and sequences for each of these were extracted using the command line version of tblastn and then translated using the command line version of EMBOSS transeq (http://www.ebi.ac.uk/Tools/st/emboss_transeq/). Each gene was then aligned separately using its protein sequence in the online version of MAFFT ([113]. A codon alignment was then obtained using the command line version of pal2nal [114] and all twelve gene codon alignments were concatenated in Excel to give a total of 20276 characters per strain. All of these characters were used to generate the phylogenetic tree. A maximum-likelihood phylogenetic tree analysis was undertaken, using the GTR + Γ + I model sequence of evolution, in the command line version of RaxML

[115] and it was verified using 100 bootstrap replicates. Lastly, the phylogenetic tree image was generated using FigTree (http://tree.bio.ed.ac.uk/software/figtree).

2.9.2 Identification of GABA permease and GABA transaminase genes

GABA permeases and GABA transaminases were identified using the command line version of tblastn. All of the genomes included in the *Pseudomonas* phylogeny were queried using representative genes from six fully sequenced strains (*Pseudomonas aeruginosa* PAO1, *Pseudomonas stutzeri* A1501, *Pseudomonas mendocina* NK-01, *Pseudomonas putida* ND6, *Pseudomonas syringae* pv. tomato DC3000 and *Pseudomonas protegens* Pf-5) and these were obtained from pseudomonas.com [110]. A manual e-value cutoff was used in each case, ranging from $1e^{-40}$ to $1e^{-100}$, depending on the query gene. Phylogenetic trees were constructed using extracted hits in the online version of MAFFT [113] and any hits which fell outside of the main clades were inspected to determine whether or not they were actual permeases or transaminases. This was done by blasting the uncertain genes against all *Pseudomonas* genomes in the NCBI database using tblastn. Additionally, where possible, gene positions and predicted functions were checked using pseudomonas.com. The majority of anomalous genes were annotated as being functionally different from GABA permeases and transaminases and, therefore, were excluded from the final analysis. The number of genes within each category (*gabP*, *gabT1*, *gabT2*, *gabT3*) were converted into a heatmap matrix using Matrix2png [116].

2.10 ICP-MS

ICP-MS analysis of the metal ion composition of tomato apoplast extracts was kindly performed by Mr. Phil Holdship (Department of Earth Sciences, University of Oxford). 100 µl of reconstituted extracted apoplast was added to 900 µl of HNO_3. This mixture was heated to 90 °C with gentle shaking for up to an hour until the sample was fully dried. 500 µl of H_2O_2 was added prior to ICP-MS analysis and the sample was diluted both 100- and 1000-fold. The technique of standard addition was employed because of the uncertainty of expected ion concentrations (due to a dearth of information in the literature). This involved spiking the sample with known standard stock solutions and the concentrations of the metal ion analytes are then extrapolated back from the total concentrations of the sample plus standard. The ion concentrations were determined using an Element2 HR-ICP-MS instrument (Thermo Fisher Scientific, Waltham, Massachusetts, USA), with a Cetac ASX-100 autosampler and PFA non-desolvating nebuliser (Cetac Technologies, Omaha, Nebraska, USA), which works at an aspirating rate of 100 µl/ml. The scan mode was set to E-mode and the analysis was performed at both medium and high mass resolutions.

2.11 ^{1}H-NMR

^{1}H-NMR profiling and analysis of apoplast extracts was kindly performed by Dr Jane Ward and Professor Michael Beale at Rothamsted Research. 70 µl of lyophilised

healthy apoplast extract, or apoplast extract that had been inoculated with bacteria and incubated for periods of time between 4 and 24 hours (after which the samples were centrifuged and the apoplast supernatant removed and re-lyophilised), were used for ^{1}H-NMR analysis. Freeze-dried apoplast samples were reconstituted in 80:20 D2O:CD3OD containing 0.05 % d4-trimethylsilylpropionate (700 µl). Samples were mixed thoroughly and then allowed to stand and re-hydrate for 45 minutes. Samples were re-agitated to ensure the final sample was thoroughly mixed and 600 µl was transferred into a 5 mm glass NMR tube for NMR analysis. ^{1}H-NMR data collection was carried out at 300 K using a Bruker Avance spectrometer (Bruker, Billerica, Massachusetts, USA) operating at 600.0528 MHz, equipped with a 5 mm selective inverse probe. Spectra were collected using a water suppression pulse sequence with a relaxation delay of 5 s. Each spectrum was acquired using 128 scans of 64,000 data points with a spectral width of 12 ppm. Spectra were automatically Fourier transformed using an exponential window with a line broadening value of 0.5 Hz. Phasing and baseline correction were carried out within the instrument software. ^{1}H chemical shifts were referenced to d4-TSP at d0.00.

Data for comparison plots was visualised in AMIX software (Bruker, Billerica, Massachusetts, USA) and compounds were identified against a library of standards run under identical conditions. Metabolite trajectories were generated by using the intensity of a characteristic, un-overlapped metabolite peak and plotting this across the time course. Orthogonal signal correction was carried out prior to constructing data models to remove variation caused by bacterial strength in the separate

independent experimental replicates.

2.12 Detection and quantification of TCA metabolites by LC-MS

A novel liquid chromatography-mass spectrometry (LC-MS) method, developed and performed by Mr Khalid Al-Qahtani (University of Oxford), was used to study changes in TCA cycle intermediates and associated metabolite concentrations. Bacterial cultures were grown in the medium of interest to densities of around OD 0.3 and then centrifuged to obtain a cell pellet. The pellets were resuspended in 1 ml of 80 % methanol by pipetting. The cell-methanol mixtures were sonicated for 30 seconds to break apart the cells and suspensions were centrifuged again. The supernatant was then dried in a speed-vacuum drier. Once fully dried, ultra pure dH_2O was added to the cell extract and D4-succinate was used as an internal standard. TCA cycle and associated metabolites were prepared in the same way, at a range of concentrations, to produce standard curves for calibration. A volume of 5 µL was used as the sample injection volume, with a partial loop size of 20 µL and using the needle overfill mode (PLNO). A hybrid stationary phase with ACE C18 pentafluorophenyl (PFP) column (2.1 x 250 mm) was used, which allows for hydrophobic and hydrophilic interactions between the stationary phase and the analyte. Chromatographic separation was performed at 45 °C. A cone voltage of 60 V and a capillary voltage of 3.0 kV were used in the negative ionization mode. The desolvation temperature was set to 190 °C and the source temperature to 120 °C.

Data was collected using Waters MassLynx v4.1 software.

2.13 GC-MS methodologies and sample preparation

GC-MS measurements were performed using an Agilent 7890 GC coupled to an Agilent 5975 quadrupole MS detector, with electron impact ionisation of 70 eV, and equipped with a Varian VF5-ms column (30 m, 10 m guard column, 0.25 mm inner diameter). Mass spectra were acquired for m/z 146-600 by scanning (at 4.38 or 3.19 scans s^{-1}). A solvent delay of 9 minutes was used in order that the mass spectrometer was turned on after the majority of the solvent had been eluted from the column. Prior to running samples, the instrument was calibrated using the autotune method. The sample volume injected into the GC was always 1 µL and this was done in the purged spitless mode.

2.13.1 Soluble metabolites

Free pool metabolites (those not bound into protein, cell wall components or other macromolecular cell constituents) were extracted from cell pellets according to an established protocol [117] with minor modifications. 140 µl of 100 % methanol was added to each frozen cell pellet (typically cells were pelleted from 10 ml cultures of at least OD_{600} 0.3) and the cells were resuspended by pipetting. 5 µl of ribitol (0.2 mg/ml) was included in the samples to act as an internal standard. The samples

were shaken at 900 rpm for 15 minutes at 70 °C (after 1-2 minutes, the caps were briefly opened to release the pressure). The tubes were then centrifuged at 14,000 rpm for 10 minutes. The supernatants were transferred to new 1.5 ml tubes and another 140 µl of methanol was added to the pellet. The cells were again resuspended and then the tubes were spun again at 14,000 rpm for 10 minutes. The resulting supernantant was added to the first volume of supernatant and the pellet was stored at -20 °C prior to protein hydrolysation. To the supernatant, 150 µl of chloroform and 300 µl of ultra pure dH_2O was added and the mixture vortexed for 15 seconds, followed by centrifugation at 4,000 rpm for 15 minutes. The upper phase was removed and then speed-vacuum dried, using a Savant SVC100H SpeedVac Concentrator (Stratech Scientific, Luton, UK) connected to a refrigerated condensation trap (Savant, Stratech Scientific, Luton, UK) and a vacuum pump (Edwards SpeediVac, Crawley, UK) for up to 4 hours. Once completely dry, 25 µl of pyridine was added and the samples were shaken at 900 rpm for 30 minutes at 37 °C. Lastly, 35 µl of MSTFA (Regis Technologies, Morton Grove, Illinois, USA) was added and the samples were shaken for a further 30 minutes at 37 °C. The samples were then transferred to GC-MS glass vials and lids were crimped on. To facilitate separation of TMS-derivatised organic acids and amino acids the oven temperature was maintained at 70 °C for 5 minutes then increased to 280 °C at 5 °C/minute and held at 280 °C for 3 minutes. The temperature was then decreased to 70 °C at 120 °C/minute. The carrier gas flow was helium at 0.6 ml/minute.

2.13.2 Protein hydrolysis and derivatisation

Proteins were hydrolysed in accordance with Zamboni *et al* (2009) [105]. First, cell pellets were resuspended in 500 µl of 6 M HCl and hydrolysed for 24 hours at 100 °C. Samples were cooled to room temperature and then centrifuged for 15 minutes at 13,000 g. The supernatant was removed and spun again if necessary (to remove any remaining cell debris). 25 µl of protein hydrolysate was speed-vacuum dried until no liquid remained. To the dried hydrolysate, 25 µl of pyridine was added and the samples shaken at 900 rpm for 30 minutes at 37 °C. Samples were briefly spun down to remove drops on the tube lids before 35 µl of MtBSTFA + 1 % TBDMS (Sigma-Aldrich Co., Gillingham, UK)) was added. Samples were shaken again at 900 rpm for 30 minutes at 60 °C. After spinning down briefly, the derivatised samples were transferred to glass GC-MS vials and lids were crimped on. TBDMS-derivatised metabolite entered the GC at an injection port temperature of 230 °C. The oven temperature was constant at 120 °C for 5 minutes, followed by an increase to 270 °C at 4 °C/minute. The temperature was held at 270 °C for 3 minutes, before a 20 °C/minute increase to 320 °C and where the temperature remained for a further minute. The carrier gas flow was helium at 1.3 ml/minute.

2.13.3 Metabolite identification and mass isotopomer data handling

Chromatograms generated by GC-MS were baseline corrected, to reduce the influence of background noise, prior to both quantification of ^{13}C incorporation and quan-

tification of metabolite abundances. This correction was carried out using MetAlign [118], with the following parameters: peak slope factor (1x noise), peak threshold factor (2x noise), peak threshold (15) and average width at half height (5 scans) and in accordance with the recommendations of Antoniewicz *et al* 2007 [119]. Baseline-corrected chromatograms were visualised using AMDIS (NIST, National Institute of Standards and Technology, Gaithersburg, Maryland, USA) and ChemStation (Agilent Technologies, Wokingham, UK) software and metabolites were identified by their elution times and by the comparison of the mass isotopomer distribution (MID) of each peak with the Golm database, using the MSSearch software (NIST), for TMS-derivatised metabolites, or with existing standard libraries of TBDMS-derivatised amino acids [120]. Once all relevant metabolite peaks had been identified, the m/z (masses) and average ion count data (abundances) off all metabolites of interest were extracted from spectra in Chemstation using customised macros which contained defined peak boundaries for each metabolite. Where chromatograms were highly similar between samples, the spectra would be processed in batches using the same macro.

In order to correct for the effect of naturally occurring heavy isotopes in the carbon backbone derivatives (for example, ^{13}C, ^{2}H, ^{15}N, ^{17}O, ^{18}O, ^{29}Si, ^{30}Si and ^{33}S), the mass correction software MSCorr [121] was used. The output from this software was both the absolute, and the proportional, abundances of the mass isotopomers of the metabolites of interest in addition to the error which can be ascribed to each measurement. The final stage in the assessment and validation of the fragment ions

was to manually check each one for the level of error from the MSCorr analysis, disregarding fragments with high levels of error (above 0.02), removing fragments which have been shown in the literature to be unreliable (such as the M-57 fragment of isoleucine, [119]) and by using the average levels of ^{13}C as a measure of validity.

Assessing the validity of mass isotopomer fragments with average ^{13}C abundances

The average amount of ^{13}C present in a fragment has been shown to be a reliable way of validating mass isotopomer fragments by S. Masakapalli [120]. By comparing the expected values of ^{13}C with the measured abundances, in samples which have and have not been labelled with ^{13}C sugars, the precision of fragment measurements can be determined. The natural abundance of ^{13}C in nature is around 1.13 % and so it can be expected that the average ^{13}C composition of fragments which have not been exposed to labelled sugars would fall close to this percentage. Samples which have been labelled with, for example, 20 % [$^{13}C_6$]glucose, would have an expected average ^{13}C composition of 20 %.

Fragments which did not display the usual natural abundances of ^{13}C or which did not become labelled to a sufficient percentage were discarded at this stage and not used in any further metabolic analyses. The equation used to determine the average ^{13}C abundance is as follows:

$$Average^{13}C = \frac{\left(\sum_{i=0-N} n_{m+i}A\right)}{N} \tag{2.4}$$

Where n_{m+i} is the number of ^{13}C-containing carbons per mass isotopomer (m+i). For example, $n = 0$ for m+0 and $n = 1$ for m+1 until $i = N$, where N is the total number of carbons in a fragment. A is the fractional abundance of the mass isotopomer.

2.13.4 Quantification of metabolites

Internal standards were used in samples where metabolite quantification was required. Amino acid standards were prepared at 1 mg/ml and a dilution series was created to provide calibration curves for the samples. For MSTFA-derived samples, 0.2 mg/ml ribitol was used as an internal standard, both for the samples and the amino acid standards, and for TBDMS-derived samples, 0.2 mg/ml of norvaline was used. The absolute abundances of the standards, produced by MSCorr, were added together for each fragment, corrected against the internal standard and then plotted against the known concentration. The samples underwent the same proceedure, with the final step calculating their actual concentration using the standard curves.

2.14 Cell biomass composition measurements

To provide accurate constraints for the metabolic models in Section 2.15.4, the macromolecular composition of *Pseudomonas syringae* pv. tomato DC3000 and *Pseudomonas fluorescens* SBW25 was determined at the point of cell harvesting during labelling experiments. For both species this was when the optical density of the cultures reached OD_{600} of between 0.35 and 0.45 (mid exponential phase). Cell

cultures were centrifuged and both the supernatant and cell pellets stored at -80 °C until required for analysis, apart from RNA measurements, which were conducted from freshly harvested cells. These measurements were converted to M/mg dry weight and the average of these values were incorporated into the metabolic models.

2.14.1 Cell dry weight

Harvested cells were lyophilised overnight in pre-weighed 1.5 ml tubes. The eppendorfs containing the dried cell pellets were then re-weighed and the weight calculated from the two measurements. At least 7 biological replicates were used for each strain and treatment condition.

2.14.2 Protein quantification

The protein content of harvested cells was quantified according to Dauner and Sauer (2001) [122]. Frozen cell pellets were resuspended in 500 µl of 10 mM $MgSO_4$. 400 µl of 4 M NaOH was added and the mixture was incubated at 100 °C for 10 minutes. The samples were cooled to room temperature before 1.6 ml of complex forming solution (10 mM $CuSO_4$, 59 mM Na-K-tartaric acid, 250 mM NaOH and 38 mM KI in dH_2O) was added. Following 30 minutes at 37 °C, the samples were centrifuged for 20 minutes at 4000 rpm. The optical densities of the samples and bovine serum albumin standards (a serial dilution of known BSA concentrations, diluted in 0.9 % NaCl) were measured at OD_{546}. The BSA standards were used to plot a standard curve, from which the protein content of the samples could be quantified.

2.14.3 Amino acid composition

Amino acid composition was determined using GC-MS. Cell pellets were analysed for both soluble and protein amino acids (see Sections 2.13.1 and 2.13.2). The identification of amino acids and the quantification of their abundances was performed as described in Sections 2.13.3 and 2.13.4 respectively.

2.14.4 Lipid quantification

Total lipid was extracted and quantified according to an established protocol [123]. Lyophilised cells (typically 20-50 mg) were finely ground in a glass vial using a micropestle. 2 ml of isopropanol was added and the samples heated to 85 °C for 10 minutes. 500 µl of dH_2O was added, followed by 3 ml of hexane. The tube was shaken vigorously and allowed to stand for 5 minutes at room temperature. 2.5 ml of 465 mM Na_2SO_4 was added, the solution was shaken again and then left to stand for until the phases separated. The upper layer was removed and transferred to a new pre-weighed glass vial and to the remaining solution 2 ml of 2:7 isopropanol:hexane was added. Following shaking, the phases were allowed to separate a final time and the new upper phase was combined with the previously collected fraction. The upper phase solution was heated to 80 °C for up to 4 hours. Once fully dry, the vial was weighed again and the percentage of lipid contributing to total biomass was calculated.

2.14.5 Glucose and fructose utilisation

The concentration of glucose and fructose remaining in the supernatant after harvesting the bacterial cells was quantified using assay kits from Sigma-Aldrich Co. (Gillingham, UK), according to the manufacturer's instructions. The concentration of sugar in the supernatant, in comparison with the uninoculated media, was used to determine the amount taken up by the cells.

2.14.6 Nucleic acids

DNA and RNA were extracted as per Section 2.6.1 and 2.6.7 respectively and quantified as described in Section 2.6.3.

2.14.7 Extracellular polysaccharides, lipopolysaccharides, peptidoglycan and phospholipids

The contribution, and composition, of extracellular polysaccharides (EPS), lipopolysaccharides (LPS), peptidoglycan and phospholipids to total biomass was estimated from the literature. Specifically, EPS was estimated from Kidambi *et al* (1995) [124] for Pst DC3000 and Read and Costerton (1987) [125] for Pfl SBW25; LPS was estimated from Zamze *et al* (1985) [126]; peptidoglycan estimates were taken from Sohn *et al* (2010) [127] and Heilmann (1972) [128] and phospholipid content was taken from Sohn *et al* (2010) [127].

2.15 ^{13}C Metabolic flux analysis

2.15.1 Chemicals

Labelled sugars were obtained from Cambridge Isotope Laboratories, Inc (Andover, MA, USA). MSTFA was purchased from Regis Technologies (Morton Grove, Illinois, USA) and MtBSTFA + 1 % TBDMS from Sigma-Aldrich Co. (Gillingham, UK).

2.15.2 Software

The following software was used in the analysis of of isotopomer measurements: 13CFLUX (www.13cflux.net; version 20050329; [129]), ChemStation (Agilent Technologies, Wokingham, UK), MSCorr [121], Matlab (Mathworks, Cambridge, UK), MetAlign (www.wageningenur.nl,), AMDIS (NIST, National Institute of Standards and Technology, Gaithersburg, Maryland, USA) and MSSearch (NIST, Golm database). Statistical analyses were performed in Excel (Microsoft, Redmond, Washington, USA) and principal component analysis in SIMCA-P 11.5 (Umetrics, Umea, Sweden).

2.15.3 Cell labelling and harvesting

Bacteria were grown overnight in LB media and then resuspended in either M9, with glucose or fructose as the sole carbon source, depending on the sugar to be used for labelling, and left to grow again overnight. The cell cultures were centrifuged and

the cell pellets washed through twice with M9 without a carbon source and the optical density adjusted to OD_{600} 0.01. The cells were centrifuged a final time and resuspended in M9 with a labelled carbon source. [$^{13}C_6$]glucose, [1-^{13}C]glucose, [2-^{13}C]glucose, [$^{13}C_6$]fructose and [1-^{13}C]fructose were used in this study in addition to non-labelled glucose and fructose (to provide both a negative control for labelling and quantification of amino acids and organic acids, and verification of the natural abundance of ^{13}C in the fragments). Once cells reached an OD_{600} of 0.35-0.45 (mid exponential phase, where the cells are in an assumed isotopic steady state [105, 130]), the cells were spun down and washed through once with M9 containing no carbon source. The washed cell pellets and supernatants were stored at -80 °C prior to analysis. Pellets were analysed by GC-MS for both soluble metabolites (Section 2.13.1) and proteinogenic amino acids (Section 2.13.2).

2.15.4 Metabolic network models and .ftbl files

Metabolic network models were constructed using network information available from KEGG (www.genome/jp/kegg/) and MetaCyc (www.metacyc.org) [89]. In addition, pseudomonas.com provided information about the presence of genes which were not included in these databases [110]. Further network verification was performed by targeted labelling strategies (see Section 2.15.6). The network model was assembled in an .ftbl file format, according to the requirements of the 13CFLUX software and the recommendations of Wiechert *et al* (2001) [129], along with the mass isotopomer distribution data, which had been analysed according to Section 2.13.3. Data from two labelling experiments (both [$^{13}C_6$] and [1-^{13}C]labelled sug-

ars, and [2-^{13}C] in the case of glucose-fed cultures), each of which included three independent repeats, were included in the .ftbl model file. This required the presence of two network models in the file for fructose-fed cells and three for glucose-fed cells. The reactions and fragment data associated with the [$^{13}C_6$] labelling strategy denoted as '_U' (for example, ALA_U denotes alanine in the [$^{13}C_6$] model) and '_1' and '_2' for [1-^{13}C] and [2-^{13}C]-derived information. All the sub-networks within a model were constrained to have the same values for the same net and exchange fluxes. The .ftbl file was checked for consistency and syntax using the Ftbl2Flx command in 13CFLUX. After amending the .ftbl file as required, the CumoNet command was then used to determine if fluxes should be assigned as free, determined or constrained, to check the feasibility of the network, and also to generate a set of isotopomer abundances for the free fluxes [120].

2.15.5 Modelling uptake flexibility

To allow for the presence of unlabelled metabolite pools resulting from the slow turn over of metabolites, discrepancies in media preparations, or bias in labelled versus unlabelled glucose uptake [131], fluxes for the uptake of both labelled and unlabelled sugars were included. This allowed the model to determine the degree to which it required the label to have been assimilated in order for the lowest discrepancy between the measured and predicted fluxes. Initially, sub-networks were run as single models and the uptake fluxes were left free to determine how much sugar assimilation was predicted by the optimisation procedure. An example of 20 % [$^{13}C_6$]glucose assimilation is given below.

The uptake of 20 % [$^{13}C_6$]glucose and 80 % unlabelled glucose is defined as:

uptU_U: GLCU_U → GLCext_U

upt0_U: GLC0_U → GLCext_U

glcupt_U: GLCext_U → G6P_U

Where the model is not constrained to a 1:4 uptake ratio of the two substrate types. Similarly for [1-^{13}C]glucose and [2-^{13}C]glucose, though these were fed in the absence of fully unlabelled glucose, the model was allowed the flexibility to determine percentage uptake of these. Once the single model simulations were run, an average was taken across the substrates to then constrain the model:

$$\frac{upt\_1 + upt\_2 + 5upt\_U}{3} \tag{2.5}$$

The result of this process allowed the models to be constrained in the percentage of labelled substrate taken up from the medium, but the total substrate uptake (*glcupt* or *frcupt*) was left as a free flux. The constraints for the glucose-fed model of Pst DC3000 are given below:

4.35uptU_U-upt0_U = 0

5uptU_U-upt1_1 = 0

upt1_1-upt2_2 = 0

In the above scenario, 93.5 % of the carbon in the cells is predicted to have come from the labelled glucose in the media.

2.15.6 Verification of metabolic pathways

The activity of the reaction, catalysed by serine dehydratase, of serine to pyruvate in both Pst DC3000 and Pfl SBW25 was determined by adding in 2 mM [2-^{13}C]glycine into cultures of Pst DC3000 and Pfl SBW25 which had reached an OD_{600} of 0.35, growing in unlabelled glucose (M9 medium). 10 ml samples were harvested at 0, 0.5, 1 and 2 hours, spun down and the pellets stored for analysis of both soluble metabolites (Section 2.13.1) and protein hydrolysate (Section 2.13.2).

2.15.7 Metabolic modelling

Metabolic flux modelling was carried out using 13CFLUX in a accordance with many of the recommendations of Wiechert *et al* [129]. The .ftbl model files were fitted with randomly generated initial values for free fluxes by using the sequential quadratic programming algorithm *Donlp2* (P. Spelluci, Technische Universität, Darmstadt, Germany) in combination with Monte Carlo simulations. The command used for this process is as follows:

> Donlp2 "model file name".ftbl -a 0.00001 m "number of simulations" -bootstrap -logAllF >"output file name".txt& watch "grep Resi "output file name".txt|tail -20"

The *Donlp2* command generates a set of solutions for free fluxes in the network, after minimising the residuum (the sum of squared standardised differences between the actual measured data and their predicted values), a specified number of times

("number of simulations"). 600 simulations were run in order to generate a large enough flux solution space (the number of Monte Carlo simulations required to fully explore the flux space is dependent on the size of the network and number of free fluxes, along with the accuracy of the data in the model) and bootstrap Monte Carlos were used in accordance with the recommendation of S. Masakapalli (University of Oxford) [120]. The simulations produced a set of flux solutions which could be classed as either feasible or infeasible (that is, they were unable to satisfy the pre-defined network requirements) and these solutions were collected using a script written by S. Masakapalli [120]. Within the feasible solutions there was a wide range of residua and a threshold was set using principal component analysis (Section 2.15.8) for flux solutions to be considered further (infeasible solutions were also rejected at this stage).

The feasible solutions that fell below the imposed threshold were then averaged for each free flux. It has been previously found that averaging all the solutions for each free flux provides a good starting point for re-optimisation and for obtaining the best fit solutions [120]. Starting from the averaged values of the free fluxes, the command *Donlp2* was run again, but without bootstrapping, as follows:

> Donlp2 "model file name".ftbl -a 0.00001 m 0 -logAllF >"output file name".txt& watch "grep Resi "output file name".txt|tail -20"

The best fit solution, generated from the averaged free flux value input, was assessed using the χ^2 criteria [129, 132]. That is, the residuum of the best fit solution must be lower than the χ^2 value of the model, where degrees of freedom (DF) are given

as:

DF = no. of measurements - no. of free fluxes - no. of metabolite fragments

Solutions that did not meet the χ^2 criteria were inspected and poorly fitting fragments were examined as a potential source of the poor fit.

2.15.8 Principal component analysis

Principal component analysis (PCA) was conducted across flux solutions from 600 Monte Carlo simulations as according to Masakapalli *et al* [133]. Flux values were mean-centred but not otherwise adjusted, scaled to unit variance, or Pareto scaled. The resulting PCA plots were used to determine the threshold for the inclusion of flux solutions into the set of values which would be averaged and then used to start the best fit optimisation. Data presented in Section 4.2.6 shows only the unit variance scaled data as little difference was seen between the three scaling methods (Appendix A.2).

2.15.9 Confidence intervals and statistical analysis

The EstimateStat component of 13CFLUX was used to generate linear standard deviation estimates for all of the flux values in the models, excluding constrained fluxes.

2.16 Unlabelling experiments

In order to track the uptake of GABA in Pst DC3000, Δ*gabP* and Δ*gabT2/T3/T1*, an unlabelling strategy was employed. As ^{13}C-GABA is not available commercially, monitoring the accumulation and metabolism of GABA was achieved by, first, fully labelling the intracellular metabolites by feeding 100 % [$^{13}C_6$]glucose, and then adding in unlabelled GABA and monitoring the depletion of label over time. Strains were grown overnight in LB 10 ml cultures and were then spun down and resuspended in M9 containing 100 % [$^{13}C_6$]glucose (22 mM) at an OD_{600} of around 0.05. The M9 cultures were again allowed to grow overnight until they reached a high density. The samples were spun down again and resuspended in fresh labelled M9 and this time resuspended at an OD_{600} of 0.05 and left to grow until reaching an OD_{600} of 0.3 (by this stage upwards of 95 % of all amino acid carbons were ^{13}C labelled). Upon reaching this desired OD, the cultures were spun down and then resuspended in 10 ml one of the modified version of M9 media in Table 2.5.

Treatment Name	**Carbon Source (Concentration)**	**Nitrogen Source (Concentration)**
Glc + NH_4	Glucose (22mM)	NH_4Cl (1.87mM)
Glc + GABA	Glucose (22mM)	GABA (22mM)
GABA + NH_4	GABA (22mM)	NH_4Cl (1.87mM)
GABA	GABA (22mM)	GABA (22mM)

Table 2.5: M9 treatments used to study GABA uptake and metabolism. The carbon and nitrogen sources were modified to include GABA as the carbon source, nitrogen source or both the carbon and nitrogen source, replacing glucose (Glc) and ammonium chloride (NH_4)

This range of treatments made it possible to test for the use of GABA as a carbon source, as a nitrogen source and as a carbon and nitrogen source, with normal M9

provided as a comparison. 1 ml aliquots of cells in the different treatments were taken at the following time points: 0, 2, 4, 6 and 8, and at 24 hours the remaining culture volume was harvested. The cells were spun down and then washed through once in 1 x M9 salts (see Section 2.3). The pellets were stored at -80 °C and samples from time points 0, 2, 4, 6 and 8 were hydrolysed and derivatised using TBDMS according to Section 2.13.2. The 24 hour samples were analysed for both soluble metabolites (as per Section 2.13.1) and protein hydrolysate (Section 2.13.2). All samples were analysed by GC-MS and data was handled in the same way as Section 2.13.3.

A second experiment was conducted to ascertain labelling patterns at 16 hours. Pst DC3000 and $\Delta gabP$ were grown in M9 (glucose and NH_4) and M9 (without NH_4Cl) with 22 mM glucose and 22 mM GABA, samples were harvested at 0 hours and 16 hours and protein hydrolysate was analysed. All experimental methods were performed as previously.

Data from both experiments were analysed in Excel and heatmap matrices were created using Matrix2png [116].

Chapter 3

The relationship between the metabolic environment and the up-regulation of virulence genes in *Pseudomonas syringae*

3.1 Introduction

The host plant apoplast is the primary site of infection for many bacterial plant pathogens, however, few studies have explored the effect of the metabolic composition of this compartment on virulence. *Pseudomonas syringae* strains are known regulate the expression of their virulence genes in response to different metabolites

and can be manipulated *in vitro* to express their type III secretion systems (T3SS) by incubation in minimal media containing sugars such as fructose and mannitol. Understanding the metabolic components of the host apoplast and their effects on the expression of bacterial virulence genes is therefore of great importance in developing a deeper understanding of the metabolic interface between plants and their bacterial pathogens.

This study has used the model pathogen, *P. syringae* pv. tomato DC3000 (Pst DC3000) and its interaction with its host, the tomato plant, to characterise the relationship between the metabolic environment of the host apoplast and the regulation of virulence genes in the pathogen. First, a non-targeted metabolomics approach was used to profile the tomato apoplast in order to identify the nutrients which are available to Pst DC3000 during infection. Second, the ability of Pst DC3000 to deplete and metabolise apoplastic metabolites was tested. Third, the effect of apoplastic metabolites on the expression of virulence genes in Pst DC3000 was monitored. Fourth, the internal metabolic changes associated with environments that induce and repress virulence genes were assessed, and, finally, a non-pathogenic T3SS-expressing *Pseudomonas* was investigated to understand if conserved mechanisms of T3SS induction exist between *Pseudomonas* species.

3.1.1 Known components of the tomato plant apoplast

Several key studies have addressed the composition of the tomato apoplast, both in the plant leaves and in the fruit. Apoplastic fluid can be extracted from plant

tissues by infiltration, either by subjecting the samples to vacuum or to pressure [134–136] and then analysed using metabolomics techniques such as HPLC [71].

Tomato leaf apoplastic components and chemical composition

An early study, by Joosten *et al* (1990) [137] identified the sugars fructose, glucose and sucrose in tomato leaf apoplastic extracts, with sucrose the most abundant of the three. Amino acids have been identified in tomato leaf apoplast in targeted analyses by Rico *et al* (2008) [71] and Solomon & Oliver (2001) [75]. Both studies found that GABA was the most abundant amino acid, and that glutamate, glutamine, alanine, aspartate and serine were also highly abundant. Neither study was able to detect cysteine or tryptophan, and Rico *et al* (2008) [71] were unable to detect arginine. Phenolic compounds have also been identified at low levels within healthy tomato leaf apoplast [138]. The pH of tomato leaf apoplast has been measured at between pH 5.0 and pH 6.5 depending on the soil moisture and nitrate levels [71, 73].

Tomato fruit apoplastic components and chemical composition

Pst DC3000 is capable of infecting tomato fruits and in this context also inhabits the apoplastic compartment. The pH of tomatoes varies according to the maturity of the fruit, with the most mature fruits at pH 4.4 [74]. Similarly to the apoplast in tomato leaves, hexose sugars and amino acids have been detected in tomato fruits, as well as organic acids and ammonia [136]. Sugars, particularly sucrose, have been shown to accumulate in the apoplast as fruits reach maturity [139]. Potassium ions are the most abundant inorganic ions, and calcium and magnesium ions have also

been detected [74].

Tomato xylem sap components and chemical composition

In addition to apoplastic metabolites, nutrient profiling of xylem sap has also been performed. All amino acids apart from tryptophan have been identified in xylem exudates, with glutamine detected in the highest concentrations [140, 141]. The organic acids, malic acid, malonic acid, maleic acid, citric acid, fumaric acid and succinic acid have all been detected in xylem sap, and malic and citric acid have been shown to be the most abundant [140–142].

Age, soil conditions and stress are known to contribute to metabolic changes occurring within tomato apoplast and sap [73, 141]. In addition, the apoplastic composition of tomato plants has been shown to change in response to invading pathogens, which is discussed in more depth in Section 3.1.2. However, no single study has sought to characterise the tomato apoplast metabolome in a non-targeted manner. An analysis of this nature would allow relative abundances of different types of metabolites to be established, creating a more complete understanding of the metabolic landscape encountered by Pst DC3000. It is also expected that the presence of additional metabolites will be detected, which may be of importance in the Pst DC3000-tomato interaction.

3.1.2 Metabolic changes known to occur in tomato and other Pst DC3000 host plants in response to pathogen infection

Numerous studies have shown that the plant apoplastic compartment responds metabolically to the presence of invading pathogens [3]. As described in Section 1.8, a large-scale metabolic reprogramming occurs, involving both primary and secondary metabolism, and this has been observed both at the transcriptomic and metabolomic levels. Changes known to occur in tomato plants in response to various pathogens are described below, as well as specific changes Pst DC3000 induces in its host plants.

In tomato leaf apoplast infected with the fungus *Cladosporium fulvum*, the abundance of mannitol markedly increases [137] along with increases in GABA, valine, tyrosine, proline, leucine, isoleucine, lysine and arginine [75]. Lopez-Gresa *et al* (2009) [8] also reported amino acid levels increasing in tomato leaves, though in response to infection with *P. syringae*. Both of these studies indicate an increase in the nitrogen content of the apoplast during infection with fungal pathogens. Another study, by Berger *et al* (2007) [98] detected pathogen-specific responses in sugar abundances: *Botrytis cinerea* inoculation caused a decrease in sugar levels in tomato leaves, whilst inoculation with *P. syringae* did not alter sugar levels. Phenolic compounds have also been shown to increase in leaf apoplast infected with viroids [138]. Transcriptional studies of tomato plants have noted changes in genes associated with

nitrogen metabolism: both asparagine synthetase and glutamine synthetase genes show a high level of induction in response to the presence of *P. syringae* cells [4, 143]. A study by Ward *et al* (2010 [7] detected metabolite changes in *A. thaliana* leaves (whole-leaf samples as opposed to apoplast extracts) in response to Pst DC3000. As in tomato, amino acid levels increased upon inoculation, specifically GABA, alanine, glutamine, isoleucine, leucine, phenylalanine, threonine, tyrosine and valine. These results imply that the nitrogen concentrations in the apoplastic environment may increase during infection, and certainly that the plant is undergoing significant metabolic changes in response to the pathogen. One of the difficulties associated with studies such as these, however, is the inability to distinguish metabolic changes which arise directly from plant defence responses, and those which arise from pathogen manipulation of the host.

Recently, Rico *et al* (in preparation) have monitored metabolic and transcriptomic changes which arise in the tomato apoplast inoculated with Pst DC3000. Over a 24 hour period, alanine, asparagine, glutamine, glutamate, citrate, trigonelline, tyrosine and adenosine all increased in abundance. GABA, inositol and valine all decreased in abundance over the same period. These results were mirrored in many of the transcriptomic results, with genes involved in aromatic amino acid metabolism and glutamate metabolism increasing in expression and genes involved in inositol metabolism decreasing. Specifically the increase in glutamine and glutamate is consistent with mobilisation of nitrogen in the apoplast. An increase in the aromatic amino acid tyrosine is indicative of upregulation of pathways involved in synthesis-

ing defence compounds, many of which use aromatic amino acids as precursors [97]. It is unknown in this study if the decrease of metabolites is due to assimilation by Pst DC3000, but the increases in metabolite abundance are most certainly due to metabolic changes in the host.

The tomato host apoplast is therefore a metabolically dynamic environment to which Pst DC3000 must be adapted in order to successfully establish infection.

3.1.3 Metabolic capabilities of Pst DC3000 in the assimilation of apoplastic components

The tomato apoplast is a complex metabolic environment, comprising several different types of carbon and nitrogen sources. A comprehensive study by Rico *et al* (2008) [71] demonstrated that Pst DC3000 is well adapted to the tomato apoplast: Pst DC3000 is able to assimilate all of the most abundant apoplastic amino acids (such as GABA, glutamate and aspartate), but is unable to grow using the lower abundance amino acids (such as threonine and isoleucine) as carbon sources. Pst DC3000 is predicted to have fewer nutrient assimilation genes than other *Pseudomonas* strains, and specifically lacks assimilation pathways for branched-chain and sulphur-containing amino acids [86]. Rico *et al*'s (2008) study also showed that extracted tomato apoplast provides a rich growth medium for Pst DC3000, as cells grew more rapidly in the extracts than rich synthetic media such as LB [71].

Current knowledge about the metabolic capabilities of Pst DC3000, provided by

the genome sequence of Pst DC3000 [30] and metabolic database analysis [86], can give an indication of which metabolites Pst DC3000 is likely to deplete *in planta*, but cannot be used to determine the rapidity of depletion of each metabolite, nor the order in which metabolites are assimilated. It is hypothesised that carbon catabolite repression (CCR), the inhibition of metabolic enzymes which are not required to assimilate preferred substrates [144], will be active in Pst DC3000 when in the plant host or in extracted apoplast, as is the case for many pathogenic bacteria in their host species [31]. In *Pseudomonas* species, CCR has been shown to favour organic and amino acids, instead of hexose sugars, which is more typical in other bacterial species [145]. The non-coding RNAs, CrcZ and CrcX, control carbon source utilisation in Pst DC3000, and the production of these molecules is governed by the two-component system CbrA-CbrB and the alternative sigma factor RpoN [146]. The involvement of another two-component system, NtrB-NtrC has also been postulated in other *Pseudomonas* species [147, 148]. CbrA-CbrB and NtrB-NtrC are described respectively as carbon and nitrogen regulatory systems and the two systems are thought to be genetically related as they share a moderate degree of amino acid sequence similarity in *P. aeruginosa* [149]. The signals which CbrA-CbrB interprets has yet to be determined [150] but these regulatory proteins are known be necessary for growth on histidine, arginine, alanine, proline and polyamines [149]. Metabolite footprinting, where the depletion of metabolites is monitored over time, of Pst DC3000-inoculated apoplast extracts should provide the evidence required to determine if CCR is in operation in the plant environment.

3.1.4 Pst DC3000 virulence gene expression in response to the host environment

Pst DC3000 is known to rapidly upregulate genes encoding its T3SS and other virulence factors, such as alginate and coronatine, when inoculated into healthy tomato plants [81, 151, 152]. Importantly, Pst DC3000 cells also upregulate virulence gene expression when incubated in extracted tomato leaf apoplastic fluid [71] and tobacco leaf sap [152], thus demonstrating that the extractable metabolic components of the apoplast are a major factor in Pst DC3000's recognition of a suitable environment for pathogenicity. Understanding fully which metabolites are present in the host apoplast therefore remains an important goal in the ongoing characterisation of the Pst DC3000-tomato interaction [3].

3.1.5 Pst DC3000 virulence gene expression in response to apoplastic metabolites *in vitro*

Whilst a complete inventory of tomato apoplastic metabolites is lacking, many metabolites have been identified and several are known to have specific effects on virulence gene expression in Pst DC3000. Fructose, sucrose and mannitol are commonly used to upregulate expression of *P. syringae* T3SS genes *in vitro* after the identification by Huynh *et al* (1989) [79] that these produce high levels of induction. All three sugars can be detected in tomato apoplast extracts [137]. Recently, Stauber *et al* (2012) [80] demonstrated optimal *hrp* induction in Pst DC3000 by

fructose. *P. syringae* virulence genes are also induced by pHs which are encountered in the tomato apoplast: the highest levels of induction have been shown to be at pH 5.5 [50, 81]. Pst DC3000 cell cultures of low density have been shown to have much higher levels of virulence gene expression than high density ones, which is unusual for a bacterial pathogen [80].

Both organic acids and amino acids have been shown to downregulate virulence gene expression in *P. syringae* strains [79–81]. Specifically, citrate and succinate, when added to fructose or mannitol media, stimulate much lower levels of induction than fructose or mannitol alone in *P. syringae* pv. glycinea [79]. Huynh *et al* (1989) [79] also found glutamate to be highly repressive in comparison with fructose and mannitol, and that different amino acids caused different levels of repression. A study by Park *et al* (2010) [88] showed that the non-protein amino acid, GABA, which is the most abundant amino acid in the tomato apoplast [71, 75], repressed virulence gene expression in Pst DC3000. The mechanisms by which external metabolites influence virulence gene expression are currently unknown.

As discussed in Section 3.1.2, the apoplast undergoes major metabolic reprogramming during infection. Understanding how Pst DC3000 regulates the expression of its virulence genes in response to apoplastic metabolites should provide novel insights into the adaptation of this pathogen to life inside the dynamic host environment. Several bacterial species have been shown to sense their metabolic environments through changes in intracellular metabolite abundances, such as *Salmonella*

typhimurium which senses low intracellular glutamine as an indication of being in a nitrogen-limited environment [153, 154]. The tomato apoplast has been suggested to be perceived as nitrogen-limited environment by Pst DC3000 cells as nitrogen-limited conditions *in vitro* induce the expression of virulence genes [71]. It was therefore hypothesised that Pst DC3000 might show differences in intracellular metabolites under virulence gene-inducing conditions which could provide the signal necessary to stimulate the transcription of T3SS genes and other virulence determinants.

An investigation of how environmental stimuli alter virulence gene expression in Pst DC3000 is likely to have a broader significance for bacterial plant pathogens more generally: *Pseudomonas*, *Erwinia*, *Pantoea*, *Ralstonia* and *Xanthomonas* species all cause economically important diseases of crop plants and all have orthologous type III secretion systems which respond to similar environmental stimuli, such as contact with plant cells, osmolarity and minimal media [50]. Whilst some differences do exist in their virulence gene expression in response to difference carbon sources, as a general rule carbon sources such as fructose, mannitol and sucrose tend to induce virulence gene expression in these pathogens, whilst succinate, citrate and glutamate tend to have a repressive effect [50]. The identification of mechanisms by which Pst DC3000 cells sense their environment may therefore be applicable to a wide range of pathogenic bacteria.

3.1.6 Statement of aims

A variety of metabolomics techniques and virulence gene expression assays were used to address the following questions:

1. What nutrients are available to Pst DC3000 in the host apoplastic environment?

2. Does Pst DC3000 show preferential depletion of certain metabolic components from host apoplastic fluid?

3. How do individual apoplastic metabolites influence virulence gene expression?

4. Do internal metabolite levels change in Pst DC3000 in environments that induce and repression virulence gene expression?

5. Are there conserved mechanisms for the induction of type III secretion systems in other *Pseudomonas* species?

3.2 Results

3.2.1 The metabolic and ionic composition of extracted tomato leaf apoplast

The host apoplast is the main site of infection for Pst DC3000 The first comprehensive study into the amino acid composition of tomato leaf apoplast demonstrated,

using high-performance liquid chromatography (HPLC), that GABA, aspartate and glutamate were highly abundant components [71]. In order to provide a broader analysis of the metabolites present in extracted tomato leaf apoplast, a non-targeted ^{1}H-NMR-based approach was taken. Apoplast from uninfected leaves was extracted on three separate occasions and Figure 3.1 shows the relative abundances of the metabolites detected. In addition to the identification of amino acids, other metabolites were able to be detected in the ^{1}H-NMR analysis, including sugars and organic acids. Notably, glycine-betaine, choline and myo-inositol were found to be relatively abundant in the apoplast and fructose was the most relatively abundant sugar present. The alkaloid trigonelline and the nucleoside adenosine were also found to be present, though in low quantities. In addition, several metabolites were found in the apoplast samples which were not able to be identified (labelled 'unknown' in Figure 3.1). These unknown metabolites are unlikely to be novel molecules; it is more probable they are uncommon enough that standards for these metabolites have not yet been entered into the metabolite library used in this study. An additional GC-MS study, conducted by Dr. Arantza Rico (personal communication) detected arginine, citrate and succinate, which were not identified in the ^{1}H-NMR analysis.

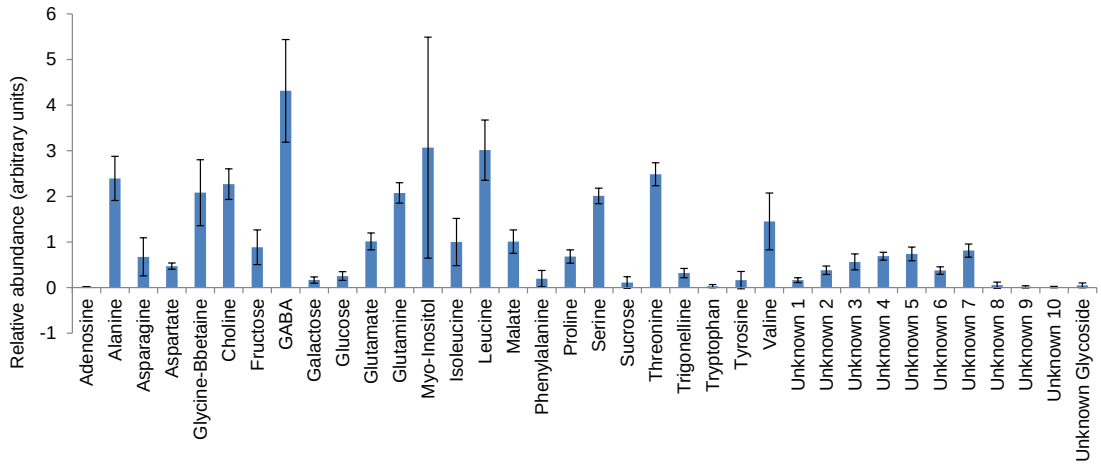

Figure 3.1: ^{1}H-NMR quantification of metabolites from extracted tomato leaf apoplastic fluid. Apoplastic fluid was extracted, lyophilised and then analysed by ^{1}H-NMR. Three independent sample sets were used, and the average abundance of each was used to standardise the measurements and provide relative quantifications. Bars represent the averages of these relative quantifications and error bars show standard deviations. Unknown metabolites were unable to be identified using current ^{1}H-NMR databases.

A comparison between the amino acids detected in the HPLC analysis by Rico *et al* (2008) [71], the GC-MS analysis (A. Rico, personal communication) and the ^{1}H-NMR analysis is shown in Figure 3.2. All three analyses show GABA to be the most abundant amino acid, however, whilst the HPLC analysis detected GABA to be four-fold higher in abundance than any other amino acid, the ^{1}H-NMR spectra show amino acids such as alanine, glutamine, leucine, serine and threonine are very much in the same abundance range as GABA. HPLC analyses identified histidine where the ^{1}H-NMR and GC-MS analyses did not, the GC-MS analysis identified arginine where the ^{1}H-NMR and HPLC analyses did not, and both the HPLC and GC-MS analyses identified methionine, lysine and glycine where the ^{1}H-NMR did not. In addition, the ^{1}H-NMR analysis was able to identify tryptophan, which was not detected in either the GC-MS or HPLC studies.

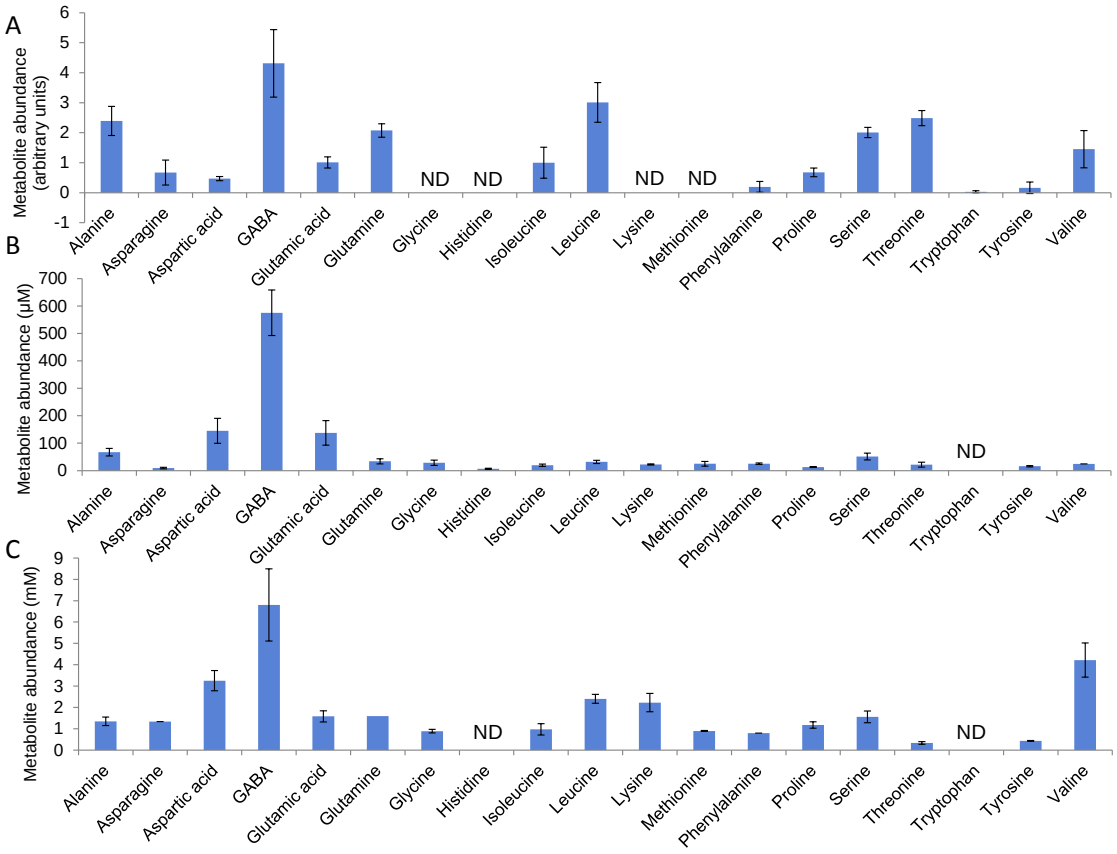

Figure 3.2: Amino acids in tomato leaf apoplastic fluid, detected and quantified using three separate approaches. (A) Amino acids detected using ^{1}H-NMR (this study). (B) Amino acids detected using HPLC by Rico *et al* (2008) [71]. (C) Amino acids detected using GC-MS, Dr Arantza Rico (University of Oxford), personal communication. ND: the amino acid was not detected during the analysis. At least three independent replicates were used in each study. Error bars represent standard deviation.

The metallic composition of tomato apoplast extracts was also analysed using ICP-MS (Figure 3.3). Metals such as iron and copper have been shown to be important for the expression of virulence determinants in *P. syringae* pathovars [124, 155], however, a full characterisation of the metals present in tomato apoplast had not previously been undertaken. Very high levels of magnesium, calcium, sodium and potassium ions were detected, and these are commonly found to be abundant in plant apoplast extracts [156]. Interestingly, copper was detected and thus may act as a signal for Pst DC3000 to upregulate its production of alginate, as has been

described for *P. syringae* pv. syringae [124]. Unfortunately, iron was found to be below the limits of detection for the ICP-MS instrument, though it has been previously detected in sugar beet leaf apoplast [70] and tomato xylem fluid [142]. It may be that iron is tightly bound to the plant cell walls and as a result is not easily extracted during the vacuum infiltration proceedure.

Several of the metal ions detected are not currently included in *hrp*-inducing synthetic media, such as cadmium, copper, zinc, nickel, manganese and molybdenum. It would therefore be interesting to assess how these metals influence the expression of virulence genes.

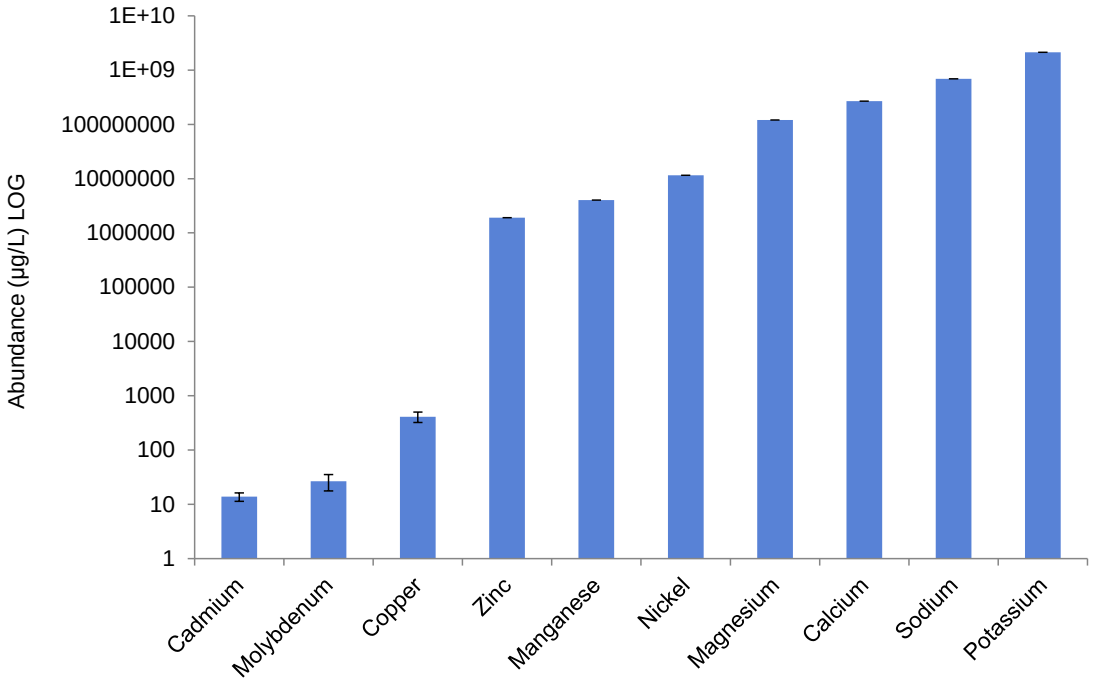

Figure 3.3: Metal ionic composition of tomato apoplastic fluid. The metal ions present in extracted tomato apoplast were determined by ICP-MS. Four independent samples were analysed and their standard deviation is shown in the error bars. Iron and cobalt ions were below the limits of detection (1.81 µg/ml and (4.60 µg/l respectively).

The tomato leaf apoplastic fluid therefore represents a rich and diverse set of metabolites, and further analysis will be required to identify the as yet unknown metabolic components. Profiling the composition of tomato apoplast extract facilitated the study of how Pst DC3000 depletes different components (Section 3.2.2) and how the expression of virulence genes responded to the individual metabolites identified in Section 3.2.5. This work will also hopefully provide the basis for creating more realistic synthetic media for the study of tomato-dwelling microorganisms.

3.2.2 Metabolite footprinting reveals preferences exhibited by Pst DC3000 in the depletion of nutrients from the host apoplast

The tomato leaf apoplast is one of the main sites of infection for Pst DC3000, and thus it can be expected that this species should be well adapted to utilising the metabolites present in this compartment. Carbon catabolite repression (CCR) has been shown to operate in many pseudomonads [145], including *P. syringae* [146], and so distinct patterns in the depletion of apoplastic metabolites were anticipated. Extracted apoplast was inoculated with Pst DC3000 and samples were taken at 8 and 24 hours. These time points were selected based on a pilot study by Dr. Aranzta Rico (University of Oxford), which showed a adaption phase of around four hours, that after 8 hours preferred substrates were beginning to be depleted, and after 24 hours a much wider set of substrates was being depleted. In order to control for any changes which might occur in the extracted apoplast under the experimental conditions,

uninoculated apoplast was left for 24 hours at 28 °C to detect any non-pathogen-associated changes. Figure 3.4 shows that metabolite abundances in uninfected apoplast extracts at 0 hours and 24 hours are highly similar. Changes detected in the subsequent depletion assays (Figure 3.5) can therefore be fully attributed to the metabolic activities of Pst DC3000 cells.

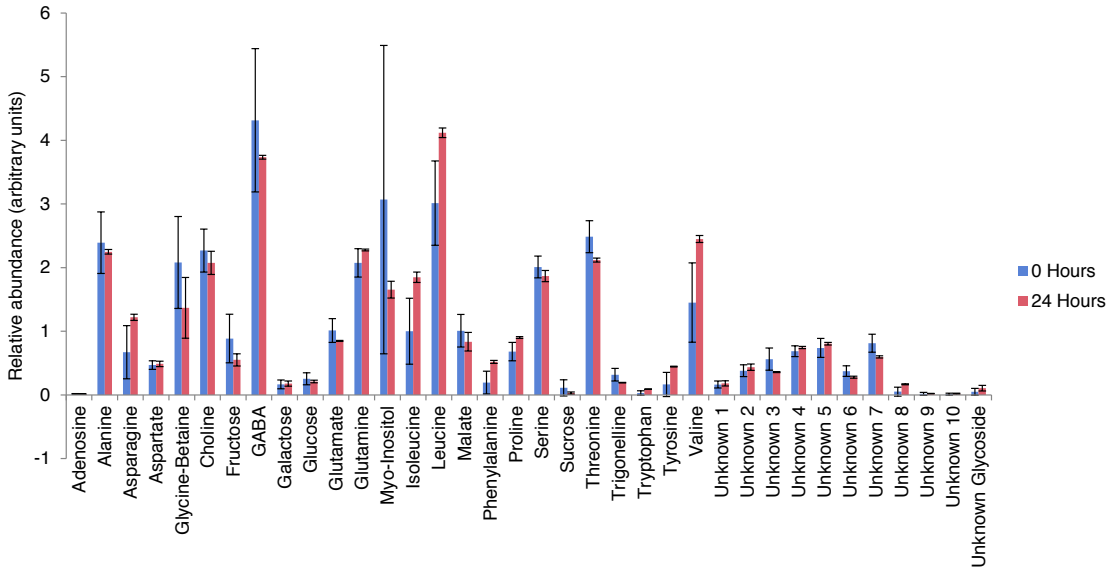

Figure 3.4: ^{1}H-NMR spectra of extracted tomato leaf apoplastic fluid does not show any significant compositional changes over 24 hours. Extracted tomato leaf apoplastic fluid was subjected to bacterial incubation conditions: 150 ml samples were incubated at 28 °C and shaken for 10 seconds every 20 minutes - for 24 hours to ensure that changes in composition in bacteria-inoculated samples was solely due to bacterial metabolic activities. Bars show averaged relative abundances and error bars indicate standard deviation over three independent sample sets.

Over the 24 hour incubation period, Pst DC3000 was able to deplete many of the metabolites present in apoplast extract almost completely (Figure 3.5). Adenosine, alanine, asparagine, aspartate, GABA, glucose, glutamine, glutamate, sucrose and tyrosine, along with unknown metabolites 2, 3, 8, 9 and the unknown glucoside were all depleted more than 70 %. Metabolites that were less than 70 % depleted after

24 hours included choline, fructose, galactose, inositol, isoleucine, leucine, malate, phenylalanine, proline, serine, threonine, trigonelline, valine and unknown metabolites 4, 5 and 7. Betaine and unknown metabolites 1 and 7 increased in abundance over the 24 hour period, indicating they are the byproducts of a bacterial metabolic pathway and are then released into the extracellular environment.

Whilst many metabolites were depleted almost fully by 24 hours post-inoculation, the 8 hour time-point samples reveal that some metabolites were more quickly removed from the apoplast than others (Figure 3.5). Asparagine, aspartate, glucose, glutamine, glutamate and unknown metabolite 8 all show at least 50 % depletion within the first 8 hours. Conversely, metabolites such as adenosine, GABA, sucrose, and unknown metabolites 2, 3 and 9, show little depletion after 8 hours, although they are almost absent from the apoplast extracts after 24 hours. Pst DC3000 therefore exhibits significant patterns of depletion of apoplastic nutrients, and it is possible that this is contolled by CCR.

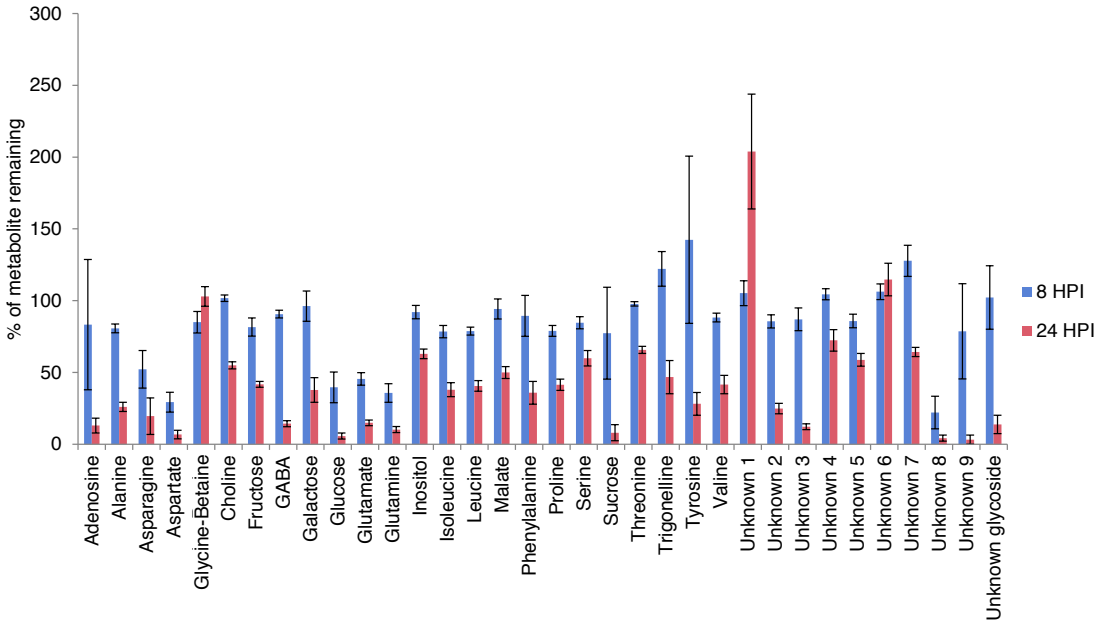

Figure 3.5: Pst DC3000 selectively depletes metabolites from tomato apoplast extracts over 24 hours. The percentage of metabolites remaining in tomato leaf apoplast extract 8 and 24 hours after inoculation with Pst DC3000. Metabolites were detected by ^{1}H-NMR. Error bars indicate standard deviation over three independent sample sets.

3.2.3 The *phrpL::luxCDABE* luminescent construct is a suitable reporter proxy for *P. syringae* virulence gene expression

Virulence gene expression has been shown to be induced in Pst DC3000 upon exposure to extracted tomato leaf apoplast [71]. One of the aims of this study was to assess the impact of different apoplastic metabolites on the expression of virulence genes in Pst DC3000 to determine if specific metabolites were responsible for this change in gene expression. In order to assess the expression of virulence genes across a range of media and treatments, a reliable reporter construct was required.

The pBS63 plasmid (courtesy of Dr. Bryan Swingle, USDA-ARS), which contains a *phrpL::luxCDABE* fusion construct, reports on the expression of the promoter region of the *hrpL* gene. *hrpL* encodes an alternative sigma factor which regulates many of the effector proteins and structural components of the T3SS, and is a key determinant of virulence in Pst DC3000 and other *P. syringae* pathovars [54]. The pBS63 plasmid was extracted from *E. coli* and electroporated into Pst DC3000 cells (as per Section 2.7), which were then selected for plasmid acquisition using kanamycin. Cells containing pBS63 luminesced when the *hrpL* promoter was induced and the amount of light produced was assessed by a plate reader. Luminescence was therefore expected to reflect the expression of the *hrpL* gene.

An assessment of different treatments on the expression of pBS63 (*hrpL*) was undertaken to identify conditions which would induce different levels of *hrpL* expression and to determine the sensitivity of the pBS63 plasmid. Historically, *hrp*-inducing minimal medium (HIM) has been used to stimulate very high levels of virulence gene expression [79]. Simple modifications of the, typically fructose-based, HIM assay were found to cause very different virulence gene expression profiles (Figure 3.6B). Fructose has been known for a long time to upregulate the expression of virulence genes [79]. The replacement of fructose with glucose in HIM caused a large decrease in the luminescence of Pst DC3000 (pBS63) and changing the pH of the medium from neutral to the pH encountered in the host plant (pH 5.5) increased expression in both glucose and fructose treatments (Figure 3.6B). This effect was also seen with the same modifications to M9 medium (Figure 3.6B). The more con-

sistent and higher levels of growth achieved in the M9-based assay (Figure 3.6A) led to these treatments being used throughout this study.

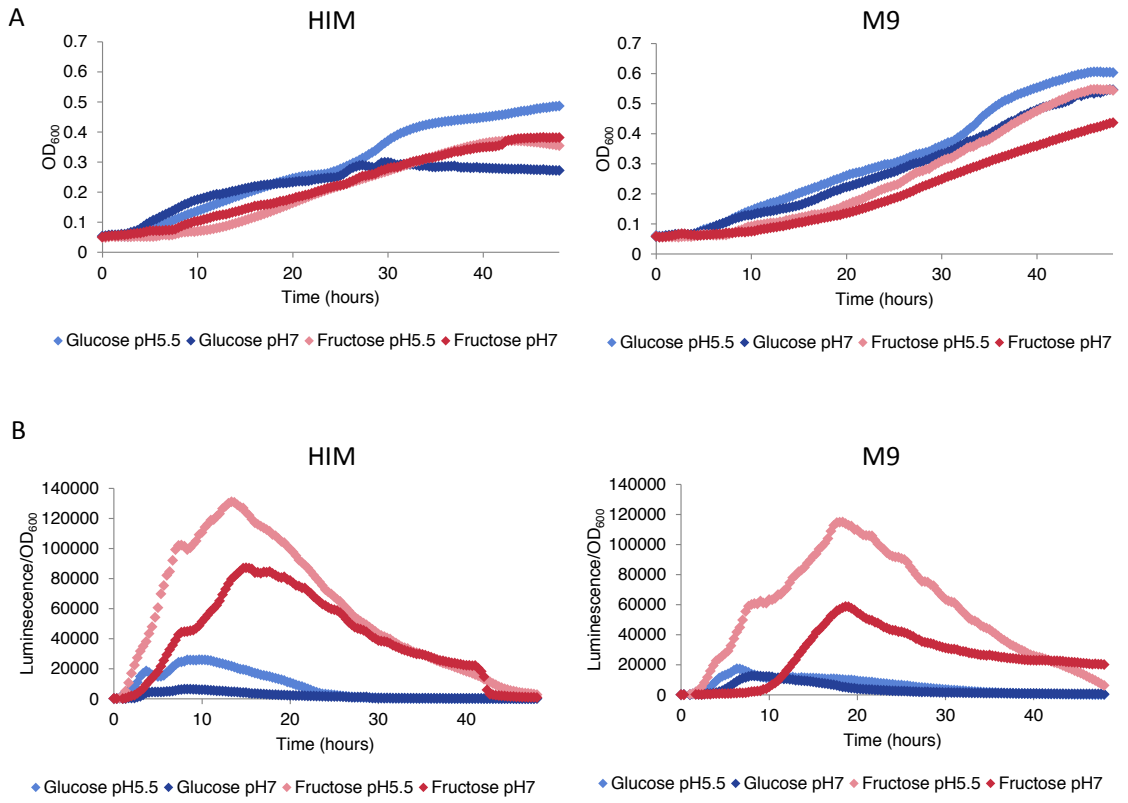

Figure 3.6: Pst DC3000 (pBS63) expresses *hrpL* to a higher level in fructose minimal media than glucose minimal media, and this induction of expression is enhanced by low pH. Glucose and fructose-based *hrp*-inducing minimal medium (HIM) and M9 minimal medium, at two pHs, pH 7 and pH 5.5, were used to investigate the effect of carbon source and pH on virulence gene expression in Pst DC3000 (pBS63). (A) Growth of Pst DC3000 (pBS63) under the different conditions. (B) Luminescence of Pst DC3000 (pBS63) cells was divided by optical density readings to give an expression per cell measure of virulence gene induction over time.

qRT-PCR was then used to determine if pBS63 luminescence reflected the expression of these genes in the absence of the reporter plasmids, and if their expression profiles could be used confidently as a proxy for the whole virulence gene cassette of Pst DC3000. The expression of *hrpL* and *hrcJ*, a structural component of the T3SS, along with genes encoding effector proteins,*avrPtoB* and *avrE*, was monitored by

qRT-PCR in the M9 conditions used previously.

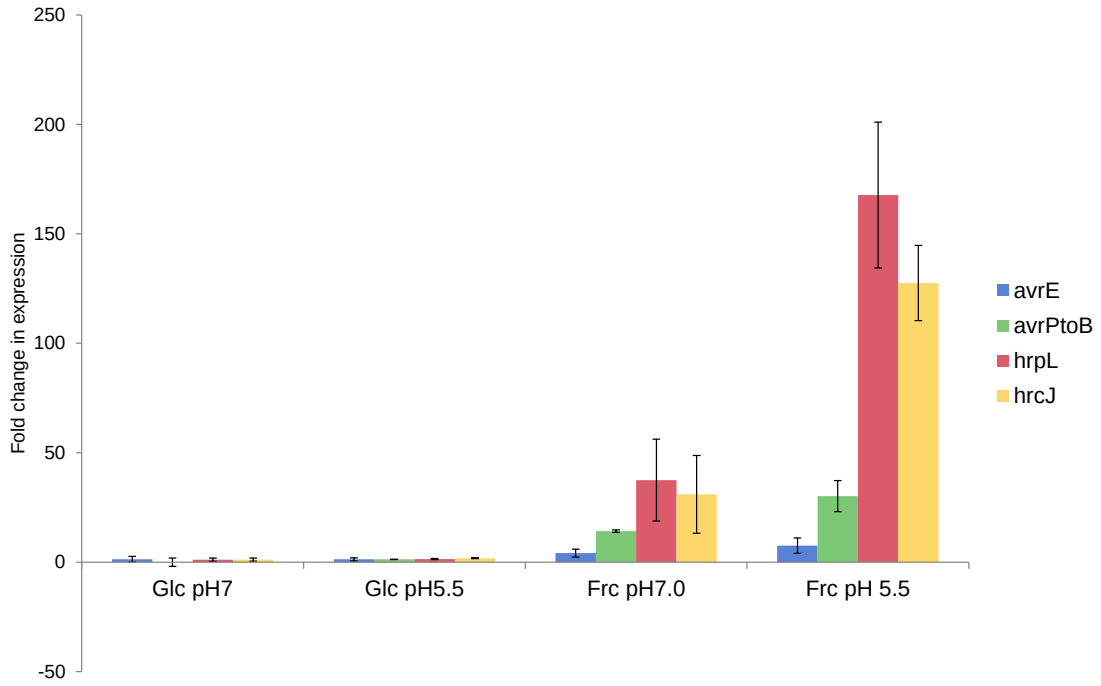

Figure 3.7: qRT-PCR analysis of *avrE*, *avrPtoB*, *hrpL* and *hrcJ* in Pst DC3000 confirms that fructose minimal media at pH 5.5 causes high levels of virulence gene expression. The fold change in expression of two T3SS genes, *hrpL* and *hrcJ*, and two T3 effector genes, *avrE* and *avrPtoB*, relative to treatment in M9-glucose pH 7, is shown in response to M9-glucose pH 5.5, M9-fructose pH 7 and M9-fructose pH 5.5. Samples were taken after 16 hours of incubation in the treatment conditions. The error bars represent standard deviation from three independent replicates.

The highest level of expression of all four target genes was in M9-fructose at pH 5.5, and the lowest in M9-glucose at pH 7, with the pattern of expression of the four genes mirroring each other across the different treatments (Figure 3.7). The data from the qRT-PCR experiment shows the same expression profiles as those seen in the pBS63-plasmid assays. There are, however, differences in the magnitude of these responses, with the highest expression observed in *hrpL*, closely followed by *hrcJ*. The expression of genes encoding the effector proteins AvrE and AvrPtoB show a much lower level of expression across the four treatments, though these genes

still showed significant levels of upregulation in the fructose treatments, which was enhanced by low pH. The use of the pBS63 reporter plasmid is therefore a valid approach for analysing the virulence gene expression responses of Pst DC3000 to different apoplastic metabolites.

3.2.4 Biolog GN2 MicroPlates can be used to identify metabolites which induce or repress virulence gene expression

Carbon-assimilation profiling can be easily and quickly performed using Biolog GN2 MicroPlates, which contain 95 different carbon sources. Metabolism is detected by the reduction of tetrazolium which is triggered by the products of cellular respiration, and which produces a purple colour that can be measured spectrophotometrically. In order to profile the expression of virulence genes, Pst DC3000 cells containing the pBS63 plasmid were used, and expression was monitored for 36 hours. Pst DC3000 was tested in Biolog GN2 MicroPlates with inoculating fluid at pH 7 and pH 5.5. Two pH values were chosen to determine if virulence gene expression with different metabolites changed under the more acidic conditions found in the host apoplast. Pst DC3000 displays significant growth on 25 out of the 95 carbon sources present in the GN2 plate. Figure 3.8A shows the metabolic activity of Pst DC3000 on the 25 different carbon sources and Figure 3.8B shows the expression of virulence genes in response to metabolites on which Pst DC3000 was able to grow. Metabolites which are known to be present in the tomato leaf apoplast are highlighted. This large-

scale profiling highlighted not only carbon sources which were readily metabolised by Pst DC3000 but also those which produced pronounced changes in virulence gene expression.

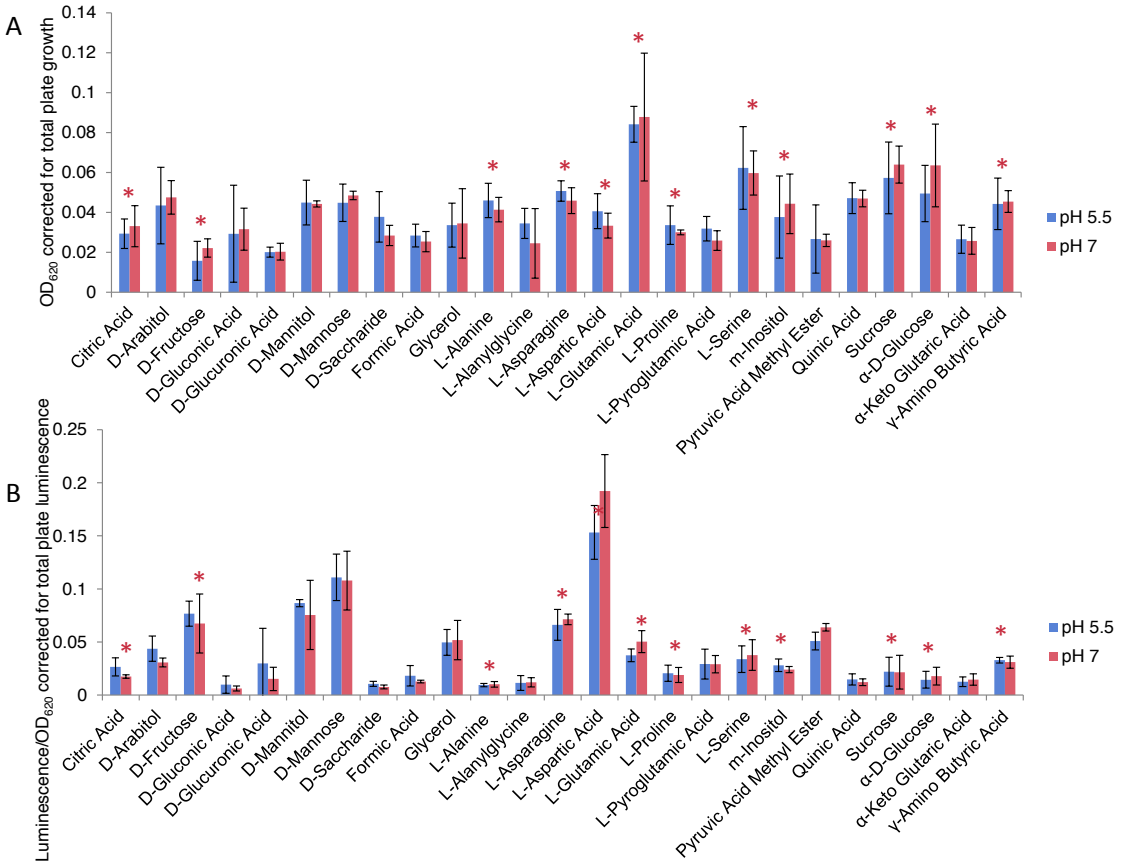

Figure 3.8: Pst DC3000 (pBS63) metabolic activity and luminescence in Biolog GN2 assay at pH 5.5 and pH 7. Pst DC3000 (pBS63) cells were inoculated into Biolog GN2 plates, which contained 95 different carbon sources. Cell were grown for 36 hours over which time the optical density and luminescence of the wells were measured. Values were integrated over the 36 hour period and values from each plate were standardised using the total plate value. Bars show averages of three independent replicates and error bars show standard deviation. Asterisks (*) highlight metabolites which have been identified in tomato apoplast extract. A full list of the 95 carbon substrates present in Biolog GN2 MicroPlates is shown in Appendix A.1

The Pst DC3000 metabolic profiles are highly similar to those obtained by Rico *et al* (2008) [71], though fewer metabolites produced strong assimilation results in this study. This is most likely due to the transposition of Biolog GN2 plate contents

to black 96-well plates. Black 96-well plates (with clear bottoms) were required to accurately measure light emittance in each well (without light contamination from neighboring wells). The process of transferring substrates almost certainly would have caused a reduction in the amount of substrate available to Pst DC3000 cells, relative to normal GN2 plates, and compounds which are not readily water-soluble would have suffered a further reduction in the amount transferred to the black plates. The highest levels of metabolic activity were observed on glutamate, serine, sucrose and glucose, all of which are present in the tomato leaf apoplast. Significant metabolic activity was also detected in the presence of mannitol, mannose, arabitol, GABA, alanine, asparagine and quinic acid, of which, GABA, alanine and asaparagine are present in high levels in extracted host apoplast. pH had no discernible significant effect on the relative assimilation profiles.

The Biolog GN2 plates reveal differential T3SS expression across the range of 25 substrates. The highest levels of expression were found in the presence of fructose, mannitol, mannose, asparagine, aspartate and pyruvic acid methyl ester, of which fructose, asparagine and aspartate are found in high abundances in the apoplast, however, the other inducing substrates have not been detected in tomato apoplast extracts. No correlation was found between substrate abundance in the analysed apoplast extracts and the degree to which it induced or repressed T3SS expression. Notably, citrate, alanine, glutamate, serine, myo-inositol, sucrose, glucose and GABA all show much lower levels of virulence gene expression in this assay. pH values did not change the relative expression in response to any particular substrate.

3.2.5 Targeted metabolite analysis: verification of Biolog results and testing of all known apoplastic metabolites

The Biolog GN2 MicroPlate luminescence assay relied on the ability of cells to metabolise a substrate in order to assess its level of virulence gene expression: substrates where no metabolic activity was observed also displayed no luminescence. The apoplast depletion assay (Section 3.2.2) demonstrated that Pst DC3000 does not deplete all of the metabolites from extracted apoplastic fluid and it is known that Pst DC3000 does not have the capability to metabolise some components of the apoplast such as valine and methionine [71, 86]. However, as these metabolites are present in the tomato apoplast they may have an effect on virulence gene expression and thus an assay was designed to be able to test the changes in virulence gene expression caused by all of the metabolites known to be present in the apoplast, even those that Pst DC3000 cannot metabolise. Fructose was used as a starting point in this set of experiments as, like the plant environment, it causes high levels of virulence gene expression [79]. M9-fructose supplemented with 5mM of different apoplastic components allowed Pst DC3000 cells to grow, and for the relative suppression or induction of virulence genes caused by the metabolite to be ascertained. Where the addition of 5mM of a substrate changed the pH of the M9-fructose, this was re-adjusted back to pH 7.

Pst DC3000 (pBS63) cells were grown in the various different treatments for 36

hours and both growth and luminescence were monitored. Luminescence was corrected for optical density and hrp expression curves were then integrated for the first six hours of the experiment and for the full 36 hours. These two time-points were chosen in order to understand initial changes in virulence gene expression (*P. syringae* strains are known to strongly upregulate their virulence genes in the first few hours after entry into the host apoplast [81]) and also expression over a longer period of time (Figure 3.9).

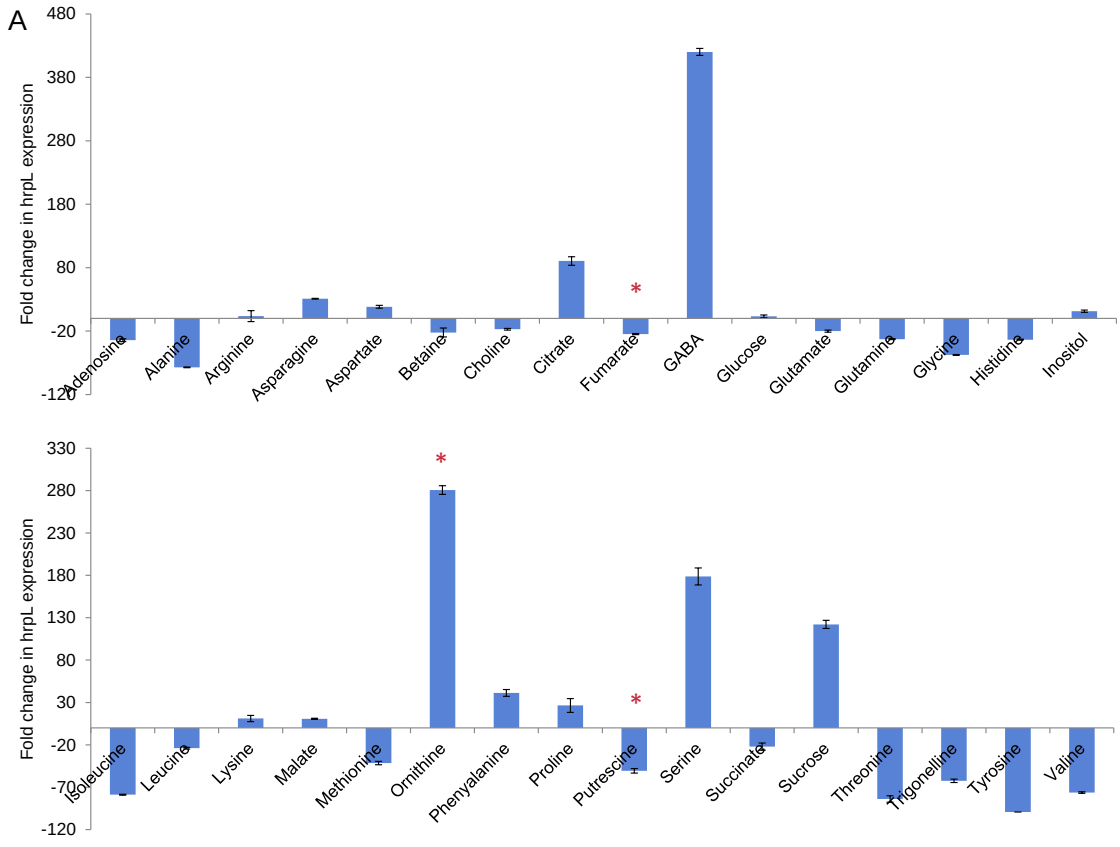

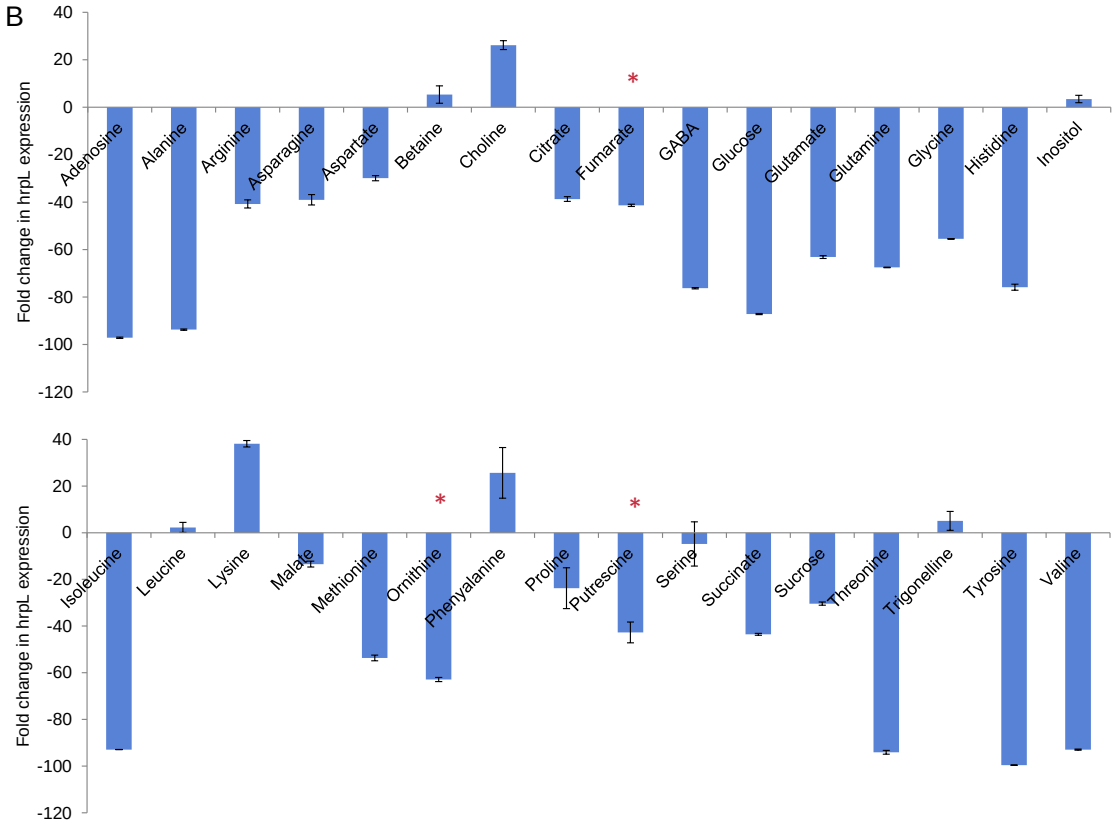

Figure 3.9: *hrpL* expression in Pst DC3000 (pBS63) differs in response metabolites present in the host apoplast. Cells were incubated in *hrp*-inducing M9-fructose media with different apoplastic components added at 5mM, as well as two GABA-related metabolites, ornithine and putrescine. Luminescence values were corrected for optical density and integrated over 6 hours (A) and 36 hours (B). The percentage change relative to *hrpL* expression in M9-fructose was then calculated for each metabolite at each time point. Asterisks (*) highlight metabolites which have not been identified in tomato leaf apoplast in this study. Error bars represent standard deviation.

After the first six hours of incubation, many of the apoplastic substrates caused repression of T3SS genes relative to the fructose-only condition. Highly repressive substrates include alanine, isoleucine, threonine, trigonelline, tyrosine and valine, and these substrates continued to cause repression of T3SS genes over the 36-hour experimental period. Notably, after six hours, GABA had caused some of the highest levels of induction, and citrate, serine and sucrose were also found to increase virulence gene expression relative to the control treatment. In all four cases this is

due to an earlier, though lower, peak of expression than that observed with fructose.

Over the 36 hour period, most of the substrates cause a net reduction of virulence gene expression relative to M9-fructose. Exceptions to this observation are choline, lysine and phenylalanine. Betaine, myo-inositol, leucine, serine and trigonelline do not seem to have any significant effect on the expression of *hrp* genes, as expression profiles in the presence of these substrates remain very similar to the M9-fructose treatment.

Aspartate was the most highly inducing substrate tested in the Biolog GN2 assay, well above the induction observed with fructose. Under pH-controlled conditions, aspartate appears to induce T3SS genes slightly above that observed with M9-fructose over the first six hours, but over 36 hours causes around a 30 % reduction in expression. It is likely that the acidic effect of aspartate accounts for the very high levels of expression displayed in the Biolog assay.

Several key metabolites were selected for experimental verification, and this was done in two ways. First, an additional reporter plasmid was used to check that all T3SS virulence genes showed similar expression with different metabolites, and second, qRT-PCR was employed to monitor the expression of *hrpL* and *avrE* with different metabolites. GABA was selected as it is the most abundance amino acid present in the host apoplast, aspartate as it is one of the least repressive amino acids (and the substrate which caused the highest levels of induction in the Biolog GN2

assay) and threonine, as it was shown to be highly repressive.

The plasmids pBS44 and pBS45 (also courtesy of Bryan Swingle), which contained the constructs empty::*luxCDABE* and *pavrPtoB::luxCDABE* respectively, were used to investigate the expression of T3SS genes with aspartate, GABA and threonine. AvrPtoB is one of the effector proteins that is injected into host cells by Pst DC3000 during infection. Pst DC3000 containing pBS44 (empty) was included to determine if the plasmid produces luminescence in the absence of a native promoter. The pBS44 (empty) was expected to produce no luminescence and pBS45 (*avrPtoB*) was expected to have a very similar expression profile to pBS63 (*hrpL*). From Figure 3.10 it can be seen that the expression of *hrpL* and *avrPtoB* showed similar levels of expression in most of the conditions tested, and that luminescence is only observed when the lux cassette is placed downstream of a functional promoter-driven construct. The pH of media used in this assay was not adjusted for the presence of acidic substrates such as aspartate (as was done for the experiment detailed in Figure 3.9), and as such, the expression of fructose + 5mM aspartate is higher than expression with just fructose. The one condition where gene expression did substantially vary was in the presence of GABA. GABA stimulates much higher levels of expression in Pst DC3000 (pBS45) (p*avrPtoB*) than in Pst DC3000 (pBS63) (p*hrpL*).

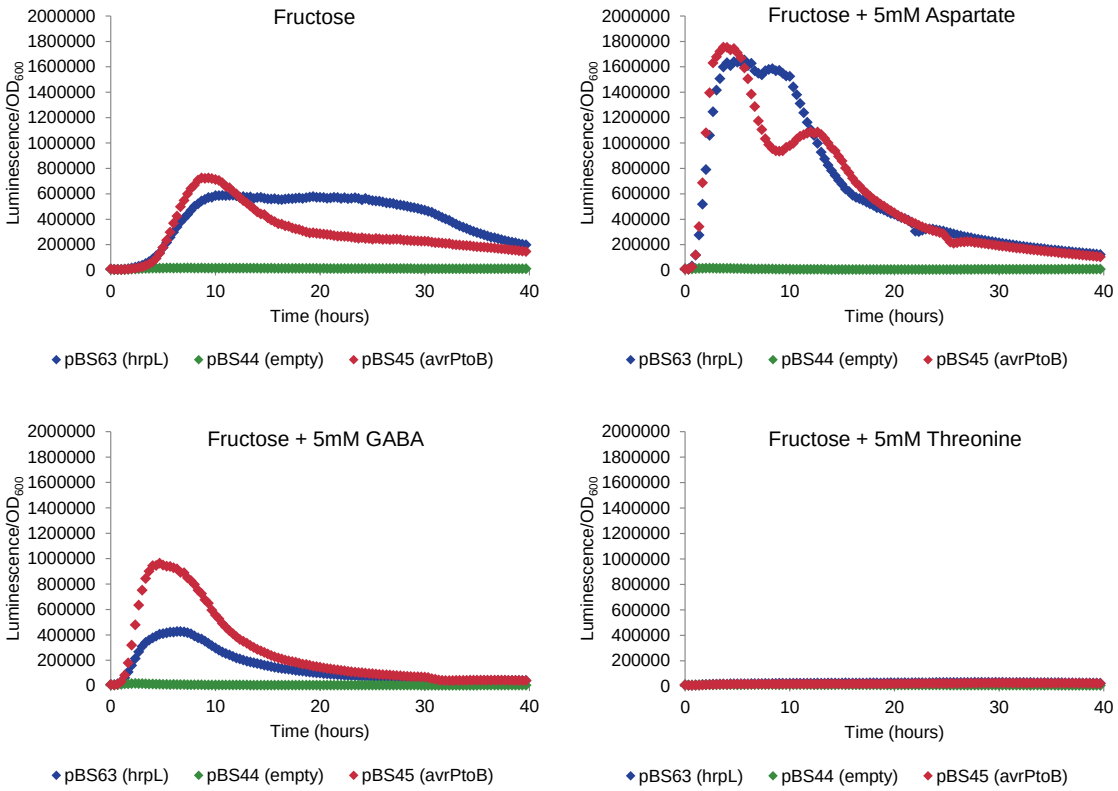

Figure 3.10: *avrPtoB* and *hrpL* show similar expression profiles in Pst DC3000 in response to different amino acids. Pst DC3000 containing three different luminescent reporter plasmids, pBS63 (phrpL::luxCDABE), pBS44 (empty::luxCDABE) and pBS45 (pavrPtoB::luxCDABE) were grown in M9-fructose and M9-fructose containing 5 mM GABA, aspartate or threonine. The graphs display the average luminescence divided by optical density from at least four technical replicates. The experiment was repeated twice, with the same patterns of expression recorded each time.

qRT-PCR analysis of *avrE* and *hrpL* expression confirmed the trends observed with the pBS63 plasmid as well. Figure 3.11 shows the fold-change in expression of these genes, relative to expression in M9-fructose, in the presence of 5mM aspartate, GABA and threonine. Again, the effector-encoding gene, *avrE*, is expressed to a lower level than *hrpL*, and this is particularly noticeable in the threonine treatment.

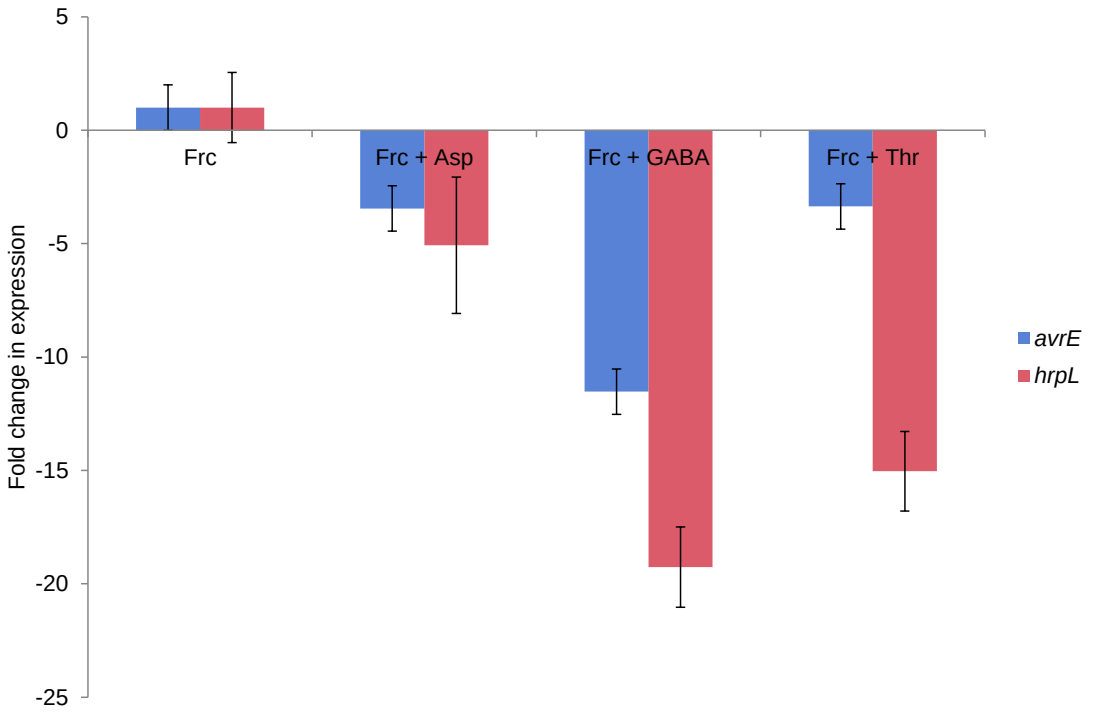

Figure 3.11: qRT-PCR of *avrE* and *hrpL* expression in Pst DC3000 demonstrates differential responses to three amino acids. M9-fructose media was used as a control, as it induces high levels of virulence gene expression in Pst DC3000, and 5 mM of different amino acids (aspartate, GABA and threonine) were added to determine how they altered virulence gene expression. Fold change in expression was normalised to the M9-fructose treatment which was given a value of 1. Samples were taken after 4-6 hours of incubation in the treatment conditions. Error bars represent standard deviation from three independent samples.

3.2.6 Soluble metabolite profiles change under virulence gene inducing conditions

Whilst it has been long established that fructose causes high levels of virulence gene expression [79], a specific reason for this has never been established. *hrp* genes are known to be regulated by RpoN, a sigma factor involved in the regulation of nitrogen assimilation, and HrpRS, which is related to the nitrogen control proteins NtrB-NtrC [40]. It was therefore hypothesised that internal amino acid proportions, which are

frequently implicated in carbon:nitrogen sensing [154, 157], may be responsible for the changes observed in virulence gene expression in the different fructose/glucose treatments. In order to establish if this was indeed the case, soluble amino acids were extracted and quantified using GC-MS as well as TCA cycle intermediates, which were quantified using LC-MS. Whilst only a subset of amino acids and organic acids could be detected from the extracts, the profiles show some key differences between the treatments (Figure 3.12). The profiles demonstrate that glutamate is the most abundant free amino acid within Pst DC3000 cells under minimal media conditions. Though pH conditions have a significant impact on virulence gene expression, they do not appear to significantly alter the metabolite profiles, however, several differences do exist between the glucose and fructose conditions. Most notably, in the GC-MS amino acid profiling, glutamate pools are higher in cells which have been grown in fructose, whilst alanine and valine are more abundant in cells grown with glucose. In the LC-MS profiles, glutamate is also the most abundant metabolite detected, across all four treatments. Again, large-scale differences can be observed between glucose and fructose-fed cells. Glutamate is proportionally lower in glucose-fed cells, whereas metabolites such as succinate, malate and 2-hydroxyglutarate are higher. In the LC-MS analysis, pH appears to have some degree of effect on the intracellular metabolite pools of glucose, but not fructose, fed cells, particularly in the levels of succinate, aspartate and 2-hydroxyglutarate.

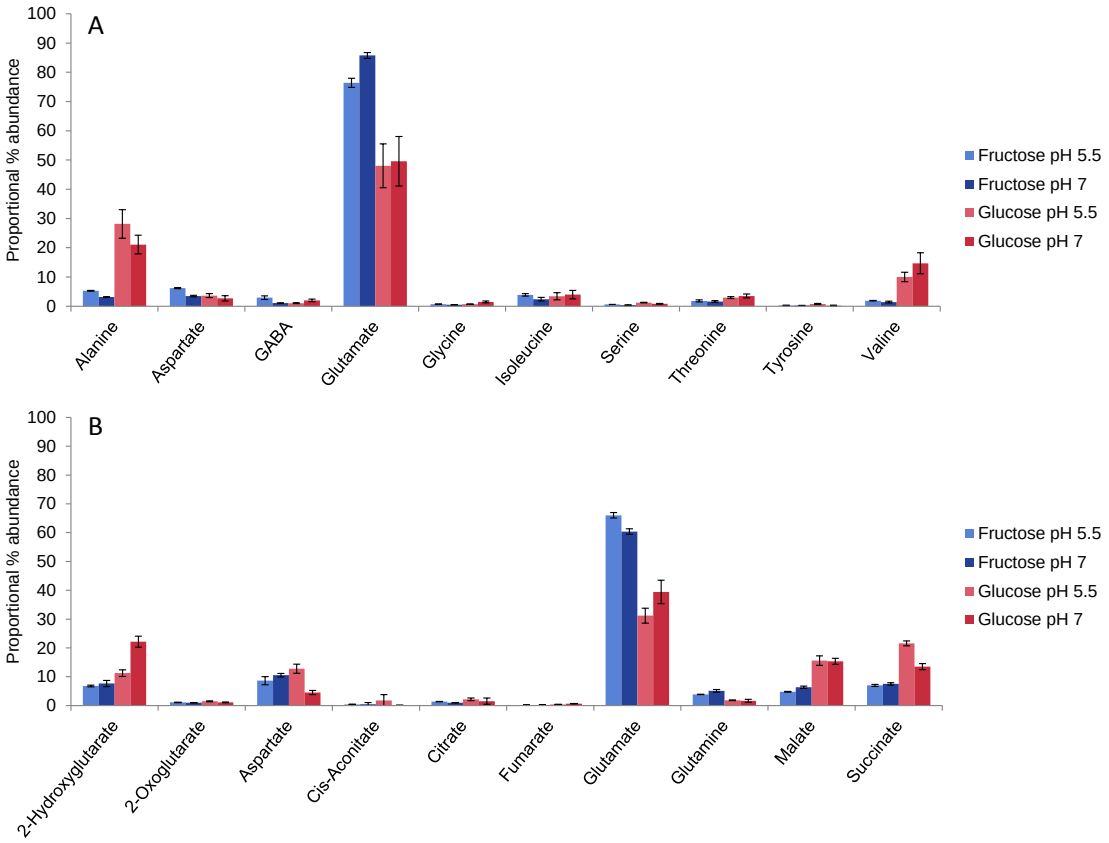

Figure 3.12: Soluble intracellular metabolite abundances in Pst DC3000 change under virulence gene inducing and non-inducing conditions. (A) Amino acid proportional abundances detected by GC-MS at peak of virulence gene expression (16 hours). (B) TCA cycle and associated metabolite proportional abundances detected by LC-MS at peak of virulence gene expression (16 hours). Metabolites are shown as the proportional percentage abundance of all the metabolites shown on each graph. Error bars represent standard deviation from three independent replicates.

3.2.7 Glutamate is the most abundant free intracellular amino acid in Pst DC3000 incubated in extracted tomato leaf apoplast

The distinct amino acid profiles observed under virulence gene inducing and non-inducing conditions were hypothesised to play a role in Pst DC3000's regulation of virulence gene expression or its perception of its environment. In order to profile

amino acid proportions in the plant environment, soluble amino acids were extracted from Pst DC3000 cells which had been incubated in extracted tomato leaf extract. Whilst not as many amino acids were detected, owing to a small cell sample size and limited apoplastic fluid, glutamate was still the most abundant amino acid, comprising up to 80 % of the total detectable amino acid pool. Alanine could not be detected and valine levels were not above levels of other amino acids (Figure 3.13).

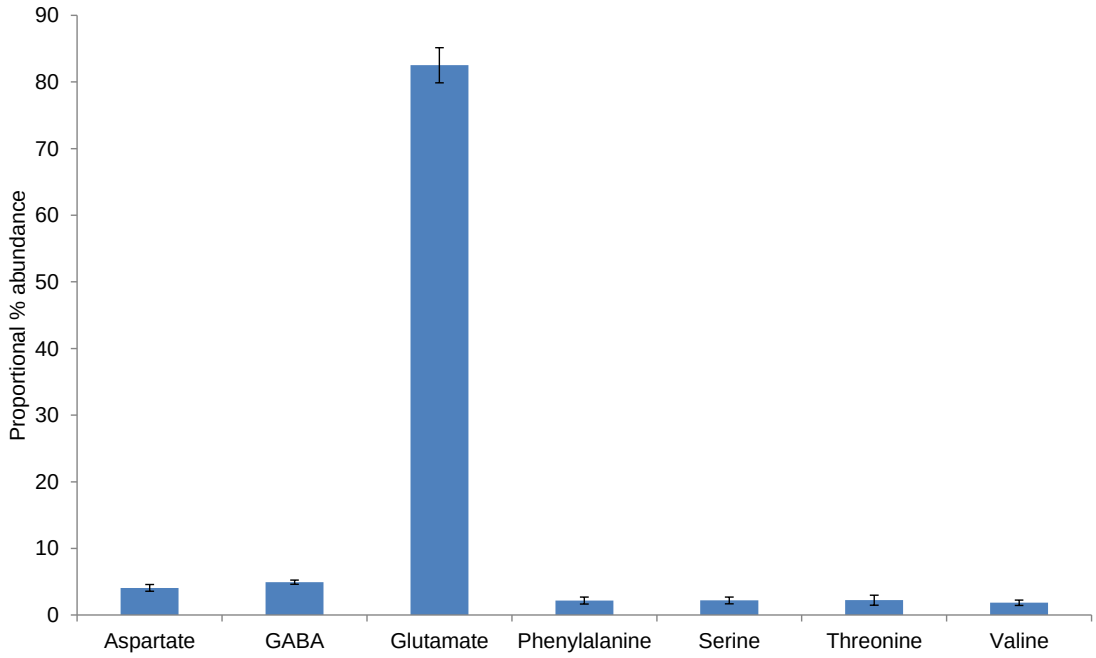

Figure 3.13: Proportional amino acid abundances in Pst DC3000 cells incubated in extracted tomato leaf apoplastic fluid. Soluble amino acids were extracted from Pst DC3000 cells that had been incubated in extracted tomato leaf apoplast for 4 hours, and analysed by GC-MS. Metabolites are shown as the proportional percentage abundance of all the metabolites shown. Error bars represent standard deviation across three independent samples.

The similarities of the amino acid profiles obtained from cells grown with fructose and those grown in apoplast extracts reinforces that these treatments provide a good *in vitro* proxy for the plant environment. It also reveals that high intracellular

glutamate may be a key factor in the induction of virulence gene expression in Pst DC3000.

3.2.8 Soluble metabolite profiles change in the presence of different amino acids

As different amino acids caused different levels of virulence gene expression in Pst DC3000 (Section 3.2.6), it was hypothesised that, as with the fructose/glucose conditions, these changes may be linked to intracellular metabolite proportions. As per Section 3.2.5, 5mM of amino acid was added to M9-fructose medium, with M9-fructose medium used as a control treatment. Aspartate, GABA, glutamate and threonine all caused different *hrp* expression profiles in Pst DC3000 when added to M9-fructose: aspartate caused little repression, GABA and glutamate both caused similar levels of repression (around 65-75 % reduction) and threonine caused a 95 % reduction over the 36 hour period. Figure 3.14 shows the different profiles obtained under the amino acid treatments and in the control treatment. In the GC-MS amino acid profiles (Figure 3.14A), there is a correlation between the proportion of glutamate present in the cells and the level of virulence gene inhibition exhibited by the Pst DC3000 cells: cells incubated with aspartate have amino acid profiles most similar to those obtained from cells which were grown in M9-fructose without any amino acids, whereas threonine, which caused the highest levels of repression in Pst DC3000 (pBS63), caused the greatest reduction in intracellular glutamate proportions. GABA, glycine and threonine show the opposite pattern to glutamate - in more repressive conditions these amino acids are proportionally greater.

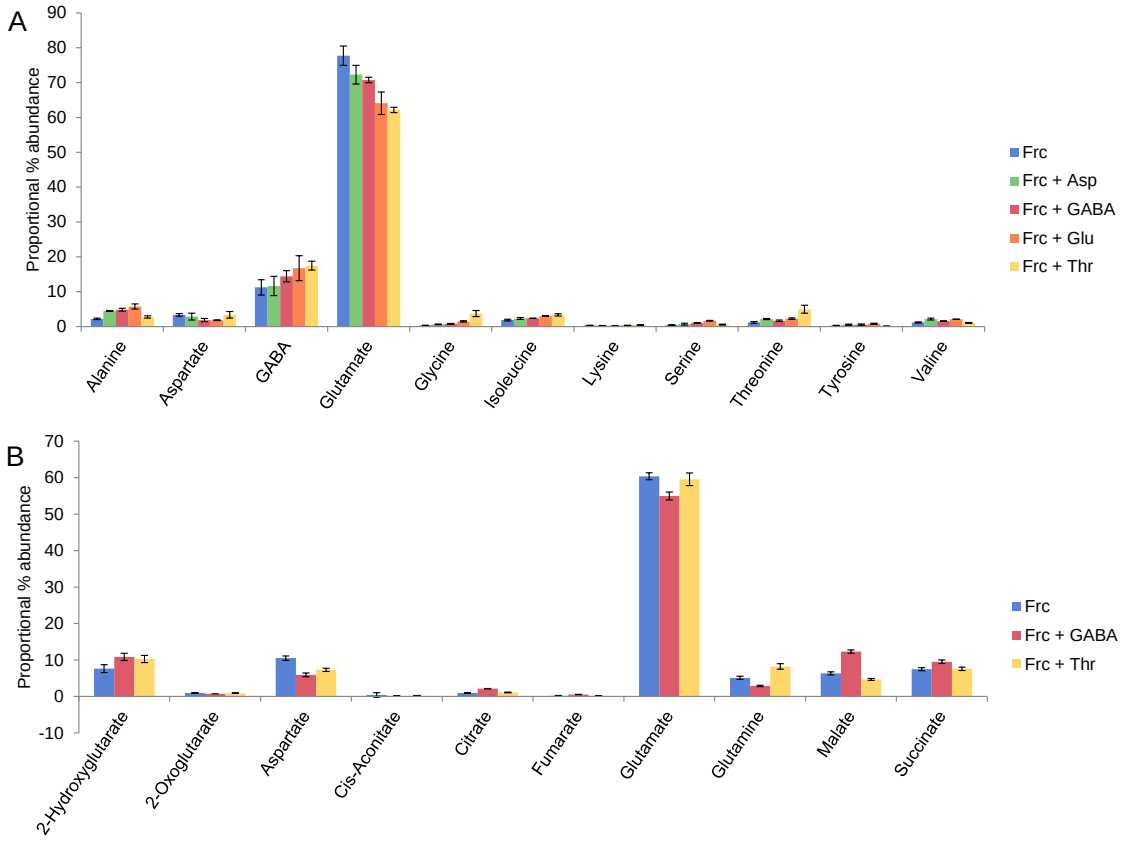

Figure 3.14: Soluble metabolite profiles for Pst DC3000 incubated with different amino acids. Pst DC3000 cells were incubated in M9-fructose (Frc) or M9-fructose with 5 mM of aspartate, GABA, glutamate or threonine, and harvested after 16 hours. (A) Soluble amino acids were extracted and analysed using GC-MS. (B) Soluble TCA cycle and associated metabolites were extracted and analysed using LC-MS. Metabolites are shown as the proportional percentage abundance of all the metabolites shown on each graph for each sample. Error bars represent standard deviation across three independent samples.

In the TCA cycle intermediates analysis by LC-MS, such a clear trend is not observed with regard to glutamate levels (Figure 3.14). GABA causes a reduction in proportional glutamate levels but threonine does not. Instead, the threonine-fed cells show very similar metabolite proportions to the fructose-fed cells. The differences between the two types of analysis may be explained by the metabolites that are being quantified and compared. For example, threonine appears to cause a notable decrease in glutamate in the GC-MS analysis as it causes a marked increase

in other amino acids, whereas in the LC-MS analysis no such differences are observed because threonine does not cause an increase of TCA cycle metabolites and thus glutamate remains proportionally high. Notably, the GABA treatment appear to show coherent results across the two experiments: GABA causes a reduction in proportional glutamate and aspartate and an increase in GABA.

3.2.9 The *phrpL::luxCDABE* pBS63 construct can be used to report on the expression of the *rsp*-encoded type III secretion system in *Pseudomonas fluorescens* SBW25

Pst DC3000 regulates its virulence genes in response to environmental stimuli, which may be due to changing internal metabolite concentrations acting as a 'virulence switch' as suggested by results in previous sections. Many species of *P. syringae* are known to show altered T3SS expression in different types of media [40, 79, 81], however little is known about whether or not non-plant-pathogenic *Pseudomonas* species that have T3SS regulate this apparatus in a similar way.

The non-pathogenic plant growth-promoting bacterium *Pseudomonas fluorescens*, whilst not possessing a set of genes which can be identified as a virulence cassette, such as the *hrp*-cluster of *Pseudomonas syringae*, does have a set of genes encoding a T3SS [158]. This T3SS is encoded by the *rsp* gene cluster. In Pfl SBW25, *rspR* has been putatively identified as the enhancer binding protein which activates

rspL, which in turn has been identified as the alternative sigma factor that drives the expression of other *rsp* genes [158]. In this way, the *rsp* genes operate similarly to the *hrp* genes of Pst DC3000, where *hrpL* acts as the alternative sigma factor and is activated by *hrpRS* [40]. The *rsp* cluster has been shown to be induced in the plant rhizosphere and in *hrp*-inducing minimal medium (though to a much lesser extent than Pst DC3000's expression of *hrp* genes). In order to determine if pBS63 could report on the expression of the *rsp* genes, pBS63 was electroporated into wild type *Pseudomonas fluorescens* SBW25 (Pfl SBW25) and Pfl SBW25 with a pRspR plasmid (an *RspR* over-producing strain). Luminescence by these strains were monitored by a photon-counting camera and is shown in Figure 3.15. The overexpression of *rspR* clearly caused an increase in luminescence on M9-fructose agar, relative to wild type Pfl SBW25. Thus, it was concluded that the pBS63 *phrpL::luxCDABE* construct was responding to RspR. The Pfl SBW25 pBS63 construct thus allowed T3SS expression to be monitored in a comparable way to Pst DC3000, and in response to different environmental stimuli.

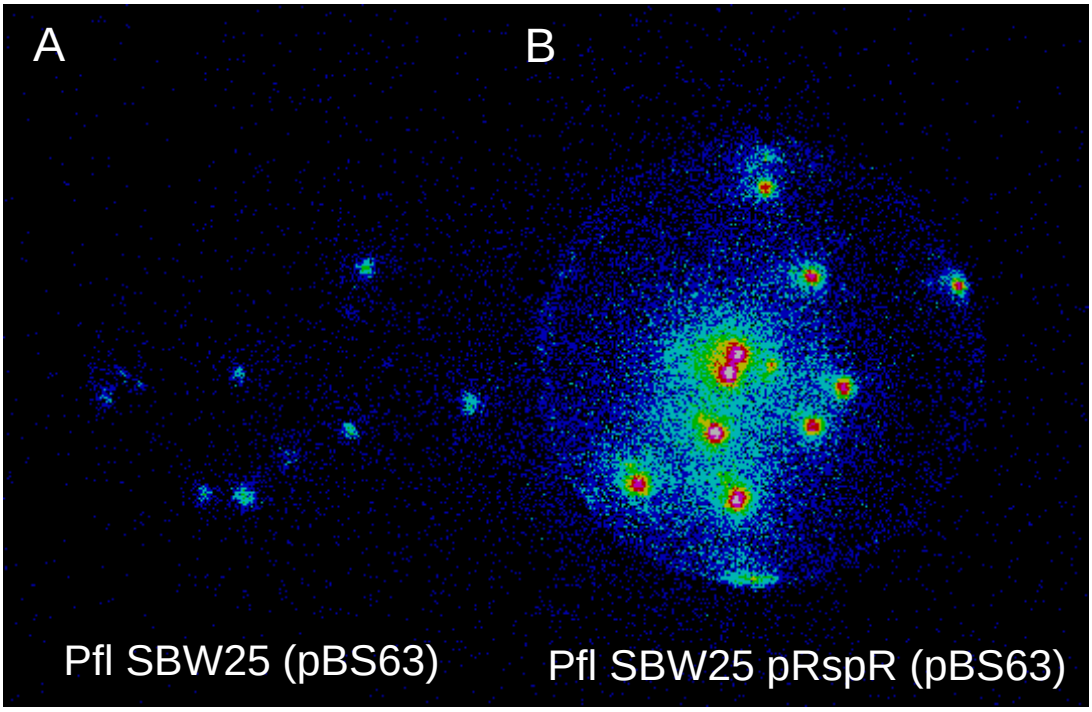

Figure 3.15: Photon camera image of Pfl SBW25 (pBS63) (A) and Pfl SBW25 pRspR (pBS63) (B). The pBS63 (*phrpL::luxCDABE*) plasmid was electroporated into wild type Pfl SBW25 and a mutant strain that overexpresses *rspR*. RspR is known to activate *rspL*, which is likely to play a similar role in the Pfl SBW25 T3SS to *hrpL*. Cells were grown on selective agar plates for 24 hours. The image was captured by a photon camera after a two minute exposure.

3.2.10 The pattern of expression of *rsp* genes in Pfl SBW25 across a range of carbon sources is different to *hrp* gene expression in Pst DC3000

The modified-M9 medium growth conditions used in Section 3.2.3 produced differential levels of *hrp* gene expression in Pst DC3000. Pfl SBW25 was also tested in the same treatments to establish if the T3SS-encoding genes of the two species responded similarly to environmental stimulants. Figure 3.16 shows the expression of the pBS63 plasmid in Pfl SBW25. Interestingly, Pfl SBW25 showed comparable

patterns of expression with the two sugars (an earlier peak with glucose and a later, longer peak, with fructose), but the magnitude of these responses in Pfl SBW25 was very similar, unlike the much higher *hrp* expression demonstrated by Pst DC3000 with fructose. In addition, Pfl SBW25 did not show an appreciable difference in *rsp* expression in response to pH with glucose and fructose, whereas the difference in *hrp* expression under different pH conditions in Pst DC3000 was very noticeable (Figure 3.16).

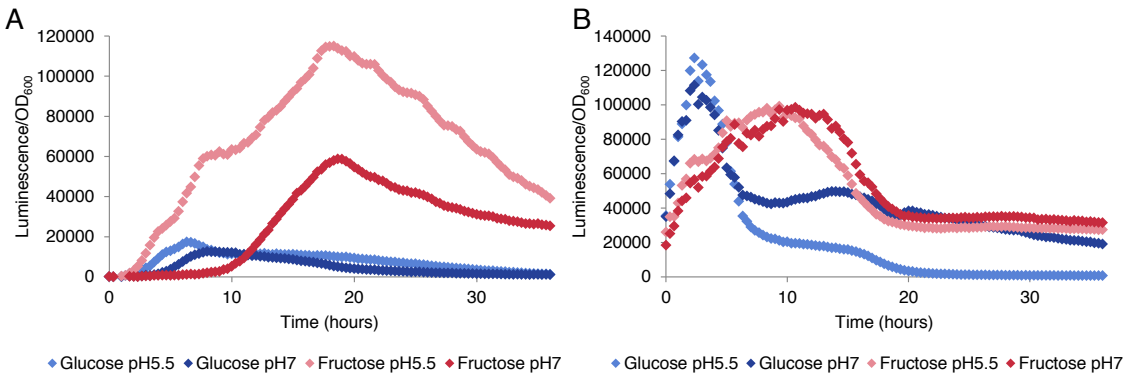

Figure 3.16: Expression of *rspL* in Pfl SBW25 (pBS63) in comparison with Pst DC3000 (pBS63) under *hrp* inducing and non-inducing conditions. Luminesence of the pBS63 (*phrpL::luxCDABE*) plasmid in Pst DC3000 (A) and Pfl SBW25 (B) was measured over 36 hours in response to M9-fructose and M9-glucose at pH 5.5 and pH 7. Luminescence values were corrected for growth by dividing by OD_{600} measurements. The experiment was repeated twice with the same patterns of expression detected each time.

Pfl SBW25 pBS63 was also tested for nutrient assimilation and *rsp* gene expression with the Biolog GN2 MicroPlates at both pH 5.5 and pH 7, as done previously with Pst DC3000 (Section 3.2.4). As noted by Rico *et al* (2008) [71], Pfl SBW25 is able to metabolise a much broader set of substrates in the Biolog GN2 plates than Pst DC3000 (Figure 3.17A), and this is consistent with the reduction in Pst DC3000's genome of genes annotated for nutrient uptake [30] and metabolism [86]. Notably, Pfl

SBW25 metabolised sorbitol, trehalose, adonitol, hydroxy-L-proline and p-hydroxy phenylacetic acid, which Pst DC3000 is unable to metabolise. Interestingly, Pfl SBW25 was unable to assimilate sucrose, which is a substrate that Pst DC3000 can metabolise.

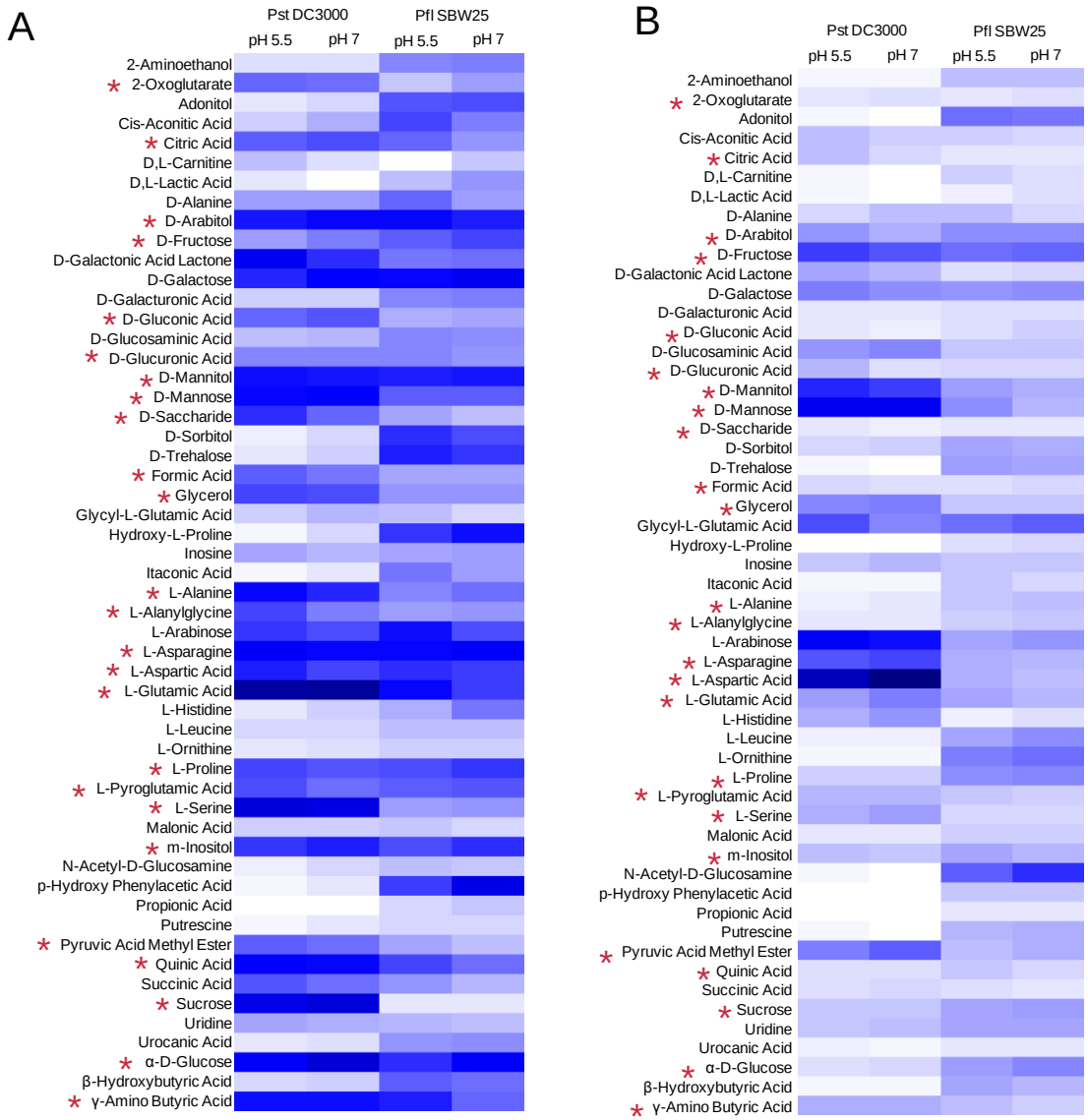

Figure 3.17: Biolog GN2 substrate assimilation and luminescence heatmaps of Pst DC3000 (pBS63) and Pfl SBW25 (pBS63) at pH 5.5 and pH 7. Pst DC3000. Biolog GN2 carbon sources which could be metabolised by either strain were included. Metabolic activity (A) and luminescence (B) measurements were integrated over the 36 hour growth period and plate averages were used to normalise experiments. The colours represent from no metabolic activity or luminescence detected (white) to the highest level of metabolic activity or luminescence recorded (dark blue). Asterisks denote the substrates Pst DC3000 was able to metabolise. A full list of the 95 carbon substrates present in Biolog GN2 MicroPlates is shown in Appendix A.1.

Pst DC3000 (pBS63) showed particularly strong induction of virulence gene expression in the presence of fructose, mannitol, mannose, aspartate and arabinose,

however, of these, only fructose caused high levels of induction in Pfl SBW25. Expression of pBS63 in Pfl SBW25 was induced by a wider range of substrates, consistent with its ability to metabolise a wider range of substrates, and in general showed lower levels of induction. Specifically, in addition to fructose, arabitol, adonitol, N-acetyl-D-glucosamine and glycyl-L-glutamic acid caused the highest levels of *rsp* expression. Pfl SBW25 therefore appears to share fructose as an inducer of T3SS gene expression, but otherwise regulates its T3SS genes differently to Pst DC3000 in response to a variety of carbon substrates.

3.2.11 Amino acid pool analysis in Pfl SBW25 shows highly similar proportions to Pst DC3000

Pfl SBW25 exhibited different T3SS gene expression in comparison with Pst DC3000 in response to many metabolites tested in Section 3.2.10, though somewhat similar patterns to Pst DC3000 in response glucose and fructose-based media (Section 3.2.9). Soluble amino acid profiling was conducted to determine if this too was similar between the two strains, as similar profiles may indicate a conserved mechanism for *Pseudomonas* T3SS expression. The analysis was performed as previously in conditions which showed differential *rsp* gene expression in Pfl SBW25. The same end-point for cell harvesting was used as for Pst DC3000: when the cells reached an OD_{600} of 0.35-0.45 in the middle of the exponential part of their growth phase. Figure 3.18 displays the amino acid profiles for Pfl SBW25.

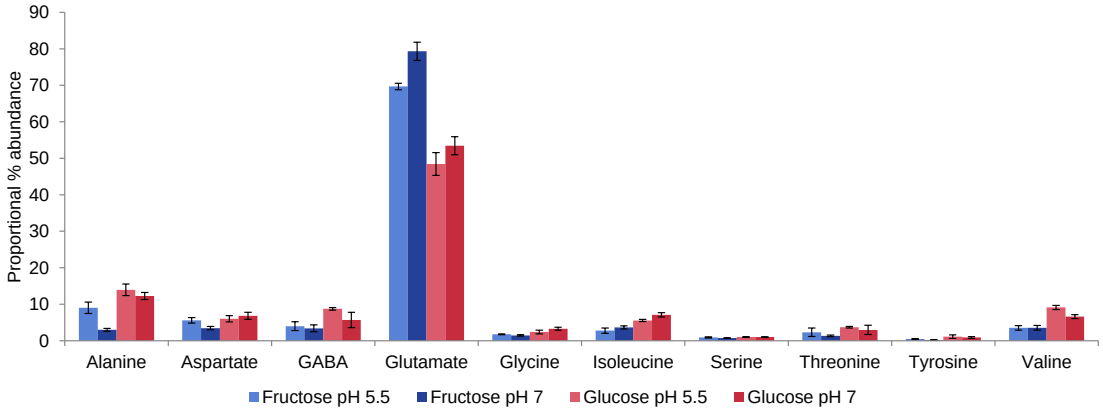

Figure 3.18: Soluble amino acid proportional abundances are different in Pfl SBW25 cells incubated in M9-fructose and M9-glucose at pH 5.5 and pH 7. Soluble (non-protein) amino acids were extracted after 16 hours of cell incubation and analysed using GC-MS. Abundances were divided by total cell amino acid abundance to give proportional values. Error bars represent standard deviation from three independent replicates.

Interestingly, the differences observed in Pst DC3000 internal metabolite abundances between the glucose and fructose treatments were also detected in Pfl SBW25: glutamate was the most abundant amino acid present in all conditions but made up a larger proportion of the total amino acid pool in M9-fructose than in M9-glucose. Relative increases in alanine and valine in M9-glucose were also detected in Pfl SBW25, however, these difference were not as marked as in Pst DC3000. Again, pH changes only caused very minor differences in metabolite profiles.

Pfl SBW25 and Pst DC3000 therefore appear to share some similarities in the ways T3SS genes are regulated in response to glucose and fructose and it is likely that sensing of internal amino acid proportions may have a bearing on the degree to which these genes are expressed.

3.3 Discussion

This study has provided detailed profiling of the tomato leaf apoplastic fluid and shown how Pst DC3000 cells exhibit preferences for the uptake of certain apoplastic components. In addition, Pst DC3000 cells were shown to change their expression of virulence genes in response to different metabolites which were detected in apoplast extracts. Notably, in synthetic media, the presence of aspartate and asparagine induced virulence gene expression whilst other amino acids such as GABA, glutamate and threonine had a repressive effect. Intracellular metabolite abundances were shown to alter in response to media which induced and repressed virulence gene expression, leading to the hypothesis that internal metabolite sensing may influence virulence gene expression. In addition, a non-pathogenic *Pseudomonas*, Pfl SBW25, was shown to undergo similar metabolic changes in response to altered environmental conditions.

3.3.1 Pst DC3000 exhibits preferences in nutrient utilisation of extracted host apoplastic fluid

The apoplast is the compartment in which Pst DC3000 profilerates and, in successful interactions, subdues the host's defence responses. Studying its composition and how Pst DC3000 responds to different elements of this compartment is therefore crucial to understanding the context in which virulence occurs. By using non-targeted ^{1}H-NMR analysis, the range of metabolites known to be present in the apoplast has

been expanded to include choline, glycine-betaine, myo-inositol, adenosine and TCA cycle intermediates, in addition to sugars such as sucrose and fructose and amino acids, which had already been detected in previous studies [71, 137]. GABA was again shown to be the most abundant amino acid present in tomato leaf apoplastic fluid.

After 24 hours of incubation in apoplastic extract, Pst DC3000 cells had assimilated over 50 % of many of the metabolites present. Pst DC3000 notably showed distinct preferences in which substrates it depleted from extracted host apoplastic fluid - specifically aspartate, asparagine, glutamate and glutamine were depleted first. The substrates which were initially depleted most rapidly from the apoplast were not necessarily those which produced the highest levels of growth *in vitro*. In the Biolog GN2 assay (Section 3.2.4), the highest levels of growth were achieved in the presence of glutamate, serine, sucrose and glucose. It therefore appears that Pst DC3000 selectively assimilates nutrient sources from the apoplast for purposes other than rapid profileration, or that some nutrient pathways must be induced by the presence of specific metabolites, as was found to be the case with citrate and fructose utilisation pathways by Rico *et al* (2008) [71]. As Pst DC3000 cells were pre-grown in LB media before inoculation into apoplast extracts, they may have become pre-adapted in the utilisation of specific nutrients, and so it would be interesting to test whether pre-growth in apoplast extracts prior to conducting a depletion assay produced different depletion patterns.

One of the explanations for the depletion patterns observed is carbon catabolite repression (CCR). CCR is known to occur in *P. syringae* [146] and in *P. putida* in response to amino acids and organic acids. Several studies have linked carbon catabolite repression with virulence gene expression in other bacterial species [31]. The Crc protein is involved in the repression of catabolic pathways in *Pseudomonas* species [159], and has been implicated in regulation of the T3SS in *P. aeruginosa* (a *crc*- mutant showed reduced type III secretion and lower virulence in its *Dictyostelium discoideum* host) [160]. However, no such link has been examined in *P. syringae* pathovars.

The Biolog GN2 analyses in Section 3.2.4 and performed by Rico *et al* (2008) [71] identified several metabolites that Pst DC3000 was able to metabolise but which were not found to be present in the tomato leaf apoplast extract, for examples, arabitol, formic acid, mannose and mannitol. This suggests that Pst DC3000 may encounter these metabolites in environments other than healthy apoplast, such as apoplastic fluid which contains defence metabolites and by-products of the hypersensitive response. In the case of mannitol, it has been found in tomato leaf apoplast infected with the fungus *Cladosporium fulvum*, but not in uninfected samples [137]. Alternatively, metabolites which were not identified in the apoplast that Pst DC3000 is able to metabolise may be assimilated by mechanisms which have broad substrate specificity.

3.3.2 Genes encoding type III effectors show differential expression to *hrp/hrc* genes in the presence of several substrates

In order to examine the relationship Pst DC3000 has with various components of the apoplastic environment, a reliable method for measuring virulence gene expression was required. The pBS63 plasmid, which luminesces upon activation of the *hrpL* promoter, was found to provide a highly sensitive and simple way of measuring virulence gene expression. HrpL is known to regulate T3SS structural genes and type III effectors [40] and so provided a useful point of reference for virulence gene expression more generally. Its suitability was demonstrated by comparison with qRT-PCR analysis: for the majority of experiments and treatments, luminescence produced by the pBS63 plasmid reliably reported the level of induction or repression relative to a control treatment.

Interestingly, the level expression of the two type III effectors tested in this study, *avrE* and *avrPtoB*, sometimes differed from that of *hrpL*. Specifically, induction of the effectors was relatively lower in response to fructose than *hrpL* and *hrcJ* (Figure 3.7), *avrPtoB* expression was much higher than that of *hrpL* in the presence of M9-fructose + 5 mM GABA, and the expression of *avrE* was less inhibited by threonine than *hrpL* expression. This result implies that the expression of type III effectors may be subject to transcriptional regulators other than HrpL. It may be worth further exploring what these additional factors may be as the success of type

III effectors is crucial to pathogensis in *P. syringae*.

3.3.3 Apoplastic metabolites have differing effects on virulence gene expression

Sections 3.2.4 and 3.2.5 established that Pst DC3000 displays different virulence profiles in the presence of different apoplastic components. As the host apoplast is metabolically dynamic in its response to Pst DC3000 [7, 9, 91], examining the response to individual metabolites should give some level of indication as to how Pst DC3000 has evolved to cope with this changing environment. GABA is the most abundant nutrient in tomato apoplastic fluid, however, this study and others have shown that it down-regulates virulence gene expression [88]. Pst DC3000 appears to have an excess of metabolic genes to catabolise GABA (three GABA transaminases and three succinic semi-aldehyde dehydrogenases, which are required to convert GABA into succinate) in comparison with other *Pseudomonas* species (Section 5.2.1), and the idea that GABA assimilation is an important virulence strategy is explored in more depth in Chapter 5.

Other metabolites which strongly repressed *hrpL* expression included threonine, glucose, alanine and tyrosine. Apoplastic metabolites which caused high levels of induction included fructose, aspartate, asparagine, betaine, choline and lysine. Interestingly, similar metabolites which are catabolised via largely the same pathways, such as glycine and serine or proline and glutamate, showed markedly different expression profiles. This result implies that the expression of virulence genes in Pst

DC3000 may not be responding to the production of catabolic products from these metabolites, but that the metabolites themselves may be binding to a regulatory protein.

In addition, there was no discernible pattern between apoplastic metabolite abundances, the rapidity of their depletion by Pst DC3000 and the degree to which they induced or repressed virulence gene expression. For example, aspartate is one of the more abundant amino acids in the apoplast, which Pst DC3000 rapidly depletes from apoplastic extracts and which causes high levels of virulence gene expression. Conversely, glutamate, which is equally as abundant as aspartate in the tomato apoplast and is depleted at the same rate as aspartate, causes virulence gene repression. These observations imply that very subtle changes in apoplastic composition could have a significant effect on the expression of virulence genes by Pst DC3000.

Rico *et al* (in preparation) have recently monitored metabolic changes which occur in the tomato apoplast inoculated with Pst DC3000 cells. Over a 24 hour period, glutamine, glutamate, alanine, asparagine, adenosine, citrate, trigonelline, and tyrosine all increased in abundance whereas GABA, inositol and valine decreased in abundance over the same period. The metabolites which increase in abundance were shown to cause a range of virulence gene responses, from high levels of induction (asparagine and trigonelline) to significant levels of repression (adenosine and tyrosine). An interesting extension of this study would be to examine the change in virulence gene expression observed in apoplast extracts spiked with these amino

acids which increase in abundance, as this would provide a more representative plant environment.

3.3.4 A link between intracellular metabolite abundances and virulence gene expression?

One of the most striking results of this study was the discovery that different intracellular metabolite profiles can be observed in Pst DC3000 in the presence of different carbon sources. The changes in metabolite abundances between fructose- and glucose-fed cells were the most notable, and the correlation between these changes and virulence gene expression presented the possibility that intracellular metabolites played a role in virulence signalling cascades, or that the intracellular metabolite pools reflect physiological changes required to produce virulence determinants.

Glutamate was consistently found to be the most abundant free amino acid, both in apoplast extracts and in synthetic media. Several studies have reported similar findings, both for *Pseudomonas* species [161] and other bacteria, such as *Bacillus* and *Erwinia* species [162, 163]. The alteration of intracellular metabolite pools in response to changing environments is also a well-documented phenomenon, with proline accumulation observed in *Bacillus subtilis* in response to osmotic shock [164] and rapid glutamate accumulation observed in *Rhizobium* species in response to sodium chloride salinity [165]. In this study, glutamate was also found to significantly change in proportional abundance under different environmental conditions. Both 2-oxoglutarate and glutamine have been implicated in bacterial nitrogen sens-

ing [153, 154, 157], and it is possible that glutamate, from which both 2-oxoglutarate and glutamine can be synthesised, is involved in a nitrogen sensing mechanism in Pst DC3000. However, other metabolites should not be excluded from further research: malate, succinate, 2-hydroxyglutarate, alanine and valine all showed significantly different abundances between the glucose and fructose treatments.

Currently, there are limited reports linking intracellular metabolite pool abundances with virulence. One of the best documented examples is the CodY transcriptional regulator in gram-positive bacteria. This protein senses the intracellular pool of branched-chain amino acids, although the exact sensory mechanism remains unknown [166]. CodY is also involved in the regulation of virulence, with mutations in the *codY* gene causing an abolition of virulence [167]. In gram-negative bacteria, no such direct relationship has been established, though the two-component systems NtrB-NtrC and CbrA-CbrB, thought to control carbon:nitrogen sensing, are possible candidates, and glutamate metabolism has been shown to be under the control of NtrC in *P. putida* [168]. Orthologues of both NtrB-NtrC and CbrA-CbrB are present in Pst DC3000 and in other *Pseudomonas* species these two-component systems have been implicated in sensing carbon:nitrogen ratios [150] as well as virulence gene regulation [169–171]. This study has provided some possible metabolites that may be causing virulence gene expression changes, namely glutamate, as well as alanine, malate, succinate and GABA, and possible mechanisms that sense these metabolites should be further investigated.

3.3.5 Does activation of the PTS system act as a virulence signal?

The changes in amino acid and TCA cycle metabolite profiles in the presence of fructose with different amino acids were notable, but not to the same extent as the changes observed between glucose and fructose treatments. *In vitro*, M9-fructose at pH 5.5 caused the highest levels of virulence gene expression, consistent with many studies which have used minimal media to stimulate the T3SS in Pst DC3000 and related pathovars [3, 79]. In Pfl SBW25, fructose and glucose also caused differential T3SS gene expression and metabolite profiles. Interestingly, fructose is the only sugar that Pst DC3000, Pfl SBW25, and other pseudomonads, take up from the outside environment by a phosphoenolpyruvate-dependent phosphotransferase system (PTS). This is in contrast to other bacterial species, such as *E. coli* and *B. subtilis*, where both fructose and glucose are assimilated thought PTS (glucose enters into *Pseudomonas* cells via the OprB-1 porin [145]). PTS-mediated transport of sugars requires the transfer of a phosphoryl group from phosphoenolpyruvate (PEP) to the sugar molecule via a cascade of phosphotransfer proteins [172]. The PTS is known to sense the ratio of PEP and pyruvate in relation to extracellular sugars and this leads to the wider regulation of carbon and nitrogen metabolism [173, 174], which may provide an explanation for the large differences observed in glutamate abundance, though there is no established link in the literature between PTS systems and the NtrB-NtrC. Interestingly, a PTS which is not thought to be involved in sugar transport, but which is clustered genetically near RpoN has been identified

in *P. putida* [175] (*pstN*, PSPTO_4455 in Pst DC3000) and is suggested to present a regulatory link between carbon and nitrogen metabolism [176]. Results from this study indicate this would be an interesting system to investigate for a possible role in virulence in Pst DC3000.

The cluster of genes known to be involved in the sugar-transporting PTS in *P. putida* is under the control of the catabolite repressor/activator protein FruR, which is responsible for the regulation of a much wider suite of metabolic genes [174]. Recently, in *P. putida*, it has been discovered that glucose and fructose metabolism result in very different internal metabolic fluxes [177] which may be another potential source the relevant signals for changes in virulence gene expression. In addition, a link between PTS sugar uptake and virulence has already been established in other gram negative bacterial species [178]. The effect of glucose and fructose metabolism on metabolic fluxes in Pst DC3000 and possible links to virulence gene expression are explored in more depth in Chapter 4.

3.3.6 Pfl SBS25 displays highly similar metabolite profiles to Pst DC3000 implying conserved metabolic processes between the species

The expression of T3SS genes in Pfl SBW25 were notably different to that of Pst DC3000 in the presence of a range of carbon and nitrogen sources. It is likely that this reflects the different environments they inhabit and the divergent roles of the

T3SS genes in either species [158]. In spite of differences in T3SS gene expression inducers and the magnitude of T3SS gene expression in Pfl SBW25, internal metabolite abundances were almost indistinguishable from Pst DC3000 under the glucose and fructose conditions. It appears therefore that the metabolic processes of these two species may be similar, irrespective of lifestyle, and that different mechanisms regulate virulence gene expression downstream of the changes in metabolite abundance. Again, this is explored further in Chapter 4 with the use of metabolic flux analysis.

3.3.7 Summary

The aim of this chapter was to further characterise the metabolic components of the host apoplast, to discover how these nutrients are assimilated by Pst DC3000 and to what extent they influence virulence gene expression. Nutrient assimilation in the apoplastic environment was shown most probably to operate under the control of catabolite repression. Several key metabolites were identified that appear to be important in the expression of virulence genes, including the intracellular abundance of glutamate and the virulence gene repressor, GABA. It appears that Pst DC3000 and the non-pathogenic Pfl SBW25, may regulate their T3SS gene expression on the basis of intracellular metabolite changes and these ideas are further explored in the following chapters.

Chapter 4

Metabolic flux analysis of *Pseudomonas syringae* and *Pseudomonas fluorescens* under *hrp*-inducing and repressing conditions

4.1 Introduction

The metabolic interaction of pathogenic bacteria with their environment has thus far received little attention, and even less so the changes in metabolic fluxes which re-

sult from those interactions. In Chapter 3, major changes in metabolite abundances were detected in *Pseudomonas syringae* pv. tomato DC3000 (Pst DC3000) cells that were grown under virulence gene inducing and non-inducing conditions. The aim of this chapter, therefore, is the characterisation of changes in central carbon metabolism in Pst DC3000 under those same experimental conditions, to determine if central carbon fluxes may be involved in the stimulation of virulence gene expression. A longer-term view was to lay the ground-work for metabolic flux analysis of Pst DC3000 during infection *in planta*. As a comparison to existing literature and in order to deduce if a pathogenic lifestyle alters metabolic fluxes, *Pseudomonas fluorescens* SBW25 (Pfl SBW25) was also included in the analysis under both conditions.

It was hypothesised that significant changes would be observed in the metabolic phenotypes of these strains, either in response to the expression of virulence genes, or to the environmental conditions. Steady-state ^{13}C metabolic flux analysis (^{13}C-MFA) was chosen for this investigation as it is a well established method for quantifying the intracellular flow of metabolites. An overview of the different ways in which metabolic fluxes can be modelled and quantified is given, with a particular focus on studies of bacterial metabolism. An in-depth introduction to the techniques involved in ^{13}C-MFA follows and finally a specific look at what is currently understood about the central carbon metabolism of *Pseudomonas* species.

4.1.1 Metabolic fluxes: the true cellular phenotype

Metabolic flux can be described as the flow of molecules through a network of metabolites, and these fluxes produce the phenotype of a cell [105, 106]. A common comparison is that of metabolic flux and traffic: whilst enzymes and metabolites can be measured (which can be represented by roads and cars respectively), neither one alone, nor in conjunction with the other, can report on the rate of turnover of the metabolites themselves (flux traffic) [179], or how this traffic responds to environmental perturbation [105, 180, 181]. Indeed, mathematical models are required for the integration of these measurable quantities [182] as metabolic fluxes usually cannot be measured directly [105].

Whilst metabolism is a complex process and can involve hundreds of different molecules [183–185], central carbon metabolic networks are highly conserved across the domains of life [105] and are, unsurprisingly, the most extensively characterised biological system [186]. The quantification of metabolic fluxes can be approached from several different angles (discussed below), though all are computationally (and often experimentally) demanding [187]. This is perhaps one of the main reasons why flux estimations have only recently gained ground as an important complement to traditional genome, transcriptome and proteome studies, though it becomes ever clearer that fluxes are not always correlated with these measurements [181]. Research into metabolic fluxes has also proven its utility with the discovery of novel pathways [188].

4.1.2 Quantifying and modelling metabolic fluxes in bacteria

The starting point for all assessments of metabolic networks is an understanding of the network stoichiometry, that is, the metabolites present and how they are connected [189]. Broadly, two main approaches to investigating metabolic fluxes then exist. Both have been used to characterise fluxes in a wide variety of organisms and are often thought of as complementary methods [190]. First, genome-scale metabolic modelling has become a popular way to examine bacterial metabolism, particularly as genome sequencing has become faster, cheaper and more reliable. Genome-scale approaches generally include many hundreds of reactions [187] and the only experimental data required is the biomass composition of the organism of interest. Flux balance analysis (FBA) is the primary method of genome-scale modelling. Second, isotopic labelling strategies can be used to monitor the redistribution of an isotpically labelled substrate throughout a metabolic network, thus allowing quantification, not just prediction, of fluxes [105]. Kinetic modelling presents a third, less commonly used method, by which fluxes may be predicted from known characteristics of enzyme kinetics. This approach requires in-depth knowledge of all enzymes within a model and this high degree of description means kinetic models can have great predictive potential [190]. Kinetic modelling has not been a primary method in the analysis of bacterial metabolism and so is not discussed further in this study.

Flux balance analysis

Flux balance analysis requires the mathematical representation of a (usually) genome-scale metabolic network reconstruction [191]. Reaction stoichiometries, predicted flux directions, and biomass composition constraints are all required for prediction of fluxes using this method [190]. The size of models for which fluxes can be predicted and fast computation of these models has made FBA an attractive option for many bacteriologists, and has proved useful in predicting drug targets for *Staphylococcus aureus* [192], in hydrogen bioengineering [193, 194] and in predicting changes in bacterial metabolism associated with viral infection [195], amongst other endeavours. However, FBA requires assumptions to be made about the system, most notably that metabolite concentrations remain constant, in addition to defining an assumed biological objective, such as minimisation of substrate utilisation or maximal biomass production [190, 191, 196]. Despite these theoretical draw-backs, FBA has been shown to produce highly accurate flux estimates across a range of species when compared with ^{13}C-MFA [197, 198] and recently the inclusion of energy-consuming transporter costs has led to even greater accuracy [199].

Isotopic labelling strategies

Quantification of metabolic fluxes using isotopically labelled substrates has frequently been heralded as the most powerful and reliable method of modelling metabolism [129, 183]. It relies on the presence of multiple pathways leading to the same products and that these pathways have different ways of rearranging carbon atoms [105].

This analytical technique is often known as ^{13}C metabolic flux analysis (^{13}C-MFA) as ^{13}C-labelled carbon substrates are commonly used. Bacteria are grown with the ^{13}C-labelled substrate either by batch culture or by continuous culture in chemostats. The redistribution of labelled carbon throughout central carbon metabolic networks can then be detected in amino acids from hydrolysed protein, or from soluble intermediates, by gas-chromatography mass-spectrometry (GC-MS) or nuclear magnetic resonance (NMR) analyses. This results in much higher levels of sample processing and data analysis than either FBA or kinetic modelling. Computationally, ^{13}C-MFA can be cumbersome as a "1000-dimensional non-linear equation system is constructed and solved repeatedly" [129]. The ^{13}C-MFA protocol which was undertaken in this study is outlined in Section 4.1.3. Several variants of this methodology exist, all of which have contributed to our understanding of bacterial metabolism.

The first distinction is the quantification of either flux ratios (the ratios of fluxes from converging pathways detectable in different metabolites) or absolute *in vivo* fluxes by isotopomer balancing. Metabolic flux ratio (METAFoR) analysis does not require knowledge about extracellular rates of substrate consumption [105] but can only give local information on fluxes and as a result is less informative than isotopomer balancing [200]. Flux ratios have been used to profile fluxes of metabolic mutants of *Escherichia coli* [130] and to confirm the role of the *yqjI* gene in *Bacillus subtilis* as an NADP$^+$-dependent 6-phosphogluconate dehydrogenase [201]. Furthermore, METAFoR analysis has been used in conjunction with isotopomer balancing to great effect in a comparative analysis of fluxes in seven different bacterial species

[188] and in identifying the conserved nature of fluxes in *B. subtilis* metabolic knock-out mutants [202]. Notably, many of the bacterial species which have been characterised by ^{13}C labelling studies are of industrial or medical relevance [188].

In contrast to METAFoR analysis, isotopomer balancing has generally been used more widely as it can give more information on a larger scale. The analysis of samples in ^{13}C-MFA can either be at a single time point when cultures are in isotopic and metabolic steady-state (isotopic enrichment is constant, as are metabolite pool sizes [203]) or samples can be taken at various points in time, in a process known as dynamic labelling, or non-stationary ^{13}C-MFA [106, 204]. The main advantage of looking at the distribution of labelling patterns over time is that it can help to resolve linear biosynthetic pathways which stationary ^{13}C-MFA cannot [106]. In addition, metabolic and isotopic steady-states do not have to be established, meaning experimental timescales can be reduced [203]. However, a major drawback of this technique is the difficulty of deducing fluxes further away from the substrate's point of entry owing to cyclical and reversible fluxes [106].

Typically, steady-state ^{13}C-MFA has been used for the absolute quantification of central metabolic fluxes, and this technique has led to important discoveries in microbes. The aforementioned analysis of seven different bacterial species [188] served to highlight the differences which exist in central carbon metabolism and thus dispelled the notion of model bacterial species, such as *E. coli* and *B. subtilis*, being representative of bacterial metabolism at large. The identification of pathways,

such as the xylose catabolic pathway in the solvent-producing *Clostridium acetobutylicum* [205] and unusual routes of metabolism, including serine biosynthesis via the hydroxymethylation of glycine rather than from 3-phosphoglycerate in *Streptococcus pneumoniae* [206], glucose catabolism through a PEP-glyoxylate cycle in *E. coli* [207] and the GAS pathway for pyruvate dissimilation (an incomplete TCA cycle with fluxes routed instead through the Glyoxylate and Anaplerotic reactions in order to produce Succinyl-CoA) in *Mycobacterium tuberculosis* [208] have all added to our understanding of bacterial metabolism.

Recently ^{13}C-MFA has been used for the identification of transcriptional regulators of central carbon metabolism [186]. Specifically, a transcriptional regulator known to be involved in carbon catabolite repression in *B. subtilis* was shown to be involved in the modulation of central carbon metabolic fluxes [209], and a large-scale analysis of transcription factor deletion mutants revealed roles for *crp*, *cra*, *ihfA*, *ihfB*, *mlc* and *nagC* in the regulation of fluxes through the PEP-glyoxylate cycle in *E. coli* [180]. Interestingly, while some studies are reporting wide-spread changes in fluxes as a result of the deletion of transcriptional regulators, other studies are reporting on the robustness of central carbon fluxes to these perturbations [206]. The role of transcriptional regulation for metabolic flux phenotypes has now been shown to less important than previously believed[180], with bacteria such as *Mycobacterium pneumoniae*, which does not have the majority of recognised metabolic transcription factors, still able to achieve complex metabolic regulation [186]. Metabolite-protein interactions and post-translational modifications have been suggested as mechanisms

that may be more important in the regulation of the metabolic phenotype [186].

As ^{13}C-MFA is now a well-established tool for the interrogation of fluxes under conditions of basic environmental or genetic alteration, attention has turned to more complex scenarios. Apart from the use of ^{13}C-MFA to study the metabolism of less well known species, such as *Geobacter metallireducens* and *Desulfovibrio vulgaris* [210], which is inherently more difficult owing to these being non-model species, other challenging systems are being addressed. Recent advances in analytical techniques should mean that metabolic flux analysis of single cells will soon be within grasp [204], allowing insights into how different fluxes are at the level of the individual cell. Currently, ^{13}C-MFA is only conducted using chemically defined media, usually only with a single carbon source [204]. Microbes, however, live in nutritionally complex environments, such as plant and animal hosts and so work towards modelling the uptake of multiple carbon sources will add to understanding of metabolism within more relevant settings. Another real-world scenario which is gathering attention is the identification of metabolic fluxes of a population within a mixed consortia of bacteria or host cells [211, 212]. The use of green fluorescent protein (GFP) as a proxy for total cellular protein allows the sampling of a specific set of GFP-expressing cells to be analysed in the context of, though separately from, other non-GFP expressing cells [213]. Advances such as these will serve the field of ^{13}C-MFA as it seeks to address the complexities of bacterial metabolic flux analysis *in situ*.

4.1.3 ^{13}C metabolic flux analysis

The approach taken in this study is based upon protocols previously outlined by Wiechert (2001) [129] and Zamboni *et al* (2009) [105]. The theoretical and practical aspects of these methods are outlined below, and a diagrammatic explanation of the protocol is given in Figure 4.1. First, a network model is constructed which contains a description of all the reactions of central carbon metabolism and the biosynthesis of cellular components. These reactions describe both the direction of the fluxes and also the movement of carbon atoms within each reaction. A labelling experiment is then carried out in which bacterial cells are fed a ^{13}C substrate until they have reached isotopic and metabolic steady state. The data collected from these labelling experiments from GC-MS or NMR analysis, known as isotopomer (isotopic isomer) abundances, are incorporated into the metabolic model along with other information to constrain the model such as biomass outputs. The model is then run using Monte Carlo simulations, which simulate predicted isotopomer abundance data, using different initial flux and measurement values, to explore the potential flux space, before a subset of these solutions with the lowest difference between the predicted and measured data are used for the final optimisation of the model.

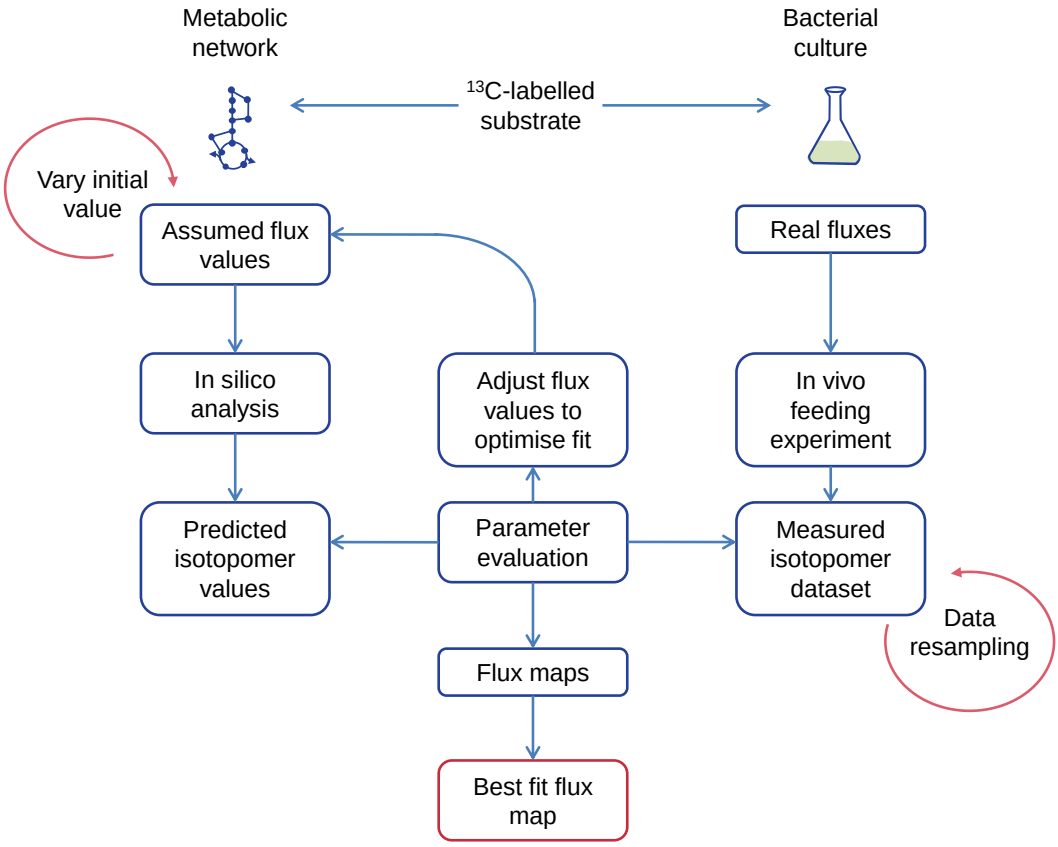

Figure 4.1: ^{13}C metabolic flux analysis work-flow. Representation of the steady-state ^{13}C-MFA protocol adapted from Kruger *et al* (2011) [187]

Theory and assumptions of ^{13}C metabolic flux analysis

^{13}C-MFA is based upon the argument that fluxes can be mathematically deduced from a set of measurements of the redistribution of label within substrates of a metabolic network. This relies on accurate measurements and knowledge about the reactions present in the network [187]. It also requires a set of assumptions to be made about the functioning of the network. These assumptions are namely that enzymes do not discriminate between ^{12}C and ^{13}C atoms and that all molecules, regardless of the degree to which they are labelled, mix thoroughly within metabolite pools [105]. However, recently it has been demonstrated that light isotopes (^{12}C)

will react faster than heavy (^{13}C) ones, meaning a bias does exist which can be significantly above the error of the instruments used for quantification [131]. This can be addressed in the modelling of reactions (Section 2.15.5) and so contravention of the assumption should not alter flux predictions. In addition, Kruger *et al* (2007) have shown that heavy isotopes do not have a significant impact on metabolic fluxes in *A. thaliana* [214]. A final assumption is that all cells within a culture have the same flux patterns. Until single cell metabolic flux analysis is possible it must be assumed that at least the majority of cells will be operating in the same way.

Fluxes through metabolic reactions can often proceed in both the forwards and reverse directions, and understanding just the net flow of carbon, whilst highly informative, is not always representative of the system as a whole. These bidirectional fluxes are not modelled as forwards and backwards reactions in 13CFLUX, a programme commonly used for ^{13}C-MFA and also in this study, instead net fluxes and exchange fluxes are calculated. The net fluxes give the direction and net magnitude of the reaction. The exchange flux quantifies how bidirectional a reaction is. This has been defined computationally by an exchange flux of 0 indicating that the reaction is only occurring in a single direction and larger values (up to a maximum of 1) indicating that both the forward and reverse reactions are occurring at a similar rate [129]. Exchange fluxes [0,1] can be defined mathematically as follows:

$$Xch[0,1] = \frac{J_{Xch}}{(1 + J_{Xch})} \tag{4.1}$$

where J_{Xch} is the true exchange flux, and, this is related to the net fluxes by the following equations:

$$J = J_f - J_r \tag{4.2}$$

$$J_{Xch} = min(J_f, J_r) \tag{4.3}$$

Where J is the net flux and , J_f and J_r are the forward and reverse fluxes respectively [129]. Often exchange fluxes can be particularly poorly defined and their contribution to our understanding of metabolism is frequently neglected [215].

Isotopic labelling and measuring fractional enrichment

Choosing the correct carbon substrate and the type of isotopic labelling for modelling a particular set of metabolic fluxes is very important. Two types of labelled carbon can be purchased from suppliers: positionally enriched substrates, where one, or sometimes two, carbons within a substrate are labelled, and uniformally labelled substrates, where there is a 99 % chance of the carbon atom at each position being ^{13}C labelled (this means that around 94 % of the total carbon atoms in a 6-carbon substrate, such as glucose, are ^{13}C labelled) [105]. Substrates which are uniformally labelled can give no information about metabolic fluxes when fed to cultures, in the same way unlabelled substrates cannot be used to resolve fluxes either. However, uniformally labelled substrates can be fed in mixture with the unlabelled version of the substrate, and typically this is done in a ratio of 20 % [$^{13}C_6$] to 80 % unlabelled which can be used to resolve fluxes [105]. Whilst the smallest experimental errors are found when both are fed in roughly equal proportions, 20 % has been shown to

be highly reliable for deducing central carbon fluxes and is also the least expensive option [207].

Different labelling strategies have individual merits, for example positionally labelled [1-^{13}C] glucose is particularly well suited to resolve fluxes through the pentose phosphate pathway [105], but they are most useful when used in combination. Fischer *et al* (2004) [216] provide an excellent example of the improvement in flux determinability when both labelling methods are either used separately and modelled together, or a mix of the two substrates is fed to the bacterial culture (for example, 20 % [$^{13}C_6$] and 80 % [1-^{13}C]).

Typically two technologies are employed in order to analyse fractional enrichment (replacement of ^{12}C with ^{13}C atoms) throughout the metabolic network: GC-MS and NMR. GC-MS is often considered to be superior to NMR as it is more sensitive and requires less processing time [105]. However, GC-MS is only able to give information on the proportion of ^{13}C found in a metabolite whilst NMR can give positional labelling information, so they are routinely used as complementary methods and sets of measurements from both analyses can be incorporated into the same model [217, 218]. A sole GC-MS approach was chosen for this study owing to time constraints and available expertise, and this has been shown to provide sufficient information for the detailed resolution of fluxes [188, 208].

Hydrolysed protein is often used to assess the redistribution of label throughout

the metabolic network as amino acids are synthesised from precursors which occupy different nodes within the central carbon network. Amino acids derived from protein hydrolysate tend to be stable and abundant analytes [105] though not all amino acids can be detected via this method as some are degraded during the hydrolysis treatment [206]. Recently, the inclusion of detectable metabolic intermediates, such as TCA cycle metabolites, in the analysis of metabolic fluxes, has been shown as a way to increase the accuracy of flux determination [105, 133, 219]. Both amino acids and free soluble metabolites are extracted and then derivatised prior to GC-MS analysis. Derivatisation makes metabolites more volatile and also less reactive.

GC-MS allows the separation of metabolites based on their elution time though the gas chromatogram and subsequent electron impact causes fragmentation of these metabolites, thus producing more than one data set for each metabolite [129]. The mass signals for each fragment are collected by the mass spectrometer, and from these patterns individual metabolites can be identified. The collected mass isotopomers must be corrected for the inclusion of naturally occurring ^{13}C atoms (which are found at around 1.13 % in nature) and for other atoms in the derivatising agent, as well as inspected for their accuracy. Fragments which have low overall reliability are not included in the modelling phase [120].

Constructing the model

First, a model must include all substrates, products and reactions known to be present in the central carbon metabolic network of the organism of interest. Many

pathways are simplified for the modelling of ^{13}C-MFA, particularly linear pathways which have no changes in carbon positions between different metabolites as these will all have the same net flux values [187]. Pathways may subsequently be removed if they are shown to have no detectable flux through them [187]. During the process of parameter fitting (Section 4.1.4), it may also become apparent that some fluxes cannot be determined from the labelling information available, and these should be considered for removal in order to generate a better overall fit of the model [187]. The directionality of a reaction can often be deduced from thermodynamic considerations and experimental evidence [129]. For example, all uptake fluxes are considered to be unidirectional, whilst internal fluxes are generally considered to be bidirectional.

The second element required is information about carbon atom transitions, that is, the movement of specific carbon atoms between substrates and products [105] and this information is present in many biochemistry textbooks. Finally, the model must be constrained by the inclusion of biomass measurements and the mass isotopomer data (Section 4.1.3).

Constraining the model

Once the bacteria have achieved steady-state in isotopically labelled culture, which for batch cultures occurs during the exponential phase of growth, they are harvested and analysed, both for their macromolecular composition and also the fractional enrichment of different metabolites. Collecting information on biomass composi-

tion typically involves measuring substrate uptake, cell dry weight, protein content and amino acid proportions, nucleic acid content, lipid content and measuring the production of any secreted products, such as extracellular polysaccharides [105]. These components are used to constrain the inputs and outputs of the model and it is important to measure these components accurately as different biomass constraints can change the outcome of flux models [220]. This is an area of metabolic flux analysis where shortcuts are often taken, for example the use of biomass composition data from *B. subtilis*, a gram positive bacterium, to constrain flux models of *Pseudomonas fluorescens*, *Pseudomonas putida*, *Agrobacterium tumefaciens*, *Sinorhizobium meliloti* and *Rhodobacter sphaeroides*, all highly divergent gram negative species [188]. This is surprising considering the ease with which these measurements may be made, or found in the literature for many species, and the degree to which these measurements can vary under different treatments [220].

The second set of measurements which are included in the model is the isotopomer values of different metabolite fragments. Precision in the measurement of mass isotopomer distributions is exceedingly important as even small errors can cause large differences in flux solutions [221]. These measurements are assigned an error, typically in the range of 1-2 % to allow for measurement noise from the GC-MS analysis, though higher errors may be assigned to allow for more unreliable fragments to be included in the model [120].

Finally, fluxes within the model must be assigned to one of three categories: free, de-

termined or constrained. The free fluxes in the model are those fluxes which cannot be calculated from knowledge of other fluxes, and determined fluxes are those than can be calculated from knowledge of other fluxes [129]. Fluxes can be constrained for two reasons: either the flux has been quantified by experimental measurements (biomass outputs) or the reaction is known to not occur. For example, if a reaction is known to proceed in only one direction, then the exchange value for this flux will be constrained to 0. If the modeller is sure that a reaction can only ever proceed in one direction then the reaction can be constrained to always have a net flux above or below 0.

4.1.4 Parameter fitting

Random initial starting values are given to the free fluxes (both net and exchange) and, in the case of 13CFLUX, Monte Carlo simulations are run to find a set of flux values that best explains the measured data. This fitting procedure seeks to minimise the variance-weighted sum of squared differences between the measured data and data that is simulated by 13CFLUX [222]. This sum of squared differences is know as the residuum and is used in conjunction with the χ^2 test (Section 4.1.4) to understand how well the model fits the data overall. Residua of individual fragments can also be used to identify any poorly fitting measurements and these can be considered for removal (if perceived to be erroneous) or the error on these measurements can be increased (if they are fitting poorly with other isotopomer values from the same metabolite). Many hundreds of simulations are run and the best fit from each is collected (the solution with the lowest residuum). Often many simulations

will converge on very similar solutions [222], but a wide variety of solutions will typically be found, and some solutions which are infeasible, that is, they contradict one or more of the model constraints [120]. All the feasible solutions are collected and analysed using principal component analysis to determine a threshold for inclusion in the best fit analysis [187]. The solutions which are included are averaged and these are taken as the starting values for the final optimisation [120]. The resulting solution is known as the global best fit and its reliability can be determined by statistical analysis.

Statistical analysis

The reliability of a set of flux quantifications can be assessed in several ways. The first method determines whether or not the model with the lowest residuum passes the χ^2 test. This gives an indication of how well the model can describe the observed labelling pattern based on the number of degrees of freedom present in the model [129]. This is a reliable way to determine how well the model is fitting the data and it is commonplace to only accept the best fit flux solution if it falls below the χ^2 value [223]. A model which fails the χ^2 test may indicate missing pathways or erroneous measurements.

The statistical element of 13CFLUX, EstimateStat, produces estimates of standard deviations for all of the best fit flux values from the parameter covariance matrix, with standard deviations greater than 0.4 indicating very poor confidence of the estimate [129]. However, this type of statistical analysis assumes linearity in the

dataset, and the data generated is more suitably analysed using non-linear statistical methods [219]. This can be done in one of two ways - either by using confidence values to map out the breadth of solution space for each flux [119] or to utilise the Monte Carlo solutions to calculate the probability distribution of the estimated fluxes [219].

4.1.5 Characterisation of metabolic fluxes in pseudomonads

This study is concerned with the characterisation of metabolic fluxes in *Pseudomonas syringae* pv tomato DC3000 and *Pseudomonas fluorescens* SBW25. Whilst no attempts have previously been made to quantify metabolic fluxes in *Pseudomonas syringae*, a flux map of *Pseudomonas fluorescens* 52-1C was produced by Fuhrer *et al* (2005) [188] in their study of seven different bacterial species. In addition, *Pseudomonas putida* KT2440 has also been analysed by ^{13}C-MFA and has been shown to have very similar fluxes to *P. fluorescens* when fed glucose as a sole carbon source [188, 224]. More recently, *Pseudomonas denitrificans*, which is used in industrial production of vitamin B12, was also analysed by ^{13}C-MFA [225]. The main findings of these flux characterisations is presented below, supplemented with evidence from other genetic and metabolic studies.

All three *Pseudomonas* species use the Entner-Doudoroff (ED) pathway almost exclusively for the initial catabolism of glucose [188, 224, 225]. This pathway was first identified in *Pseudomonas saccharophila* and has since been found to be present

in a wide variety of bacterial species [226]. It is also thought, evolutionarily, to be one of the oldest routes of catabolism [226]. The ED pathway is an alternative route to glycolysis: glucose is metabolised via 6-phosphogluconate to glyceraldehyde-3-phosphate (G3P) and pyruvate instead of via glucose- and fructose-6-phosphate. The absence of 6-phosphofructokinase in both species, and indeed in almost all *Pseudomonas* species, means glycolysis cannot proceed from fructose-6-phosphate (F6P) to fructose-1,6-bisphosphate (FBP) [145]. This pathway has been previously treated as completely non-functional in *P. fluorescens* [188], whilst in *P. putida* a small flux was shown to operate in the reverse direction making the ED pathway essentially cyclical [224]. Cyclical ED fluxes operating via gluconeogenesis had been hypothesised in pseudomonads for some time [226] and it is likely these gluconeogenic fluxes occur in order to produce polysaccharides, for which F6P is a precursor [188]. Very small fluxes through the oxidative pentose-phosphate (PP) pathway are present but appear to serve largely biosynthetic requirements in *P. fluorescens* and *P. putida* [188], though a larger flux through this pathway was observed in *P. denitrificans* [225]. The tricarboxylic acid (TCA) cycle has large fluxes through it, though in *P. fluorescens* and *P. putida* the conversion of malate to oxaloacetate (OAA) has a much smaller flux than the rest of the cycle (this reaction has been incorporated into an OAA to citrate flux in the *P. denitrificans* model). This is due to the high activity of the so-called pyruvate shunt, whereby malate is converted to pyruvate by malic enzyme (decarboxylating malate dehydrogenase) and then pyruvate is converted to OAA by pyruvate carboxylase. A small, though detectable, flux could also be identified from OAA to phosphoenolpyruvate (PEP) [188, 224]. These three

reactions are often collectively referred to as anaplerotic pathways owing to the replenishing of TCA cycle metabolites by pyruvate carboxylase, a reversal of the anabolic removal of said intermediates [227]. Whilst perhaps erroneous to extend this name to the reactions performed by malic enzyme and PEP carboxykinase, it has become commonplace in the literature, and so for consistency, will be used here.

4.1.6 Statement of aims

The following questions are addressed in this chapter:

1. How similar are Pst DC3000 and Pfl SBW25 in terms of genes involved in central carbon metabolism, metabolic network structure and biomass composition?

2. What differences can be observed in fluxes in Pst DC3000 under conditions that induce and repress virulence gene expression, and are the same differences observed in Pfl SBW25?

3. Do these changes indicate any parts of central carbon metabolism which may influence virulence?

4.2 Results

4.2.1 Establishment of growth conditions for metabolic flux analysis

Currently, metabolic flux analysis is only commonly performed using a single carbon source. In order to investigate the changes in metabolism when Pst DC3000 is grown under virulence gene-inducing and non-inducing conditions, growth media were required which caused large-scale differences in gene expression with minimal changes to the composition of the media and the growth of the bacteria, so that the two maps might be comparable. Previously (Section 3.2.3), modified M9 media, with either glucose or fructose as the sole carbon source, and at pH 5.5 or pH 7, were found to cause dramatic changes in the expression of virulence genes (Figure 4.2), and also to the proportions of soluble amino acid pools (Section 3.2.6). A trade-off was encountered in choosing the harvesting point for the cells: the bacteria needed to have grown enough to have entered mid-exponential phase (to achieve steady-state metabolism and sufficient labelling) but not so much that type III gene expression would have become too low, as virulence gene expression has been found to be inversely proportional to cell density in Pst DC3000 [80]. Harvesting cells at an OD_{600} of between 0.35 and 0.45 seemed to satisfy both considerations: cells were at mid exponential phase and, in the case of Pst DC3000, this was the density at which *hrpL* expression peaked. As ^{13}C-MFA is experimentally and computationally non-trivial, only two conditions could be chosen, and therefore the two conditions

which produced the lowest type III expression (glucose pH 7) and the highest type III expression (fructose pH 5.5) in Pst DC3000 were selected. The similarity in the level of induction of *rsp* genes in Pfl SBW25 in all experimental treatments meant that the degree of *rsp* induction was not a factor when choosing the treatments for flux analysis or the point of harvesting.

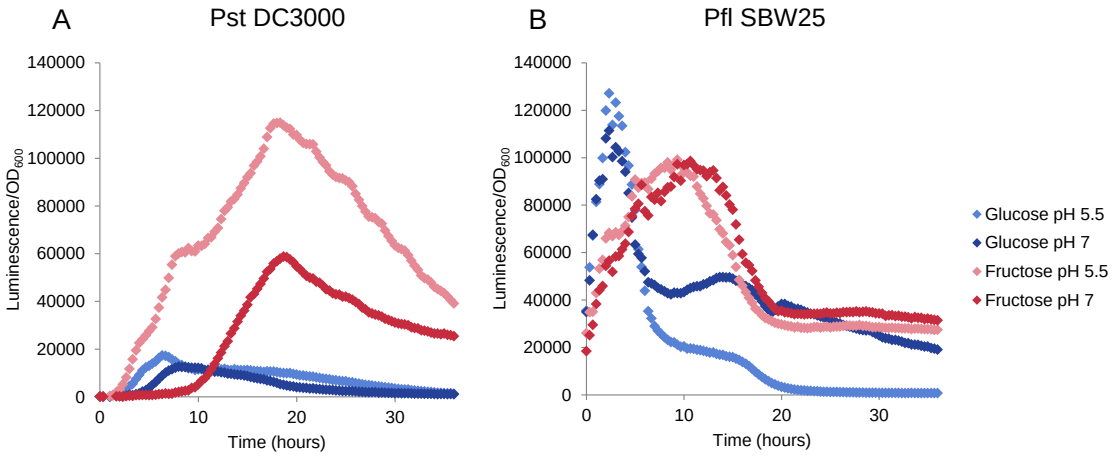

Figure 4.2: Expression of *hrp* and *rsp* genes using the pBS63 luminescent reporter plasmid.The pBS63 plasmid reports on the expression of *hrpL* in Pst DC3000 (A) and *rspL* in Pfl SBW25 (B). In Pst DC3000 it can be seen that fructose induces the expression of *hrpL* whilst glucose is repressive. In Pfl SBW25, both sugars induce *rsp* expression but this is found to be sustained for longer in fructose conditions, and therefore at the point of cell harvesting in mid-exponential phase, *rsp* genes were more highly expressed in the fructose treatment. Pfl SBW25 is not as sensitive to pH in the expression of *rsp* genes as Pst DC3000 appears to be in the expression of *hrp* genes. Luminescence values are corrected against optical density readings for each time point measurement. From the information about T3SS expression in this experiment, Pst DC3000 cells were harvested at 16 hours and the faster growing Pfl SBW25 cells at 8 hours. Figure is the same as Figure 3.16.

4.2.2 Biomass measurements for Pst DC3000 and Pfl SBW25 show similar molecular composition under the same growth conditions

In order to provide information on the macromolecular composition of both Pst DC3000 and Pfl SBW25, measurements were made of cell dry weight, protein, protein composition, DNA, RNA, lipid and sugar utilisation of cells grown in both glucose (pH 7) and fructose (pH 5.5). The macromolecular composition under these treatments is shown in Figure 4.3, and were found to be very similar between strains under the same treatments, with small differences in protein content providing the only notable difference between strains: Pfl SBW25 has a greater amount of protein per cell than Pst DC3000. Several differences were observed between the treatment conditions: when fed fructose, both strains produced more lipid and less RNA. The amino acid composition of the protein hyrolysate showed very similar profiles across the four sets of samples (Figure 4.4). Soluble metabolites were extracted and analysed for the inclusion of TCA cycle metabolites in the network model, however, these were found to be at such low abundances that they were not included as biomass outputs (Data not shown). The final biomass outputs used to constrain the models are shown in Figure 4.5.

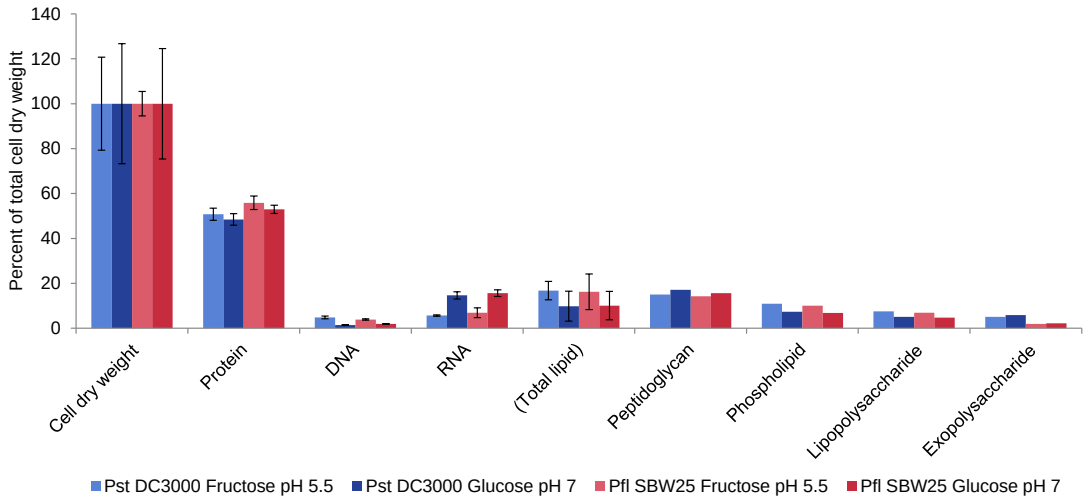

Figure 4.3: The macromolecular composition of Pst DC3000 and Pfl SBW25 under type III-inducing and repressing conditions. Data is shown for components which were measured (with error bars) and those components for which estimates were taken from the literature (without error bars). Total lipid measurements were used to estimate phospholipid and LPS percentages, and as these measurements are not included in the total sum of components they are presented in brackets. Where error bars are shown they represent the standard deviation of at least 7 independent sample measurements.

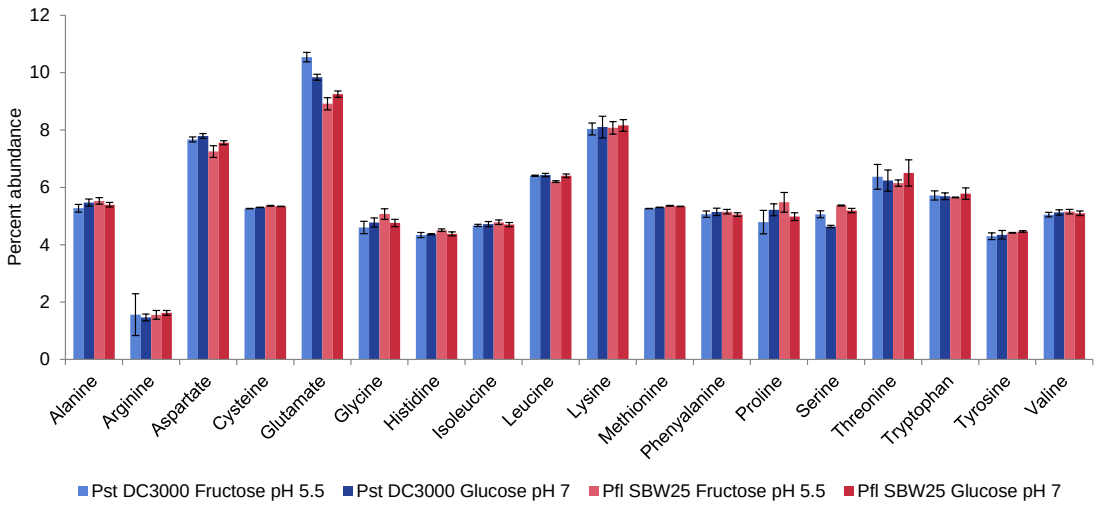

Figure 4.4: Amino acid proportions in protein hydrolysate from Pst DC3000 and Pfl SBW25 cells. Hydrolysed protein was analysed by GC-MS in order to obtain the percentage abundance of each amino acid. Cysteine, methionine and tyrosine could not be detected by GC-MS and so these were taken from the literature. Error bars represent the standard deviation from three biological replicates.

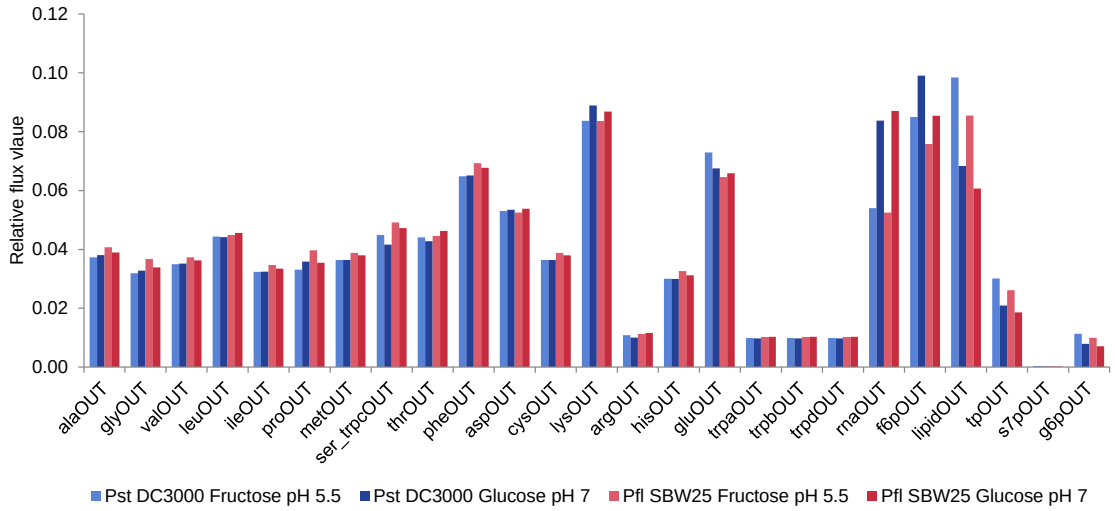

Figure 4.5: Biomass output fluxes used to constrain Pst DC3000 and Pfl SBW25 metabolic models. All macromolecular components were converted into flux values relative to cell dry weight and total substrate uptake. They were then assigned a relevant output flux, for example, alaOUT encompasses alanine that is incorporated into protein and also the alanine required for the synthesis of lipopolysaccharides. Error bars are not shown as some of the initial values come from estimates from the literature.

4.2.3 Metabolic network analysis reveals highly conserved central carbon pathways in Pst DC3000 and Pfl SBW25

A comprehensive examination of the literature and metabolic databases (KEGG and MetaCyc) was undertaken to build detailed network models. The pathways involved in the central carbon metabolic pathways that are typically included in metabolic flux analyses are shown in Table 4.1. The genomes of both Pst DC3000 and Pfl SBW25 are annotated to include all of the enzymes required for these reactions, however, the number of genes encoding certain enzymes do vary in number between these *Pseudomonas* species.

Enzyme	Reactant(s)	Product(s)	Gene locus ID DC3000	Gene locus ID SBW25
Glucokinase	Glucose	Glucose-6-phosphate	PSPTO_1289	PFLU4963
Glucose-6-phosphate isomerase	Glucose-6-phosphate	Fructose-6-phosphate	PSPTO_0959	PFLU5243
Fructose-PTS	Fructose	Fructose-1-phosphate	PSPTO_0954	PFLU0804
			PSPTO_0956	PFLU0806
1-phosphofructokinase	Fructose-1-phosphate	Fructose-1,6-bisphosphate	PSPTO_0955	PFLU0805
Fructose-1,6-bisphosphatase	Fructose-1,6-bisphosphate	Fructose-6-phosphate	PSPTO_5168	PFLU0355
Fructose-bisphosphate aldolase	Fructose-1,6-bisphosphate	Glyceraldehyde-3-phosphate	PSPTO_0390	PFLU5701
		Dihydroxyacetone-phosphate		
Triosephosphate isomerase	Dihydroxyacetone-phosphate	Glyceraldehyde-3-phosphate	PSPTO_4494	PFLU5257
Glyceraldehyde-3-phosphate deydrogenase	Glyceraldehyde-3-phosphate	3-phosphate-glycerate	PSPTO_1287	PFLU1566
			PSPTO_2102	PFLU4965
Phosphoglycerate kinase			PSPTO_0387	PFLU5705
Phosphoglycerate mutase	3-phosphate-glycerate	2-phosphate-glycerate	PSPTO_5327	PFLU0337
Enolase	2-phosphate-glycerate	Phosphoenolpyruvate	PSPTO_1554	PFLU1291
			PSPTO_4616	PFLU1903
Pyruvate kinase	Phosphoenolpyruvate	Pyruvate	PSPTO_4337	PFLU1799
				PFLU4949
Phosphoenolpyruvate synthase	Pyruvate	Phosphoenolpyruvate	PSPTO_2292	PFLU4620
Glucose-6-phosphate 1-dehydrogenase	Glucose-6-phosphate	6-phosphogluconate	PSPTO_1300	PFLU2692
			PSPTO_3121	PFLU4838
6-phosphogluconolactonase	Glucose-6-phosphate	6-phosphogluconate	PSPTO_1301	PFLU4837
			PSPTO_2765	
6-phosphogluconate dehydrogenase	6-phosphogluconate	Ribulose-5-phosphate	PSPTO_3122	PFLU2691
		Carbon dioxide		
Ribulose-phosphate 3-epimerase	Ribulose-5-phosphate	Xylulose-5-phosphate	PSPTO_0566	PFLU5563
Ribulose-5-phosphate isomerase A	Ribulose-5-phosphate	Ribose-5-phosphate	PSPTO_0404	PFLU5824
Transketolase	Xylulose-5-phosphate	Sedo-heptulose-7-phosphate	PSPTO_0385	PFLU3599
	Ribose-5-phosphate	Glyceraldehyde-3-phosphate	PSPTO_2401	PFLU3724
			PSPTO_2402	PFLU3724
				PFLU5707
Transketolase	Xylulose-5-phosphate	Fructose-6-phosphate	As before	As before
	Erythrose-4-phosphate	Glyceraldehyde-3-phosphate		
Transaldolase	Fructose-6-phosphate	Glyceraldehyde-3-phosphate	PSPTO_2119	PFLU1585
	Erythrose-4-phosphate	Sedo-heptulose-7-phosphate		PFLU2091
				PFLU3732
Phosphogluconase dehydrogenase	6-phosphogluconate	2-keto-3-deoxy-6-phosphogluconate	PSPTO_1288	PFLU4964

Enzyme	Reactant(s)	Product(s)	DC3000	SBW25
2-dehydro-3-deoxyphosphogluconate aldolase	2-keto-3-deoxy-6-phosphogluconate	Glyceraldehyde-3-phosphate Pyruvate	PSPTO_1302	PFLU4836
Pyruvate dehydrogenase	Pyruvate	Acetyl-CoA	PSPTO_3860	PFLU0460
		Carbon dioxide	PSPTO_5005	PFLU3193
			PSPTO_5006	PFLU3120
				PFLU0459
Oxaloacetate decarboxylase	Pyruvate	Oxaloacetate	PSPTO_5510	PFLU6070
	Carbon dioxide		PSPTO_5511	PFLU6071
Citrate synthase	Oxaloacetate	Citrate	PSPTO_2194	PFLU1815
	Acetyl-CoA			
Citrate lyase	Citrate	Oxaloacetate	-	PFLU3472
Aconitase hydratase	Citrate	Isocitrate	PSPTO_2016	PFLU1542
			PSPTO_2286	PFLU3489
			PSPTO_3752	PFLU4630
Isocitrate dehydrogenase	Isocitrate	2-keto-glutarate	PSPTO_3356	PFLU3808
		Carbon dioxide		PFLU3809
2-oxoglutarate dehydrogenase	2-keto-glutarate	Succinyl-CoA	PSPTO_2199	PFLU1820
		Carbon dioxide	PSPTO_2200	PFLU1821
Succinyl-CoA synthetase	Succinyl-CoA	Succinate	PSPTO_2202	PFLU1823
			PSPTO_2203	PFLU1824
Succinate dehydrogenase	Succinate	Fumarate	PSPTO_2195	PFLU1816
			PSPTO_2196	PFLU1817
			PSPTO_2197	PFLU1818
			PSPTO_2198	PFLU1819
Fumarate hydratase	Fumarate	Malate	PSPTO_1731	PFLU0874
			PSPTO_4399	PFLU4314
			PSPTO_4461	PFLU4952
Malate dehydrogenase (quinone)	Malate	Oxaloacetate	PSPTO_1136	PFLU0904
				PFLU1613
Isocitrate lyase	Isocitrate	Glyoxylate Succinate	PSPTO_3364	PFLU3817
Malate synthase	Glyoxylate	Malate	PSPTO_0480	PFLU5623
	Acetyl-CoA		PSPTO_3559	
Malate dehydrogenase (Malic enzyme)	Malate	Pyruvate Carbon dioxide	PSPTO_3924	PFLU0405
Phophoenolpyruvate carboxykinase	Oxaloacetate	Phosphoenolpyruvate Carbon dioxide	PSPTO_0239	PFLU0267
Phosphoenolpyruvate carboxylase	Phosphoenolpyruvate Carbon dioxide	Oxaloacetate	PSPTO_1508	PFLU1239

Table 4.1: Genes involved in central metabolic pathways in Pst DC3000 and Pfl SBW25. Gene locus tags are given for each enzyme, and where multiple genes are annotated to encode the same enzyme, these appear in the table in no specific order.

As the genomes are annotated to be capable of all the same reactions in both species, identical metabolic network models could be used for metabolic flux analysis. Where differences do arise in Table 4.1, these are in the number of genes annotated for specific enzymes. Notably, there are only two enzymes, 6-phosphogluconolactonase and malate synthase, where Pst DC3000 has more copies of the encoding genes than Pfl SBW25 (one additional gene in either case). Pfl SBW25 has six enzymes for which which multiple copies exist in the genome that are not found in Pst DC3000: pyruvate kinase, transketolase, transaldolase, pyruvate dehydrogenase, isocitrate dehydrogenase and malate dehydrogenase. It is unsurprising that Pfl SBW25 has higher levels of genetic redundancy than Pst DC3000, as the reduction of metabolic components of the genome of the latter pathogenic species is well documented [86].

This network is also illustrated in Figure 4.6 in which reversible reactions are indicated by double-headed arrows and irreversible reactions are identified by single-headed arrows pointing in the direction of metabolic flow.

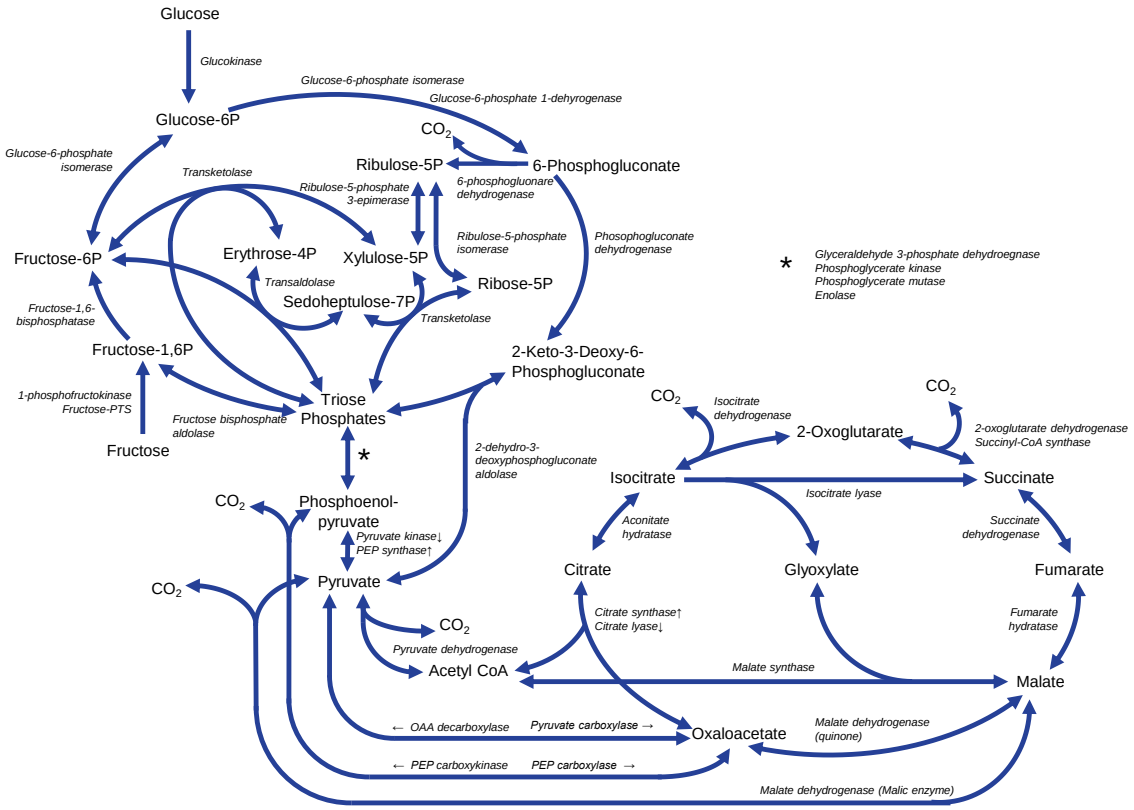

Figure 4.6: Network map of central carbon metabolism with enzyme annotations. This metabolic map describes the central reactions of carbon metabolism in both Pst DC3000 and Pfl SBW25. Metabolite abbreviations are used which correspond to those in the network model. Some pathways, notably those between the triose phosphates and PEP have been condensed for brevity. Here, TP describes both glyceraldehyde-3-phosphate and dihydroxyacetone phosphate, which are readily interchangeable.

4.2.4 Construction of network models used for ^{13}C-metabolic flux analysis

Metabolic flux analysis relies on accurate knowledge about the carbon transitions that occur during metabolic reactions. That is, the movement of carbon atoms during the conversion of reactants to products. Table A.3 (Appendix A.3) shows the carbon transitions involved in central carbon metabolism and the names of the pathways used in the .ftbl file model. Carbon atom transitions were used from pre-

vious ^{13}C-MFA studies [105, 120, 222]. The following section outlines experimental and modelling evidence that led to the inclusion of the reactions which are present in the final model.

The non-oxidative branch of the pentose phosphate pathway, specifically those steps catalysed by transketolase and transaldolase, can be described in a metabolic network model in one of two ways. The first, as shown in Figure 4.6, is the conventional way that these reactions are usually drawn and often described in metabolic flux models [105, 183], and which assumes multiple independent metabolite pools. However, Kleijn *et al* (2005) [228] showed that this method can misrepresent label distribution and proposed half reactions as a better descriptor of the underlying fluxes resulting from the ping-pong action of the enzymes involved [133]. Half reaction modelling of the pentose phosphate pathway has therefore been used in all metabolic models described in this chapter.

Several reactions in the model were condensed as no differences in carbon atom positions can be observed. These included introducing a pool of triose phosphate to replace dihydroxyacetone-phosphate (DHAP) and G3P. DHAP and G3P are products of FBP and so originally have different carbons present, however, DHAP can be converted to G3P and vice versa, meaning a pool of these metabolites is a reasonable modification to the model and this reaction is generally regarded to operate very close to equilibrium *in vivo*. The reaction pathway from G3P to PEP was condensed to a single reaction as there are no carbon positional changes, nor are

any biomass components synthesised from any of the intermediates. In addition, the extracellular conversion of glucose to gluconate and its subsequent conversion 2-ketogluconate was not included in the model as the carbon atom transitions are the same as that between glucose-6-phosphate (G6P), 6-phosphogluconate and 2-keto-3-deoxy-6-phosphogluconate. These reactions are known to occur in *P. fluorescens* [188] and predicted to occur in *P. syringae* [224] but without directly measuring the extracellular quantities of gluconate in the culture supernatant or the rate of gluconate uptake by cells, it would not be possible to resolve these fluxes.

The model contained all of the reactions of Table 4.2.3, reactions which describe the biosynthesis of amino acids, nucleic acids, polysaccharides, lipids and peptidoglycan, and also the recycling of amino acids. The biosynthetic reactions were adapted from a previous study [120] and checked in KEGG for the presence of annotated genes. Again, both Pst DC3000 and Pfl SBW25 contained all of the same pathways, and neither bacterium is auxotrophic for any amino acid. Amino acid recycling reactions were included, though in most cases it was expected that these would not have significant fluxes. The conversion of histidine to glutamate by histidine ammonia-lyase, urocanate hydratase, imidazolonepropionase and finally formimidoylglutamase was included in the model to begin with as a single reaction step, though later removed as no flux was evident through this pathway in either strain. It is likely this pathway is only active when histidine is being metabolised as a primary carbon or nitrogen source. The conversion of serine to pyruvate by L-serine dehydratase was also initially incorporated, but later removed after exper-

imental evidence showed it was non-operational, as described in Section 4.2.5. In addition, the conversion of threonine to glycine and acetaldehyde (in the model this appears as acetyl-CoA, owing to their interconversion) was included in the original model. Interestingly, this reaction was predicted by 13CFLUX to have small fluxes in all of the strains and treatments, and this is in agreement with Wang *et al* 2012 [225] who found around 10 % of glycine molecules were derived from threonine in their analysis of *P. denitrificans*.

The glyoxylate shunt was added to the network model as both Pst DC3000 and Pfl SBW25 are annotated as having isocitrate lyase and malate synthase. It is notable that in none of the previously published *Pseudomonas* flux maps is the glyoxylate shunt included [188, 224, 225] and it is unclear whether or not this is due to an absence of flux detected through this pathway or if the authors did not consider including it.

Initially the labelling strategy employed for both glucose and fructose experiments involved the use of 20 % [$^{13}C_6$]hexose + 80 % unlabelled hexose and 100 % [1-^{13}C]hexose. This combination has been widely reported in the literature to yield accurate flux estimates [105, 188, 216] for bacterial flux maps. However, in both Pst DC3000 and Pfl SBW25 cells fed with glucose, these labelled substrates were not able to give enough information to resolve fluxes through the anaplerotic reactions or between malate and OAA (the standard deviations of the net fluxes, provided by EstimateStat, were consistently above 10, and thus more than an order of mag-

nitude greater than the estimated flux values), though this was not the case in the fructose-fed cultures. In order to increase the resolution of the fluxes through these pathways a second set of feeding experiments was conducted, this time including [2-^{13}C]glucose as well. The inclusion of [2-^{13}C]glucose meant that the reliability of the anaplerotic flux estimates was improved such that the standard estimates were deemed to be acceptable (lower than 0.5). The inclusion of additional positionally-labelled substrates can therefore help to increase the accuracy of flux estimates.

A representation of the model used in all metabolic flux analysis in this study is shown in Figure 4.7. Half reactions are shown for the non-oxidative branch of the pentose phosphate pathway and the short-hand names of the reactions in the model are annotated onto the map.

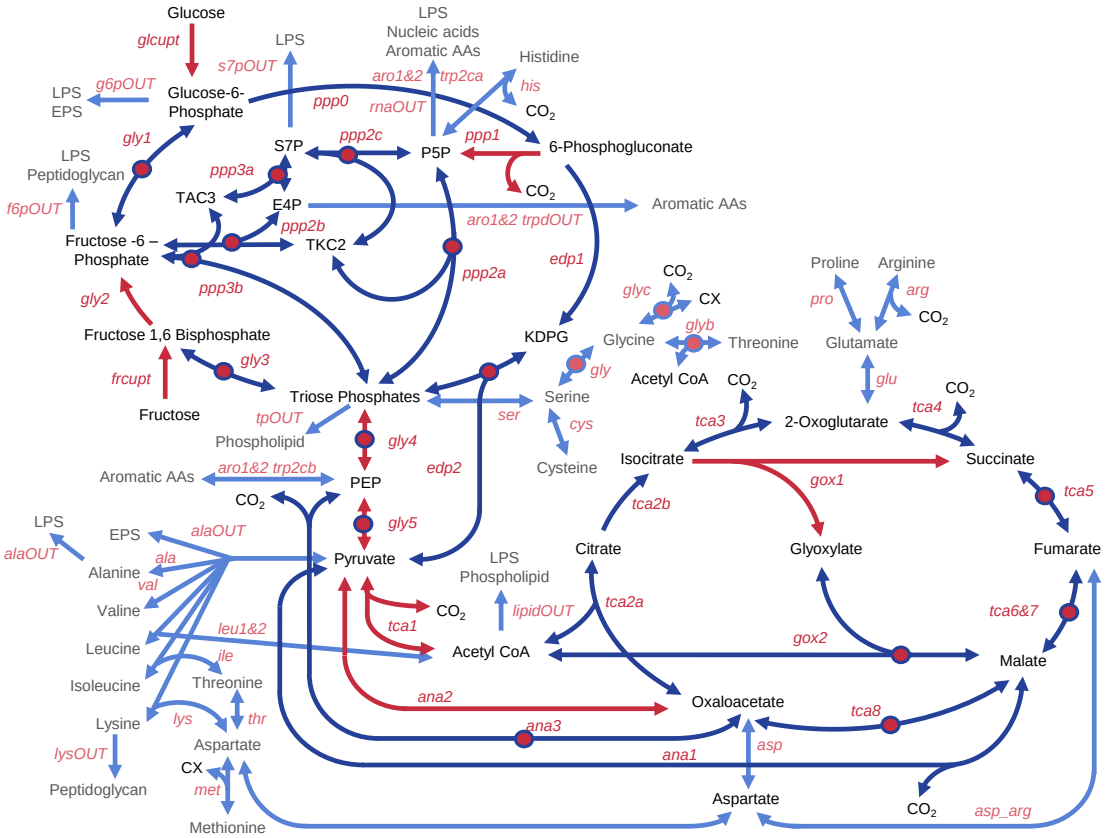

Figure 4.7: Full metabolic map of Pst DC3000 and Pfl SBW25. A diagrammatic representation of the fluxes included in network models of both strains with reaction names annotated onto the relevant fluxes in light red (flux name and reactions can be found in Appendix Table A.13). Dark blue arrows indicate central fluxes, whilst light blue represents reactions which lead to biomass outputs. Red arrows indicate fluxes which were modelled as free in the network. Double-headed arrows indicate the reaction was not constrained as to the direction of the flux and dots indicate free exchange fluxes. The follow abbreviations have been used: LPS, lipopolysaccharide; EPS, exopolysaccharide; S7P, sedoheptulose-7-phosphate; E4P, erythrose-4-phosphate; P5P, pentose-5-phosphates; AA, amino acid; KDPG, 2-keto-3-deoxy-6-phosphogluconate; PEP, phosphoenolpyruvate; CX, 5,10-methylenetetrahydrofolate; TAC3 and TKC2 are representative of intermediates of the pentose phosphate half reactions, as described by Kleijn *et al* (2005) [228] (these reactions can be found in Appendix Table A.13).

4.2.5 [2-^{13}C]glycine feeding shows no flux is present from serine to pyruvate

Initially a recycling pathway from serine to pyruvate was included in the models as annotations for L-serine dehydratase (*sdaA*) are present in the genomes of both Pst DC3000 (PSPTO_1886) and Pfl SBW25 (PFLU1035). A large flux from the triose phosphates to serine and from serine to pyruvate was predicted by 13CFLUX as the best explanation of the measurements provided. The size of these fluxes were thought to be unlikely, and a similar problem had also been encountered by Kruger *et al* (2011) in ^{13}C-MFA of *Arabidopsis thaliana* cell suspension culture [187]. In order to investigate whether this 'serine shunt' should be included in the model, a feeding experiment with [2-^{13}C]glycine was undertaken [187]. Glycine can be metabolised by conversion to serine and, in the presence of the proposed 'serine shunt', subsequent conversion into pyruvate. If the serine recycling flux was active under the glucose feeding conditions, carbon from the labelled glycine would be expected to be found in amino acids derived from pyruvate, such as alanine, valine and leucine. 2 mM [2-^{13}C]glycine was added to cultures of Pst DC3000 and Pfl SBW25 that had been growing in non-labelled glucose M9 overnight and had reached an OD of 0.35. These cultures were harvested at 0, 0.5, 1 and 2 hours and the resulting mass isotopomer abundances of a range of metabolites were determined (Figure 4.8). The results show that ^{13}C abundance is high in glycine (50.1 % in Pfl SBW25 and 33.5 % in, the slower-growing, Pst DC3000 after 2 hours) and also in serine (18.4 % in SBW25 and 30.9 % in DC3000). Interestingly, labelled glycine is more readily converted

into serine in Pst DC3000 after 2 hours than in Pfl SBW25. Labelled carbon can also be observed to increase over time in histidine (7.4 % in Pfl SBW25 and 7.5 % in DC3000 after 2 hours) and methionine (6.0 % in Pfl SBW25 and 7.8 % in Pst DC3000 after 2 hours). Glycine can be broken down to carbon dioxide and 5,10-methylenetetrahydrofolate (MTHF) by glycine dehydrogenase (decarboxylating), and MTHF is incorporated into the synthesis of both histidine and methionine.

Whilst labelled carbon is observed in glycine, serine, methionine and histidine, there is no evidence of labelled carbon in amino acids derived from pyruvate or in those derived from TCA cycle intermediates in either species. The data presented here is for protein hydrolysate, but the same patterns were observed in soluble metabolites. Thus the pathway from serine to pyruvate, whilst providing a better fit of the data, was discarded as no evidence was found of a major flux through this pathway. It is still currently unclear why the inclusion of this pathway should provide a better explanation of the measured data.

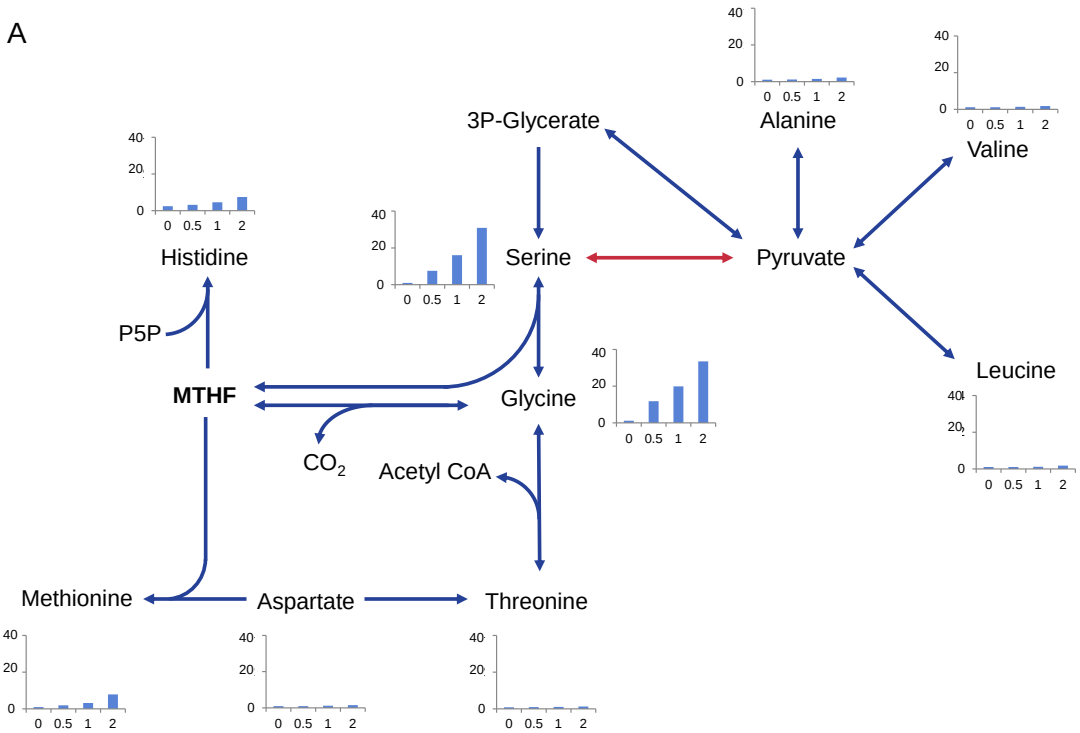
A
3P-Glycerate
Alanine
Valine
Histidine
Serine
Pyruvate
P5P
MTHF
Glycine
Leucine
CO_2
Acetyl CoA
Methionine
Aspartate
Threonine
40
20
0
0 0.5 1 2

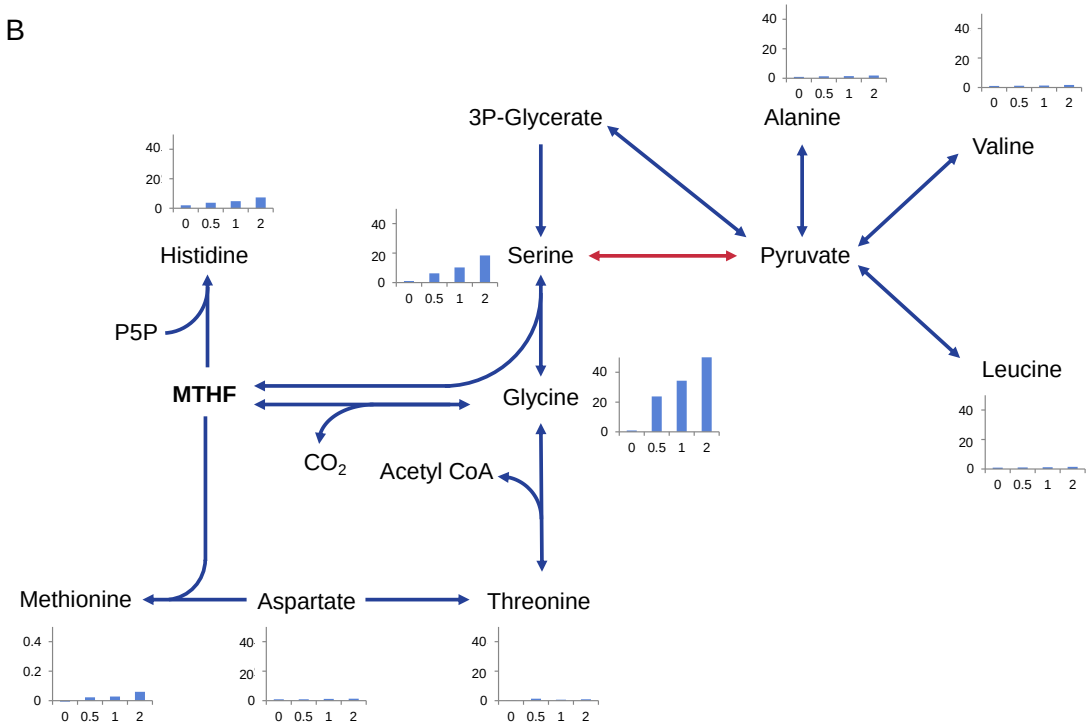

Figure 4.8: ^{13}C label present in amino acids in Pst DC3000 and Pfl SBW25 incubated with [2-^{13}C]glycine over 2 hours. Isotopomer abundances show an increase in label in certain amino acids over a 2 hour period in A) Pst DC3000 and B) Pfl SBW25. The red arrow indicates the pathway being assessed for activity, which is shown to be inactive in both species under the conditions tested as ^{13}C abundance does not increase in pyruvate-derived amino acids. Data shown is from protein hydrolysate and graphs show % abundance of label over time (hour). Samples were also analysed for soluble metabolites and these displayed the same patterns of label distribution. The following abbreviations have been used: P5P, pentose-5-phosphate; MTHF, 5,10-methylenetetrahydrofolate.

4.2.6 Metabolic flux analysis of Pst DC3000 and Pfl SBW25 under *hrp*-inducing and repressing conditions reveals differences in central carbon metabolism between treatments, but not between strains

Exploration of flux solution space using Monte Carlo simulated data

Six hundred Monte Carlo simulations were run of the final models for Pst DC3000 and Pfl SBW25 in the glucose (*hrp*-repressing) and fructose (*hrp*-inducing) treatments in order to fully explore the multi-dimensional flux space defined by the observed labelling data. Figure 4.9 shows the distribution of residua for all of the feasible solutions. The residua for these sets of solutions encompassed a wide range of values, though tended to cluster at the lower end of the spectrum. The identification of the first and second principal components in PCA analysis helped to better understand the nature of these solutions and how they grouped together [133]. Figures 4.10 and 4.11 were used to identify a subset of the solutions which could be used to generate the best fit starting values. In every model, a threshold for the inclusion of solutions was evident based on the tight clustering of solutions of the lowest values.

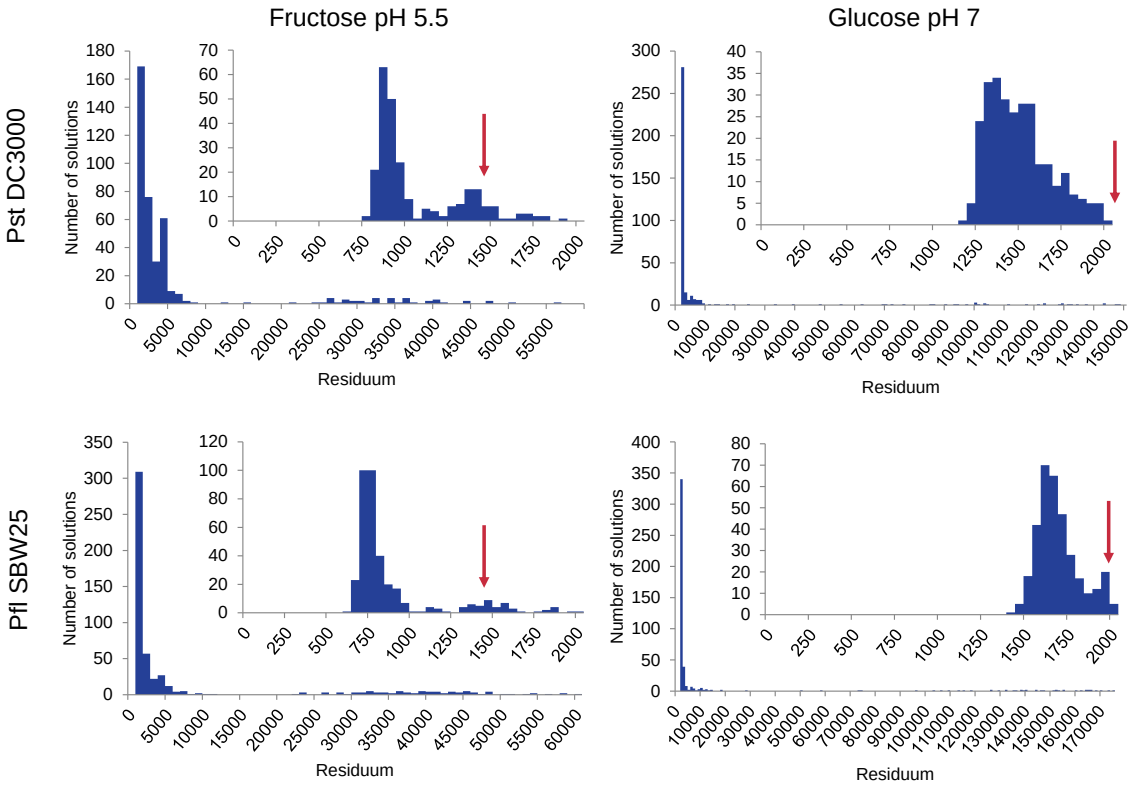

Figure 4.9: Histograms of the residua for feasible flux solutions. Histograms for each of the four models display the frequency distribution of the residua obtained from 600 Monte Carlo simulations. Intervals used were 1000 and 50 (inset histograms). Red arrows show the threshold value for inclusion into the set of best fit solutions which were used to generate starting values for the final model optimisations.

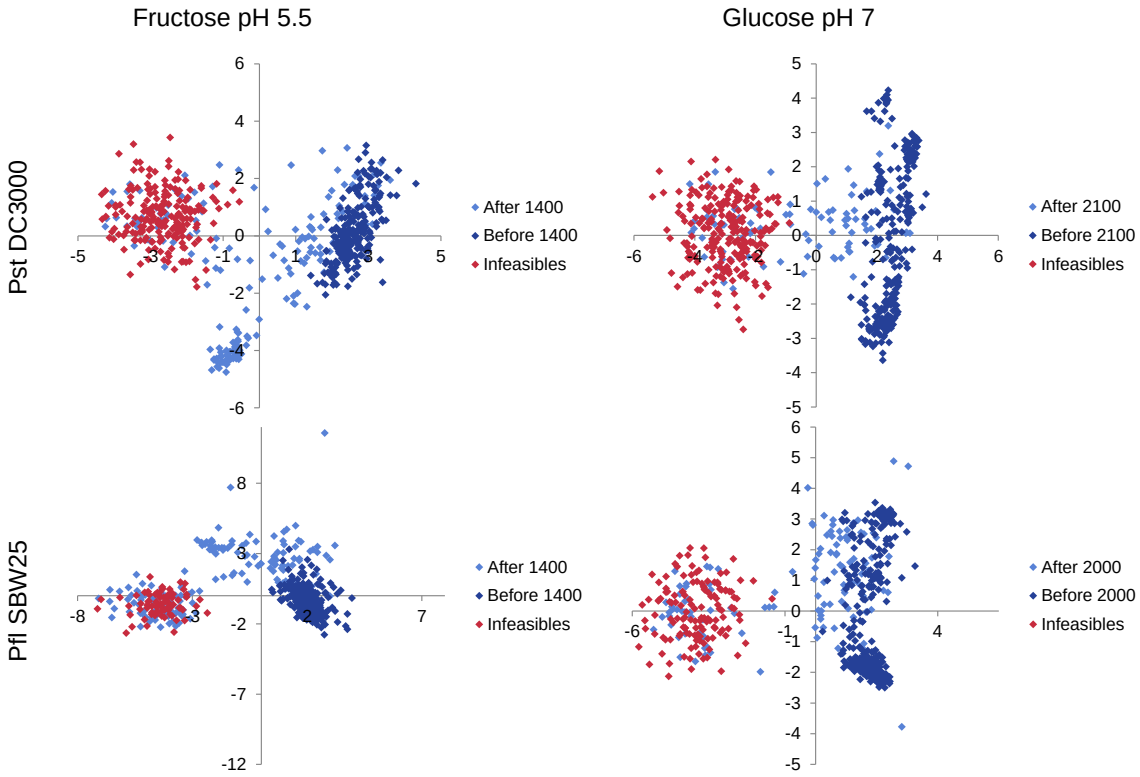

Figure 4.10: Distribution scores of the first two principal components plotted against one another show clustering of the selected best fit solutions. The scatterplots shown were obtained by principal component analysis using unit variance scaling of the data. Infeasible solutions are shown in red whilst feasible solutions are shown in blue. Feasible solutions which were used in the subsequent generation of the global best fit are shown in the darker blue, feasible solutions which were not included in this analysis are shown in light blue. The x-axis represents the first principal component and the y-axis the second.

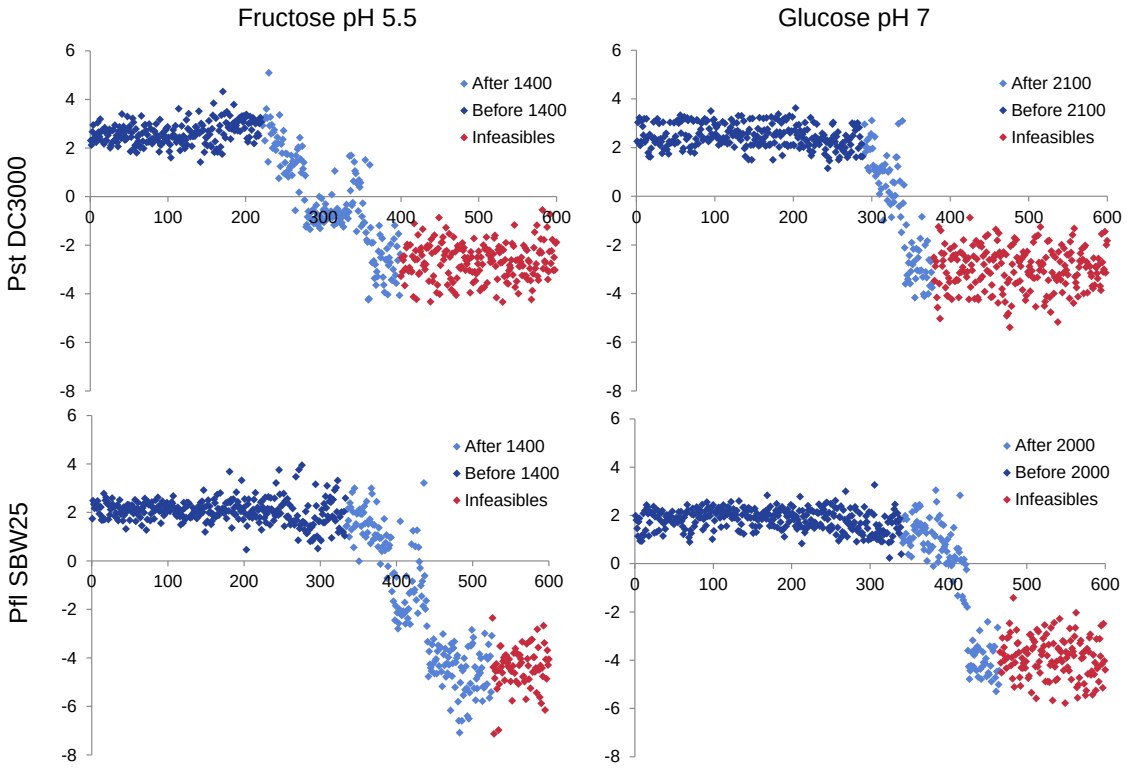

Figure 4.11: Distribution scores of the first principal component ranked in order of residua value. Principal component analysis identified the principal component from a set of 600 flux solutions for each of the models. The distribution scores were then arranged in order of lowest to highest residua along the x-axis. As previously, infeasible solutions are shown in red and feasible solutions in blue. The feasible solutions included in the best fit analysis (and coloured dark blue) can be seen to all have tightly correlated distribution scores.

Best fit solutions: goodness of fit

Following the averaging of the best fit solutions and the generation of the best fit flux estimates, each model was analysed by the χ^2 test. Table 4.2 displays a summary of the statistics for the best fit solutions. This gives an overview of the ability of the models to explain the given measurements. All four models passed well below the χ^2 threshold for an acceptable fit. The fructose models have the lowest residua, owing to fewer measurements present in the model as a result of data from only two labelling strategies being incorporated. The best fit residuum is, inevitably,

correlated with the number of measurements in the model.

	Pst DC3000		**Pfl SBW25**	
	Glucose pH 7	**Fructose pH 5.5**	**Glucose pH 7**	**Fructose pH 5.5**
Model type	Triple	Double	Triple	Double
Datasets	[$^{13}C_6$]Glucose [1-^{13}C]Glucose [2-^{13}C]Glucose	[$^{13}C_6$]Fructose [1-^{13}C]Fructose	[$^{13}C_6$]Glucose [1-^{13}C]Glucose [2-^{13}C]Glucose	[$^{13}C_6$]Fructose [1-^{13}C]Fructose
No. measurements	1099	804	1197	748
No. metabolite fragments	201	149	216	142
Degrees of freedom	28	28	28	28
χ^2 (95% significance)	939.7	686.4	1025.9	635.0
Best fit residuum	409.5 (pass)	208.5 (pass)	567.6 (pass)	107.8 (pass)

Table 4.2: χ^2 statistical analysis of the best fit models. χ^2 values are given at the 95 % confidence levels in accordance with Antoniewicz *et al* 2007 [119]

The measured isotopomer abundances were also assessed against the predicted isotopomer abundances of the best fit solutions (Figure 4.12). In all four cases, the measured data and predicted data were tightly correlated (R^2 were all above 0.99) and, therefore, in good agreement [120].

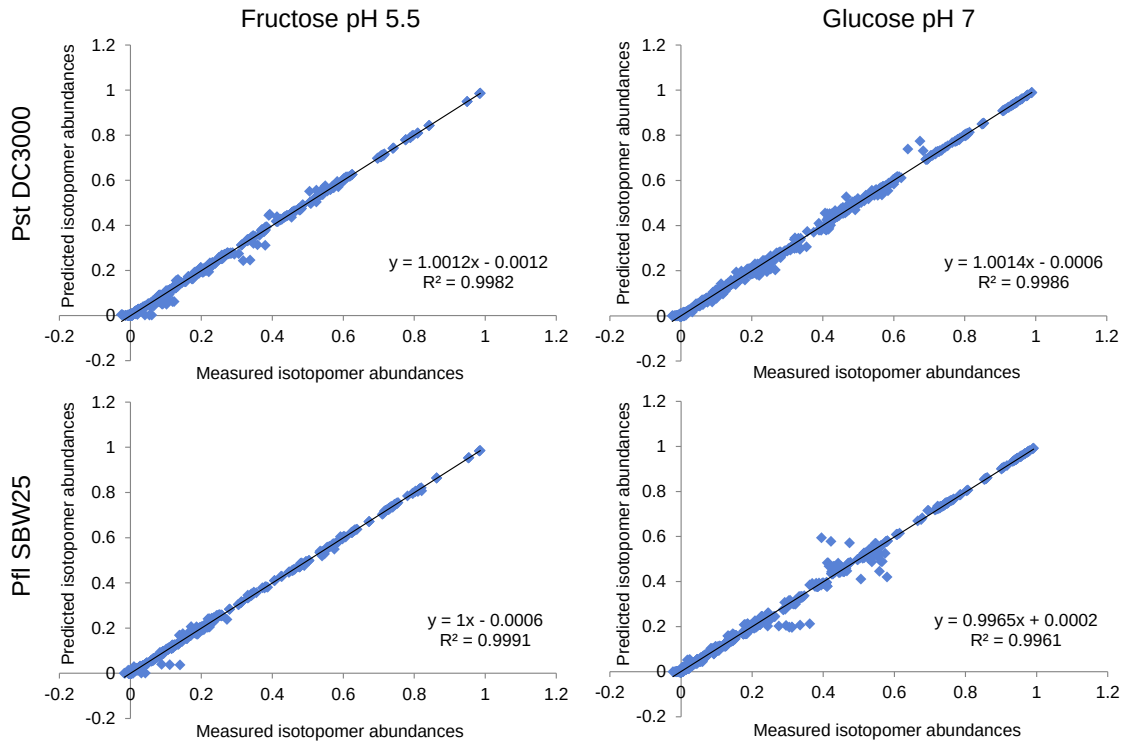

Figure 4.12: Measured versus predicted isotopomer abundances. Both measured isotopomer abundances and those predicted by 13CFLUX in the global best fit solutions were plotted against one another. This analysis shows there are very few changes to measurements which 13CFLUX predicts would improve the fit of the models.

Best fit solutions: flux maps and statistical reliability

The final flux estimates for all of the four models are presented in Table 4.3 along with the standard deviation estimates for free fluxes obtained from EstimateStat. The data shown has been normalised to the initial uptake flux (value=1). Comparative analyses of the four solutions show that there are no significant differences in flux estimate between the strains for either of the two treatments, though there are differences in the flux estimates between the two treatments (Figures 4.13 and 4.14).

	Fructose pH 5.5		**Glucose pH 7**	
Flux	**Pst DC3000**	**Pfl SBW25**	**Pst DC3000**	**Pfl SBW25**
upt	1.000±0.034	1.000±0.032	1.000±0.029	1.000±0.020
upt1	0.926±0.032	0.893±0.028	0.935±0.027	0.964±0.020
upt0	0.074±0.003	0.107±0.003	0.065±0.002	0.036±0.001
uptU_U	0.185±0.006	0.179±0.006	0.187±0.005	0.193±0.004
upt0_U	0.815±0.028	0.821±0.026	0.813±0.023	0.807±0.016
cxupt	0.000±0.008	0.000±0.024	0.010±0.048	0.026±0.063
CO2upt	0.530±0.089	0.581±0.063	0.581±0.075	0.508±0.052
gly1	-0.831±0.040	-0.785±0.023	-0.040±0.137	0.017±0.039
gly2	-0.888±0.054	-0.856±0.036	-0.134±0.047	-0.084±0.020
gly3	0.112±0.053	0.144±0.037	-0.134±0.047	-0.084±0.020
gly4	0.743±0.074	0.775±0.063	0.551±0.046	0.574±0.033
gly5	0.807±0.098	0.778±0.088	0.535±0.063	0.525±0.050
ppp0	0.822±0.040	0.776±0.023	1.034±0.149	0.977±0.044
ppp1	0.124±0.097	0.109±0.059	0.078±0.148	0.080±0.052
ppp2a	0.012±0.064	-0.005±0.039	-0.024±0.099	-0.034±0.035
ppp2b	-0.025±0.032	-0.037±0.020	-0.039±0.049	-0.048±0.017
ppp2c	0.036±0.032	0.032±0.020	0.015±0.049	0.014±0.017
ppp3a	0.036±0.032	0.032±0.020	0.014±0.049	0.014±0.017
ppp3b	0.036±0.032	0.032±0.020	0.014±0.049	0.014±0.017
edp1	0.698±0.082	0.667±0.054	0.956±0.030	0.897±0.022
edp2	0.698±0.082	0.667±0.054	0.956±0.030	0.897±0.022
tca1	0.779±0.105	0.720±0.078	1.138±0.063	1.033±0.060
tca2	0.673±0.074	0.611±0.068	0.848±0.046	0.737±0.035
tca2b	0.673±0.074	0.611±0.068	0.848±0.046	0.737±0.035
tca3	0.673±0.097	0.611±0.083	0.634±0.053	0.521±0.035
tca4	0.579±0.097	0.512±0.083	0.553±0.053	0.432±0.035
tca5	0.579±0.074	0.512±0.068	0.768±0.046	0.648±0.035
tca6	0.294±0.037	0.261±0.034	0.388±0.023	0.329±0.017
tca7	0.294±0.037	0.261±0.034	0.388±0.023	0.329±0.017
tca8	0.326±0.400	0.250±0.036	0.106±0.037	-0.078±0.447
gox1	0.000±0.070	0.000±0.044	0.215±0.036	0.216±0.035
gox2	0.000±0.070	0.000±0.044	0.215±0.036	0.216±0.035
ana1	0.261±0.450	0.272±0.070	0.884±0.074	0.952±0.434
ana2	0.735±0.386	0.718±0.081	1.011±0.072	1.087±0.442
ana3	0.169±0.068	0.123±0.065	0.076±0.036	0.057±0.043
g6pOUT	0.009	0.009	0.006	0.006
f6pOUT	0.069	0.066	0.070	0.067
s7pOUT	0.000	0.000	0.000	0.000
co2	2.673±0.208	2.498±0.185	3.162±0.148	2.746±0.100
rna	0.044	0.045	0.059	0.068
rnaOUT	0.044	0.045	0.059	0.068
tpOUT	0.024	0.023	0.015	0.015
lipidOUT	0.079	0.074	0.048	0.048
glu	0.086	0.090	0.073	0.079
gluOUT	0.059	0.056	0.048	0.052
asp	0.219±0.009	0.233±0.005	0.192±0.002	0.214±0.002
aspOUT	0.043	0.045	0.038	0.042
arg	0.009	0.010	0.007	0.009
argOUT	0.009	0.010	0.007	0.009
asp_arg	0.009	0.010	0.007	0.009
ser	0.130±0.006	0.121±0.013	0.083±0.016	0.093±0.015
cys	0.029	0.034	0.026	0.030
cysOUT	0.029	0.034	0.026	0.030

	Fructose pH 5.5		**Glucose pH 7**	
Flux	**Pst DC3000**	**Pfl SBW25**	**Pst DC3000**	**Pfl SBW25**
gly	0.065±0.006	0.045±0.013	0.028±0.016	0.026±0.015
glyb	0.009±0.009	0.004±0.005	0.005±0.002	0.003±0.002
glyc	0.048±0.008	0.017±0.014	0.009±0.017	0.002±0.016
glyOUT	0.026	0.032	0.023	0.027
cxeff	0.059±0.016	0.000±0.050	0.000±0.081	0.000±0.094
ala	0.030	0.035	0.027	0.031
alaOUT	0.030	0.035	0.027	0.031
leu1	0.064	0.071	0.056	0.064
leu	0.036	0.039	0.031	0.036
leuOUT	0.036	0.039	0.031	0.036
val	0.028	0.032	0.025	0.028
valOUT	0.028	0.032	0.025	0.028
met	0.029	0.034	0.026	0.030
metOUT	0.029	0.034	0.026	0.030
thr	0.071±0.009	0.072±0.005	0.058±0.002	0.065±0.002
thrOUT	0.036	0.038	0.030	0.036
ile	0.026	0.030	0.023	0.026
ileOUT	0.026	0.030	0.023	0.026
aro1	0.026	0.030	0.023	0.027
aro2	0.026	0.030	0.023	0.027
phe_tyr	0.052	0.060	0.046	0.053
pheOUT	0.052	0.060	0.046	0.053
pro	0.027	0.034	0.025	0.028
proOUT	0.027	0.034	0.025	0.028
lys	0.034	0.036	0.032	0.034
lys1	0.034	0.036	0.032	0.034
lysOUT	0.068	0.072	0.063	0.068
his	0.024	0.028	0.021	0.024
hisOUT	0.024	0.028	0.021	0.024
trp2ca	0.008	0.009	0.007	0.008
trpaOUT	0.008	0.009	0.007	0.008
trp2cb	0.008	0.009	0.007	0.008
trpbOUT	0.008	0.009	0.007	0.008
ser_trpcOUT	0.066	0.076	0.055	0.067
trpdOUT	0.008	0.009	0.007	0.008

Table 4.3: Flux values for each of the global best fit solutions as determined by 13CFLUX. Values are given to three decimal places and standard deviations were obtained using EstimateStat. Constrained fluxes do not have standard deviations.

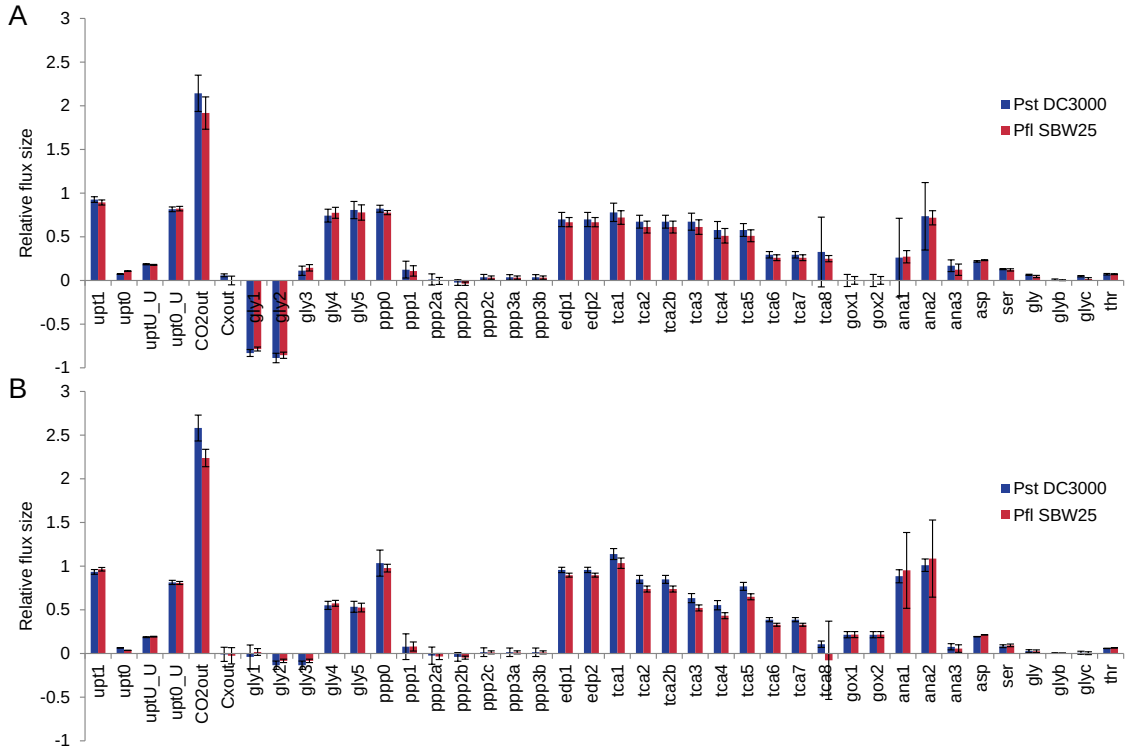

Figure 4.13: Net fluxes of global best fit solutions. The bar charts represent the net flux values of the models, normalised to the uptake flux (uptake flux = 1). A) The two fructose pH 5.5 models are plotted together as they show no significant differences from one another. This is also true of the glucose pH 7 models, B). All non-constrained net fluxes (free or determined) are shown with error bars representing standard deviations obtained from EstimateStat.

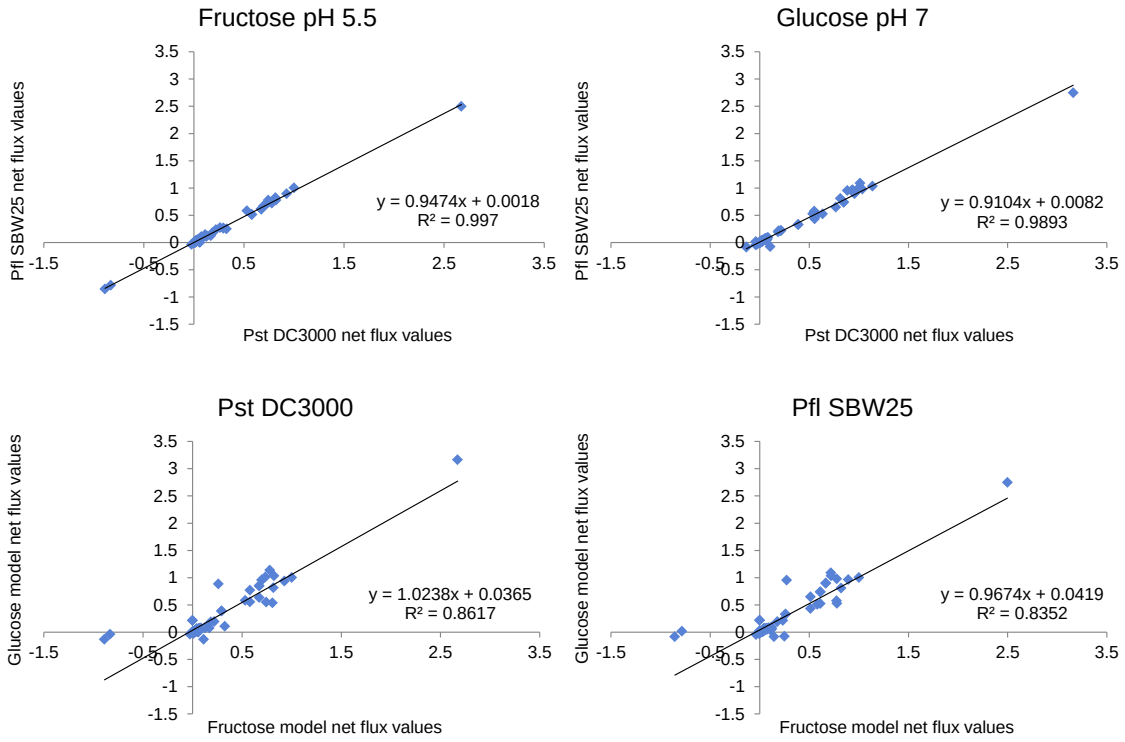

Figure 4.14: A comparison of flux values between treatments and between strains. Net flux solutions from different models were plotted against one another to show the differences and similarities between the global best fit solutions. Exchange fluxes were not used in this analysis owing to the unreliability of many of the estimates. The comparisons show that strains measured under the same treatment are have highly similar fluxes, whilst larger differences exist in the solutions for the same strain under different treatments.

Almost all of the net fluxes in the two models are well defined apart from *tca8*, *ana1* and *ana2* (malate to OAA, malate to pyruvate and pyruvate to OAA)in the Pst DC3000 fructose and Pfl SBW25 glucose models. Notably, both these models lack isotopomer abundance data for malate and it is possible that the absence of information on the label distribution in malate is creating this uncertainty. Thus, malate may be an important TCA intermediate for the resolution of the anaplerotic node in pseudomonads.

The exchange flux values of the best fit solutions are shown in Figure 4.15. Only a

few of these fluxes are well defined. In the fructose-fed models, *gly3*, *ppp2a*, *ppp2b*, *gly*, *glyb* and *glyc* (as well as *tca8* for Pfl SBW25) all have low standard deviations (less than 100 % of the exchange flux). In the glucose-fed models, *gly5*, *ppp2a*, *tca6*, *tca7*, *tca8*, *gox2*, *gly*, *glyb* and *glyc* (as well as *tca5* for Pfl SBW25) all have low standard deviations (less than 100 % of the exchange flux). The glucose-fed models have more exchange fluxes which are well defined: this is likely to be due to the inclusion of [2-^{13}]glucose, which appears to add particular accuracy to the resolution of TCA cycle exchange fluxes.

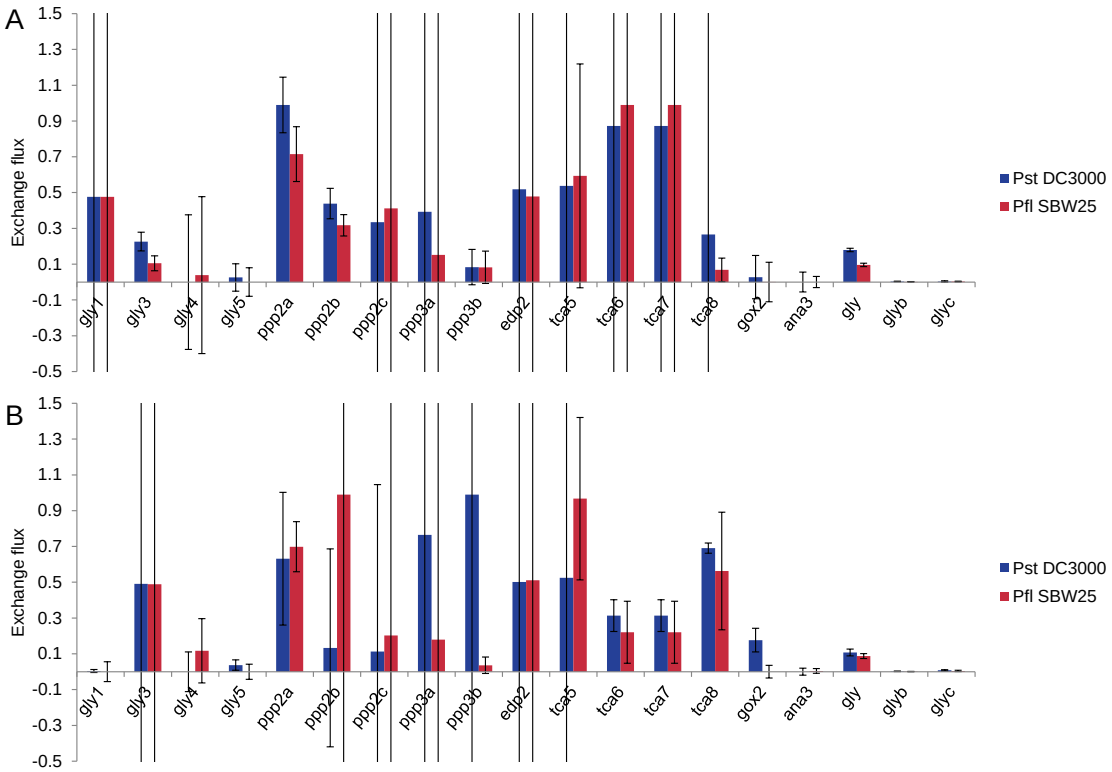

Figure 4.15: Exchange fluxes of global best fit solutions. Exchange flux values are shown for reactions where the exchange flux was allowed to be free, that is, the reaction was expected to show some level of reversibility. (A) Exchange fluxes for fructose pH 5.5 models and (B) exchange fluxes for glucose pH 7 models. Standard deviations of these measurements, obtained from EstimateStat, were used as error bars. The large size of the error associated with some of the fluxes means the extent of these errors is not shown. Exchange fluxes with deviations larger than 0.4 are thought to be very poorly defined, and therefore, beyond this point, the size of the error is immaterial.

In addition to analysing the best fit solutions using EstimateStat, the set of solutions generated by Monte Carlo simulations was used to provide a separate estimate of the degree to which the free fluxes in the models were defined. Of the solutions included in the final best fit optimisation, each free flux was sorted into ascending order and the 25^{th} and 75^{th} percentile values were obtained for each set of fluxes. These values, along with the best fit solution are shown plotted in Figure 4.16 for each of the models. This analysis show very similar results to that of the standard deviations obtained from EstimateStat, that is, specific fluxes are very tightly defined (such as *ana3*_XCH), whilst others appear to have a broader range of solutions (such as *gly1*_XCH).

A particular issue occurred with the *gly2* flux in Pst DC3000 under glucose-fed conditions: both large and small fluxes were found in the set of solutions and the average of these led to an intermediate value which the final optimisation struggled to resolve to a suitably low residuum. It was noticed that in solutions with a high flux through *gly2* there would be small fluxes through *gly4* and *gly5* and that the reverse was also true. Both types of solutions were found evenly distributed amongst solutions with the lowest residua, and so it was not immediately evident which solution was most accurate. Therefore, both sets of extreme starting values were examined and two additional final optimations were run. The solution with the lowest residuum was included in the final set of solutions, where the flux through *gly2* was smaller and the fluxes through *gly4* and *gly5* larger, and this also was in agreement with the best fit solution of Pfl SBW25 under glucose-fed conditions.

Interestingly, the range of solutions for *ana2* (pyruvate to OAA) in the glucose models varied by a large amount - from 1.45 to -1.25 in Pst DC3000 and from 1.39 to -2.1 in Pfl SBW25. A reverse flux as large as this would have a knock-on effect on other reactions, and it is likely that *ana1* would operate in reverse to compensate (though only information on free fluxes is available in this analysis). Thus, it appears that whilst the best fit solution has these two reactions operating in their conventional directions with acceptable levels of error, the isotopomer balancing data can be used to describe these fluxes as acting in either direction.

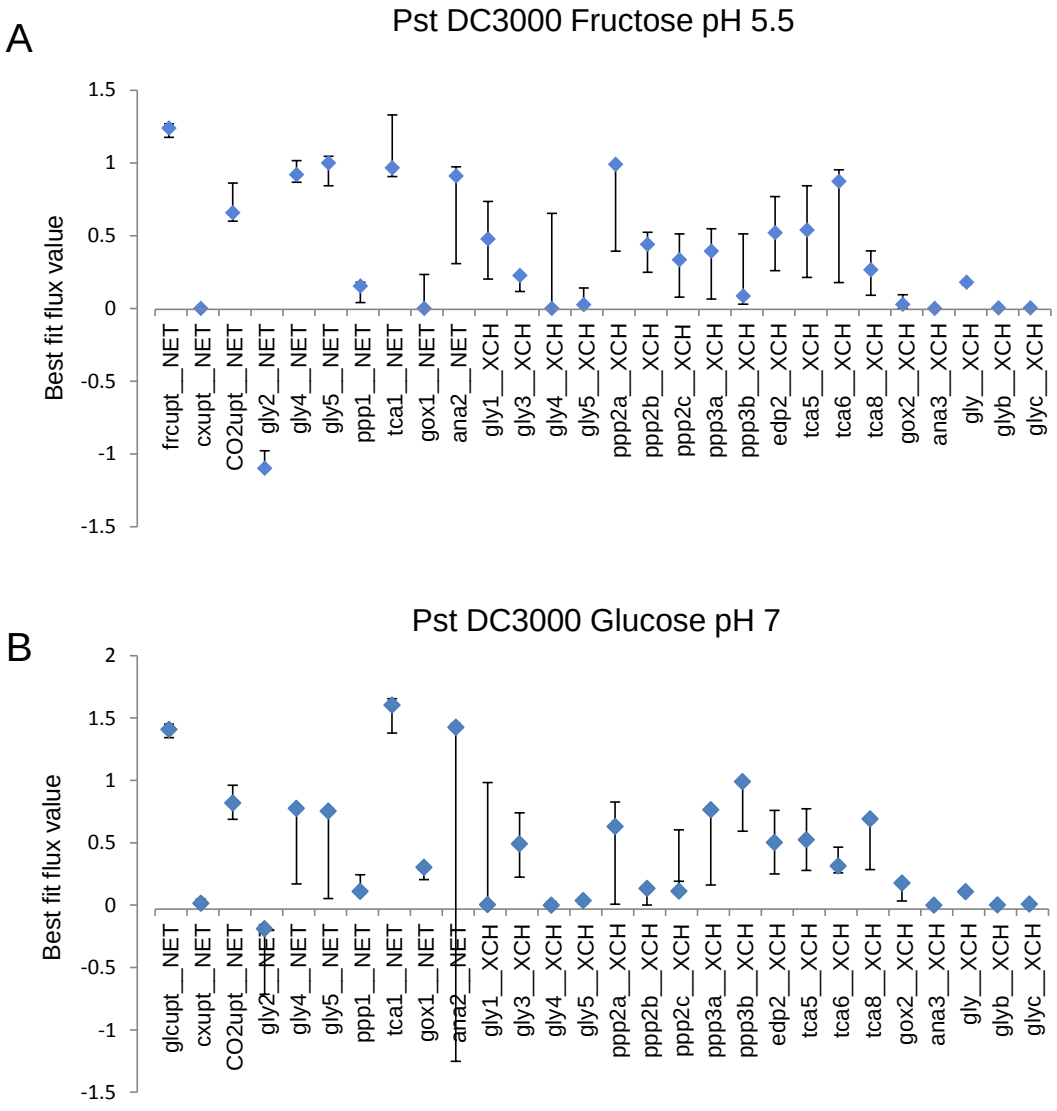
A
Pst DC3000 Fructose pH 5.5
Best fit flux value
1.5
1
0.5
0
-0.5
-1
-1.5
frcupt__NET
cxupt__NET
CO2upt__NET
gly2__NET
gly4__NET
gly5__NET
ppp1__NET
tca1__NET
gox1__NET
ana2__NET
gly1__XCH
gly3__XCH
gly4__XCH
gly5__XCH
ppp2a__XCH
ppp2b__XCH
ppp2c__XCH
ppp3a__XCH
ppp3b__XCH
edp2__XCH
tca5__XCH
tca6__XCH
tca8__XCH
gox2__XCH
ana3__XCH
gly__XCH
glyb__XCH
glyc__XCH
B
Pst DC3000 Glucose pH 7
Best fit flux value
2
1.5
1
0.5
0
-0.5
-1
-1.5
glcupt__NET
cxupt__NET
CO2upt__NET
gly2__NET
gly4__NET
gly5__NET
ppp1__NET
tca1__NET
gox1__NET
ana2__NET
gly1__XCH
gly3__XCH
gly4__XCH
gly5__XCH
ppp2a__XCH
ppp2b__XCH
ppp2c__XCH
ppp3a__XCH
ppp3b__XCH
edp2__XCH
tca5__XCH
tca6__XCH
tca8__XCH
gox2__XCH
ana3__XCH
gly__XCH
glyb__XCH
glyc__XCH

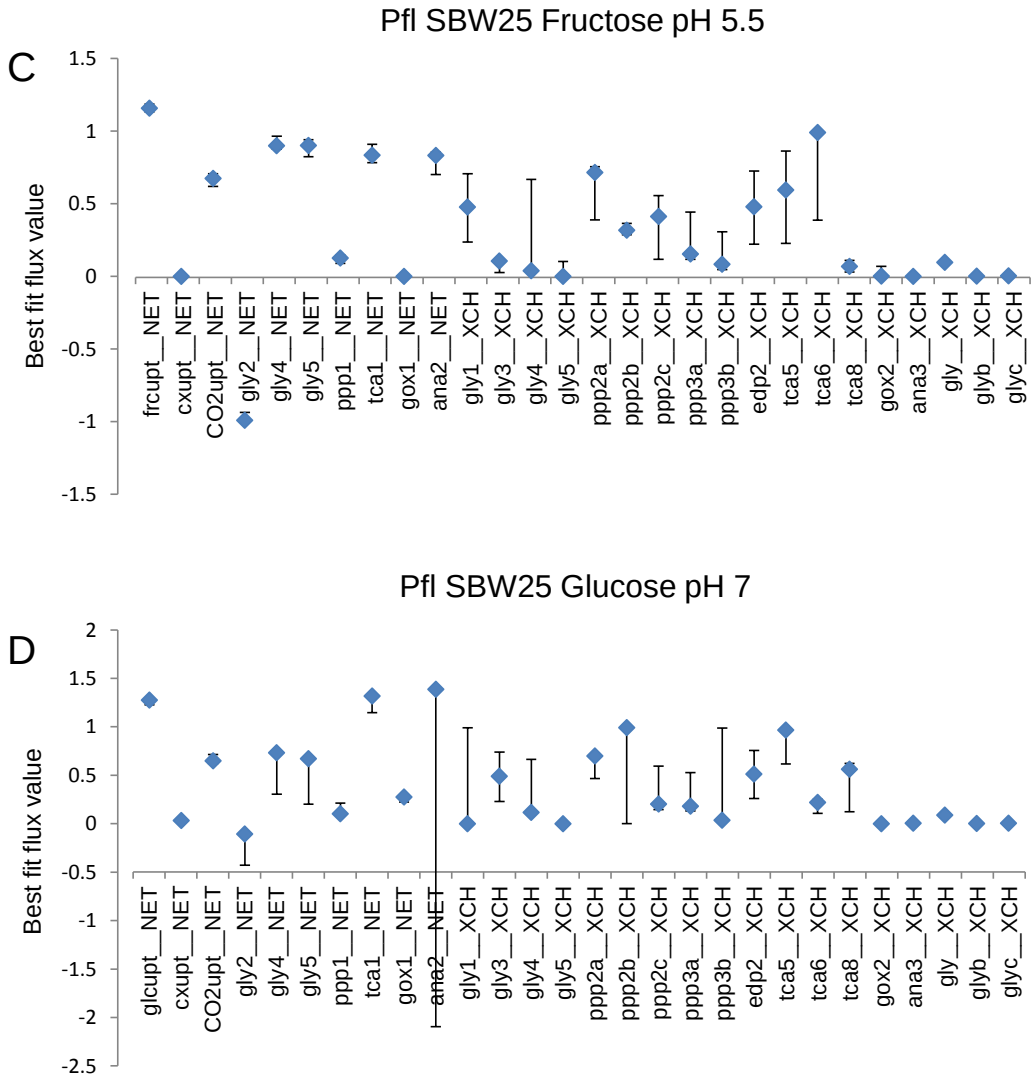

Figure 4.16: Free fluxes plotted with the 25^{th} and 75^{th} percentile values from ranked feasible solutions. All feasible solutions which were included in the best fit analysis were ranked, for each free flux, in order of magnitude. The 25^{th} and 75^{th} percentile values were obtained and these were plotted alongside the global best fit solution values. This analysis gives some indication of the confidence level associated with each of the free fluxes.

Description of changes in fluxes associated with *hrp* inducing and non-inducing media

As the fluxes between Pst DC3000 and Pfl SBW25 were found to be very similar for each of the treatments, they will be discussed together, and this is perhaps indicative

of a '*Pseudomonas*' response to these two carbon sources. This is interesting as type III expression differs between the two species (virulence expression is strongly induced by fructose in Pst DC3000 in comparison to treatment with glucose, but to a much lesser extent in Pfl SBW25). The maps in Figures 4.17 and 4.18 show the fluxes of the four models and compares each of the two treatments.

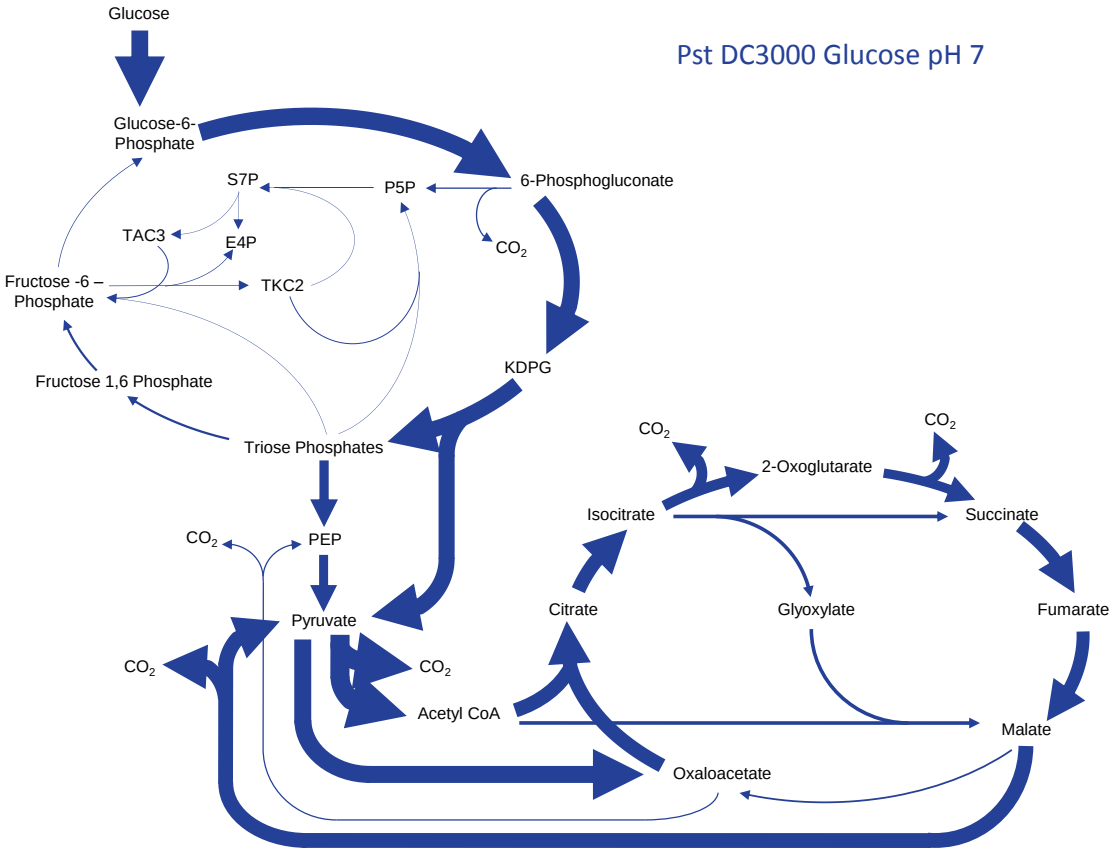

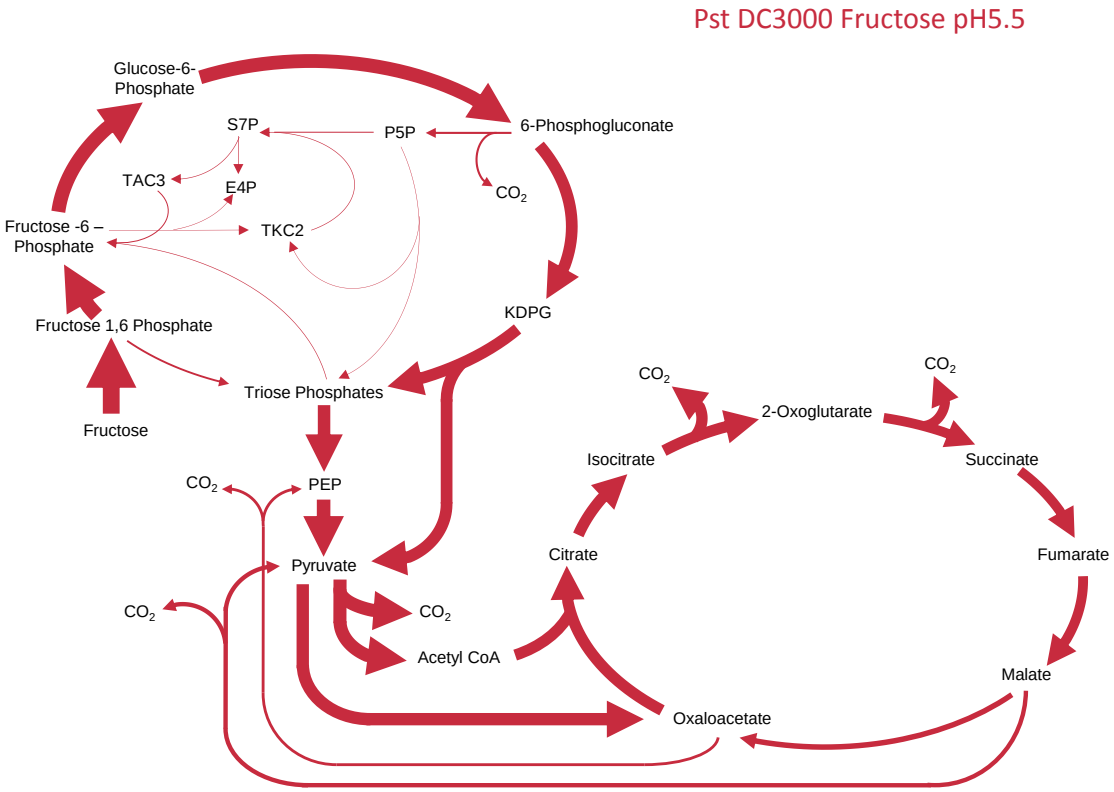
Pst DC3000 Fructose pH5.5
Glucose-6-Phosphate
6-Phosphogluconate
P5P
S7P
TAC3
E4P
TKC2
CO2
Fructose -6 – Phosphate
KDPG
Fructose 1,6 Phosphate
Triose Phosphates
Fructose
PEP
CO2
Pyruvate
Acetyl CoA
Citrate
Isocitrate
2-Oxoglutarate
Succinate
Fumarate
Malate
Oxaloacetate

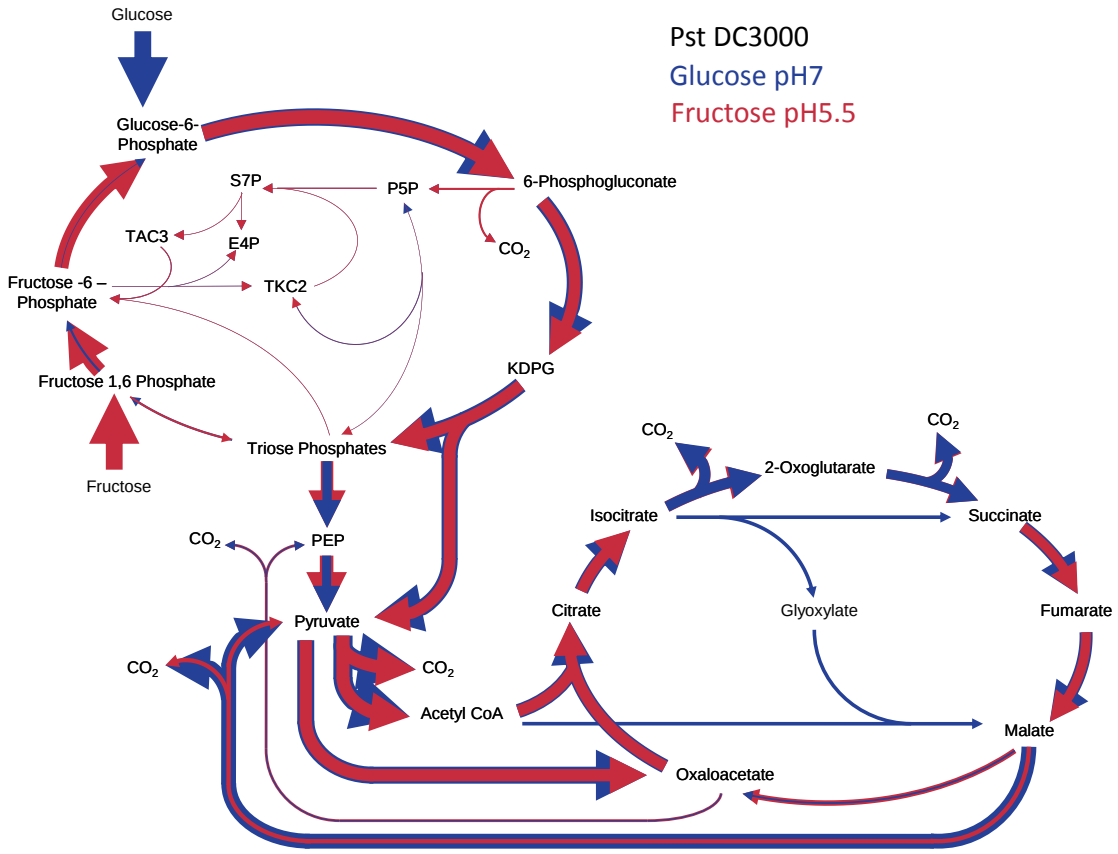

Figure 4.17: Metabolic flux maps of Pst DC3000 in fructose pH 5.5 and glucose pH 7 conditions. The global best fit solution of each of the treatment models can be displayed as a metabolic map, where the arrow direction and size indication the direction and size of the flux. Standard deviations and exchange flux values are not shown in order to retain clarity in the diagrams. In addition, only the central pathways of metabolism are included. The maps can be compared by superimposing one on another and this has been done where the greatest differences were observed: between treatments.

In all four models, the primary route of glucose metabolism is through the ED pathway, rather than the PP pathway or glycolysis. Indeed, for the fructose-fed models, though the point of entry for fructose is fructose-1,6-bisphophate, the carbon is routed primarily in the reverse direction through glycolytic pathways in order that it can flow through the ED pathway. ED pathway fluxes in the glucose-fed models were notably larger than those of the fructose-fed ones (around 0.92 in comparison to 0.68), due to a larger recycling flux through the triose phosphates from the ED

pathway. The reaction *gly3*, which is the conversion of FBP to triose phosphates (G3P and DHAP), operated a small flux in the forwards direction in fructose models but in the reverse direction (from the triose phosphates to FBP) in the glucose models (though this flux was also small), thus providing the recycling flux for the ED pathway. Fluxes through the PP pathway are small, particularly through the non-oxidative section and several of these fluxes operate in the reverse direction (primarily *ppp2b* in both models). The PP exchange fluxes also reveal a high level of uncertainty, though where exchanges can be deduced, reversibility appears to be high, apart from in *ppp3b*. It is likely that these PP fluxes serve a purely biosynthetic function, with the precursors for nucleic acids, aromatic amino acids and histidine all drawn from this section of the metabolic network.

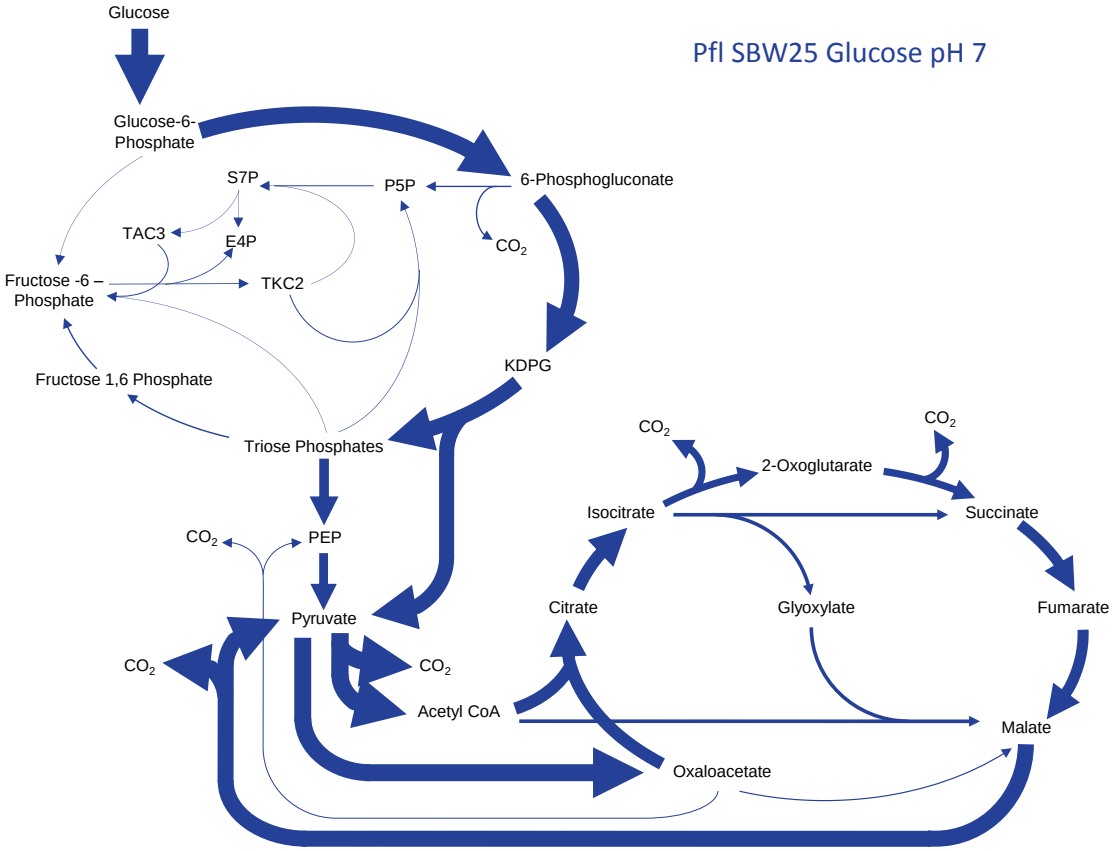

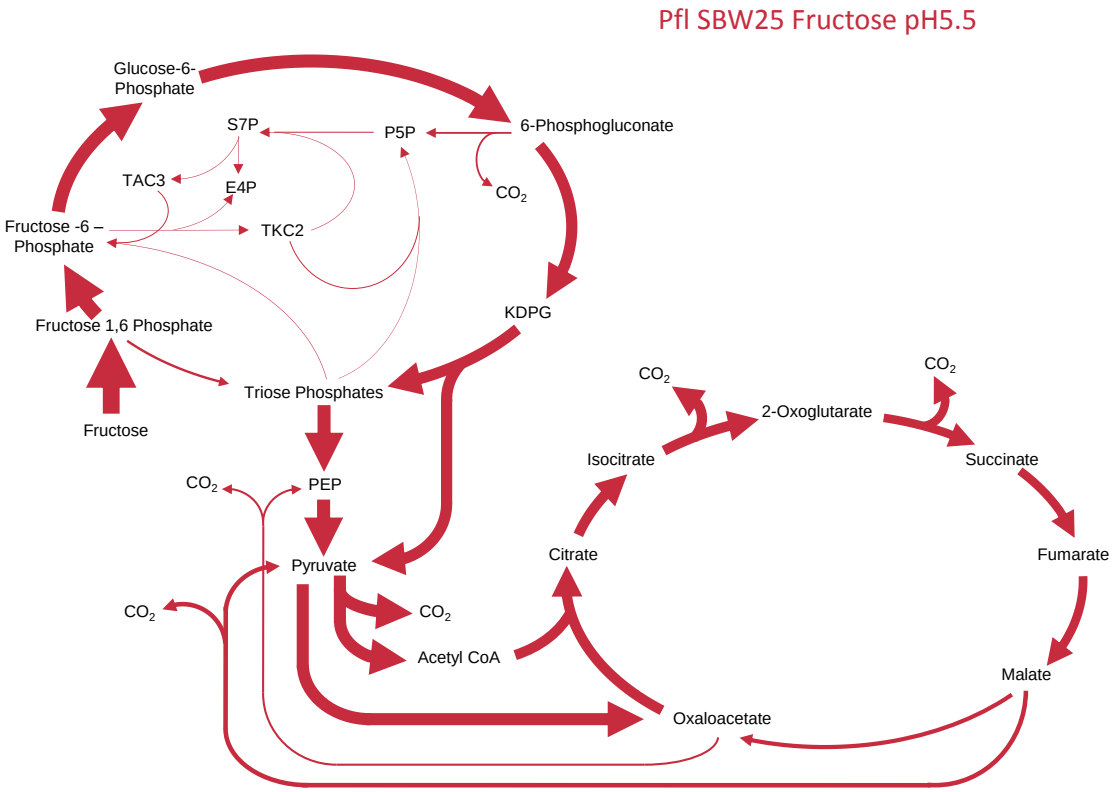
Pfl SBW25 Fructose pH5.5
Glucose-6-Phosphate
6-Phosphogluconate
S7P
P5P
TAC3
E4P
CO2
Fructose -6 – Phosphate
TKC2
KDPG
Fructose 1,6 Phosphate
Triose Phosphates
Fructose
CO2
2-Oxoglutarate
CO2
Isocitrate
Succinate
CO2
PEP
Citrate
Fumarate
Pyruvate
CO2
CO2
Acetyl CoA
Malate
Oxaloacetate

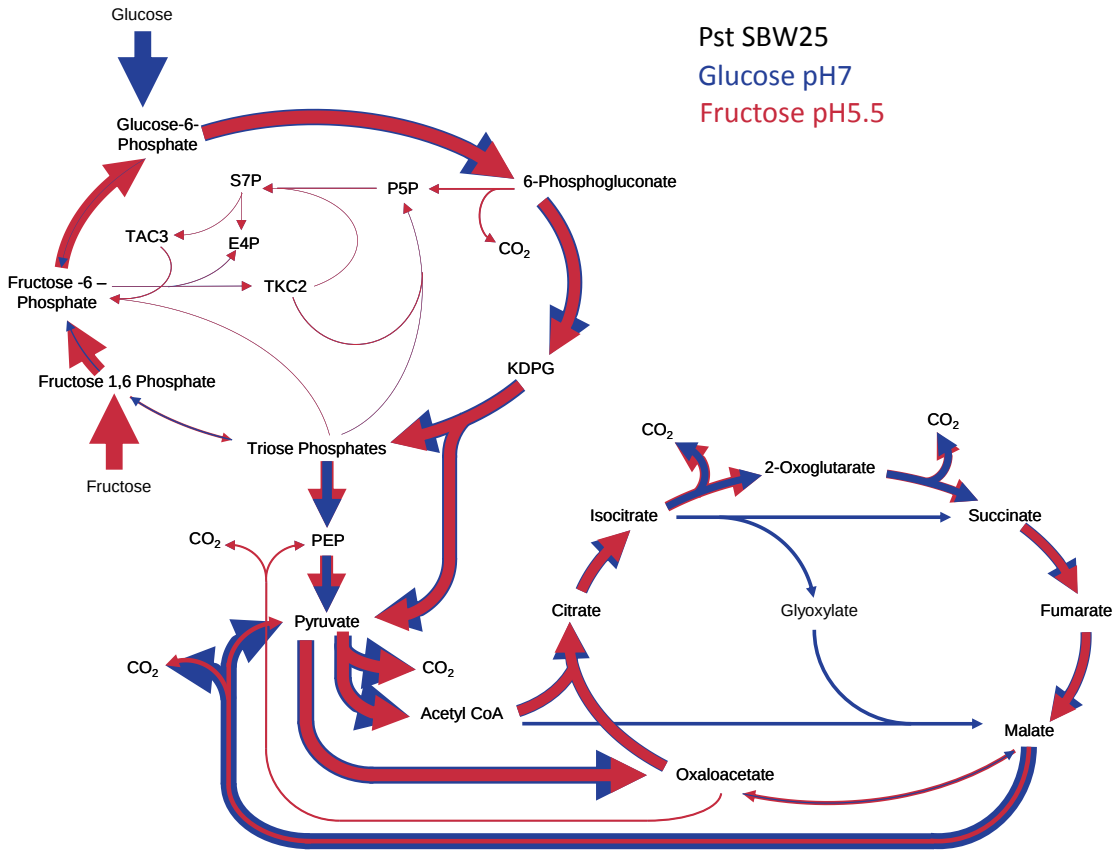

Figure 4.18: Metabolic flux maps of Pfl SBW25 in fructose pH 5.5 and glucose pH 7 conditions. The global best fit solution of each of the treatment models can be displayed as a metabolic map, where the arrow direction and size indication the direction and size of the flux. Standard deviations and exchange flux values are not shown in order to retain clarity in the diagrams. In addition, only the central pathways of metabolism are included. The maps can be compared by superimposing one on another and this has been done where the greatest differences were observed: between treatments.

Fluxes though the lower part of glycolysis, from the triose phosphates to pyruvate, were substantial in all models, though in the glucose-fed models they were around 0.56 whilst in the fructose-fed models this flux was larger at around 0.76. Fluxes entering the TCA cycle were also large, though these were higher in the glucose models (glucose-fed models: 1.1, fructose-fed models: 0.75). A notable difference around the TCA cycle was the presence of the glyoxylate shunt in the glucose models and its absence in the fructose models. The flux between malate and OAA provides

another difference: the fructose models have a larger flux than the glucose models for this reaction, though in both feeding strategies this flux is much smaller than other fluxes of the TCA cycle.

Finally, the anaplerotic reactions show largely similar patterns between the two models, though these differ in magnitude. The pathway between OAA and PEP is estimated to have a small forwards flux with very little reversibility in all models. *ana1* (malate to pyruvate) and *ana2* (pyruvate to OAA) have very large fluxes in the glucose models (around 0.92 and 1.05 respectively) as does *ana2* in the fructose models (0.72), however, the *ana1* flux is much smaller in the fructose models (0.27).

All of these observed differences are discussed and compared against existing *Pseudomonas* models in the following section.

4.3 Discussion

4.3.1 Similarities in metabolic capabilities and biomass composition between Pst DC3000 and Pfl SBW25

The process of producing metabolic flux maps involves collecting information about the metabolic capabilities and outputs of the organism(s) of interest. In this study, biomass composition, identifying the genes involved in central carbon metabolism and predicted metabolic pathways were all required for the model used to build

flux maps for Pst DC3000 and Pfl SBW25. Pst DC3000 is predicted to have fewer genes involved in central carbon metabolic pathways than Pfl SBW25, however, both species were predicted to have at least one gene for each pathway, making their central carbon metabolic networks identical. This implies that central carbon metabolism is strongly conserved across the *P. syringae*/*P. fluorescens* clade of the *Pseudomonas* phylogeny. The biomass measurements also showed a high degree of similarity between the strains, with the only notable difference being the proportion of protein that made up cell dry weight: Pfl SBW25 had slightly more protein per cell than Pst DC3000. The major differences in this analysis were found between cells placed under different treatments, and not between species, and this was reflected in the resulting flux maps.

4.3.2 Comparison of new flux maps with flux data from the literature

Four flux maps were produced in this study in order to investigate the response of two *Pseudomonas* species to conditions known to alter type III expression. As with all studies into the metabolic fluxes associated with *Pseudomonas* growth on glucose, both strains metabolised glucose almost solely through the ED pathway [188, 224, 225, 229]. Recycling of metabolites through gluconeogenesis to the ED pathway was observed in Pst DC3000, and possibly in Pfl SBW25 (whilst the net flux is shown going from G6P to fructose-6-phosphate, the error on this measurement is large enough that the flux may be operating in the reverse direction, or alternatively the flux through this part of the network may be negligible). Cyclical

operation of the *Pseudomonas* ED pathway has been well established in the literature [226]. Additionally, the glucose maps were in keeping with reported fluxes round the anaplerotic node, with large fluxes through both *ana1* and *ana2* and a small flux through *tca8* [188, 224].

Fluxes round the TCA cycle were found to be high in both treatments and this appears in keeping with the literature [188, 224, 225, 229]. One major departure, however, is the presence of the glyoxylate shunt in glucose-fed cells. This has not been reported in the literature previously and its absence from models described in the literature remains unexplained. This study clearly demonstrated the activity of the glyoxylate shunt in the presence of glucose as a carbon source and it therefore should be included in future *Pseudomonas* models. The glyoxylate shunt bypasses the the reactions in the TCA cycle which produce CO_2, thus allowing more carbon to be passed though anabolic pathways [230], a trend which is observed in the glucose maps. Why this should be of importance during glucose metabolism currently unclear.

The only paper to have previously reported on fluxes arising in a *Pseudomonas* strain as a result of growth on fructose was conducted by Chavarría *et al* (2012) [177]. This study described flux ratios of *P. putida* when grown on glucose and on fructose. Interestingly, they also observed that whilst glucose was metabolised solely though the ED pathway, fructose was metabolised through the ED pathway, the PP pathway and though the lower section of glycolysis (FBP to triose phosphates) in a

ratio of around 52:34:14. In the present study, a small amount of glycolytic activity was observed in fructose-fed cells (ratios of ED:PPP:glycolysis were 75:13:12 for Pst DC3000 and 73:12:15 for Pfl SBW25), but not to the extent of that found by Chavarría *et al* (2012) [177]. It was also found that, in agreement in Chavarría *et al* (2012), the fructose-fed cultures had larger fluxes through the PP pathway than glucose-fed cells. Chavarría *et al* (2012) [177] noted that fructose-fed cells, though being capable of metabolising fructose via the glycolytic pathway still use the less energy efficient route of the ED pathway. Precursor requirements aside, why the majority of fructose is metabolised through the ED pathway is unclear, but appears to be a common feature of *Pseudomonas* fructose and glucose metabolism [226].

The predicted fluxes from the triose phosphates to pyruvate in this study agreed with those flux ratios observed by Chavarría *et al* (2012) [177]: larger fluxes through this part of the network were observed in the presence of fructose than with glucose. Chavarría *et al* (2012) [177] also reported a corresponding larger flux from OAA to PEP with fructose and this was also observed in both Pst DC3000 and Pfl SBW25. In contrast to the earlier study that reported an increase around the pyruvate shunt (malate to pyruvate to OAA) under fructose conditions [177], the present results suggest the opposite, with a major reduction in flux from malate to pyruvate.

The results from the ^{13}C-MFA in this study are very much in keeping with the literature indicating that *Pseudomonas* central carbon metabolism is highly conserved under minimal media conditions. One important improvement to the modelling of

Pseudomonas metabolism is the discovery of an active glyoxylate shunt when glucose is the sole carbon source. This TCA-cycle bypass is clearly of importance to both Pst DC3000 and Pfl SBW25 under these conditions and the role the glyoxylate shunt plays in glucose metabolism merits further investigation.

4.3.3 A link between metabolic flux and virulence gene expression?

Differences in metabolic fluxes were observed between cells grown under the different culture conditions in both Pst DC3000 and Pfl SBW25. The similarity of the responses of Pst DC3000 and Pfl SBW25 to the two treatments show that at as far as can be detected at the level of central carbon fluxes, there are no obvious candidate areas of metabolism which might explain why Pst DC3000 is virulent and Pfl SBW25 is not. It must be assumed that the metabolic differences which arise in Pst DC3000 and Pfl SBW25 in the glucose and fructose treatments, if they do have an effect on the expression of T3SS genes, is because they are interpreted differently by the two strains.

Is it possible that these observed metabolic differences could contribute to the virulent and non-virulent outcomes of the treatments in Pst DC3000? Recently, Kochanowski *et al* (2013) [231] showed that *E. coli* cells are able to sense glycolytic fluxes and that specifically the concentration of FBP (which they found to be an accurate reporter of glycolytic flux) acts as a switch for the transcription factor Cra. Thus, they describe the FBP-Cra interaction as a flux sensor [231] and this

constitutes one of the first reports of a mechanism of this nature. Cra is a global regulator of carbon metabolism, a catabolite repressor/activator, known to regulate the expression of *gapA* (G3P dehydrogenase A), *eno* (enolase), and to repress genes associated with fructose metabolism in the absence of fructose [232]. As yet, no such flux sensing mechanisms have been reported for *Pseudomonas* strains, but they are known to possess global metabolic regulators, such the CbrAB/Crc system, which may interact with many different metabolites [233]. The expression of virulence genes in *Pseudomonas* is known to be regulated by Crc [233, 234] and CbrA-CbrB [149, 170]. Thus, testing flux-sensing characteristics of known global regulators may be a strong starting point in the elucidation of a regulatory cascade that controls type III expression in Pst DC3000.

The major differences occurring between metabolism with fructose and with glucose included the magnitude of fluxes between FBP, F6P and G6P, the presence and absence of the glyoxylate shunt, and the magnitude of fluxes between malate and pyruvate, and malate and OAA. First, as previously described, FBP is known in *E. coli* to interact with the global regulator Cra. In this study, fluxes through FBP are shown to be large in fructose-fed cells (as this is the entry point for fructose into the metabolic network) and very small in glucose-fed cells. No link between FBP fluxes and virulence has been established in *Pseudomonas* strains, though FBP aldolase is a known moonlighting protein in other bacterial species (that is, it serves more cellular functions than just its conventional catalytic purpose) [235] and is part of a group of central carbon metabolic enzymes shown to have multiple purposes,

including acting as virulence factors [236].

The glyoxylate shunt has also been implicated in virulence in other bacterial species. It is essential for the persistence of *Mycobacterium tuberculosis* infections in macrophages [237], and isocitrate lyase (ICL) activity is known to upregulate T3SS expression in *P. aeruginosa* under anaerobic conditions [230]. ICL is also required for the virulence of *P. aeruginosa* in alfalfa seedlings and in rat lungs [238], and is negatively regulated by the global nitrogen regulator RpoN [239]. As RpoN is known to regulate virulence genes in *P. syringae* [240], the possibility exists that the glyoxylate shunt will only operate under conditions where the T3SS is not expressed. Fluxes through the glyoxylate shunt may therefore be associated with avirulence.

A role for malate dehydrogenase (quinone) in virulence in Pst DC3000 has already been postulated: mutants lacking *mqo*, which catalyses the conversion of malate to OAA (*tca8*), were shown to be much less virulent on host plants. However, this was shown not to be as a result of lower T3SS expression and it was hypothesised that *mqo* must encode a novel virulence factor [241]. Notably, little evidence exists for a role for any of the genes involved in the pyruvate shunt in virulence. Malic enzyme is upregulated in *M. tuberculosis* in response to the host environment and a *Salmonella typhimurium* strain unable to convert malate to pyruvate shows strongly attenuated virulence [237]. In *Pseudomonas putida*, Crc has been shown to repress the activity of pyruvate carboxylase, but to have no effect on the expression of malic enzyme [144]. This, therefore, may provide an explanation for the differences in *ana1*

fluxes between fructose and glucose conditions (lower in fructose-fed cells) and the similarity in flux levels through *ana2*, although flux sizes are not always correlated with a change in activity of a single enzyme [242].

As large-scale changes in metabolic fluxes are observed between fructose and glucose-fed cultures, it is likely, though not certain, that these make some contribution to the cell's understanding of their environment that gives rise to the expression or repression of virulence genes. As several notable changes are observed, including alterations in glyoxylate, glycolytic and anapleurotic fluxes, it is possible that one, or all, are required to signal, via a flux sensing mechanism, the suitability of an environment for the expression of virulence genes. The analysis of metabolic mutants under these conditions may help to elucidate the complexities of the metabolism-virulence regulatory system.

4.3.4 Summary

The aim of this chapter was to quantify fluxes through central carbon metabolism in Pst DC3000 and Pfl SBW25 in conditions known to upregulate virulence gene expression. The flux maps generated show central carbon fluxes are highly conserved between the two species under the same conditions and this agreed with the relevant literature. Significant changes were observed between glucose- and fructose-fed models and these differences have identified areas of metabolic regulation and pathways which may be important in the up and down regulation of virulence genes. These findings have taken on a greater level of significance in the light of the dis-

covery of flux sensing mechanisms and the potential existence of such mechanisms and involvement in virulence in *Pseudomonas* species merits further investigation.

Chapter 5

The importance of GABA for the virulence of *Pseudomonas syringae* pv. tomato

5.1 Introduction

γ-aminobutyric acid (GABA) is an important metabolite in many species and has been implicated in a wide range of biological functions. It is the most abundant amino acid in tomato leaf apoplast and one of the most abundant amino acids in the tomato fruit apoplast, both sites of infection for the plant pathogen *Pseudomonas syringae* pv. tomato DC3000 (Pst DC3000) [71, 243]. Genome sequencing revealed that this metabolite may be a preferred host nutrient for Pst DC3000 as it

possesses three GABA transaminase genes and three succinic semialdehyde genes, which encode the enzymes required to metabolise GABA to succinate (a TCA cycle intermediate) [30]. In addition, Pst DC3000 was noted to have a much reduced selection of amino acid transporter genes in comparison to other pseudomonads. Of the four it does have, one of these is orthologous to an *Escherichia coli* GABA permease (*gabP*) [30, 244].

GABA has recently been shown to repress virulence gene expression in wild type Pst DC3000 and to a much greater degree in GABA transaminase mutants [88]. Thus, it appears GABA may be of importance during the process of infection, as a carbon and nitrogen source, and because of its impact on virulence gene expression.

The experimental focus of this study is the evaluation of the role of GABA in bacterial virulence. The following sections review the literature on GABA in both plant and bacteria, and in plant-bacteria interactions, however the role of GABA in plants is not further explored experimentally in this study. Previous work with GABA and Pst DC3000 will also be discussed and the aims of this chapter explained.

5.1.1 A ubiquitous and multi-purpose non-proteinogenic amino acid

GABA was first identified in potato tubers in the middle of the last century and has since be found to be a very common metabolite across all domains of life [245, 246]. It is a four-carbon, non-protein amino acid. In both vertebrates and

invertebrates, GABA has a well-established function as a major inhibitory neurotransmitter [247, 248], and perturbation of GABAergic neurotransmission is known to be associated with several neurological disorders in humans [249]. However, the role of GABA, and GABA metabolism, in plants and bacteria is slightly more contentious [246]. The accumulation of GABA in response to various environmental stresses is particularly well documented in plants and a range of possible functions have been assigned, such as osmoprotection and signalling roles [87, 250, 251], whilst in bacteria, GABA has received far less attention, but still has been shown to have significant roles in quorum sensing and virulence [247, 252, 253].

As GABA transport and metabolism genes have been shown to be upregulated in response to the host environment in *P. syringae* cells [10], GABA assimilation has been suggested to be of important for Pst DC3000 during infection. The mechanisms by which GABA can be transported and metabolised are discussed in the following sections, before current hypotheses on the role of this ubiquitous amino acid are described.

5.1.2 GABA transport

Currently, the majority of identified GABA transport proteins belong to the 2.A subclass of the Transport Classification (TC) system [247]. Within this subclass, GABA transporters are divided between the APC (amino acid/polyamine/organocation) family (TC 2.A.3), the AAAP (amino acid/auxin permease) family (TC 2.A.18) and the NSS (neurotransmitter:sodium symporter) family (TC 2.A.22), for bacte-

ria, eukaryotic microbes and mitochondria, plants, and mammals, respectively [247].

The APC family member proteins share a common topology: each have twelve transmembrane α-helical spanners in a single polypeptide [254]. Within the APC family, GABA permeases are classified as members of the amino acid transporter (AAT) subfamily [254]. AAT GABA permeases have been well characterised in *Escherichia coli* and *Bacillus subtilis* with *gabP* mutants in both species shown to be incapable of metabolising GABA. [255, 256]. *gabP* in *B. subtilis* is regulated by CodY and TnrA [256], nitrogen-responsive global regulators, and the *gabP* gene in *E. coli* is regulated by RpoS [257], an alternative sigma factor which controls the expression of many genes in stationary phase. *Saccharomyces cerevisiae* also has a specific GABA permease but is known to have two alternative routes of GABA uptake: a proline permease and a general amino acid permease [258].

In addition to the 2.A subclass of transport proteins, a second subclass, 3.A, the ATP-binding cassette (ABC) transporters, also contains GABA transporting proteins. These have been identified in *Rhizobium* and *Agrobacterium* species [247]. In *Agrobacterium tumefaciens*, two GABA ABC transporters have been discovered - one specific to GABA (Atu4243) and one with a broader substrate range (Atu2422-BraDEFG) [247, 259]. *Rhizobium leguminosarium* has also been found to have two GABA ABC transport systems, one of which is also the *bra* locus. Mutations in the *bra* operon have been shown to severely impair the ability of *R. leguminosarum* to growth on minimal media containing GABA [260].

In *E. coli*, a glutamate-GABA antiporter, known as GadC, is involved in acid resistance [261]. GadC works in the reverse direction to GabP and Bra proteins as it transports GABA out of the cell. GadC is highly selective in its transport of substrates, and in addition to glutamate will also transport glutamine, methionine and leucine, though will only operate under acidic conditions [261].

5.1.3 GABA metabolism

GABA can be synthesised by two routes in many plants and bacteria - via the decarboxylation of glutamate or via polyamine metabolic pathways. The majority of GABA in most organisms tends to be synthesised from glutamate [262]. Figure 5.1 shows the different known routes of GABA synthesis and catabolism.

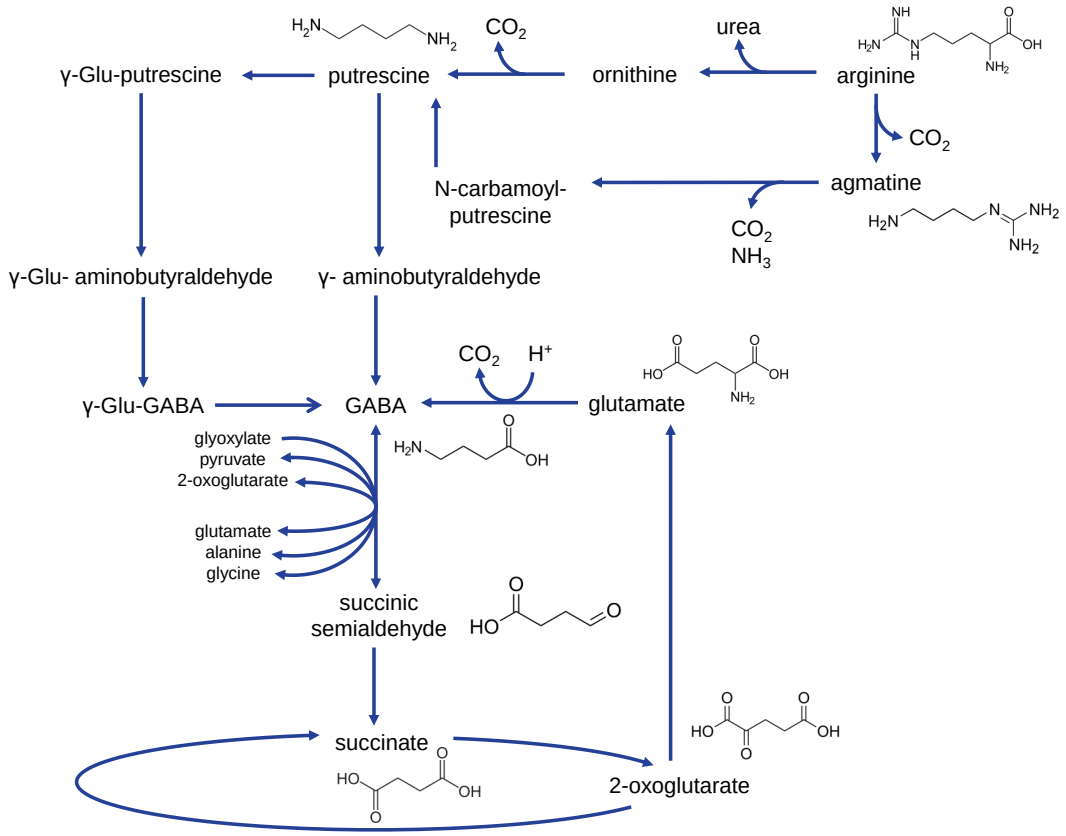

Figure 5.1: GABA metabolism. Metabolic pathways involved in the synthesis and catabolism of GABA. All known routes, in both bacteria and plants, are shown.

GABA from glutamate

The GABA shunt is a well-characterised pathway and comprises the H^+-consuming decarboxylation of glutamate to form GABA and the subsequent transamination of GABA to succinic semialdehyde, which is then converted to succinate [87]. It is known as a 'shunt' because it provides a bypass of the TCA cycle, from 2-oxoglutarate (from which glutamate is formed) to succinate. Whilst the GABA shunt is energetically less efficient than oxidation of 2-oxoglutarate through the TCA cycle [258] it is active in many species and under many different environmental conditions. Thus, it can be assumed that it must serve an important physiological

function.

In plants, glutamate decarboxylase (GAD) is located in the cell cytosol [250] and the H^+-consuming decarboxylation of glutamate proceeds optimally at acidic pHs [262]. Most plant GAD proteins possess a calmodulin (CaM)-binding domain which allows activation at higher pHs due to stimulation by a Ca^{2+}/CaM complex [246] but a notable exception is a GAD enzyme present in rice (*Oryza sativa*) that does not depend on the Ca^{2+}/CaM mechanism for activation [251]. In *E. coli*, GAD, which is encoded by the *gadA* and *gadB* genes, is also induced under acidic conditions [263]. The reaction catalysed by GAD produces CO_2, along with GABA, in the cytosol [251].

GABA from polyamines

An alternative route of GABA synthesis is via polyamine metabolic pathways. Polyamines, similarly to GABA, are known to accumulate in plants in response to abiotic stresses. GABA can be synthesised from the polyamine putrescine in plants by the action of diamine oxidase and, subsequently, pyrroline dehydrogenase [262]. In *E. coli*, this process occurs by the ATP-dependent γ-glutamylation of putrescine, followed by oxidation of γ-glutamylputrescine to γ-glutamyl-γ-aminobutyraldehyde and a final hydrolysis step that produces GABA [264]. Interestingly, arginine is the precursor of putrescine, which itself is synthesised from glutamate. In a way, therefore, the polyamine pathway of GABA synthesis is another route for GABA to be synthesised from glutamate.

The conversion of GABA to succinate

To complete the GABA shunt, or the catabolism of GABA from putrescine, two further enzymatic reactions are required: GABA is converted to succinic semialdehyde by GABA transaminase (GABA-T) and then succinic semialdehyde is converted to succinate by succinic semialdehyde dehydrogenase (SSADH) [246]. In plants and bacteria, both GABA-T and SSADH, encoded by *gabT* and *gabD* genes respectively, are located in mitochondria [265]. A mitochondrial GABA permease is required to transport GABA from the cytosol into the mitochondria [266]. A variation on this set of reactions is the reduction of succinic semialdehyde to γ-hydroxybutyrate (GHB) by succinic semialdehyde reductase [87]. This reaction is known to occur in mammals, where GHB has been proposed as a neurotransmitter [267], and is also thought to occur in plants [268].

The transamination step requires an amino group acceptor. In *Rhizobium* bacteria 2-oxoglutarate and pyruvate have been found to act as the amino acceptor for different GABA transaminases, with the production of glutamate or alanine resulting from the reactions, along with succinic semialdehyde [269]. Interestingly, the use of 2-oxoglutarate could lead to futile cycling as the resultant glutamate could be used for subsequent GABA synthesis [251]. Pst DC3000 GABA transaminases are predicted to use 2-oxoglutarate as their amino group acceptor owing to their similarity with the 2-oxoglutarate-dependent GABA transaminase in *R. leguminosarum* [252], however, this remains to be experimentally tested. In plants, pyruvate, 2-oxoglutarate and glyoxylate can act as the amino group acceptor substrates [265].

Regulation of GABA metabolism

Genes involved in GABA metabolism appear to be regulated in several different ways. *gabT* and *gabD* genes are often found within the same operon, as in *Pseudomonas* species and *E. coli* [88, 270], and are therefore co-transcribed. In *E. coli*, two other genes appear in the gab operon: *gabC*, a regulator and *gabP*, a GABA permease [270]. This operon has been shown to be regulated in response to nitrogen limitation, which produces an increase in expression of *gabD*, *gabT* and *gabP*, and by nitrogen assimilation control protein (Nac)-mediated induction [270]. Notably, the *E. coli gab* operon is only involved in the catabolism of GABA and no other nitrogen source [270].

In *Bacillus thuringiensis*, *gabD* and *gabT* are not found as part of the same transcriptional unit. Instead, *gabD* and *gabR* are co-transcribed, with *gabR* encoding a transcriptional activator which regulates both *gabD* and *gabT* and which is activated itself by an alternative sigma factor, σ^{54} (RpoN), which is involved in the regulation of nitrogen limitation responses in bacteria [253] along with the NtrB-NtrC two-component system.

GABA uptake and metabolism therefore appears to be intrinsically linked to the ability of different bacteria to sense nitrogen and assimilate it from the environment, and this study will address if the same is true of Pst DC3000 in the plant apoplast.

5.1.4 The role of GABA in plants

Many studies have been conducted into the role of GABA in various plant species and a wide range of suggestions have been put forward as to the functions this metabolite might perform. It is known to accumulate in response to both biotic and abiotic stresses and has been shown to have protective, regulatory, transport and signalling functions [271]. A few of these roles are explored below.

GABA accumulates in response to insect herbivory in many plants as a result of an upregulation of GAD activity [272]. GAD activity is stimulated by an increase in Ca^{2+}/calmodulin, a common plant response to damage, and also a drop in pH associated with the acid release from cellular compartments [272]. GABA is a potent inhibitory and excitatory neurotransmitter in insects and its production as a result of mechanical wounding may serve as a deterrent for insect species. Indeed, in a study conducted by MacGregor *et al* (2003) [273], tobacco plants engineered to overexpress GAD were subject to much less feeding by budworm larvae than wild type plants.

Communication and signalling roles have also been described for GABA. A gradient of GABA is required to guide the pollen tube through the style apoplast in *Arabidopsis thaliana* [274] and GABA increases in tomato plants in response to the presence of attacking *Cladosporium fulvum* hyphae (though this increase may constitute manipulation by the pathogen instead of a specific defence response by the

host) [75, 246].

Both GABA and polyamines have been observed to accumulate in plants in response to abiotic stresses such as salinity, oxidative stress and drought [262]. Osmotic stress has also been shown to stimulate the conversion of glutamate to GABA in soybean and *A. thaliana* [275, 276], and thus GABA has been hypothesised to have a protective role within plants [251].

GABA has also been proposed as a key metabolite in carbon:nitrogen metabolism [247, 271]. Specifically, the GABA shunt is thought to act as a link between secondary metabolism and central carbon:nitrogen metabolism [251]. GABA becomes more abundant in plants in response to changing the plants' nitrogen supply from an unreduced nitrogen source (KNO_3) to reduced sources (ammonium, glutamate and glutamine) [87]. An increased production of GABA induces a nitrate transporter in *Brassica napus* roots [277] and exogenously applied GABA also promotes NO_3 uptake when NO_3 is limited in *A. thaliana* seedlings [278].

Whilst many putative functions have been assigned to GABA and its metabolism, there does not seem be be a generic role for GABA in all plants - indeed it appears that generalisations cannot be made from one species to another. Many questions also remain about this metabolite, including how fluxes through GABA assimilation pathways are regulated and whether or not additional pathways exist for GABA synthesis and catabolism [279].

5.1.5 The role of GABA in bacteria

GABA has been extensively studied in plant species, but much less attention has been paid to possible biological functions that GABA might have in bacteria [253]. In many bacteria GABA can be used as both a carbon and a nitrogen source [157], and is known to produce rapid growth in *R. leguminsarum* and *P. syringae* cultures [71, 252]. As in plants, it is has been implicated in the regulation of cellular pH, owing to the H^+-consuming decarboxylation of glutamate to produce GABA [280]. *Lactobacillus brevis*, *Listeria monocytogenes* and *E. coli* all are known to increase their production of GABA in response to low pH conditions in order to increase intracellular pH [281–283]. Polyamines are also known to be involved in bacterial acid survival [263].

GABA has been shown to be involved in nitrogen regulation, as nitrogen limitation in *E. coli* causes the induction of pathways that catabolise GABA and related metabolites, ornithine, putrescine and arginine [270]. A more striking role for GABA in metabolism may be found in *L. monocytogenes*, *M. tuberculosis* and *B. thuringiensis*, where the TCA cycle is incomplete and the GABA shunt can provide succinate [280]. Specifically, *M. tuberculosis* cells are unable to produce 2-oxoglutarate decarboxylase in the host environment, whereas SSADH is detected along with other components of the GABA shunt [284]. *L. monocytogenes* and *B. thuringiensis* also lack the ability to convert 2-oxoglutarate to succinate [285, 286].

A role for GABA in bacterial virulence?

In the last few years, several studies have shown that GABA is involved in the regulation of virulence determinants in bacteria. In *Pseudomonas aeruginosa*, virulence towards nematodes is increased in the presence of GABA. This upregulation of virulence is due to changes in quorum sensing: incubation with GABA produced an earlier and higher peak of the 3-oxo-dodecanoyl-L-homoserine lactone quorum-sensing molecule which led to a reduction in oxygen accessibility and much higher expression of oxygen-scavenging proteins, which created a higher cytotoxic potential in host nematodes [248]. The interaction of *P. aeruginosa* with GABA is an important relationship to explore as this opportunistic bacteria has been known to invade the central nervous system of humans, where GABA concentrations are high [248]. GABA is also involved in the regulation of quorum sensing in *Agrobacterium tumefaciens*, a pathogen that causes tumors in its host plants, which is discussed in Section 5.1.6. Recently, genes for GABA metabolism have been shown to be expressed in the human plague pathogen *Yersinia pestis* when cells are in their insect vector [287], though the role of GABA in virulence in this context remains unclear.

Polyamines, potential metabolic precursors of GABA, are involved in various aspects of pathogenicity in a range of bacterial species as well. For example, a spermidine transporter is one of the regulators of T3SS expression in *P. aeruginosa* [288] and polyamines regulate the production of biofilm formation, an important virulence determinant, in *Y. pestis* [263].

The implication of GABA in general stress responses in bacteria, including acid stress and oxidative stress [289], may also be of importance during the infection process, as the host tries to destroy invading cells using a suite of stress-inducing defensive molecules.

5.1.6 The role of GABA in plant-bacteria interactions

Several important studies have shown that GABA is a key metabolite in the interactions between plants and bacteria. An example of GABA playing an important role in plant-bacteria symbiosis is the abundance of GABA in pea nodules, where the symbiont *Rhizobium leguminosarum* is involved in nitrogen fixation, and a GABA transaminase gene has been shown to be induced in *R. leguminosarum* and highly expressed within this environment [252, 269].

Chevrot *et al* (2006) [290] demonstrated that, unlike in *P. aeruginosa*, GABA caused a down-regulation of virulence in *A. tumefaciens*. This down regulation was caused by GABA inducing the expression of the *attKLM* operon which in turn inactivated the production of quorum-sensing proteins. Quorum-sensing molecules are involved in the conjugation of the Ti plasmid into the host which induces the expression of nutrients for the pathogen, opines, and stimulates the formation of a tumor. Interestingly, this process is antagonised by proline as it interferes with GABA transport via the Bra locus, and the Bra locus is required for the expression of the *attKLM* operon [291]. Most recently, it has been shown that the deletion of *atu4243*, a periplasmic binding protein involved in GABA uptake in *A. tumefaciens*, causes

changes in tumour development [292]. Yuan *et al* (2008) have hypothesised that *A. tumefaciens* hijacks plant signals such as GABA for its own benefit during the course of infection [293].

GABA levels increase during the course of the susceptible interaction of *A. thaliana* and *Pseudomonas syringae* pv. tomato DC3000 by the action of GAD enzymes [7] and Pst DC3000 stimulates very similar responses to those induced by abiotic stresses [9]. GABA may therefore be involved in the plant defence response to invading pathogens. Finally, mutations in GABA transaminase genes in *Pseudomonas syringae* pv. tomato DC3000 cause a reduction in bacterial virulence [88], and this is further discussed in the following section.

5.1.7 GABA transport and metabolism in *Pseudomonas syringae* pv. tomato DC3000

In Section 3.2.1, GABA was shown to be the most abundant amino acid in the tomato leaf apoplast and after 24 hours of incubation Pst DC3000 was able to almost fully deplete this metabolite from apoplast extract (Section 3.2.2). Pst DC3000 has a much reduced set of APC family proteins and within this group, a much reduced set of amino acid permease genes in comparison with other pseudomonads (Tables 5.1 and 5.2 respectively) but is still able to deplete many of the nutrients from apoplast extracts [30, 71]. One of the transport proteins Pst DC3000 has retained is a single GABA permease. The expression of this GABA permease gene, *gabP*, is increased by low pH, the presence of GABA, in tomato leaf apoplast ex-

tract and in 'low nitrogen' (NH_4Cl) conditions [85]. It was also found to be the most highly expressed of the four amino acid permease genes present in Pst DC3000 upon exposure to apoplast extracts and in the tomato host [85]. An RpoN binding site has been identified upstream of GABA permease genes in *P. putida* KT2440 (PP0284 and PP4407) and *P. entomophila* L48 (PSEEN5205) [85], indicating these genes are RpoN-regulated, and it is therefore highly likely that *gabP* in Pst DC3000 will also be regulated by RpoN. As RpoN is involved in the regulation of *hrpL* [40], this provides a previously untested link between GABA transport and virulence in Pst DC3000.

There is good evidence that *gabP* is may be important enzyme for Pst DC3000 during the infection process: Pst DC3000 appears to actively assimilate GABA when in the host and the import of GABA may be controlled by the same regulator as virulence genes. By using a ΔgabP mutant of Pst DC3000, the roles of *gabP* in growth, metabolism and virulence in Pst DC3000 are investigated in this study.

Pfam domain family	Ppu KT2440	Ppu F1	Ppr Pf5	Pfl Pf0-1	Pae PAO1	Psy DC3000	Psy 1448A	Psy B728a
Cytosine, purine, uracil, thymine, allantoin transporter	7	7	8	9	6	2	2	3
Sulfate transporter	4	5	6	3	4	4	4	4
Na^+:alanine symporter	1	1	1	1	3	1	1	1
Branched chain amino acid: Na^+/H^+ transporter	1	1	1	1	2	1	1	1
Transmembrane amino acid transporter	1	0	0	0	0	0	0	0
Benzoate: H^+ symporter	3	3	3	3	1	1	1	1
Tryptophan/tyrosine permease	0	1	1	1	3	1	1	1
Xanthine/uracil permease	6	6	8	8	7	3	3	3
Na^+: solute symporter	7	6	7	5	6	4	5	6
Amino acid permease	21	21	21	14	21	4	5	6
Total	**51**	**51**	**56**	**45**	**53**	**20**	**22**	**23**

Table 5.1: APC superfamilies present in selected pseudomonads. *Pseudomonas syringae* strains are underrepresented in several families within the APC superfamily. Full strain names can be found in Table A.14 (Appendix A.4). Adapted from Rachel Jones' DPhil thesis [85]

Amino acid permease domain	Ppu KT2440	Ppu F1	Ppr Pf5	Pfl Pf0-1	Pae PAO1	Psy DC3000	Psy 1448A	Psy B728a	Pen L48
GABA	6	6	1	2	1	1	1	1	4
Ethanolamine	1	1	2	2	2	1	1	1	2
Aromatic	2	2	2	1	2	1	1	1	2
Proline	1	1	2	0	1	1	1	1	1
Arginine/ornithine	2	2	2	2	1	0	0	1	2
D-serine/alanine/glycine	1	1	1	0	0	0	0	0	1
Lysine	0	0	0	0	1	0	0	0	0
Unknown function	8	8	11	7	13	0	1	1	7
Total	**21**	**21**	**21**	**14**	**22**	**4**	**4**	**6**	**19**

Table 5.2: Amino acid permease domains present in selected pseudomonads. *Pseudomonas syringae* strains have notably fewer domains than other pseudomonads. Full strain names can be found in Table A.14 (Appendix A.4). Adapted from Rachel Jones' DPhil thesis [85]

Pst DC3000 also has three GABA transaminase (*gabT*) and three SSADH (*gabD*) genes encoded in its genome [30]. Both *gabT1* and *gabT2* are linked with *gabD* genes (*gabD1* and *gabD2* respectively) and are therefore likely to be transcribed together [88]. *gabT2* has been shown to be the primary GABA transaminase in this species: only *gabT2* was able to partially restore growth on GABA in a triple

transaminase mutant, though all three genes (*gabT1*, *gabT2* and *gabT3*) have some level of transaminase activity [88]. Unlike in *A. tumefaciens*, GABA appears to cause a general down-regulation of virulence gene expression in Pst DC3000 and this effect is amplified in a triple transaminase mutant, Δ*gabT2/T3/T1*, in which all three GABA transaminase genes have been deleted [88]. Park *et al* (2010) [88] hypothesised that this may be due to the build-up of intracellular GABA unbalancing the carbon:nitrogen ratio, and they demonstrated that GABA increases in Pst DC3000 cells upon increasing extracellular GABA concentrations. In addition, *P. syringae* pv. tabaci showed reduced symptoms on GAD-overproducing tobacco lines (which have elevated GABA [85]) and the same result was obtained with Pst DC3000 and an *Arabidopsis thaliana* line which accumulates higher levels of GABA [88]. In Section 3.2.5, GABA was again shown to cause a strong down-regulation of virulence genes (after an initial upregulation) in Pst DC3000.

Notably, Pst DC3000, like many other pseudomonads, is predicted to lack glutamate decarboxylase-encoding genes (GAD), and therefore is thought to be unable to synthesise GABA from glutamate [88]. Pst DC3000 is predicted to lack the genes required to synthesise GABA via polyamine catabolism, though it is not unreasonable to assume that the import of GABA from the host environment (uninfected tomato plants are abundant in GABA, whereas in other plants GABA accumulates in response to infection) would be the more energetically favourable route. Figure 5.2 shows the routes of import, synthesis and catabolism of GABA available to Pst DC3000.

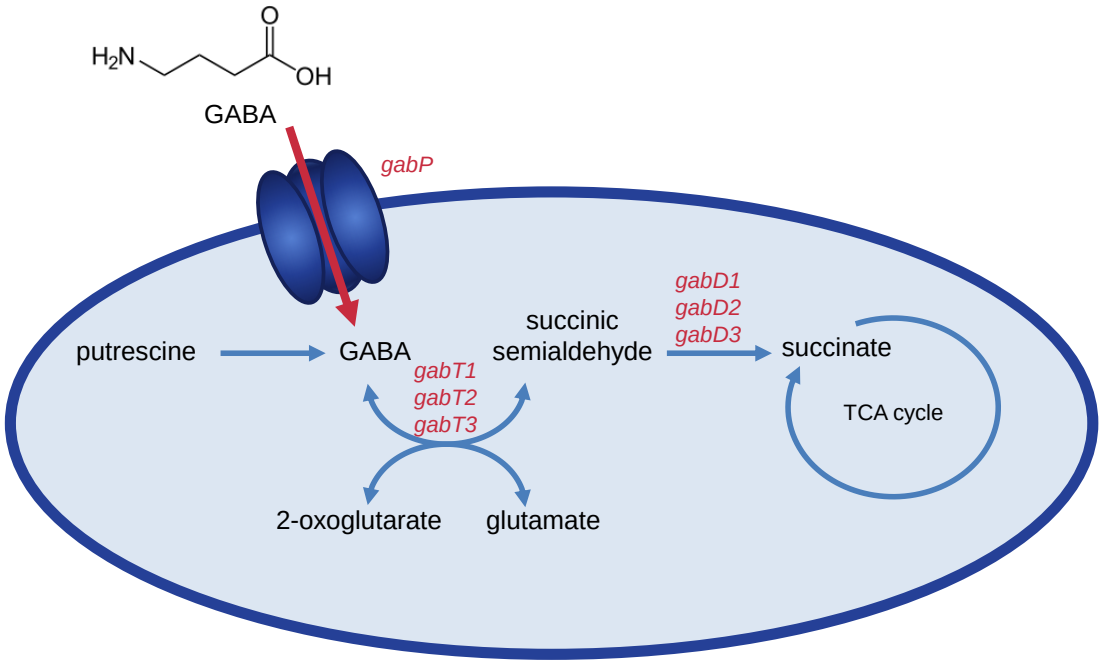

Figure 5.2: GABA import and metabolism in Pst DC3000. All described routes of GABA transport and metabolism in Pst DC3000, with gene annotations where known.

GABA therefore appears to be a key metabolite for Pst DC3000 during the infection process. However, whilst an impact of GABA on virulence has been noted in Pst DC3000 and other species, the metabolic changes associated with GABA assimilation and metabolism, along with mutations in GABA transaminase genes, have never been examined in a bacterial species prior to this study. The triple GABA transaminase mutant, $\Delta gabT2/T3/T1$, created by Park *et al* (2010) [88], which is impaired in the expression of virulence genes in the presence of GABA, was used to understand the role the GABA transaminase genes play in Pst DC3000 virulence.

5.1.8 Statement of aims

Pst DC3000 strains with mutations in genes for GABA uptake and metabolism were used to address the following hypotheses:

1. *P. syringae* strains are unique amongst *Pseudomonas* species in the number of genes annotated for GABA transport and metabolism

2. An inability to transport and metabolise GABA will reduce growth in the GABA-abundant host environment

3. Mutations in GABA transaminase and permease genes will alter virulence gene expression in the host environment

4. GABA over-accumulation in Δ*gabT2/T3/T1* will alter the internal carbon:nitrogen ratio

5. *gabP* is regulated by RpoN

6. GABA assimilation and metabolism in Pst DC3000 plays a role in abiotic stress protection

5.2 Results

5.2.1 Phylogenetic analysis reveals the *Pseudomonas syringae* clade is unique among pseudomonads in the number of genes annotated for GABA utilisation

The genome of Pst DC3000, the first fully sequenced *Pseudomonas syringae* strain, revealed an abundance of genes involved in the metabolism of GABA [30]. Pst DC3000 has three GABA transaminase genes and three succinic semialdehyde dehydrogenase genes, and it was hypothesised that this may imply that the utilisation of GABA is of importance during infection [30]. Buell *et al* (2003) [30] noted that Pst DC3000 has a much reduced set of amino acid transport genes in comparison with *P. fluorescens* and *P. putida* but that one of the remaining four amino acid permease genes present in Pst DC3000 is annotated as a GABA permease (*gabP*). In order to understand how *P. syringae* strains differ from other *Pseudomonas* strains in the number of genes they have for GABA transport and metabolism, a phylogenetic tree of all sequenced pseudomonads was constructed and to this was mapped the numbers of GABA permeases and transaminases present in the genomes of each strain (Figure 5.3).

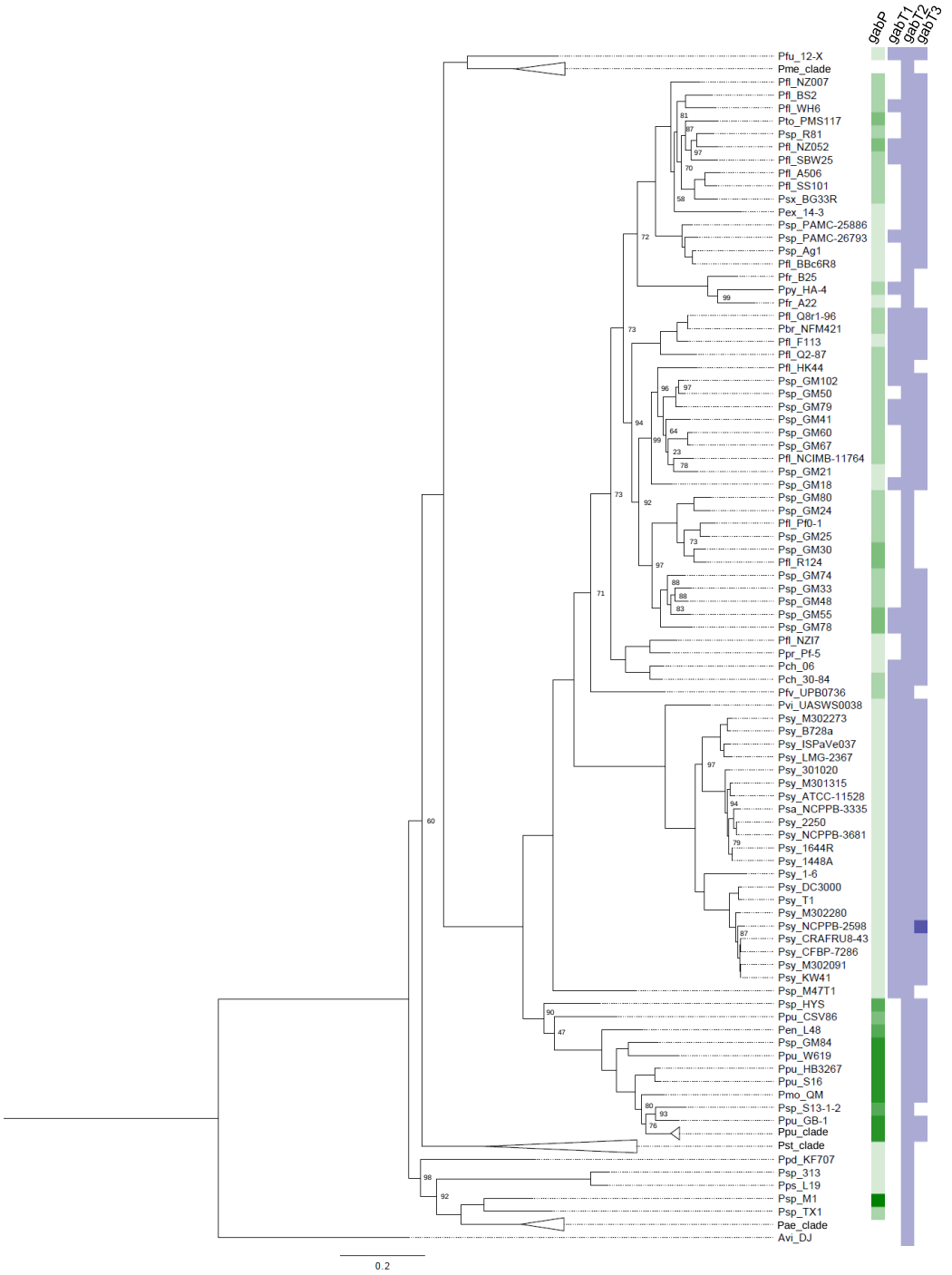

Figure 5.3: Phylogenetic tree of *Pseudomonas* species with annotations for the number of GABA permease and GABA transaminase genes present in each genome. Clades which exhibited the same pattern of GABA genes were collapsed for clarity (for example, the *P. aeruginosa* clade). *Azotobacter vinelandii* was used as the outgroup. Bootstrap values are only shown if below 100. The scale bar corresponds to the number of substitutions per site. GABA permease gene numbers are shown in green, where the absence of any GABA permease genes is shown in white, whilst increasing numbers of GABA permease genes are shown in increasingly intense shades of green (the maximum value is six). GABA transaminase genes are shown in blue, and white is shown for the absence of a gene. The full names for all of the strains shown can be found in Appendix A.4.

First, the phylogenetic tree is in good agreement with other recently published phylogenies of *Pseudomonas* species [13, 14] and highlights the diversity present within this genus.

All of the *Pseudomonas* species which have been analysed here are predicted to have a *gabT2* gene within their genomes, with many species having *gabT1* or *gabT3* in addition. Notably, only the strains in the *P. syringae* clade consistently all possess three GABA transaminases. One strain within the *P. syringae* group has four GABA transaminases, though the fourth is not a novel gene, but instead a duplication of *gabT3* (inferred from gene homology). Several species of *P. fluorescens* and *P. chlororaphis* (as well as some as yet un-named species in the *P. fluorescens* clade) also have three putative GABA transaminase genes, orthologous to those found in *P. syringae*.

The variation in the presence or absence of putative GABA transaminase genes in the *P. fluorescens* clade is reflected in the number of putative GABA permeases present in different *P. fluorescens* strains. All of the strains within this group have at least one permease, though up to three were detected in several instances. The *P. fluorescens* group is known to be highly diverse, both in the environments different strains inhabit and also genetically, with hundreds of unique genes present in many of the strains [14]. Longer branch lengths within the *P. fluorescens* clade (more time has passed between the time of sequencing and the last common ancestor) may explain a significant degree of the variation observed.

Putative GABA permease genes were found in all species, apart from the *P. aeruginosa* and *P. mendocina* clades, where no orthologues were detected. The GABA permease genes were found to all be highly related to one another, and where multiple versions exist, such as in *P. putid*a and *P. entomophila*, these are due to duplication events. The radiation of GABA permeases in these strains has not received any attention in the literature, though induction of *gabP* expression in *P. putida* in the maize rhizosphere has been noted [294]. It is likely that this proliferation of GABA permease genes confers some advantage to these strains in their current environments, or perhaps were advantageous to the ancestral strain [85]. Interestingly, in strains where more GABA permeases are present, this is often accompanied by large numbers of other amino acid transporters and APC family genes (Tables 5.1 and 5.2.

5.2.2 Mutations of GABA permease and transaminase genes in Pst DC3000 render it unable to utilise GABA as a carbon and nitrogen source

In order to assess the impact of GABA metabolism on the survival and virulence of Pst DC3000, *gabP*, *gabT1*, *gabT2* and *gabT3* deletion mutations were constructed by Dr. Duck-Hwan Park (Kangwon National University). Mutants with deletions in the GABA transaminase genes were previously described to some degree by Park *et al* (2010) [88], however, the ability of these strains to utilise GABA as a car-

bon or nitrogen source was not fully tested. *gabT2* was shown to be the primary GABA transaminase, but all three genes were concluded to have some level of GABA transaminase activity [88]. The finding that all three genes have GABA transaminase activity led to the triple GABA transaminase mutant, Δ*gabT2/T3/T1*, being used throughout this study. Initially, the ability of Δ*gabP* and Δ*gabT2/T3/T1* to utilise GABA as a carbon source, a nitrogen source and both a carbon and nitrogen source was tested using a modified version of M9 minimal media, shown in Table 2.5.

The chart in Figure 5.4 shows that after 36 hours Pst DC3000 was able to grow to higher densities in all treatments where GABA was present than in standard M9 medium (Glc + NH_4). Δ*gabP* and Δ*gabT2/T3/T1* were unable to utilise GABA as a carbon and nitrogen source, and as a carbon source (GABA + NH_4). Δ*gabP* was able to grow better in the presence of GABA as a nitrogen source (Glc + GABA) than in the normal M9 medium (Glc + NH_4) and Δ*gabT2/T3/T1* was able to achieve similar densities to those observed in normal M9 medium. Thus, DC3000 is able to use GABA as a carbon and nitrogen source, whilst the Δ*gabP* and Δ*gabT2/T3/T1* are only able to use GABA as a nitrogen source. The observation that Δ*gabP* and Δ*gabT2/T3/T1* could use GABA as a nitrogen source led to the following testable hypotheses: GABA is chemically altered in the presence of glucose to allow both for its depletion and metabolism by alternative means (amino sugars are known to be produced by pseudomonads for lipopolysaccharide synthesis [295], though a reaction between glucose and GABA has never been reported); Pst DC3000 is able to remove nitrogen from GABA extracellularly and transport it into

the cell; as yet unidentified transport and metabolism mechanisms exist for GABA in Pst DC3000 (which only operate to any great extent in the presence of glucose).

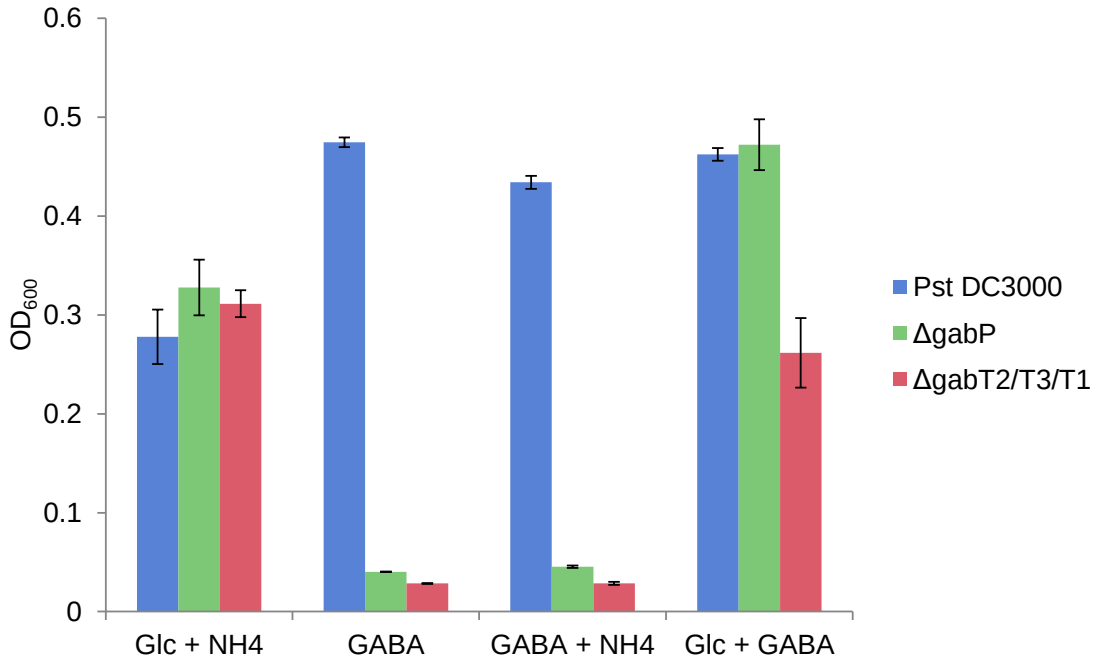

Figure 5.4: Utilisation of GABA as a carbon source, a nitrogen source, and as a carbon and nitrogen source by Pst DC3000, Δ*gabP* and Δ*gabT2/T3/T1*. Cells were incubated in modified M9-glucose for 36 hours, where GABA replaced glucose, ammonium chloride, or glucose and ammonium chloride. Error bars represent standard deviations over four independent replicates.

Δ*gabT2/T3/T1* has previously been shown to have GABA-utilisation partially restored by the addition of the complementation plasmid pBS46:*gabT2* [88]. This broad host-range plasmid (kindly supplied by Dr. Bryan Swingle, USDA-ARS) was constructed to express *gabP* by Dr. Duck-Hwan Park (Kangwon National University). The complemented strain, Δ*gabP* pBS46:*gabP* was tested in the above carbon and nitrogen conditions and the results, displayed in Figure 5.5, show a partially rescued phenotype.

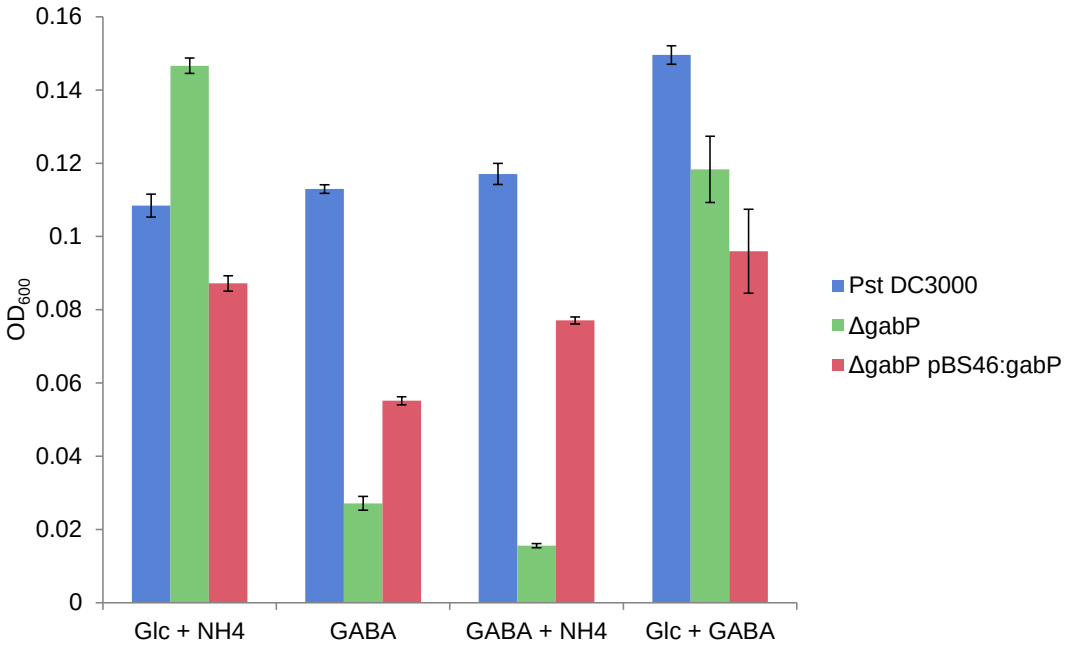

Figure 5.5: Complementation of Δ*gabP* with pBS63:gabP restores growth on GABA as a carbon source. Strains were tested for their ability to utilise GABA as a carbon source, a nitrogen source and a carbon and nitrogen source over 24 hours (beyond 24 hours the growth of strains containing the complementation construct was limited). Error bars represent the standard deviations from four independent replicates.

5.2.3 Δ*gabP* and Δ*gabT2/T3/T1* can use GABA as a nitrogen source in conjunction with several different carbon sources

A possible explanation for the ability of Δ*gabP* and Δ*gabT2/T3/T1* to use GABA as a nitrogen source is the complexing of GABA with glucose and the subsequent transport and metabolism of this hypothesised sugar-amine. The GABA-M9 assay was conducted as previously but with fructose and mannitol as replacement carbon sources for glucose. Figure 5.6 shows that changing the carbon source does not seem

to significantly change the growth patterns observed previously. Thus, if GABA is being co-transported, it is not in a glucose-dependent manner.

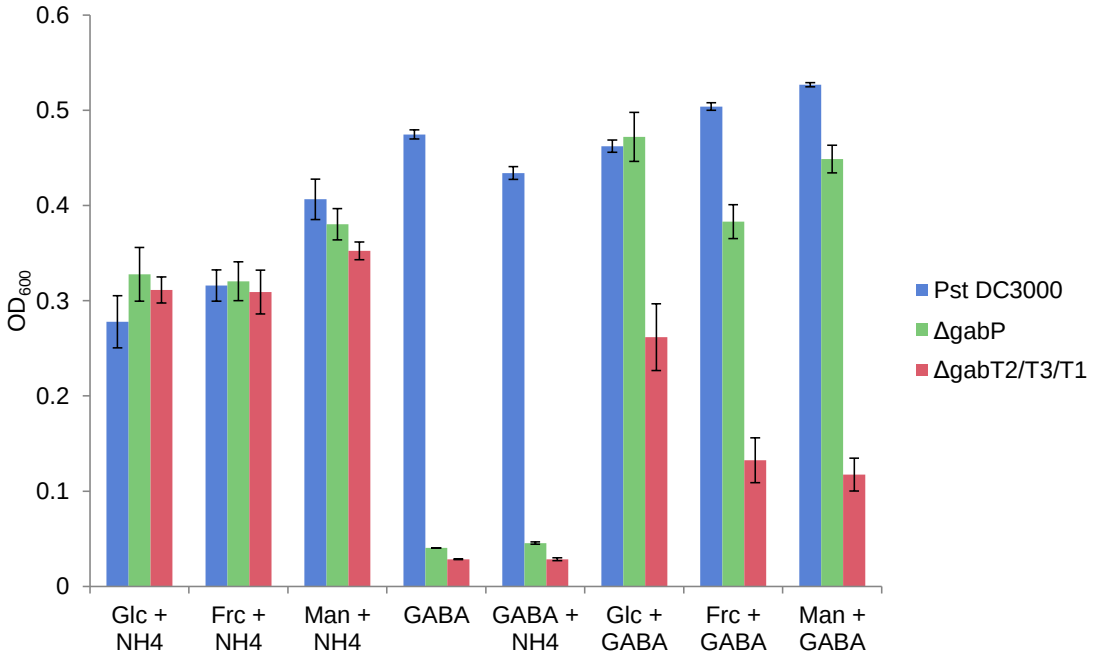

Figure 5.6: Utilisation of GABA as a nitrogen source in the presence of different carbon substrates. Pst DC3000, Δ*gabP* and Δ*gabT2/T3/T1* were incubated in modified M9 for 36 hours, where either glucose was replaced with fructose and mannitol or GABA, and ammonium chloride was replaced with GABA. Error bars show the standard deviations from four replicates. Data for the Glc + NH_4, GABA, Glc + GABA and GABA + NH_4 treatments is repeated from Figure 5.4.

5.2.4 A unlabelling experiment resolves the fate of extracellular GABA in Pst DC3000, Δ*gabP* and Δ*gabT2/T3/T1*

The GABA utilisation assay (Section 5.2.2) raised questions about the ability of Δ*gabP* and Δ*gabT2/T3/T1* to metabolise GABA as a nitrogen source. A second hypothesis to explain the growth observed in the treatment Glc + GABA, and the

absence of growth of Δ*gabP* and Δ*gabT2/T3/T1* in the GABA and GABA + NH_4 treatments, was that Pst DC3000 can break down GABA extracellularly to releases a transportable nitrogen compound that does not contain carbon. The existence of such a mechanism was explored by monitoring the metabolic fate of GABA within Pst DC3000, Δ*gabP* and Δ*gabT2/T3/T1*.

The tracing of labelled carbon substrates to resolve the fate of metabolites is a widely used technique, however, ^{13}C-labelled GABA is not available commercially and so an alternative strategy was developed. An unlabelling approach was taken: cells were labelled using [$^{13}C_6$] glucose prior to the start of the experiment and then once almost all the carbon atoms in the cells had been replaced with ^{13}C atoms, unlabelled GABA was introduced into the culture medium. The experimental conditions used were those established in Section 5.2.2: Glc + NH_4, GABA, GABA + NH_4 and Glc + GABA as the carbon and nitrogen sources but with 100 % [$^{13}C_6$] glucose used throughout. The detection of any unlabelled carbon during the experiment would be a result of the incorporation of GABA into the cells, and thus the unlabelling strategy is theoretically identical to a label-tracing experiment. Incorporation of unlabelled carbon was expected for all GABA treatments in Pst DC3000 and for none of the GABA treatments in Δ*gabP* and Δ*gabT2/T3/T1*, as only (unlabelled) nitrogen from GABA was expected to enter the cells.

Aliquots of bacterial culture were extracted at 0, 2, 4, 6, 8 and 24 hours (after GABA was added to the medium) and the labelling patterns of amino acids derived

from protein hydrolysate were measured. At the end point of the experiment, soluble metabolites were also analysed, both for their labelling patterns and for the proportion in which different amino acids were present. The growth curves of the three strains over the experimental period are shown in Figure 5.7. The following section outlines the conclusions which can be drawn from this investigation. The metabolic network model presented in Chapter 4, specifically the routes of amino acid synthesis, forms the basis of these conclusions.

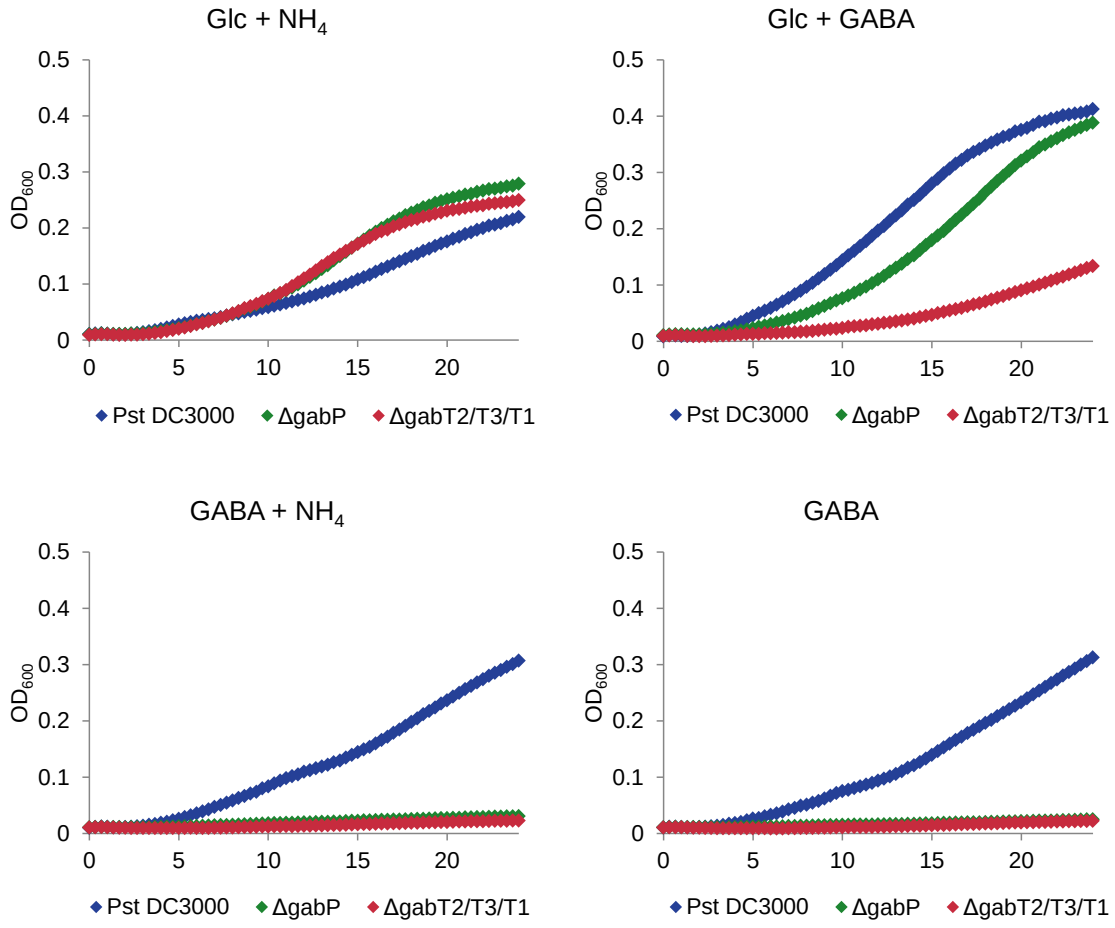

Figure 5.7: Growth curves of Pst DC3000, Δ*gabP* and Δ*gabT2/T3/T1* with GABA as a carbon source, a nitrogen source and a carbon and nitrogen source. Cells were incubated in modified M9-glucose for 24 hours, where GABA replaced glucose, ammonium chloride, or glucose and ammonium chloride. The experiment was repeated three times with the same levels of growth recorded each time.

Protein hydrolysate analysis shows distinct amino acid labelling patterns

Fragments for 14 different amino acids were obtained from GC-MS analysis of protein hydrolysate. The fragment M-57 has been used in the analysis wherever possible, though in the case of serine, leucine, isoleucine and glutamate, alternative fragments have been shown due to the error on the M-57 measurements or known unreliability of the M-57 fragment. In all instances, where more than one fragment per amino acid could be acquired, the differences between the labelling patterns of the different fragments were negligible (Figure 5.8). The results obtained from each different treatment are examined below.

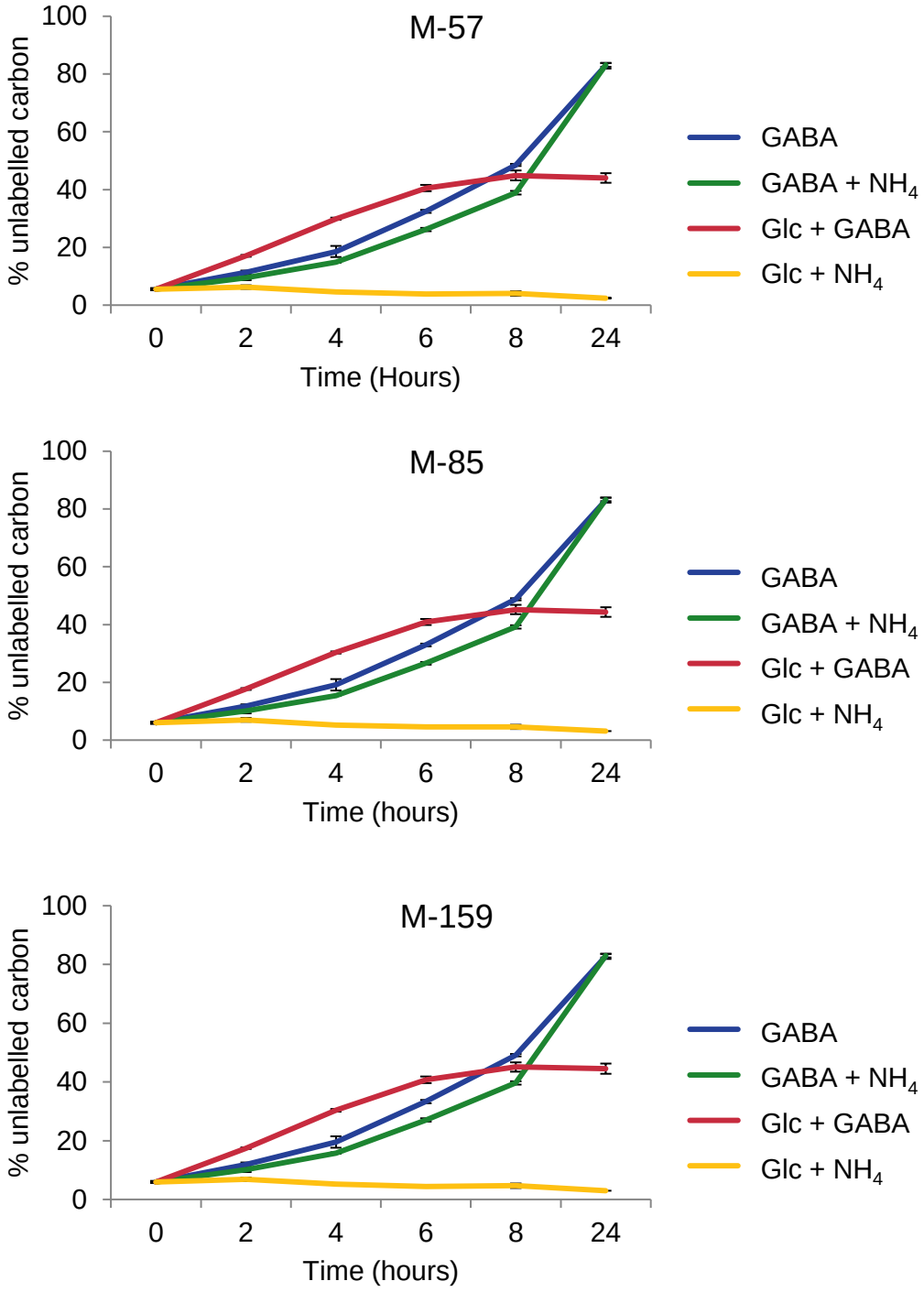

Figure 5.8: Three different fragments of aspartate extracted from Pst DC3000 in four experimental conditions over 24 hours show highly similar labelling patterns. Pst DC3000 was incubated with [$^{13}C_6$] glucose prior to incubation with unlabelled GABA as a carbon source, as a nitrogen source, and as a carbon and nitrogen source ([$^{13}C_6$] glucose was used throughout the experiment). The degree of unlabelling observed in three fragments of aspartate was recorded over a 24 hour period in three independent samples. Errors bars show standard deviation.

At the beginning of the experiment (time point 0), almost all amino acids measured were around 94-96 % labelled. By the final time point (24 hours), in the Glc + NH_4 treatment, a slight increase in labelled carbon was observed across all amino acids, in the range of 2-4 % (Figure 5.9). This pattern was observed across all three strains and indicated that the cultures were not fully labelled at the start of the experiment. However, it is unlikely that this caused a major hindrance to the interpretation of the following results.

Interestingly, there were some differences in the time point 0 labelling percentages in different amino acids. Specifically, lysine (91 %) and arginine (92 %) fragments had less labelled carbon than other amino acid fragments. The amount of unlabelled carbon in arginine may be explained by the inclusion of environmental (unlabelled) CO_2 into the carbon skeleton (CO_2 is required for the synthesis of carbamoyl phosphate, one of the precursors of arginine), however, this explanation cannot also be applied to lysine as CO_2 is not one of its precursors. Whilst these fragments have lower labelling percentages, they followed the same labelling patterns observed over 24 hours in other amino acids which are derived from the same precursor metabolites (lysine is synthesised from oxaloacetate and arginine from glutamate) and therefore were included in the analysis.

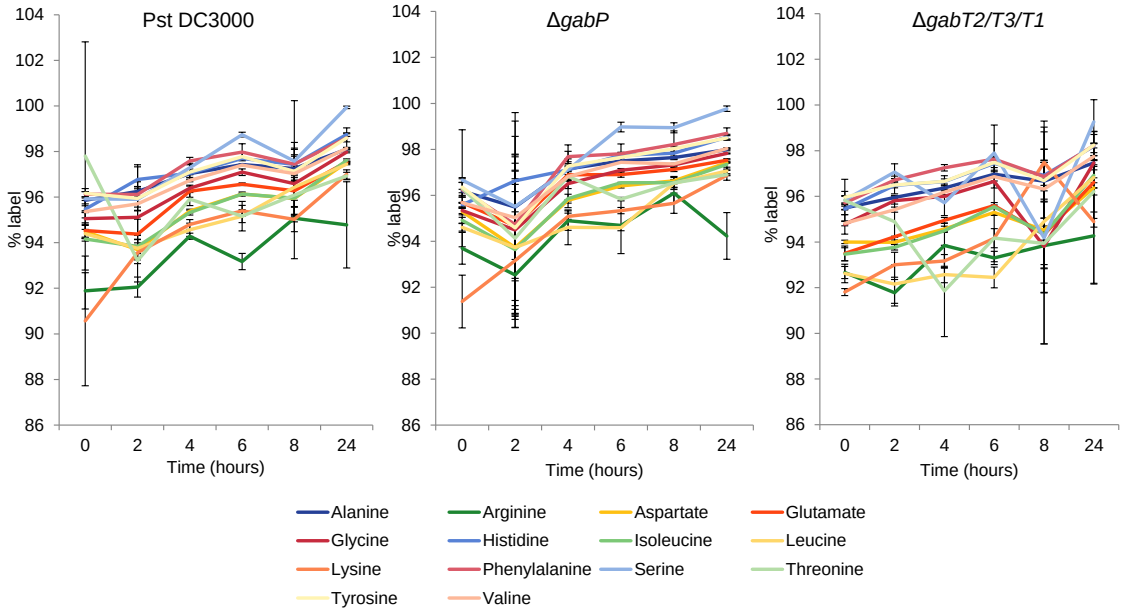

Figure 5.9: The percent of labelled carbon amino acids extracted from Pst DC3000, Δ*gabP* and Δ*gabT2/T3/T1* in the Glc + NH4 treatment increased over 24 hours. The percentage of label present in amino acids derived from protein and extracted from cells incubated with [$^{13}C_6$] glucose was measured by GC-MS over a 24 hour period. Error bars indicate standard deviation from three independent replicates.

The two conditions where GABA was present as the sole carbon source (GABA and GABA + NH_4) can be examined together as they exhibited highly similar labelling patterns within each strain. Indeed, the growth kinetics in these two treatments were virtually indistinguishable in the wild type (Figure 5.7), with growth in GABA + NH_4 being only fractionally higher. In Pst DC3000, a small, but gradual decline in the percentage of label present in all amino acids was observed across the first four hours of the experiment, with a more rapid decline observed between four and eight hours, consistent with the observed lag phase in growth. In all detectable amino acids, a greater degree of unlabelled carbon was observed in the GABA treatment in comparison with the GABA + NH_4 treatment from 2 to 8 hours (Figure 5.10). By 24 hours the percentage of labelled carbon in both treatments was essentially the

same, and ranged from 16-22 % depending on the amino acid measured. A possible explaination for the greater degree of unlabelling and slightly lower growth in the GABA treatment is that Pst DC3000 was restricted to utilising GABA for both the carbon and nitrogen it required, whereas when NH_4 is also present, more labelled carbon reserves were metabolised with in the presence of NH_4, and a lag phase for adaptation to GABA uptake is avoided.

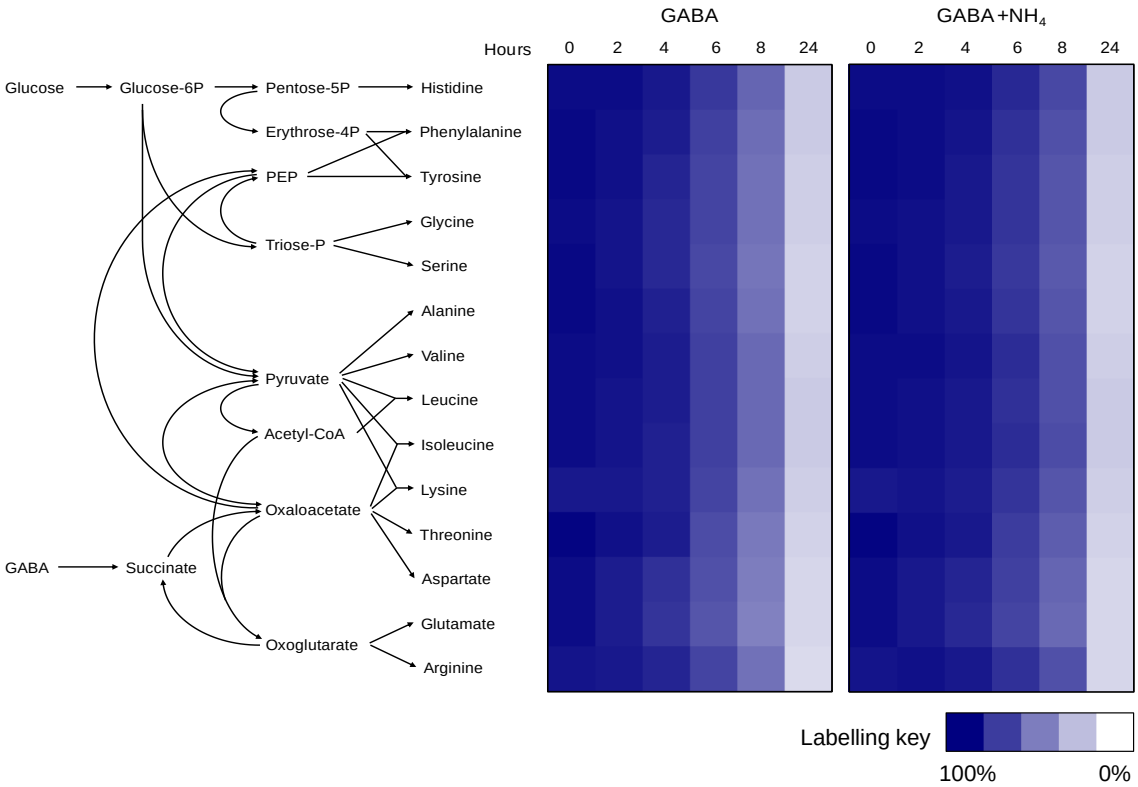

Figure 5.10: Pst DC3000 incubated with GABA and GABA + NH4 shows very similar unlabelling patterns across 14 amino acids. Pst DC3000 was incubated with [$^{13}C_6$] glucose prior to incubation with unlabelled GABA, both as a carbon source, and as a carbon and nitrogen source. The heatmap squares represent the degree of labelling measured for each fragment: the darkest blue represents 100 % labelling and white represents 0 % labelling. The metabolic map demonstrates the primary routes of synthesis for each amino acid.

In both ΔgabP and ΔgabT2/T3/T1, in treatments with GABA and GABA+NH_4, no significant change was seen in the percentage of labelled carbon across all amino

acids over 24 hours (Figure 5.11). This is consistent with the lack of growth observed when GABA is present as the sole carbon source (Section 5.2.2).

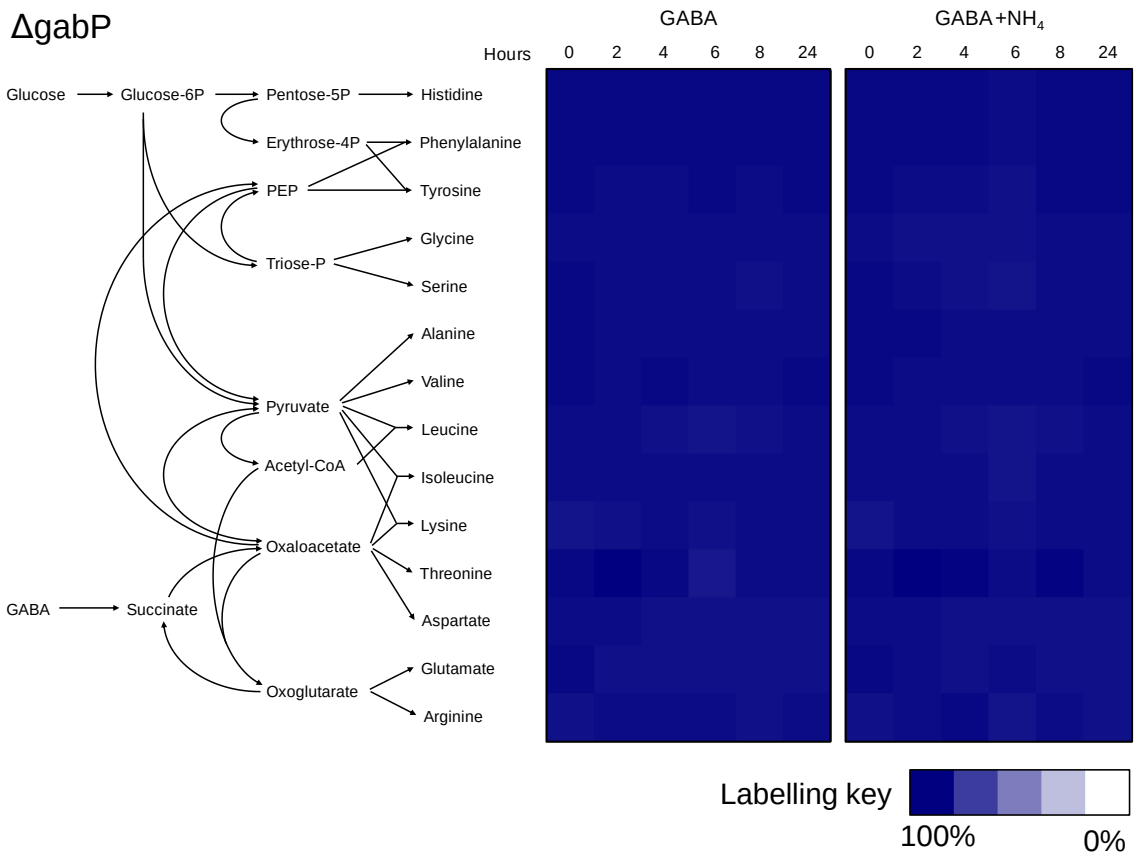

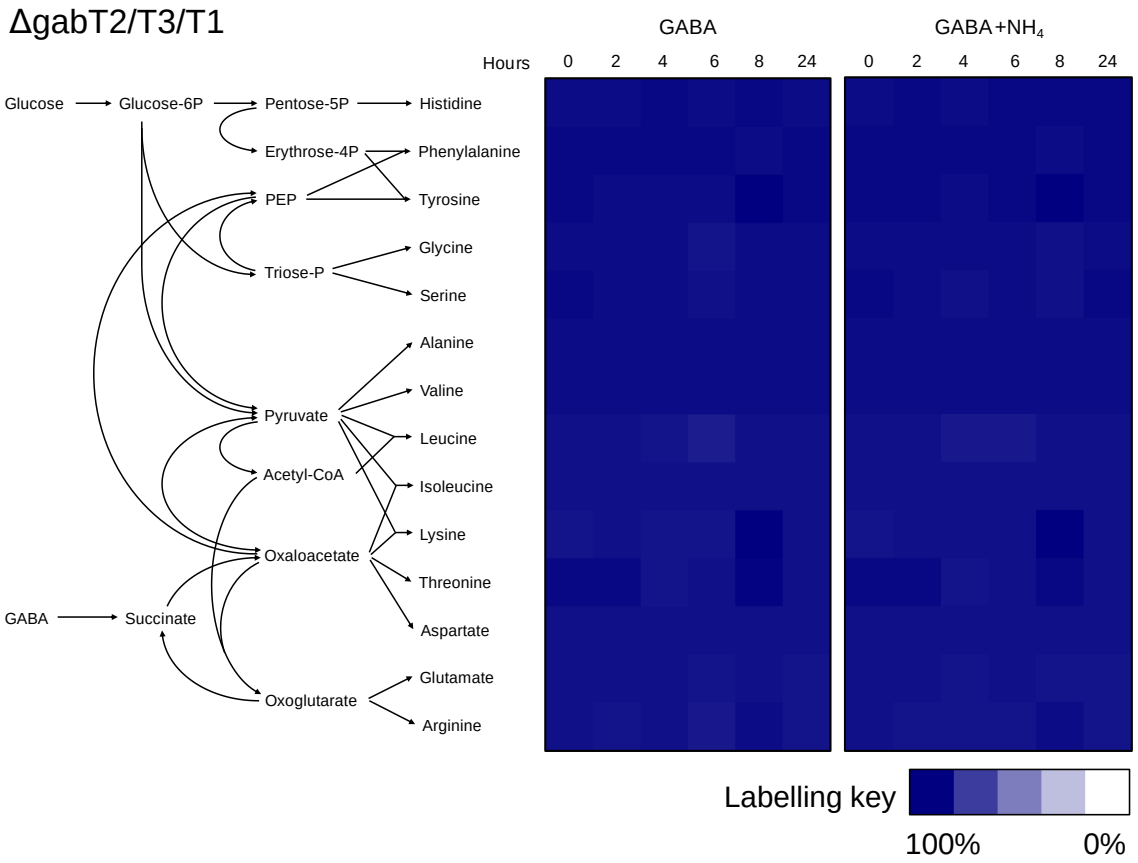

Figure 5.11: Δ*gabP* and Δ*gabT2/T3/T1* cells show no unlabelling after 24 hours when GABA is the sole carbon source. Δ*gabP* and Δ*gabT2/T3/T1* were incubated with [$^{13}C_6$] glucose prior to incubation with unlabelled GABA, both as a carbon source, and as a carbon and nitrogen source. The heatmap squares represent the degree of labelling measured each fragment: the darkest blue represents 100 % labelling and white represents 0 % labelling. The metabolic map demonstrates the primary routes of synthesis for each amino acid.

The Glc + GABA treatment is perhaps the most informative as to the metabolism of GABA in an environment where multiple carbon sources are available, such as the host apoplast. In Pst DC3000 several distinct labelling patterns were detected depending on the precursor from which an amino acid is formed (Figure 5.12). Glycine, serine, phenylalanine, tyrosine and histidine showed little or no increase in the amount of unlabelled carbon present over the 24 hour period. In particular, histidine and serine actually increased in the percentage of label measured over time.

Glycine, phenylalanine and tyrosine showed very small decreases in the percentage of labelled carbon measured over 24 hours (2.3 %, 5.1 % and 4.8 % decreases respectively).

Amino acids which derive from TCA cycle intermediates such as aspartate (synthesised from oxaloacetate), threonine (synthesised from aspartate), glutamate (synthesised from 2-oxoglutarate), arginine (synthesised from glutamate), isoleucine (synthesised from threonine and pyruvate) and lysine (synthesised from aspartate and pyruvate) were unlabelled most rapidly and to the greatest degree (aspartate showed a 41.7 % decrease in label after 24 hours). By between 6-8 hours these amino acids showed a levelling off in their degree of unlabelling, perhaps indicating that a steady state had been achieved (or would have been achieved) in the amounts of glucose and GABA-derived carbon entering the TCA cycle.

The third group of metabolites is composed of alanine, valine and leucine, which are all derived from pyruvate. These amino acids showed a steady decline in the amount of labelled carbon present, to around 80 %. Interestingly, lysine and isoleucine, which are formed from both TCA cycle amino acids and pyruvate, had unlabelling patterns which mimic most closely those amino acids formed solely from TCA cycle intermediates and did not display, the perhaps expected, intermediate labelling patterns.

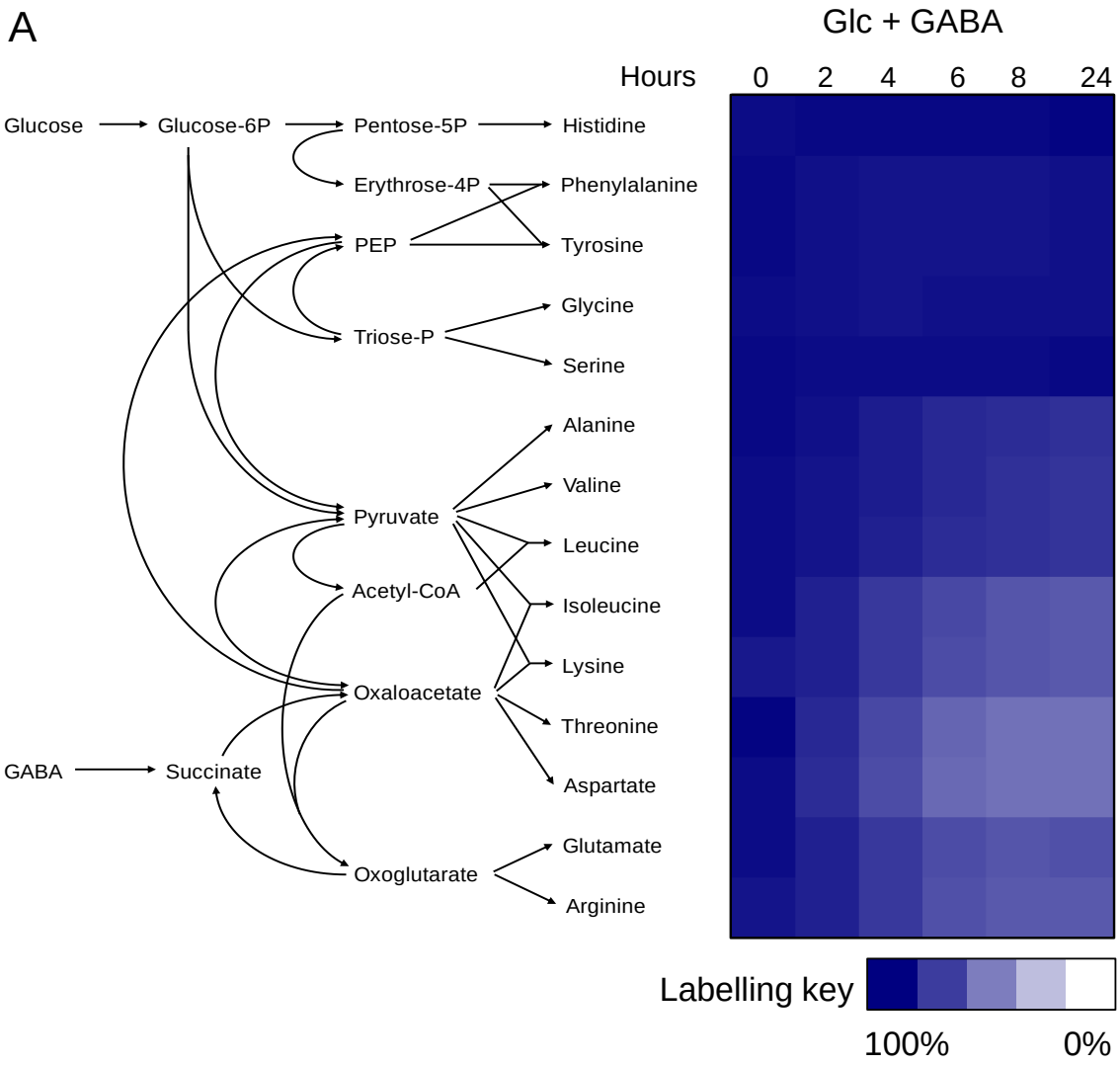
A
Glc + GABA
Hours
0
2
4
6
8
24
Glucose
Glucose-6P
Pentose-5P
Histidine
Erythrose-4P
Phenylalanine
PEP
Tyrosine
Triose-P
Glycine
Serine
Alanine
Valine
Pyruvate
Leucine
Acetyl-CoA
Isoleucine
Lysine
Oxaloacetate
Threonine
GABA
Succinate
Aspartate
Glutamate
Oxoglutarate
Arginine
Labelling key
100%
0%

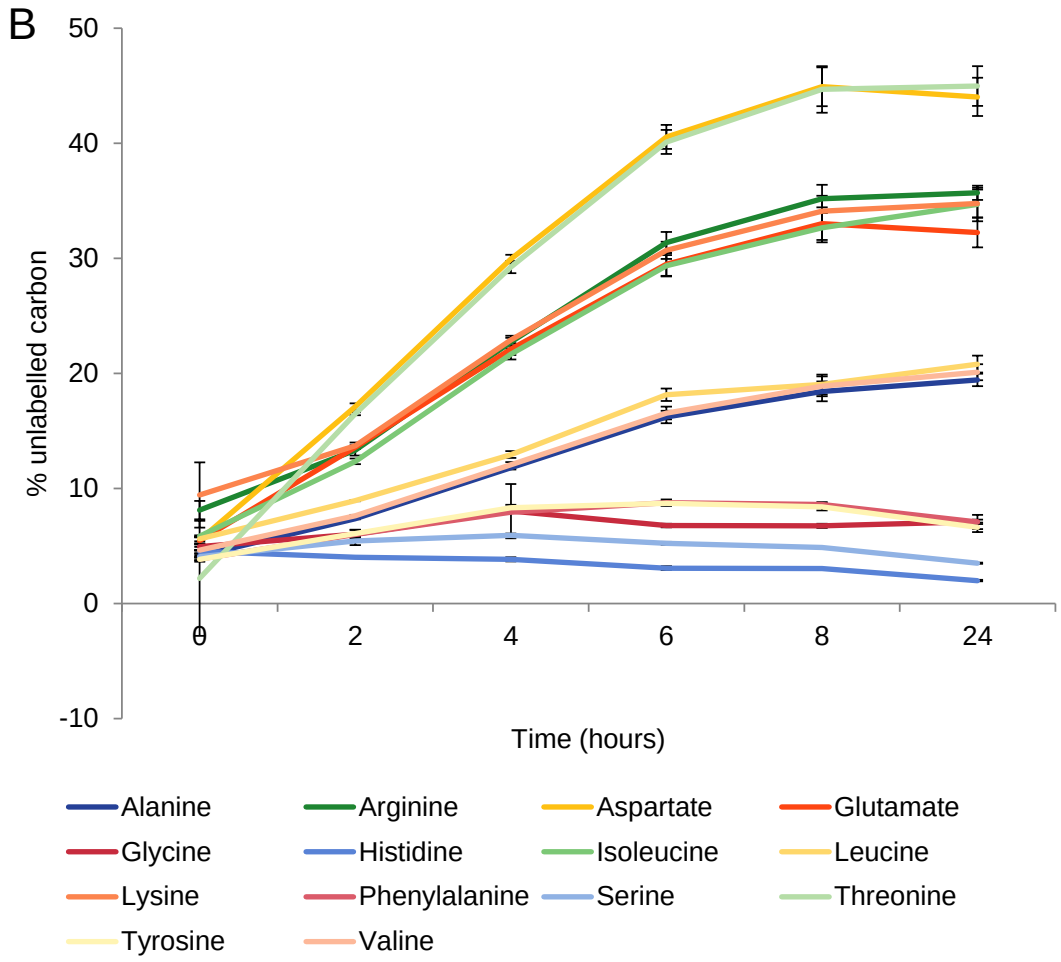

Figure 5.12: Unlabelling patterns in Pst DC3000 incubated with Glc + GABA show carbon from GABA is mainly assimilated into TCA-cycle derived amino acids. (A) Pst DC3000 was incubated with [$^{13}C_6$] glucose prior to incubation with [$^{13}C_6$] glucose and unlabelled GABA. The heatmap squares represent the degree of labelling measured for each fragment: the darkest blue represents 100 % labelling and white represents 0 % labelling. (B) The percentage of unlabelled carbon measured in different amino acids (derived from hydrolysed protein) in Pst DC3000 incubated in [$^{13}C_6$] glucose and unlabelled GABA, error bars represent standard deviation from three independent sample measurements.

ΔgabP and Δ*gabT2/T3/T1* were both able to grow in the Glc + GABA treatment: Δ*gabP* is able to grow as well as the wild type, whilst Δ*gabT2/T3/T1* only showed significant growth after around 10 hours (Section 5.7). In both strains, unlabelled carbon had been metabolised into many amino acids by 24 hours, and to a greater

degree in Δ*gabP* than in Δ*gabT2/T3/T1*. As in Pst DC3000, no substantial amount of unlabelled carbon was incorporated into histidine, phenylalanine or tyrosine after 24 hours (Figure 5.13).

By 24 hours a flux between malate and pyruvate appeared to be active in Δ*gabP* as unlabelled carbon was observed in alanine, valine and leucine, consistent with results from Section 4.2.6, where a large flux from malate to pyruvate was detected in the glucose treatment. In Δ*gabT2/T3/T1* less unlabelled carbon was observed in these amino acids implying that not as much GABA was metabolised as in Δ*gabP*. Alanine was the most unlabelled of the three pyruvate-derived amino acids in Δ*gabT2/T3/T1* which may indicate that alanine was more rapidly synthesised than the others.

The TCA cycle amino acids in Δ*gabP* showed a small increase in unlabelled carbon over the first 8 hours, when growth in this condition was very low. By 24 hours, Δ*gabP* had managed to assimilate some of the unlabelled carbon from extracellular GABA. This implies that an alternative route for GABA uptake is present in Pst DC3000, but that it operates with much lower efficiency than GabP. An additional time-point, between 8 and 24 hours was required to establish if this is the case, and that Δ*gabP* is assimilating GABA throughout its growth curve.

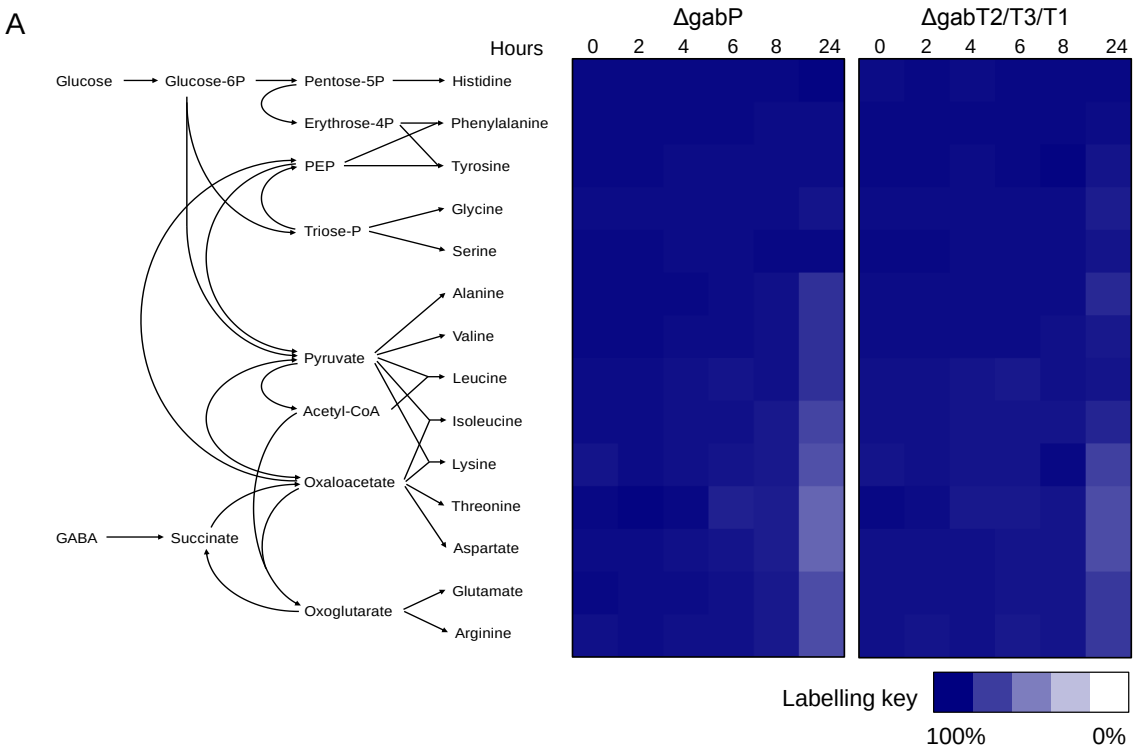
A
ΔgabP
ΔgabT2/T3/T1
Hours
0 2 4 6 8 24
0 2 4 6 8 24
Glucose
Glucose-6P
Pentose-5P
Histidine
Erythrose-4P
Phenylalanine
PEP
Tyrosine
Triose-P
Glycine
Serine
Alanine
Valine
Pyruvate
Leucine
Acetyl-CoA
Isoleucine
Lysine
Oxaloacetate
Threonine
GABA
Succinate
Aspartate
Glutamate
Oxoglutarate
Arginine
Labelling key
100%
0%

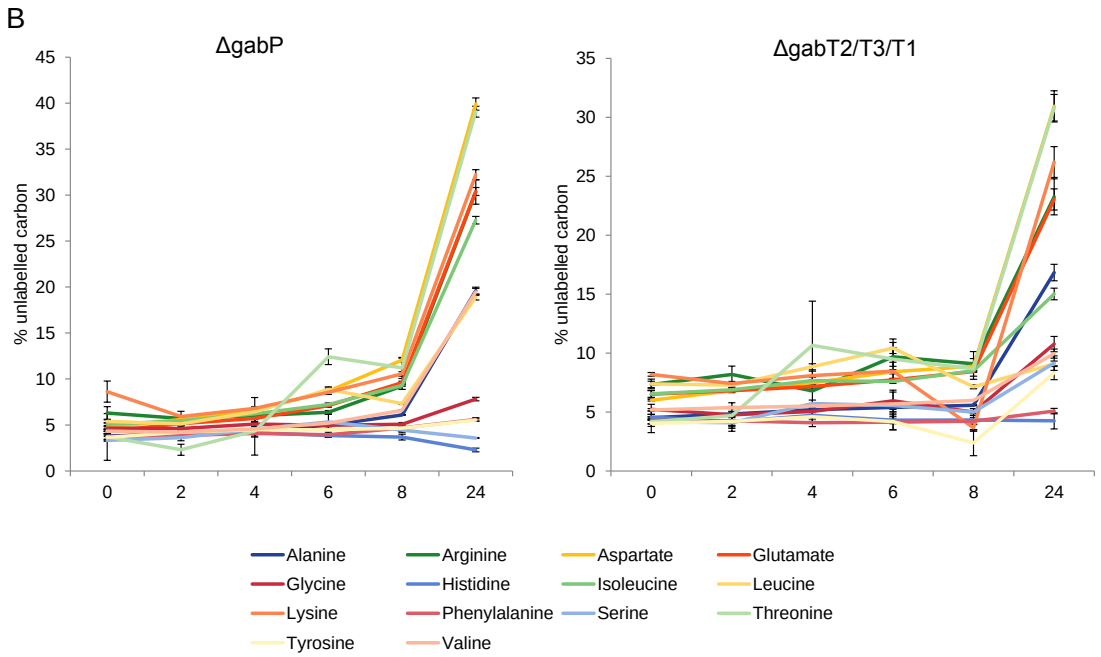

Figure 5.13: Unlabelling patterns in Δ*gabP* and Δ*gabT2/T3/T1* in Glc + GABA treatment reveal alternative mechanisms for GABA uptake and metabolism. (A) Δ*gabP* and Δ*gabT2/T3/T1* were incubated with [$^{13}C_6$] glucose prior to incubation with [$^{13}C_6$] glucose and unlabelled GABA. The heatmap squares represent the degree of labelling measured for each fragment: the darkest blue represents 100 % labelling and white represents 0 % labelling. (B) The percentage of unlabelled carbon measured in different amino acids (derived from hydrolysed protein) in Δ*gabP* and Δ*gabT2/T3/T1* incubated in [$^{13}C_6$] glucose and unlabelled GABA, error bars represent standard deviation.

Conversely, Δ*gabT2/T3/T1* showed no assimilation of unlabelled carbon into any amino acids in the first 8 hours of the experiment. The late onset of growth in the Glc + GABA treatment appeared to be linked to the ability to metabolise GABA, developed between 8 and 24 hours. GABA is most probably metabolised into the TCA cycle first as amino acids derived from oxaloacetate have greatest percentage of unlabelled carbon by 24 hours.

Soluble metabolite analysis confirms analysis of protein hydrolysate-derived amino acids

After 24 hours of incubation in the four treatments, reliable fragments were obtained for 10 soluble metabolites from Pst DC3000, ΔgabP and ΔgabT2/T3/T1. The M-117 fragment has been used in the analysis for the majority of metabolites, though in the case of GABA (M-145), succinate (M-15) and citrate (M-105) alternative fragments have been used.

The unlabelling experiment demonstrated that GABA is produced intracellularly in Pst DC3000 (this was also observed in the analysis of amino acid pool proportions in Sections 3.2.6 to 3.2.8) as it can be detected in the soluble metabolite extract at 24 hours in all strains and across all treatments. GABA is therefore synthesised *de novo* from polyamines, or perhaps via the reverse action of GABA transaminase genes. However, Pst DC3000 did not require the presence of the GABA transaminases, to produce GABA, thus indicating that GABA is likely to be synthesised via polyamine catabolism.

By the 24 hour time point both Δ*gabP* and Δ*gabT2/T3/T1* had assimilated unlabelled carbon from GABA into soluble metabolites in all treatment conditions that contained GABA (Figure 5.14). It is likely in both cases, as was observed in the protein hydrolysate analysis, that GABA has first been metabolised into the TCA cycle as citrate, malate and succinate show the greatest percentage of unlabelled carbon in Δ*gabP* and Δ*gabT2/T3/T1*.

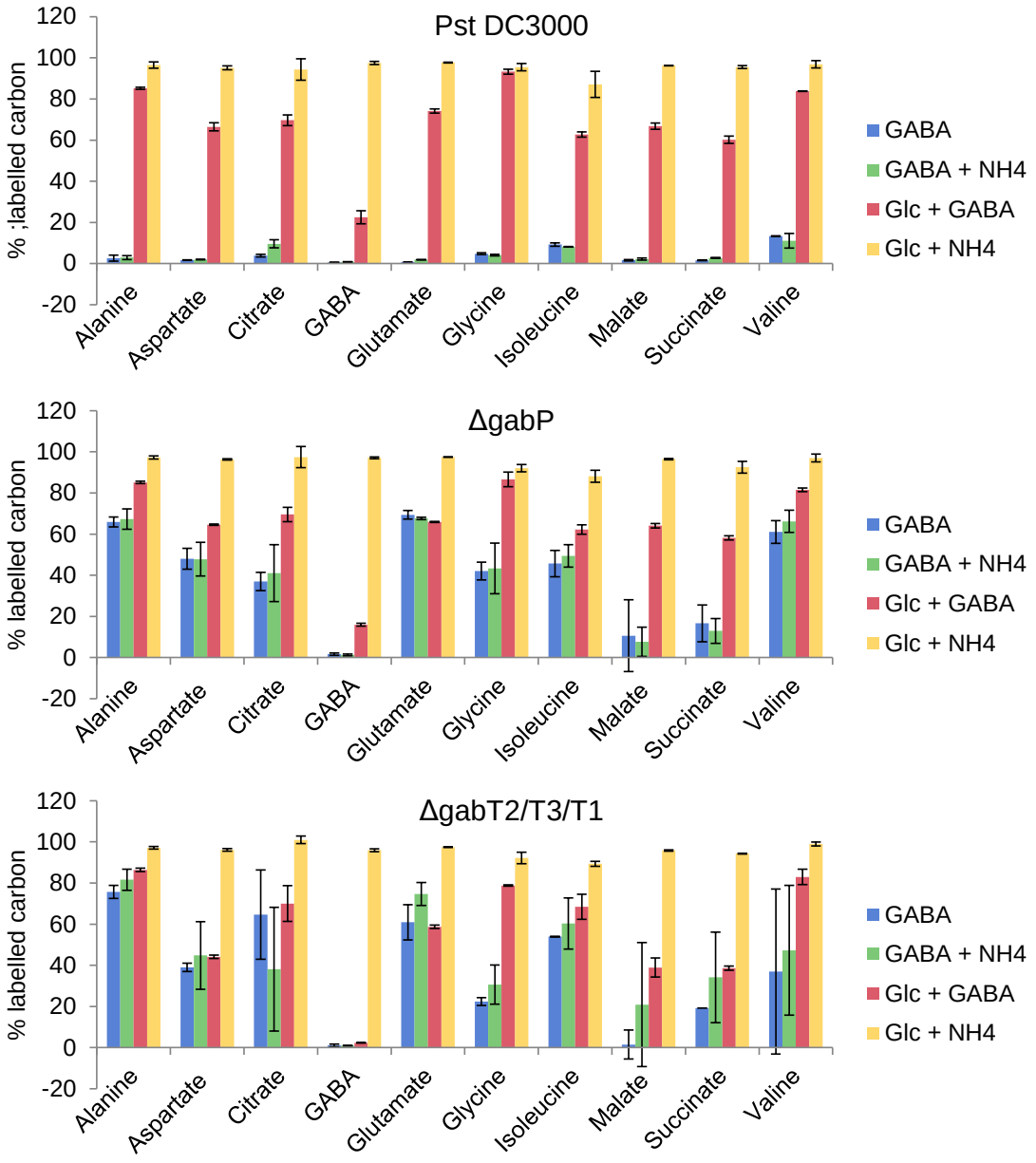

Figure 5.14: Percent of ^{13}C label remaining in soluble metabolites after 24 hours of incubation in four different GABA treatments. Pst DC3000, Δ*gabP* and Δ*gabT2/T3/T1* were incubated with [$^{13}C_6$] glucose prior to incubation with [$^{13}C_6$] glucose and unlabelled GABA to monitor the uptake of GABA as a carbon source, nitrogen source and as a carbon and nitrogen source. Soluble metabolites which could be detected in cell extracts at the 24 hour endpoint of the experiment are shown. Error bars represent standard deviations of three independent samples.

In both Δ*gabP* and Δ*gabT2/T3/T1*, when GABA was the sole source of carbon, glycine showed a greater degree of unlabelled carbon after 24 hours than other

amino acids. As alanine showed a higher percentage of labelling than glycine, we can exclude the possibility of a gluconeogenic flux from pyruvate to the triose phosphates as the source of the unlabelled carbon. Instead, it is most likely that glycine either exists in a much smaller pool (which the amino acid pool proportions below indicate is the case) and is rapidly turned over or that glycine is synthesised by glycine decarboxylase, which would incorporate (increasingly) unlabelled CO_2. However, in Section 4.2.6, under both glucose and fructose conditions, glycine decarboxylase was not predicted to be active.

Intracellular amino acid pool proportions

In addition to the degree of unlabelling, the proportions of amino acids present in soluble metabolites at 24 hours were also examined. In the Glc + NH_4 treatment, the proportions are as those described for the glucose pH 7 treatment in Chapter 3 (Section 3.2.6): glutamate comprises just over 50 % of total measurable amino acid, with alanine the next most abundant amino acid at 20 % (Figure 5.15). The same pattern is observed in Δ*gabP* and in ΔgabT2/T3/T1.

Interestingly, proportionally more intracellular GABA was found in the Δ*gabT2/T3/T1* mutant across all treatments (Figure 5.16). Even when no GABA is present in the medium, the GABA levels in Δ*gabT2/T3/T1* were almost twice that of Pst DC3000 and Δ*gabP*. In the Glc + NH_4 treatment it is possible that GABA was synthesised *de novo* from polyamines but cannot be converted into succinate, resulting in an intracellular build-up.

In the GABA and GABA + NH_4 treatments, the Δ*gabP* and Δ*gabT2/T3/T1* mutants appeared to have large quantities of GABA stored intracellularly. For Δ*gabT2/T3/T1* this is unsurprising as it has been shown to deplete GABA from both complex medium (Section 5.2.8) and minimal medium [88]. The presence of excessive amounts of GABA in Δ*gabP* however must be explained by the presence of an alternative transport system for GABA which is only induced after an incubation period, or that *gabP* normally has the dual function of GABA import and export (which has been reported for the *E. coli* GABA/glutamate antiporter, GadC [296]) and in Δ*gabP* GABA builds up because it cannot leave the cell.

In the Glc + GABA treatment, Δ*gabT2/T3/T1* had amino acid proportions that were highly similar to those that it exhibited in extracted apoplast (Section 5.2.17): higher GABA and proportionally lower glutamate than in the Glc + NH_4 treatment.

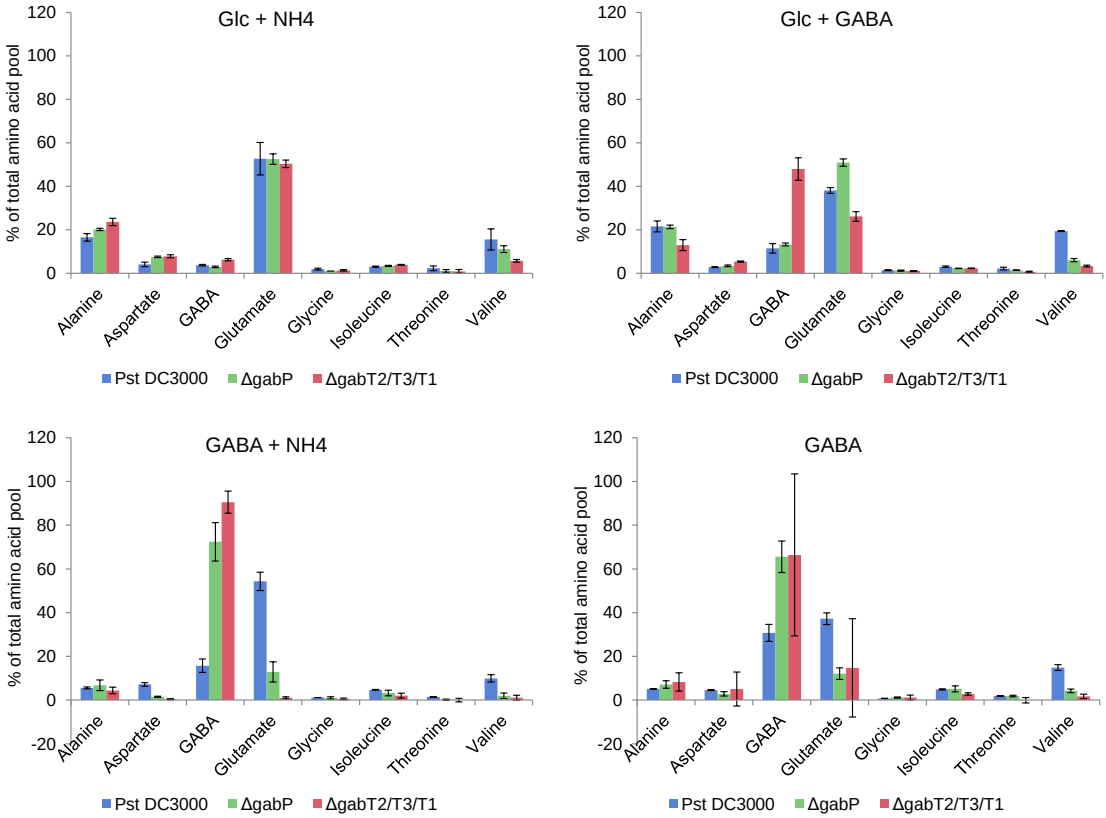

Figure 5.15: Proportional abundances of detectable soluble amino acids after 24 hours of incubation in four different GABA treatments. Pst DC3000, Δ*gabP* and Δ*gabT2/T3/T1* were incubated in M9 modified to monitor the uptake of GABA as a carbon source, nitrogen source and as a carbon and nitrogen source. Soluble amino acids were extracted, quantified and proportional abundances were calculated. Error bars represent standard deviation.

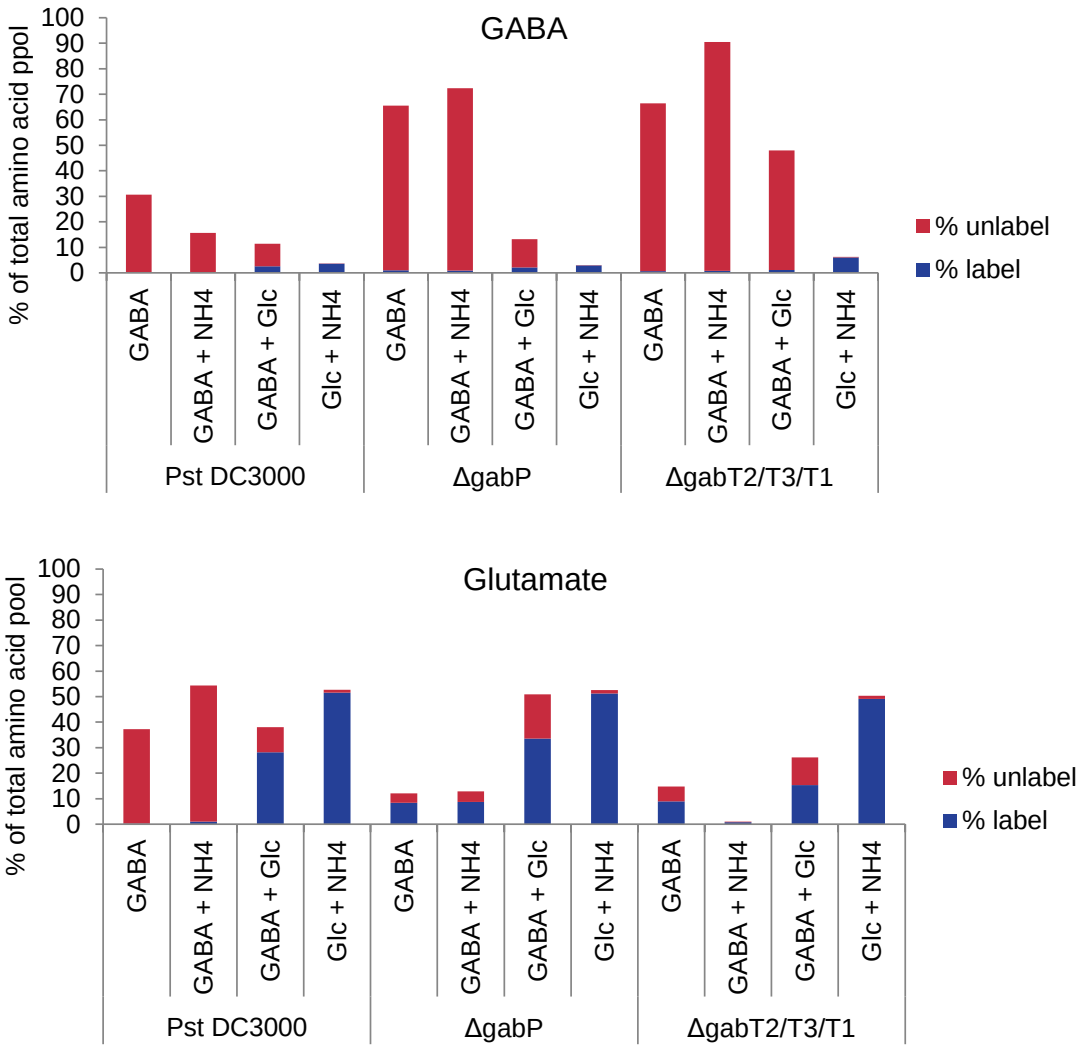

Figure 5.16: Proportion of soluble amino acid attributable to GABA (A) and glutamate (B), and the percentage of which is labelled or unlabelled. Pst DC3000, Δ*gabP* and Δ*gabT2/T3/T1* were incubated with [$^{13}C_6$] glucose prior to incubation with [$^{13}C_6$] glucose and unlabelled GABA to monitor the uptake of GABA as a carbon source, nitrogen source and as a carbon and nitrogen source. Soluble metabolites were extracted and analysed for proportional abundance relative to other amino acids, and the percentage of label remaining in the fragments after 24 hours.

Analysis of unlabelling patterns at an additional time point shows that Δ*gabP* has an alternative GABA transport mechanism

Both the protein hydrolysate and soluble metabolite analyses demonstrated that by 24 hours Δ*gabP* was able to metabolise carbon from GABA in the presence of glucose and that GABA was present intracellularly. However, up until 8 hours very little change in label percentage in protein-bound amino acids was observed. This did not fully resolve the question of whether or not Δ*gabP* was removing NH_4 extracellularly as little growth had occurred by 8 hours (Section 5.2.2). The experiment was therefore repeated on a much smaller scale, with only Pst DC3000 and Δ*gabP* grown in Glc + NH_4 (as a control) and in GABA + Glc. The new time point integrated into the previous set of results is shown in Figure 5.17. This additional sample set revealed that GABA was metabolised by Δ*gabP* throughout the exponential growth phase, though at a much lower level than Pst DC3000, revealing the presence of an alternative GABA transport mechanism. This transport system seems to have a low affinity for GABA, with only enough GABA transported to fulfill the nitrogen requirements of the system and not enough GABA transported to allow growth in the absence of an alternative carbon source.

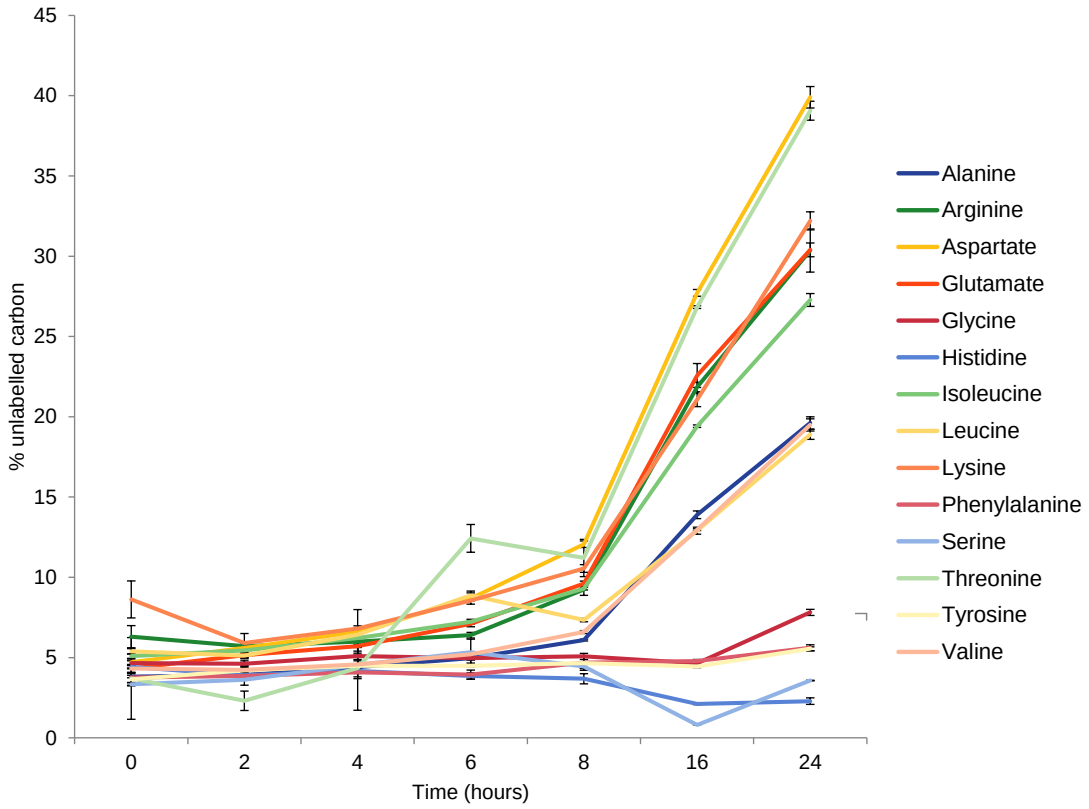

Figure 5.17: Unlabelled carbon present in Δ*gabP* incubated with GABA + Glc, including additional 16 hour time point, demonstrated the presence of an alternative GABA uptake mechanism. Δ*gabP* was incubated with [$^{13}C_6$] glucose prior to incubation with [$^{13}C_6$] glucose and unlabelled GABA to monitor the uptake of GABA as a nitrogen source. Protein was extracted from cells after 16 hours (in addition to time points taken in an earlier experiment) and analysed for the percentage of unlabel that had accumulated in different amino acid fragments.

5.2.5 Characterisation of nutrient utilisation reveals little difference between Δ*gabP*, Δ*gabT2/T3/T1* and Pst DC3000

As polyamines may provide a route for GABA synthesis in Pst DC3000, the ability of the wild type and GABA mutants to use putrescine and ornithine as carbon and nitrogen sources was tested. Pst DC3000 was unable to grow using either putrescine

or ornithine as sole carbon and nitrogen sources, nor was it able to grow when either polyamine was present just as a carbon source (Figure 5.18). The wild type was able to grow using polyamines as nitrogen source to around half the cell densities which would normally be observed in M9. Δ*gabP* and Δ*gabT2/T3/T1* largely showed similar trends, and these were not changed in the presence of GABA. It is likely that polyamines are not rapidly transported, and thus only meet the nitrogen demands of the cell and not the glucose demands, as was previously observed for GABA uptake and metabolism by Δ*gabP* and Δ*gabT2/T3/T1* (Section 5.2.4).

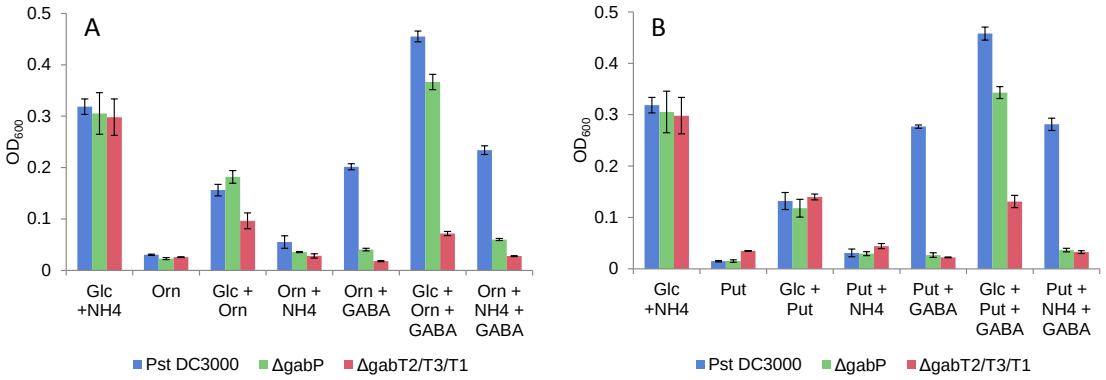

Figure 5.18: Polyamine utilisation by Pst DC3000, Δ*gabP* and Δ*gabT2/T3/T1*. Pst DC3000, Δ*gabP* and Δ*gabT2/T3/T1* were incubated with modified M9, where the polyamines ornithine (A) and putrescine (B) were tested as carbon sources, nitrogen sources and carbon and nitrogen sources. The data shows a 24 hour time point and error bars show standard deviations.

A broader set of profiling was carried out in order to determine if deletions in *gabP* and the GABA transaminase genes would have an adverse effect on the ability of Pst DC3000 to metabolise other nutrient sources. Biolog GN2 96-well plates were used for this analysis and pBS63 plasmid (*luxCDABE::phrpL*, Section 3.2.3) versions of Pst DC3000, Δ*gabP* and Δ*gabT2/T3/T1*. As previously (Section 3.2.4), the phenoarrays were conducted at 2 pHs: a neutral pH (pH 7) and an acidic

pH (pH 5.5). The resulting measurements were adjusted for total plate metabolic activity. Pst DC3000 was able to metabolise 25 different substrates at both pHs and Δ*gabP* and Δ*gabT2/T3/T1* were able to metabolise many of the same set of substrates, with the notable exception of GABA (Figure 5.19). Interestingly, metabolic activity in the presence of glutamate was significantly higher in both Δ*gabP* and Δ*gabT2/T3/T1* at pH 5.5 than Pst DC3000. In assays where the pH was neutral, this higher metabolic activity with glutamate was observed only in Δ*gabT2/T3/T1*. At pH 5.5, citric acid, formic acid and aspartate all presented instances where Δ*gabP*'s metabolic activity was higher than Pst DC3000 relative to total plate metabolic activity. It is likely that these substrates, and glutamate, would be further lowering the pH beyond the inoculating fluid pH (adjusted to pH5.5) and thus might present more favourable growth conditions. Δ*gabT2/T3/T1* is unable to metabolise formic acid or 2-oxoglutarate at either pH. This indicates that Pst DC3000 may not able to convert 2-oxoglutarate to glutamate except via the action of the GABA transaminases, and that 2-oxoglutarate is a amino acceptor during the transamination of GABA in Pst DC3000. Both Δ*gabP* and Δ*gabT2/T3/T1* are unable to metabolise proline. Why this would be the case for either strain is unclear.

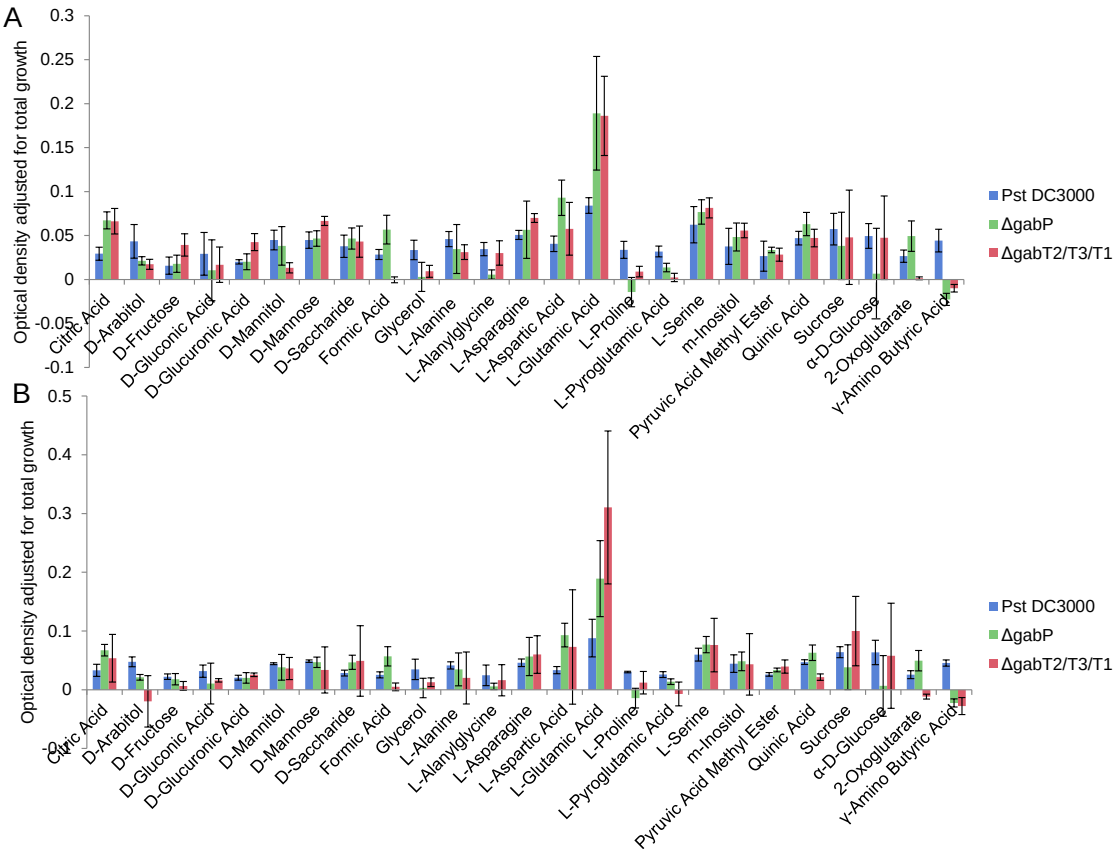

Figure 5.19: Biolog GN2 metabolism profiles of DC3000, Δ*gabP* and Δ*gabT2/T3/T1* show differences in the metabolism of specific substrates. Metabolism of Pst DC3000, Δ*gabP* and Δ*gabT2/T3/T1* after 36 hours in Biolog GN2 plates with inoculating fluid adjusted to pH 5.5 (A) or pH 7 (B). Data has been adjusted for total plate metabolic activity and only metabolites where significant levels of growth were observed have been shown. Error bars represent standard deviations. A full list of the 95 carbon substrates present in Biolog GN2 MicroPlates is shown in Appendix A.1.

5.2.6 Mutations in GABA genes do not affect growth in extracted host apoplast

As GABA is a major amino acid component of the tomato leaf apoplast [71], the ability of Δ*gabP* and Δ*gabT2/T3/T1* to grow in extracted apoplast was tested against that of the wild type. A commonly used rich media, LB, was also included in the assay to act as a point of comparison. All strains grew to the highest densities

in extracted apoplast and there was no significant difference in the densities achieved by Pst DC3000, Δ*gabP* and Δ*gabT2/T3/T1* after 24 hours (Figure 5.20). As the apoplast is an environment rich in carbon sources, it seems likely, as in the Glc + GABA treatment of Section 5.2.2 that Δ*gabP* and Δ*gabT2/T3/T1* are able to metabolise GABA to sufficient levels to support normal growth. Rico *et al* [71] discovered that tomato leaf apoplast acts as a complete growth medium for Pst DC3000, and the same is true for Δ*gabP* and Δ*gabT2/T3/T1*.

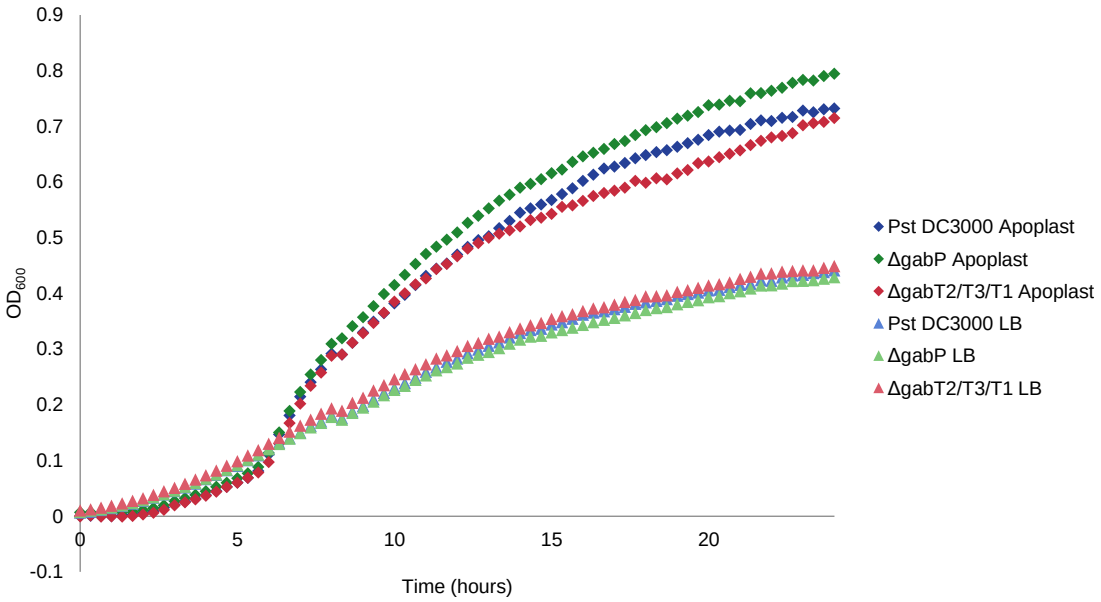

Figure 5.20: Pst DC3000, Δ*gabP* and Δ*gabT2/T3/T1* show higher growth in tomato leaf apoplast in comparison with growth in LB media. Pst DC3000, Δ*gabP* and Δ*gabT2/T3/T1* were incubated in extracted tomato leaf apoplastic fluid and LB medium and monitored for growth over a 24 hour period. This experiment was performed twice and the same growth patterns were obtained each time.

5.2.7 Mutations in GABA genes do not affect growth in tomato plants

The wild type and GABA mutants were also tested for their ability to grow within tomato leaves. Park *et al* had previously shown that Δ*gabT2/T3/T1* grew less well than the wild type in *A. thaliana* [88]. *A. thaliana* is known to upregulate GABA production in the presence of Pst DC3000 [7] and as GABA has been shown to inhibit the growth of GABA transaminase mutants [88] it is possible this is the cause of the growth inhibition. An increase in GABA production in tomato leaves has not been observed in response to infection by Pst DC3000, and though GABA levels are naturally high in tomato leaves, it can be seen in Figure 5.21 that there is no significant difference in viable cell counts between Pst DC3000 and Δ*gabT2/T3/T1* when grown in tomato leaves. Δ*gab*P is also able to grow as well as Pst DC3000. This result, in conjunction with the apoplast growth assay, confirm that mutations in the GABA permease gene and in the GABA transaminase genes do not inhibit growth in the plant environment.

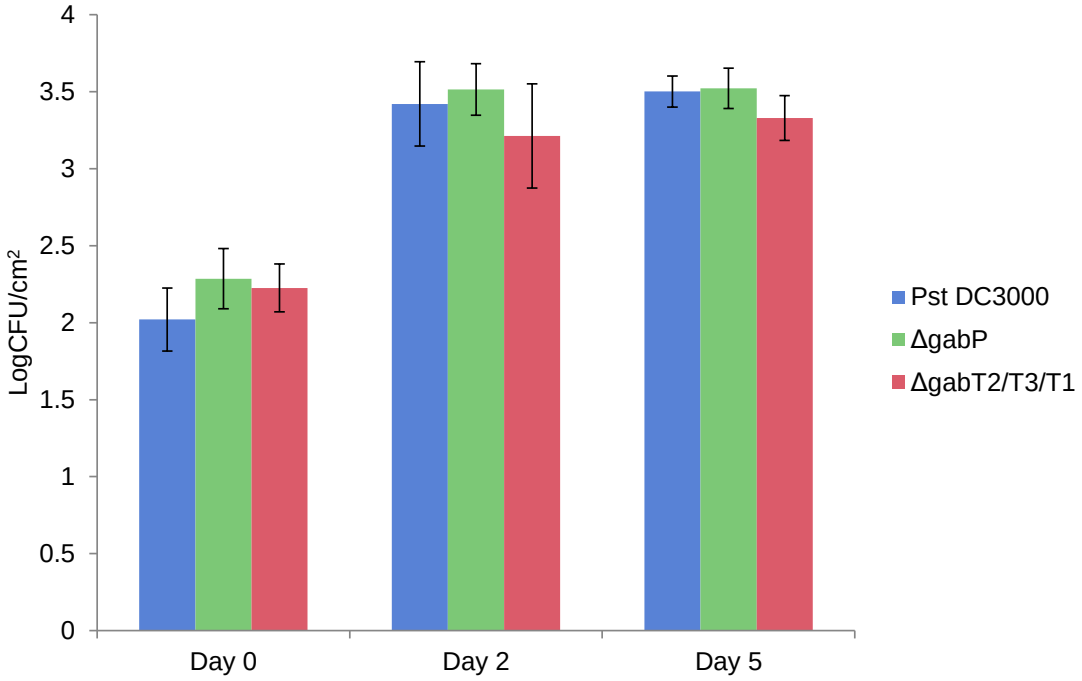

Figure 5.21: Pst DC3000, Δ*gabP* and Δ*gabT2/T3/T1* grow to the same density in tomato leaves over 5 days. Pst DC3000, Δ*gabP* and Δ*gabT2/T3/T1* cells were suspended in 10mM MgCl2 and inoculated into tomato leaves. Leaf disks were excised and cell counts were made after 2 days and after 5 days. Error bars show standard error from four independent samples on each day.

5.2.8 Δ*gabP* and Δ*gabT2/T3/T1* have highly similar apoplast depletion profiles to Pst DC3000, including GABA depletion

In order to test if the GABA mutants were impaired in their ability to deplete nutrients from extracted host leaf apoplast, Δ*gabP* and Δ*gabT2/T3/T1* were grown in apoplast which was then profiled using ^{1}H-NMR, as per Section 3.2.2. The Biolog GN2 analysis revealed there are notable differences in the ability of the GABA mutants to metabolise certain metabolites, and so the pace of metabolite depletion

in the GABA mutants compared with Pst DC3000 was investigated. Figure 5.22 demonstrates the similarity in depletion profiles both at 8 hours post inoculation and 24 hours. At 24 hours post inoculation (Figure 5.22B) there were no significant differences in the depletion profiles of Pst DC3000, Δ*gabP* and Δ*gabT2/T3/T1*. As with Pst DC3000, the GABA mutants were able to fully deplete many of the metabolites in the apoplast extract including amino acids such as asparagine, aspartate, glutamine and glutamate, and deplete little of the betaine, inositol, serine and threonine present. Most notably, by 24 hours GABA had been depleted from the apoplastic extract by Δ*gabP* and Δ*gabT2/T3/T1* to the same degree as observed in the wild type.

At the 8 hour time point, there is an appreciable difference in the depletion of GABA by the three strains (Figure 5.22A). Pst DC3000, by 8 hours, had begun to deplete GABA (around 10 % has been removed from the extract), however Δ*gabP* was unable to do so, and in fact a small increase is observed in the GABA in the apoplast (7 %). The delay in GABA uptake is consistent with the results oberved in the GABA unlabelling experiment (Section 5.2.4): Δ*gabP* was able to assimilate GABA from 8 hours onwards, and the delay was likely to be due to the slow induction of an alternative transport system. The small increase in extracellular GABA must be explained by extracellular synthesis of GABA, or the expulsion of intracellular GABA from the bacteria. A smaller decrease in GABA was observed in the apoplast extracts incubated with Δ*gabT2/T3/T1* (an average of around 3 %), though this level of depletion is not significantly different from that of Pst DC3000.

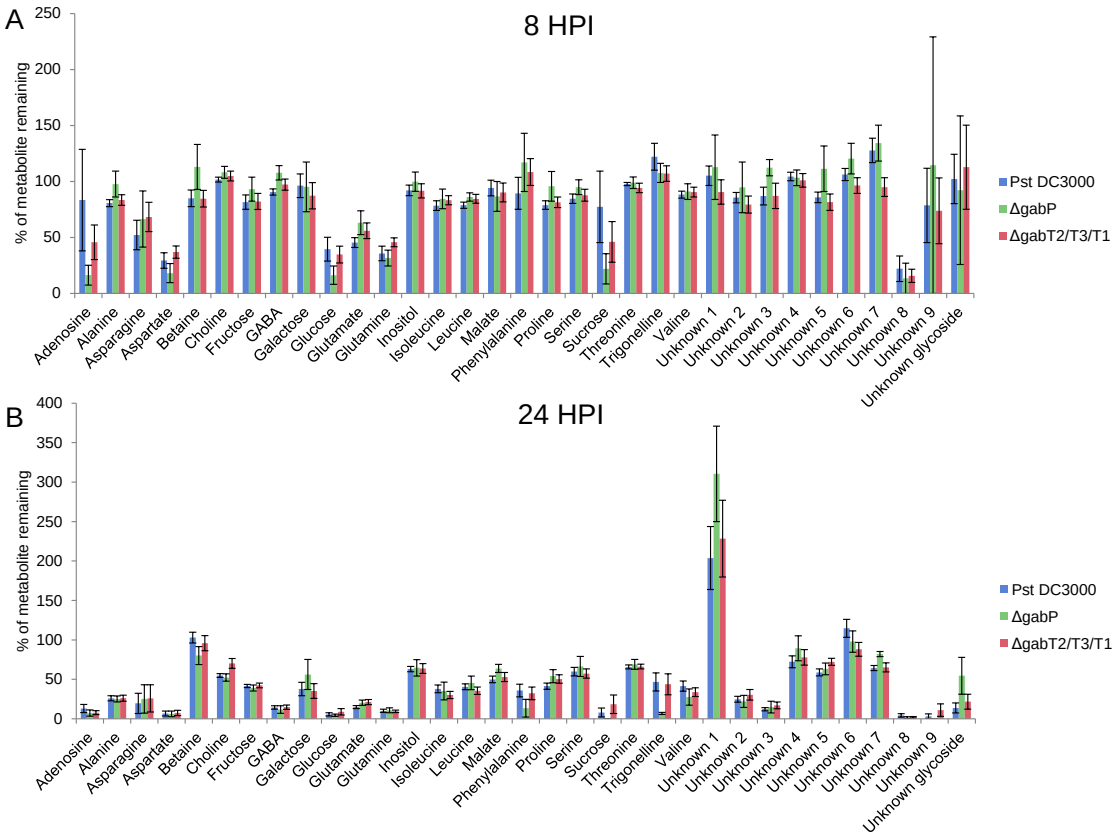

Figure 5.22: Percentage of tomato leaf apoplastic metabolites remaining, 8 and 24 hours, post inoculation with Pst DC3000, Δ*gabP* and Δ*gabT2/T3/T1*. Cells were inoculated into extracted tomato leaf apoplast and metabolite changes were monitored after 8 (A) and 24 (B) hours by ^{1}H-NMR. Error bars show the standard error from three independent sample sets. Tyrosine is not shown owing to very large errors.

5.2.9 Mutations in GABA transaminase genes affect the ability of Pst DC3000 to cause disease symptoms in tomato plants

Park *et al* (2010) [88] demonstrated that Δ*gabT2/T3/T1* was impaired in it's ability to cause a hypersensitive response in the non-host plant tobacco, and that this effect was amplified in the presence of exogenous GABA at concentrations of 1 mM or more. However, the ability of Δ*gabT2/T3/T1* to cause disease symptoms in the

native host, tomato, was not tested. In this study, Δ*gabT2/T3/T1* was inoculated into tomato leaves at a CFU of 1 x 10^5 alongside Pst DC3000, Δ*gabP* and 10 mM $MgCl_2$ as a negative control. Whilst growth of Δ*gabT2/T3/T1 in planta* did not differ from that of the wild type (Section 5.2.7), the elicitation of disease symptoms was notably different. Δ*gabT2/T3/T1* was unable to produce disease symptoms (necrosis in this case) to the same degree as the wild type (Figure 5.23). Δ*gabP* did not show a reduction in disease symptoms.

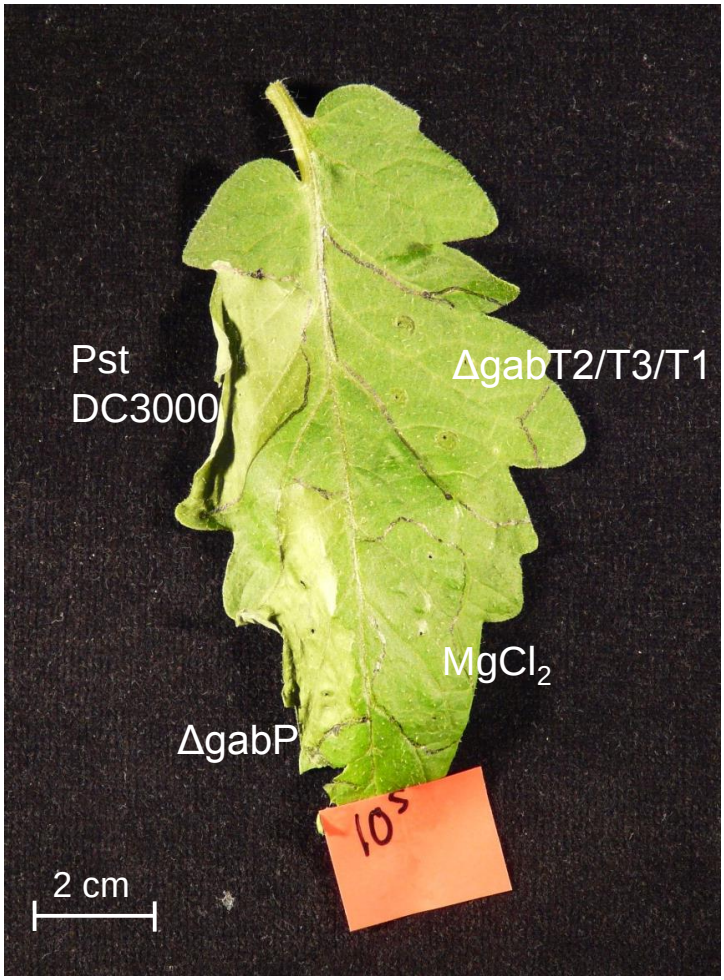

Figure 5.23: Δ*gabT2/T3/T1* does not cause visible disease symptoms in the host plant. Pst DC3000, Δ*gabP* and Δ*gabT2/T3/T1* cells were suspended in 10 mM $MgCl_2$ at 10^5 CFU and inoculated into tomato leaves (black lines mark the inoculation area). 10 mM $MgCl_2$ was also inoculated into leaves to act as a control. After 2 days, necrosis could be observed in parts of the leaves inoculated with Pst DC3000 and Δ*gabP*. Three leaves were inoculated on four different plants, and the photo is representative of the results observed on all leaves.

5.2.10 Δ*gabP* induces a stronger hypersensitive response in tobacco leaves in the presence of excess GABA

In Section 5.2.9, Δ*gabP* was shown to cause the same level of disease symptoms as the wild type on the tomato host plant, implying Δ*gabP* expresses its virulence

genes to the same degree as the wild type. Another useful way of examining *in planta* virulence gene expression is the use of non-host plants to monitor the hypersensitive response (localised cell death in the plant in response to the expression of virulence genes by the invading pathogen). In order to determine if $\Delta gabP$ was impaired in eliciting the hypersensitive response in a non-host, and in a non-host with excess apoplastic GABA, tobacco lines (seeds supplied by Prof. Barry Shelp, University of Guelph) were inoculated with Pst DC3000 and $\Delta gabP$ in 10-fold dilution series. MacLean *et al* (2003) described a set of tobacco lines which all overproduced GABA by the action of glutamate decarboxylase overexpression [297]. An additional copy of a gene encoding glutamate decarboxylase, the GAD enzyme, from petunia, was included in each line. Two of the lines (GADΔC1 and 2) were transformed with a truncated version of the gene, lacking the autoinhibitory calmodulin-binding domain. In young GADΔC1 seedlings, GABA was found to be produced at concentrations of 17 nmol g^{-1} FW in comparison with 7 nmol g^{-1} FW in wild type seedlings [297], which was among the highest levels of GABA observed in the transgenic lines. All lines were subsequently analysed by Dr. Rachel Jones [85] for their leaf apoplast amino acid content and GADΔC1 was found to have the highest levels of GABA. GABA accounted for 61% percent of total amino acid in extracted GADΔC1 leaf apoplast in comparison with 36% in wild type leaves [85].GADΔC1 was therefore used in this study in conjunction with the wild type line Delgold.

Upon inoculation into the wild type tobacco, $\Delta gabP$ elicited a very similar hypersensitive response to Pst DC3000 (Figure 5.24A): both were able to produce

hypersensitive responses at densities of 1 x 10^7 and 1 x 10^6. However, ΔgabP elicited a stronger hypersensitive response relative to Pst DC3000 when inoculated into GADΔC1 plants (Figure 5.24B): ΔgabP was able to produce a hypersensitive response at 1 x 10^6 whereas Pst DC3000 was not. The expression of virulence genes by Pst DC3000 is inhibited by GABA [88] and this appears to occur in GADΔC1 plants, whereas Δ*gabP* does not suffer the same levels of inhibition.

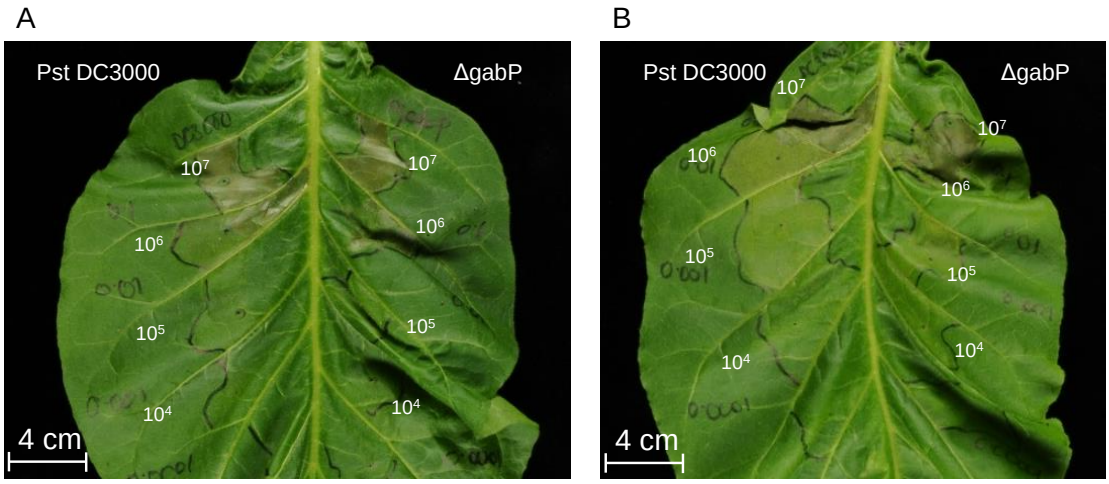

Figure 5.24: Δ*gabP* is able to elicit a stronger HR from tobacco plants that overproduce GABA than Pst DC3000 . Pst DC3000 and Δ*gabP* cells were suspended in 10 mM $MgCl_2$ at 10^7, 10^6 , 10^5 and 10^4 CFU/ml and inoculated into wild type tobacco leaves (A) or tobacco GADΔC1 leaves (B). After 24 hours, HR symptoms could be observed in parts of the leaves inoculated with Pst DC3000 and Δ*gabP*. Three leaves were inoculated on four different plants, and the photo is representative of the results observed on all leaves.

5.2.11 ΔgabT2/T3/T1 shows a decreased ability to elicit the hypersensitive response in tobacco plants with elevated levels of GABA

ΔgabT2/T3/T1 was tested in tobacco plants for its ability to cause a hypersensitive response by Park *et al* [88]. Park *et al* [88] looked at the effects of co-inoculating

the GABA transaminase mutants with different concentrations of GABA and found that concentrations of 1 mM and above inhibited the production of a hypersensitive response, whereas Pst DC3000 was able to elicit a strong hypersensitive response with up to 10 mM of co-infiltrated GABA. As previously (Section 5.2.10), wild type and GADΔC1 tobacco plants were used to monitor the HR-inducing abilities of ΔgabT2/T3/T1. The results obtained from this study (Figure 5.25) matched those found by Park *et al* [88]: the absence of GABA transaminase genes results in a milder hypersensitive response in a non-host plant when GABA is present in excess of natural abundances when compared with the wild type.

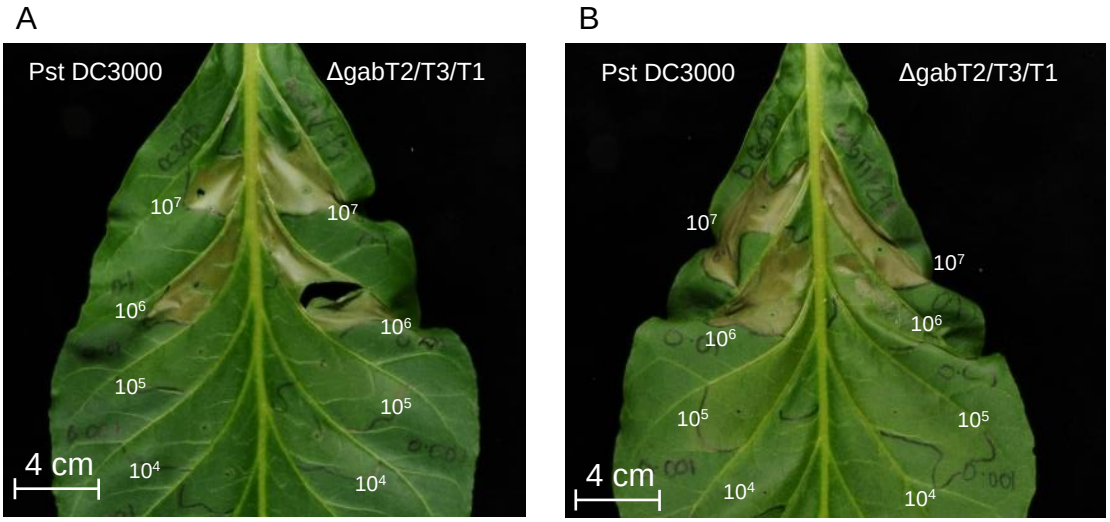

Figure 5.25: Δ*gabT2/T3/T1* is not able to elicit an HR from tobacco plants that overproduce GABA at the same cell densities as Pst DC3000. Pst DC3000 and Δ*gabT2/T3/T1* cells were suspended in 10 mM $MgCl_2$ at 10^7, 10^6 , 10^5 and 10^4 CFU/ml and inoculated into wild type tobacco leaves (A) or tobacco GADΔC1 leaves (B). After 24 hours, HR symptoms could be observed in parts of the leaves inoculated with Pst DC3000 and Δ*gabT2/T3/T1*. Three leaves were inoculated on four different plants, and the photo is representative of the results observed on all leaves.

5.2.12 Virulence gene expression by Δ*gabT2/T3/T1* is lower in extracted tomato apoplast than expression by Pst DC3000

To test whether the reduction in symptoms and hypersensitive responses observed in Δ*gabT2/T3/T1*-infected plants (Section 5.2.9) was due to the apoplastic environment encountered by the bacteria, extracted tomato leaf apoplast was inoculated with bacteria containing the pBS63 (*luxCDABE::phrpL*) plasmid. Pst DC3000, Δ*gabP* and Δ*gabT2/T3/T1* were grown for 36 hours in a 96-well plate in the presence of both rifampicin (to prevent the growth of any other microorganisms present in the extracts) and kanamycin (for the retention of the pBS63 plasmid). Whilst virulence gene expression was many fold lower than observed in minimal media, differences in expression could be detected (Figure 5.26). Most notably, *hrpL* expression by Δ*gabT2/T3/T1* was 54 % lower than in Pst DC3000 (value taken from integrated expression curves over 40 hours). Δ*gabP* showed a slight reduction (23 % lower) in comparison with Pst DC3000, however, this reduction was not significant enough to impair the strain's ability to cause disease symptoms in the host (Section 5.2.9).

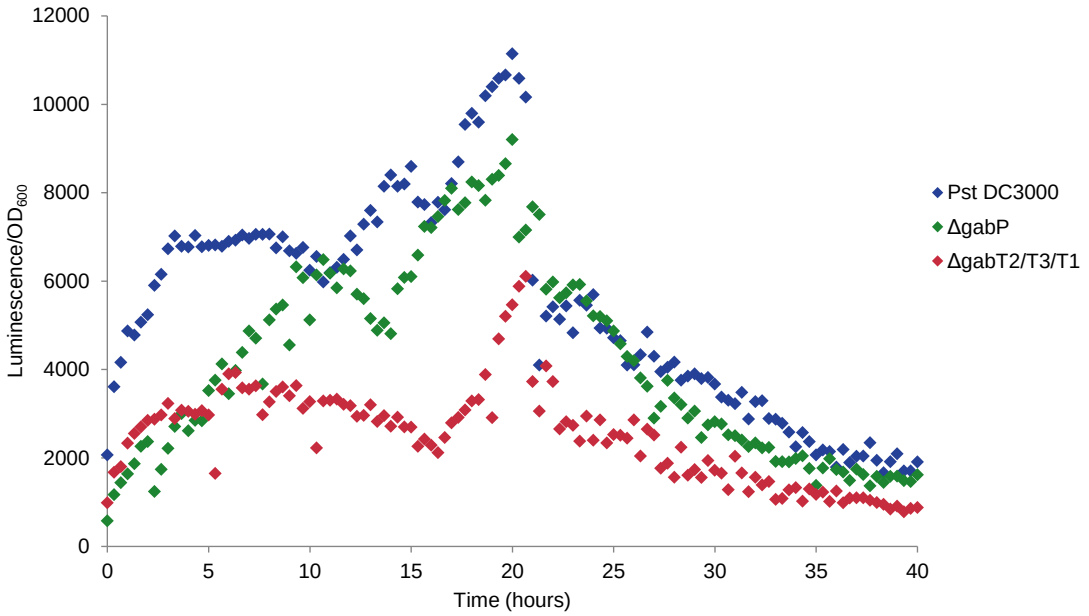

Figure 5.26: Expression of *hrpL* in Pst DC3000 (pBS63), Δ*gabP* (pBS63) and Δ*gabT2/T3/T1* (pBS63) in extracted tomato apoplastic fluid shows virulence gene expression is notably reduced in Δ*gabT2/T3/T1* (pBS63). Pst DC3000 (pBS63), Δ*gabP* (pBS63) and Δ*gabT2/T3/T1* (pBS63) cells were incubated in extracted tomato leaf apoplast over 40 hours. Luminescence readings are adjusted for optical density. The experiment was repeated twice and the same patterns of expression obtained both times.

As noted by Rico *et al* (2008) [71], virulence gene expression in extracted apoplastic fluid is much lower than the levels of expression observed in minimal media (for example, Section 5.2.15) and this was the case for all three strains.

5.2.13 Virulence gene expression by Δ*gabT2/T3/T1* is inhibited by GABA *in vitro* more than Pst DC3000; Δ*gabP* shows little inhibition

Sections 5.2.9, 5.2.10 and 5.2.11 present the possibility that GABA does not significantly inhibit virulence gene expression in Δ*gabP* (although Δ*gabP* does show

mild repression relative to Pst DC3000 in extracted host apoplast in Section 5.2.12), but does so in Pst DC3000 and to a much greater degree in Δ*gabT2/T3/T1*. To test this hypothesis, all three strains were incubated with M9 (with fructose as the main carbon source to stimulate high levels of virulence gene expression) and GABA ranging in concentration from 10 μM to 10 mM. The virulence gene expression data clearly demonstrated inhibition of Pst DC3000 at GABA concentrations of 100 μM and above, with the most significant decease in expression observed between 100 μM and 1 mM (Figure 5.27). Δ*gabT2/T3/T1* was inhibited at all GABA concentrations and consistently showed a much greater degree of repression than Pst DC300, with up to a 77.6 % reduction observed in Δ*gabT2/T3/T1* and 63.3 % in Pst DC3000 (values from integrated expression curves over 36 hours). Δ*gabP* is inhibited most in the presence of 1 mM GABA (a 12.3 % reduction in comparison to the no GABA treatment). Strong virulence gene repression by GABA therefore requires the entry of GABA into the intracellular environment, with higher concentrations of GABA likely to lead to higher levels of inhibition.

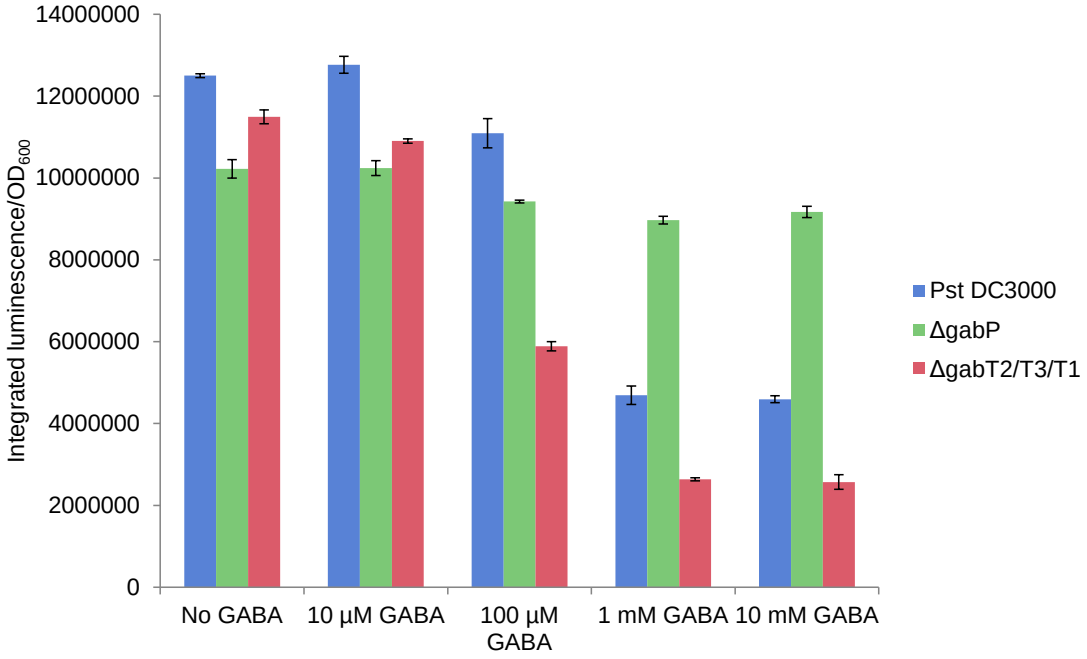

Figure 5.27: *hrpL* expression of Pst DC3000 (pBS63), Δ*gabP* (pBS63) and Δ*gabT2/T3/T1* (pBS63) with different concentrations of GABA. Cells were grown in M9-fructose with different amounts of GABA. Luminescence of the pBS63 plasmid was monitored over 36 hours. Luminescence values, corrected for optical density, were integrated over 36 hours to give the total luminescent expression over the period. Error bars represent standard deviation.

5.2.14 Biolog assays highlight differences in *hrpL* expression by GABA mutants in response to different carbon sources

Virulence gene expression in Δ*gabP* and Δ*gabT2/T3/T1* has been shown to be different to that of the wild type, both *in planta* and in extracted apoplast (Sections 5.2.10, 5.2.11 and 5.2.12). In order to determine if this effect was solely due to differential *hrp* expression in response to the presence of GABA, Biolog GN2 plates were used to test virulence gene expression in response to 95 different carbon sources.

hrpL expression was monitored, using the pBS63 versions of Pst DC3000, Δ*gabP* and Δ*gabT2/T3/T1*, under the same experimental conditions as used previously (Section 5.2.5). Again, the data from the Biolog assays were integrated and normalised within the set of data so as to make the data more comparable across repeats. Figure 5.28 shows the relative *hrp* expression on substrates where a significant amount of metabolic activity was observed. General trends in *hrpL* expression are retained across the three strains, such as upregulation in response to asparagine, aspartate, fructose, mannitol and mannose, in both pH treatments. However, there are some notable differences in *hrp* responses to specific metabolites. Asparagine, aspartate, GABA, glutamate and proline create notably different *hrp* expression profiles in the three strains. This may be due to the different growth levels these strains exhibited on these substrates, particularly in the case of glutamate.

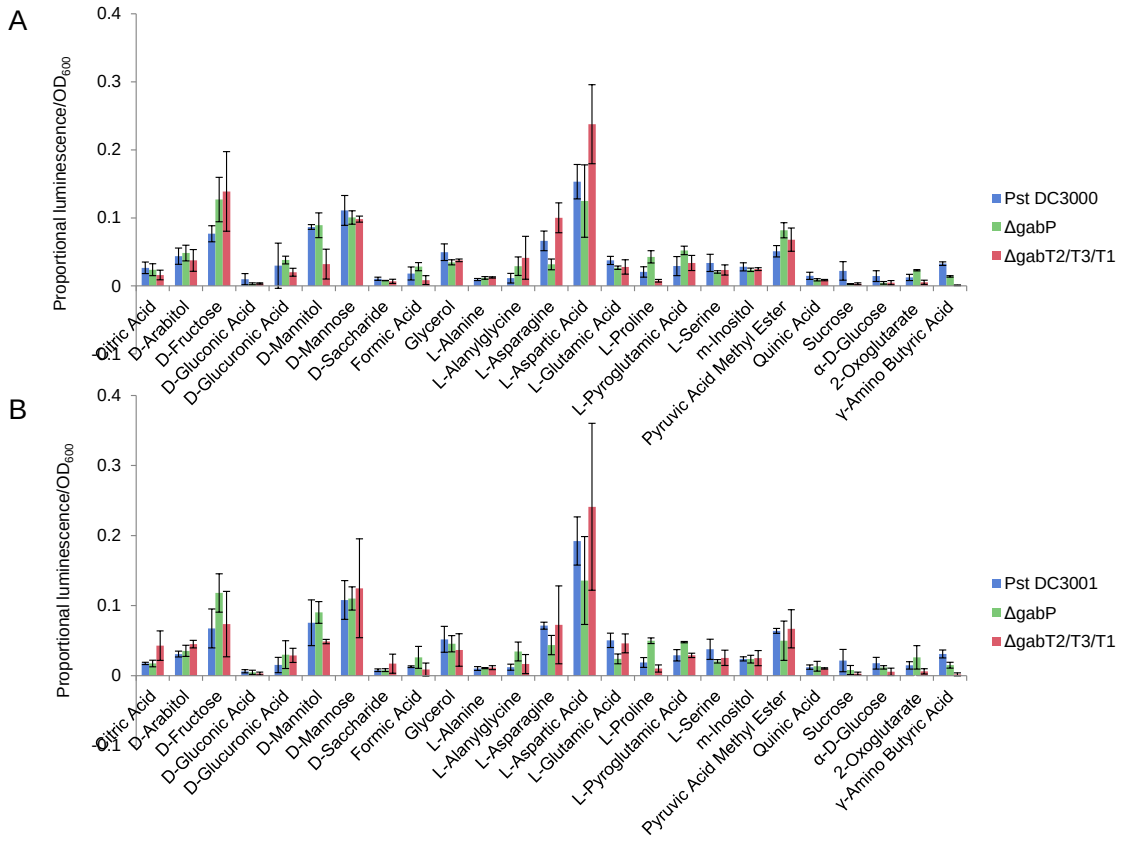

Figure 5.28: *hrpL* expression of Pst DC3000 (pBS63), Δ*gabP* (pBS63) and Δ*gabT2/T3/T1* (pBS63) in response to Biolog GN2 substrates at pH 5.5 and pH 7. Cells were suspended in inoculating fluid at pH 5.5 (A) or pH 7 (B) and added to the Biolog GN2 plates. Luminescence was recorded over a 36 hour period, corrected for optical density values and then integrated. Only substrates for which growth was observed have been included. Error bars show standard deviation. A full list of the 95 carbon substrates present in Biolog GN2 MicroPlates is shown in Appendix A.1.

5.2.15 Targeted metabolite analysis: verification of Biolog results and virulence gene expression in response to apoplastic metabolites

The previous Biolog GN2 analysis (Section 5.2.14) gave a helpful overview of potential differences which may exist between the wild type and the GABA mutants, however, the Biolog assay can produce noisy data, and also does not allow for the

testing of *hrp* gene responses to substrates which cannot be metabolised. Therefore, to further understand how different metabolites affect virulence gene expression in Δ*gabP* and Δ*gabT2/T3/T1*, a M9-fructose assay was used, for reasons discussed previously (Section 3.2.5). All of the known carbon sources present in the apoplast were tested (from studies using HPLC, GC-MS and ^{1}H-NMR), and each was included at 5mM (actual apoplast concentrations were not used owing to discrepancies between detection methods giving different concentrations, however metabolites can reach these levels of concentration as shown in Section 3.2.1). In addition, some other metabolites related to GABA, such as the polyamines putrescine and ornithine, were included in the assay. Where metabolites would have caused a change in pH, for example aspartate, this was corrected so that all experimental treatments were at pH 7. Figure 5.29 shows the *hrpL* expression curves for Pst DC3000, Δ*gabP* and Δ*gabT2/T3/T1*, which all express *hrpL* to the same degree and in the same pattern of expression. Expression curves (once adjusted for OD), were integrated over the first six hours (typically the time period when virulence genes are most upregulated in the host [50]) and over 36 hours (which encapsulates growth up to stationary phase and the peak of *hrp* expression when just fed fructose). Integrated values with different metabolites were then compared against fructose-only fed cells to give a fold change in expression (Figures 5.29 and 5.30).

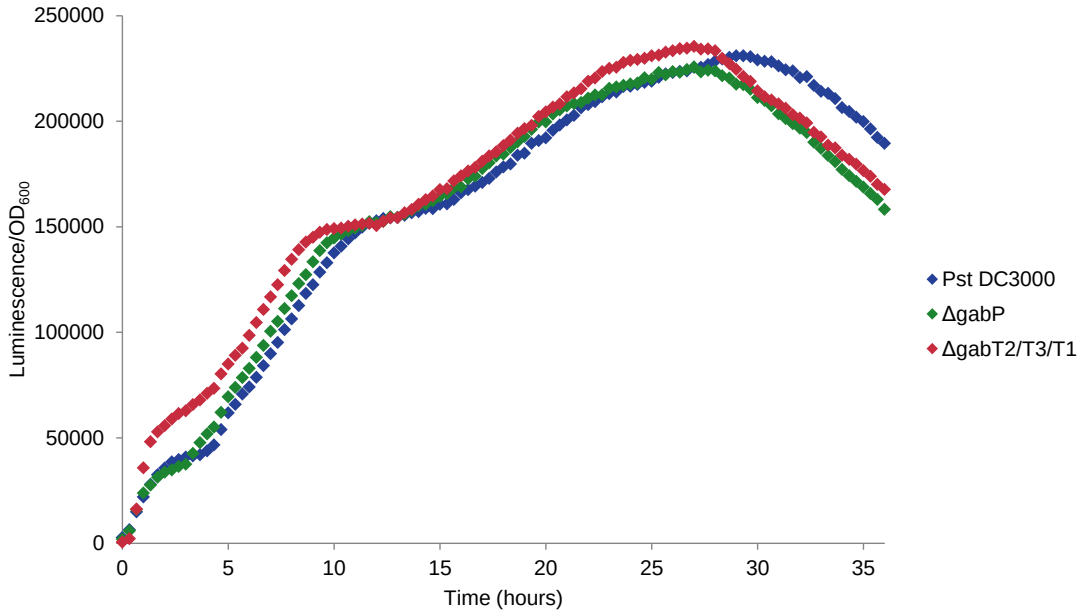

Figure 5.29: Expression of *hrpL* is highly similar in Pst DC3000 (pBS63), Δ*gabP* (pBS63) and Δ*gabT2/T3/T1* (pBS63) in response to M9-fructose. Cells were incubated with M9-fructose over 36 hours. Luminescence values were corrected for optical density. The experiment was repeated three times and showed the same expression patterns each time.

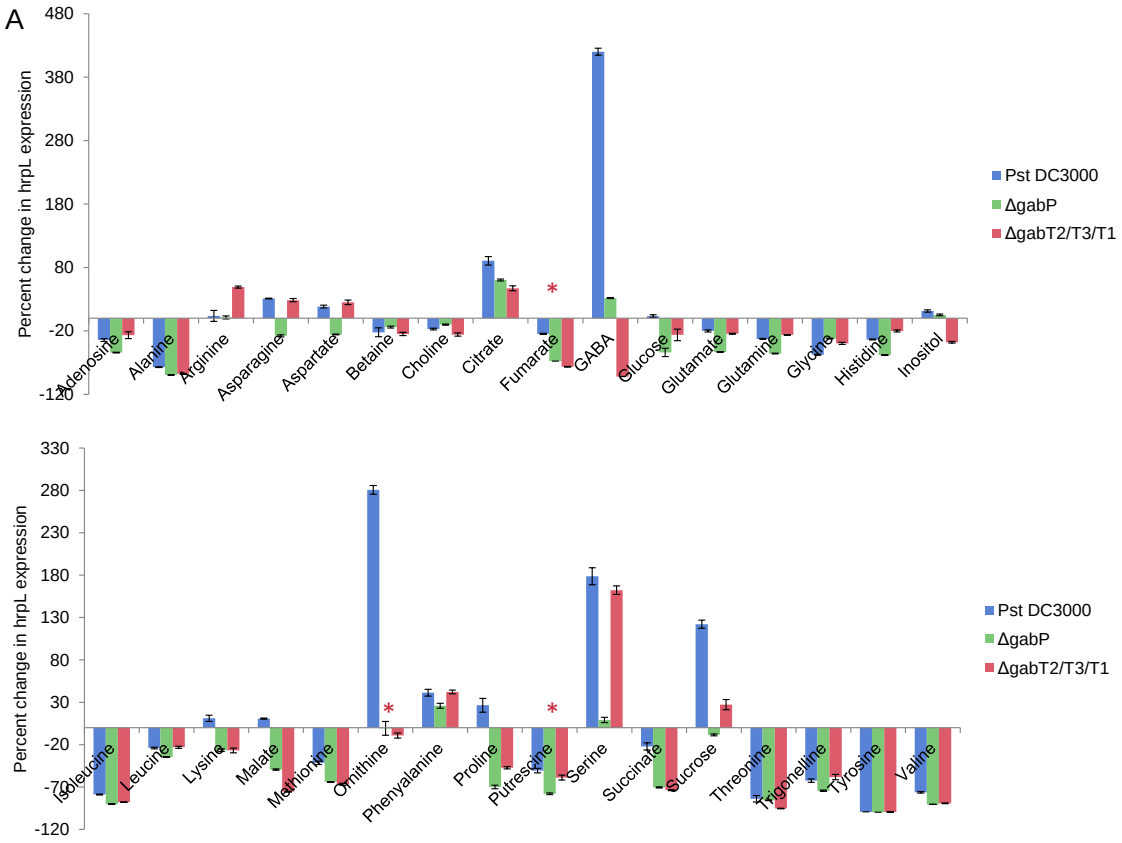
A
Percent change in hrpL expression
480
380
280
180
80
-20
-120
Adenosine
Alanine
Arginine
Asparagine
Aspartate
Betaine
Choline
Citrate
Fumarate
GABA
Glucose
Glutamate
Glutamine
Glycine
Histidine
Inositol
Pst DC3000
ΔgabP
ΔgabT2/T3/T1
Percent change in hrpL expression
330
280
230
180
130
80
30
-20
-70
-120
Isoleucine
Leucine
Lysine
Malate
Methionine
Ornithine
Phenylalanine
Proline
Putrescine
Serine
Succinate
Sucrose
Threonine
Trigonelline
Tyrosine
Valine
Pst DC3000
ΔgabP
ΔgabT2/T3/T1

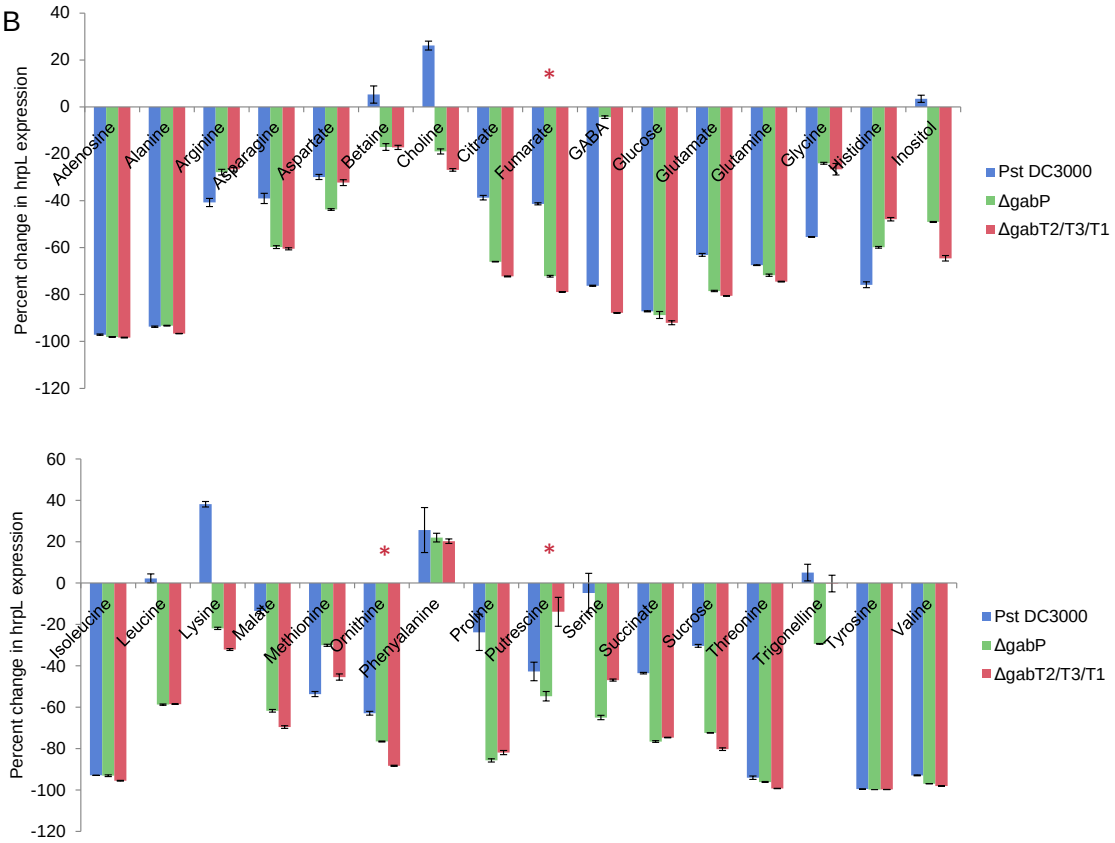

Figure 5.30: *hrpL* expression differs in Pst DC3000 (pBS63), Δ*gabP* (pBS63) and Δ*gabT2/T3/T1* (pBS63 in response to metabolites present in the host apoplast. Cells were incubated in *hrp*-inducing M9-fructose media with different apoplastic components added at 5mM, as well as two GABA-related metabolites, ornithine and putrescine. Luminescence values were corrected for optical density and integrated over 6 hour and 36 hours. The percentage change relative to *hrpL* expression in M9-fructose without additional metabolites was then calculated for each metabolite at each time point. Asterisks (*) highlight metabolites which have not been identified in tomato leaf apoplast in this study. Error bars represent standard deviation.

The results show that several of the metabolites tested caused very similar levels of repression of virulence genes in all three strains. After six hours, alanine, isoleucine, threonine, trigonelline, tyrosine, valine had all reduced virulence gene expression to the extent that *hrp* expression was almost fully repressed. Over 36 hours of expression, large-scale repression was observed with the following metabolites: adenosine, alanine, glucose, glutamate, glutamine, isoleucine, ornithine, threonine, tyrosine and

valine. The only metabolite to cause a net increase in virulence gene expression in all three strains over 36 hours was phenylalanine.

Different patterns of expression can be observed between the three strains in many of the metabolites tested. In particular, Δ*gabP* seems to show greater repression, or less induction, after 6 hours than Pst DC3000 and Δ*gabT2/T3/T1* with adenosine, asparagine, aspartate, glucose, glutamate, glutamine, histidine, leucine, phenylalanine, putrescine, serine and trigonelline. It is possible, as with other bacterial species, that GabP transports metabolites, other than GABA, at a low level, and so the Δ*gabP* mutant has a changed virulence gene expression profile in comparison with the wild type in the presence of these substrates. An alternative hypothesis would be that the Δ*gabP* mutant responds differently to certain nitrogen sources because of a changed internal nitrogen status.

After 6 hours, Pst DC3000 showed either higher levels of induction, or lower levels of inhibition, than Δ*gabP* and Δ*gabT2/T3/T1* in the presence of several metabolites: lysine, ornithine, proline, sucrose. The link between these substrates and GABA is not entirely clear. However, proline is known to be imported through GABA permeases of other species [291], and interestingly proline metabolism is very low for both Δ*gabP* and Δ*gabT2/T3/T1.* In addition, ornithine is catabolised via GABA. Interestingly, all the TCA cycle intermediates tested, citrate, fumarate, malate and succinate, stimulated very similar patterns of expression across the three strains: expression of virulence genes was always highest in Pst DC3000 and lowest

in Δ*gabT2/T3/T1*, both after 6 hours and 36 hours. As GABA is metabolised via the TCA cycle, it appears these intermediates may be involved in the sensing of carbon:nitrogen ratios in Pst DC3000, which may be unbalanced by an inability to metabolise or transport GABA.

Over the 36 hour period, most of the metabolites caused a strong downregulation of virulence genes relative to expression with fructose in all three strains. Pst DC3000 was more down-regulated in the presence of arginine, glycine, histidine and methionine than Δ*gabP* and Δ*gabT2/T3/T1*, and the reverse was true for asparagine, aspartate, betaine, choline, inositol, leucine, lysine, proline, serine, sucrose and succinate.

Aspartate was one of the substrates in the Biolog assay which caused the greatest upregulation of virulence genes in all three strains, above that of fructose. It is likely this was due mainly to the pH effect of aspartate, as aspartate is one of the most acidic amino acids, and Pst DC3000 expresses its virulence genes more highly under acidic conditions [71]. Whilst aspartate is not repressive under pH-adjusted conditions, it does not cause an increase in virulence gene expression above that observed with fructose.

qRT-PCT confirms the patterns of virulence gene expression observed with different apoplastic metabolites

In order to validate some of the results from the previous section (5.2.15), qRT-PCR was used to monitor the expression of both *hrpL* and the HrpL-regulated T3SS effector *avrE*. The effect of 5mM aspartate, GABA and threonine was tested in Pst DC3000, Δ*gabP* and Δ*gabT2/T3/T1*. RNA was harvested after 4-6 hours of incubation with the various metabolites. Figure 5.31 shows very similar profiles to that observed with the pBS63 construct (Section 5.2.15). One notable difference was the down-regulation of Pst DC3000 with GABA, whereas in the same time-scale in the pBS63-based experiment, a large upregulation is observed. Why this is the case is unclear, but it may due to a physiological effect of GABA, which will not affect the results of the qRT-PCR results but may alter luminescence values as luminescence is dependent on ATP production, oxygen and the synthesis of precursors. Aspartate was again seen to cause minimal repression, whilst threonine is highly repressive. GABA caused different expression levels in each of the three strains: GABA repressed virulence gene expression in Pst DC3000 and to a much greater degree in Δ*gabT2/T3/T1*, whereas Δ*gabP* was not effected by the presence of GABA in an M9-fructose environment and continued to highly express its virulence genes.

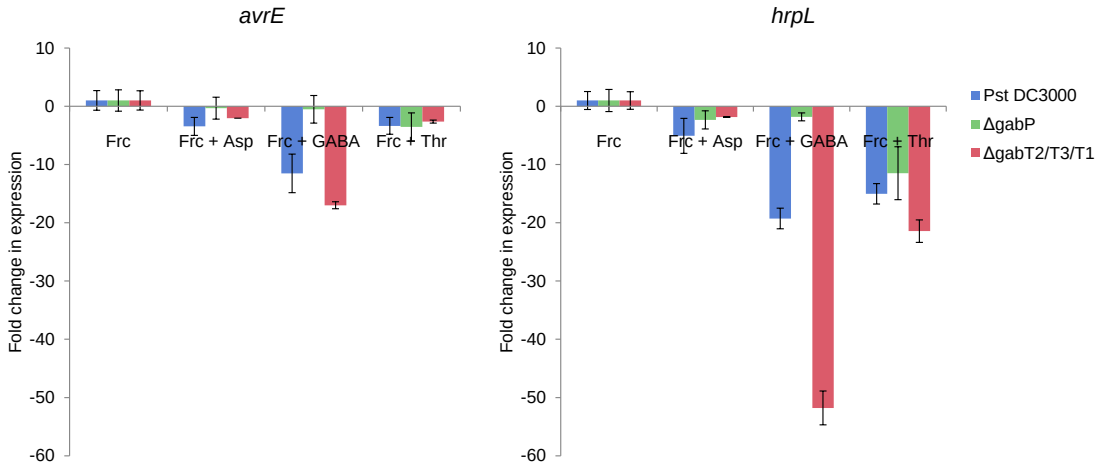

Figure 5.31: qRT-PCR of *avrE* and *hrpL* expression in Pst DC3000, Δ*gabP* and Δ*gabT2/T3/T1* in the presence of M9-fructose supplemented with aspartate, GABA and threonine. Cells were incubated in M9-fructose with 5 mM of each amino acid. Cells were harvested after 4-6 hours and RNA was extracted and converted to cDNA, which then underwent qRT-PCR. *groEL* and *rpoD* were used as the reference genes to calculate fold change. Fold change is shown in relation to expression of the virulence genes in M9-fructose without any amino acid supplements. Error bars show standard deviation.

5.2.16 Metabolite profiling of GABA mutants in the presence of different amino acids

In Section 3.2.6, the soluble amino acids in Pst DC3000 were profiled using GC-MS and this revealed distinct differences in metabolite pools between cells which had been grown on glucose and those which had been grown on fructose, as well as more subtle differences for those grown with different amino acid supplements. As virulence gene expression profiles differed for the GABA mutants in comparison with Pst DC3000 in the presence of several amino acids, metabolite profiling was performed under these conditions: amino acid profiles were analysed by GC-MS (Figure 5.32) and TCA cycle metabolite profiles by LC-MS (Figure 5.33). In addition

to the M9-fructose control medium and M9-fructose +5 mM GABA treatment, for the amino acid profiles, aspartate, glutamate and threonine were also used.

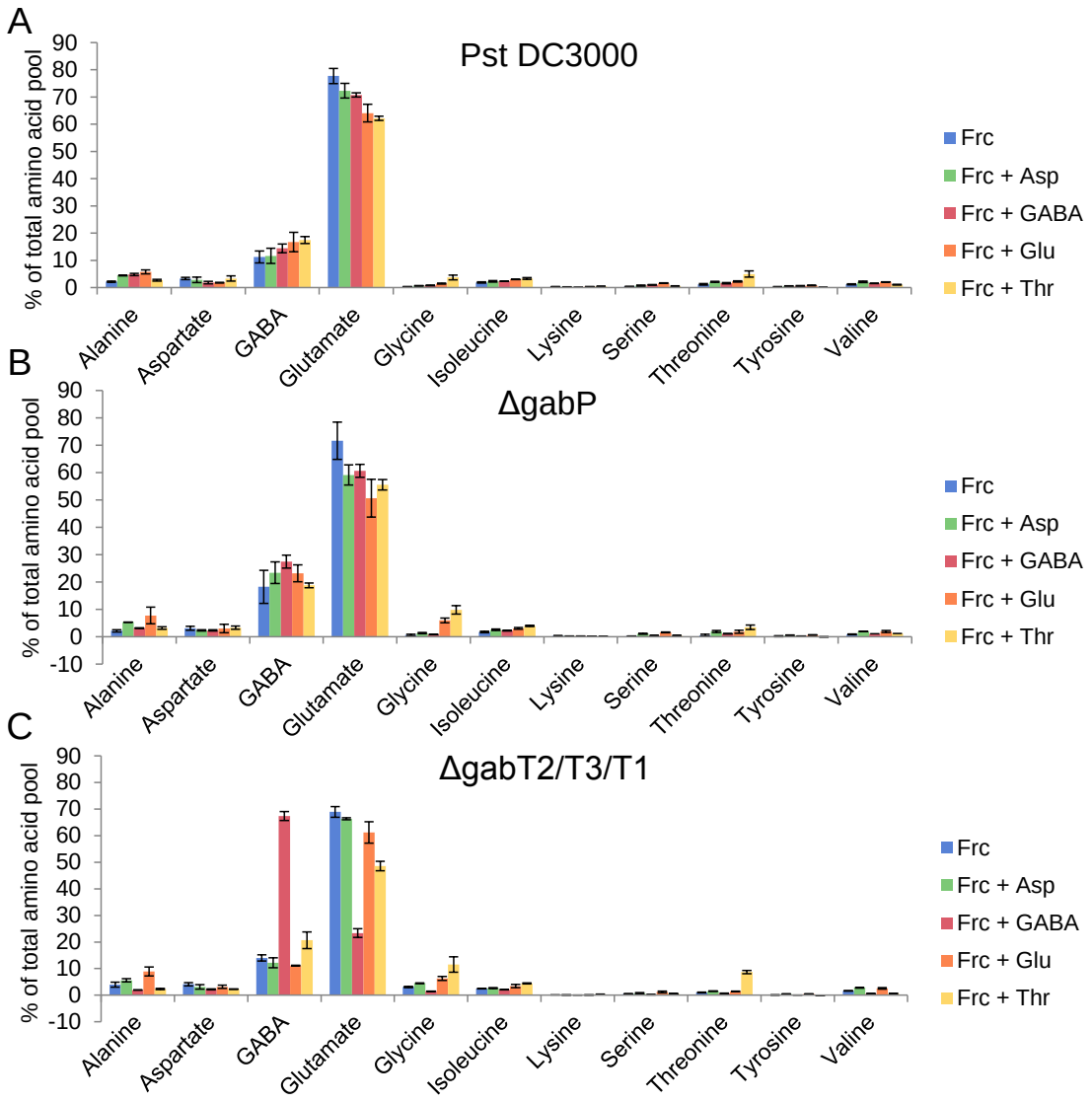

Figure 5.32: Proportional abundances of detectable soluble amino acids in Pst DC3000 (A), Δ*gabP* (B) and Δ*gabT2/T3/T1* (C) in the presence of aspartate, GABA, glutamate and threonine. Cells were incubated in M9-fructose and M9-fructose + 5 mM of different amino acids. After 16 hours the cells were harvested and soluble amino acids were extracted and analysed using GC-MS. The detectable metabolites were quantified and proportional abundances were generated by normalising samples to total amino acid quantities. Error bars show standard deviations.

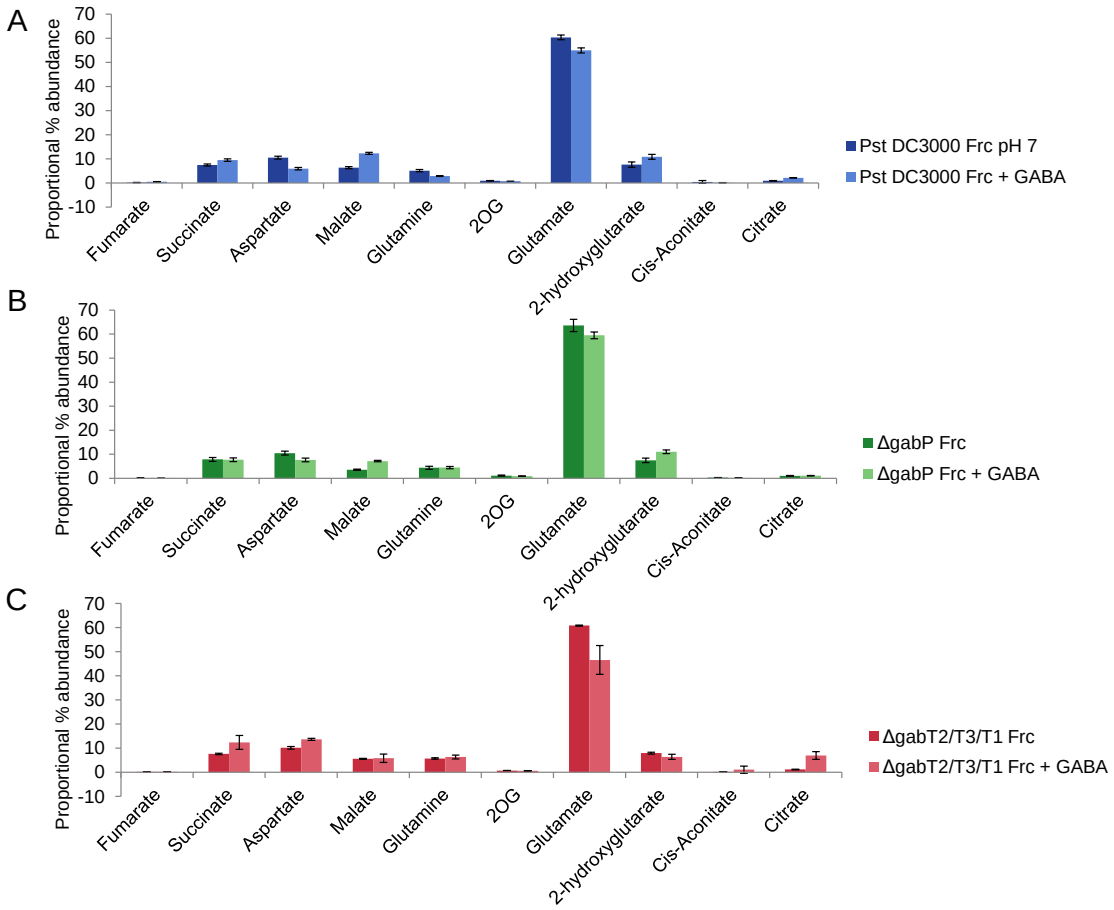

Figure 5.33: Proportional abundances of detectable TCA cycle and associated metabolites in Pst DC3000 (A), Δ*gabP* (B) and Δ*gabT2/T3/T1* (C) in the presence of GABA. Cells were incubated in M9-fructose and M9-fructose + 5 mM GABA. After 16 hours the cells were harvested and soluble metabolites were extracted and analysed using LC-MS. The detectable metabolites were quantified and proportional abundances were generated by normalising samples to total amino acid quantities. Error bars show standard deviations of three independent samples.

In both the GC-MS and LC-MS profiles, Pst DC3000, Δ*gabP* and Δ*gabT2/T3/T1* had metabolite profiles which were indistinguishable from one another (Figure 5.32). This implies that neither *gabP* nor *gabT2/T3/T1* hold any influence over the metabolism of fructose or ammonium in so far as can be discerned through metabolite profiling. In the presence of GABA, the most notable change occurred in Δ*gabT2/T3/T1*, where a large intracellular pool of GABA had accumulated, as it could not be

metabolised in the absence of the three GABA transaminase genes (Figures 5.32). As observed previously (Section 3.2.8), in the presence of GABA, Pst DC3000 showed a slight decline its proportional levels of glutamate, both in the amino acid and TCA cycle metabolite profiles. Interestingly, a similar pattern was observed in Δ*gabP*, though this strain showed very little inhibition in the presence of GABA. Intriguingly, there was proportionally more GABA present in Δ*gabP* than in Pst DC3000, a result which was also found in Section 5.2.4.

Repression of virulence genes in Δ*gabT2/T3/T1* appeared more marked in the presence of threonine than in Pst DC3000 or Δ*gabP* (Figures 5.31), and this appears to be acompanied by relatively higher intracellular levels of GABA and threonine, and lower levels of glutamate.

5.2.17 Amino acid profiling of Δ*gabP* and Δ*gabT2/T3/T1* in tomato apoplast extracts reveals differences in GABA accumulation

Amino acid profiling of strains that had been incubated in extracted apoplast was undertaken to investigate whether intracellular metabolite pools were contributing to observed differences virulence gene expression, and to compare the profiles against other experimental conditions (Section 5.2.16). Pst DC3000, Δ*gabP* and Δ*gabT2/T3/T1* were inoculated into extracted apoplast (filtered, and with pH adjusted to 5.5) at a starting OD of 0.4 and cells were harvested after two hours.

Unfortunately, only the most abundant amino acids could be detected in this analysis, as not enough cells were collected to get full profiles owing to the constraints of using apoplast extract (obtaining extracts is a lengthy process and only around 0.3 ml of liquid can be collected from 8 leaves). However, notably Pst DC3000 and $\Delta gabP$ show very similar profiles to those detected in M9-fructose media (Section 5.2.16). Very high levels of glutamate, relative to other amino acids, appear to be correlated with virulence gene expression. $\Delta gabT2/T3/T1$ conversely displayed a different proportional profile, with GABA being the most abundant amino acid (Figure 5.34). The change in relative abundance of amino acids in $\Delta gabT2/T3/T1$ may well contribute to the repression of virulence gene expression observed in Section 5.2.12.

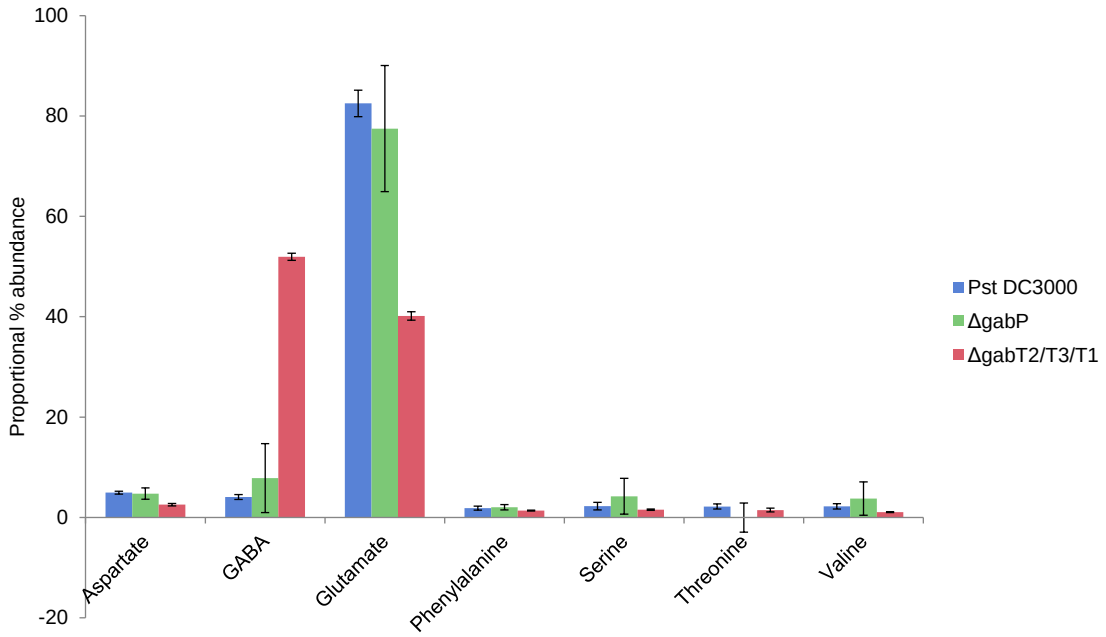

Figure 5.34: Proportional abundances of detectable soluble amino acids in Pst DC3000, Δ*gabP* and Δ*gabT2/T3/T1* after incubation in extracted tomato leaf apoplast demonstrate the accumulation of GABA in Δ*gabT2/T3/T1*. Cells were incubated in extracted tomato leaf apoplast for 4 hours. The cells were then harvested and soluble amino acids were extracted and analysed using GC-MS. The detectable metabolites were quantified and proportional abundances were generated by normalising samples. Error bars represent standard deviation.

5.2.18 *gabP* is regulated by RpoN

The alternative sigma factor σ^{54}, encoded by *rpoN*, is required for the transcription of many genes involved in nitrogen assimilation, type III secretion and other virulence factors such as coronatine, alginate production, flagella and pili in *Pseudomonas syringae* and other plant pathogenic bacteria [240, 298, 299]. An *rpoN* mutant of Pst DC3000 has been shown to be unable to cause disease symptoms in tomato leaves or elicit the HR in tobacco [85]. It was also found to be deficient in its ability to utilise many carbon sources, including GABA [85]. Previous work has identified RpoN binding sites upstream of GABA permease genes in *P. putida* KT2440 (PP0284

and PP4407) and *P. entomophila* L48 (PSEEN5205) [85]. In *E. coli*, the expression of *gabP* (and *gabT* and *gabD*) was found to be regulated by an alternative sigma factor, RpoS [257, 300], which interacts antagonistically with RpoN [301]. It was therefore hypothesised that *gabP* in Pst DC3000 may be regulated by RpoN.

Pst DC3000 and Pst DC3000 *rpoN*- were grown overnight in glucose M9 and then resuspended at an OD of 0.4 in glucose M9 (Glc + NH_4) or M9-GABA (GABA + NH_4) and grown at 28 °C for four hours. RNA was then extracted and converted to cDNA. qRT-PCR was performed using primers for *gabP* and *gabT2*, as well as reference genes *groEL* and *rpoD*.

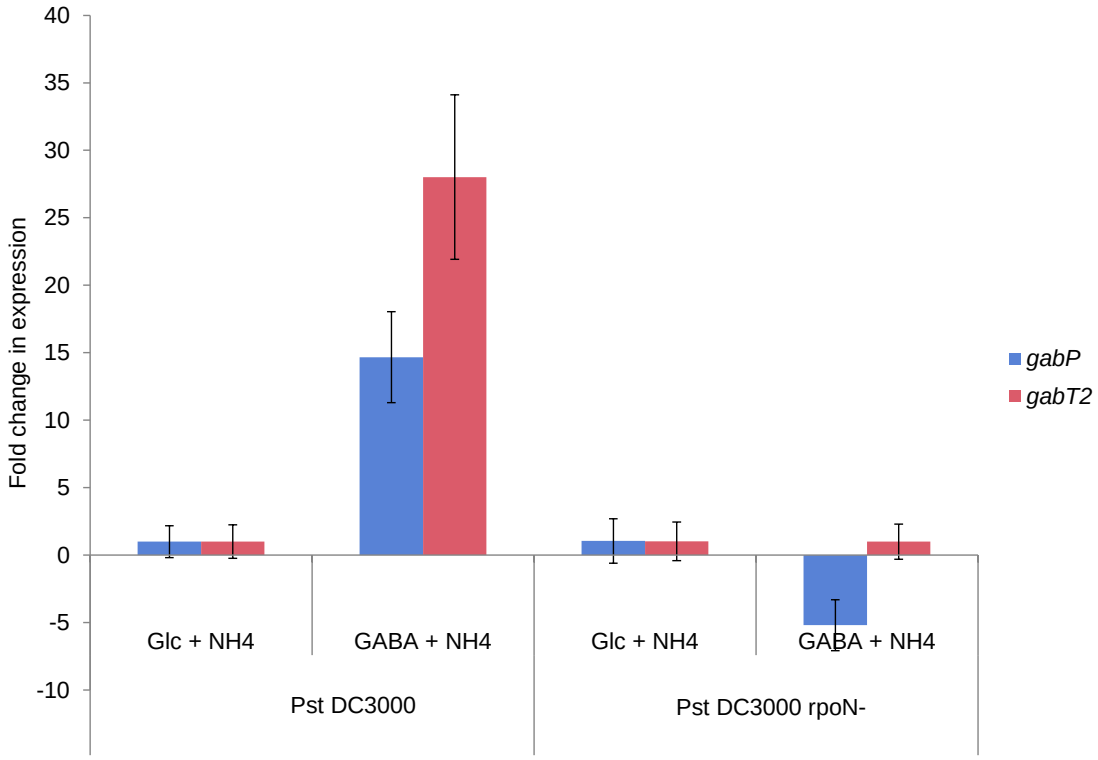

Figure 5.35: qRT-PCR of *gabP* and *gabT2* expression in wild type and *rpoN*- strains demonstrates *gabP* is RpoN-regulated. Both Pst DC3000 and Pst DC3000 rpoN- were incubated in M9-glucose and M9-GABA (22 mM of GABA replaced 22 mM of glucose). RNA was extracted after 4 hours of incubation and converted to cDNA and the expression of both *gabP* and *gabT2* analysed used qRT-PCR. *groEL* and *rpoD* were used as the reference genes to calculate fold change. Fold change is shown in relation to expression of *gabP* and *gabT2* in M9-glucose without GABA. Error bars show standard deviation from three independent sample sets.

The results show that the expression of both *gabP* and *gabT2* is upregulated in Pst DC3000 in the presence of GABA (Figure 5.35). In Pst DC3000 *rpoN*-, *gabP* is expressed 5-fold less than in the presence of GABA and the expression of *gabT2* does not change. Notably, Pst DC3000 grows over the 4 hours of incubation, whilst Pst DC3000 *rpoN*- is unable to derive any nutritional benefit from the GABA + NH_4 treatment (data not shown). This implies that GABA is unable to enter the cells.

Thus, *gabP* does appear to be regulated by RpoN and the non-induction of *gabT2* is likely to be due to a hypothesised low level of GABA in the cells, which is inferred from the lack of growth of Pst DC3000 *rpoN*- in the GABA + NH_4 treatment.

5.2.19 GABA metabolism is involved in responses to various environmental stresses

GABA is known to rapidly accumulate in plants and bacteria in response to a variety of environmental stresses, such as salinity, anoxia and cold stress [262, 300, 302]. The ability of Pst DC3000 to withstand different environmental stresses was tested to determine if GABA metabolism plays a role in stress protection, as it is possible that the apoplastic environment, over the course of infection, becomes a stressful environment for Pst DC3000 cells. The growth ability of the wild type, Δ*gabP* and Δ*gabT2/T3/T1*, and the expression of virulence genes, was tested under different pH conditions, high temperature (34 °C), heat-shock (42 °C), oxygen levels and salt concentrations, both in the presence and absence of GABA. All experiments were carried out in M9-fructose minimal media (pH 7, unless specified), and where GABA was present, it was used at a concentration of 5 mM, a concentration known to cause significantly higher growth and virulence gene repression in Pst DC3000 based on previous experiments (Section 5.2.13).

Of all the conditions tested, only the heat-shock treatments did not cause any differences in growth or expression of virulence genes (Figure 5.36) and therefore was

not considered to have caused any level of measurable physiological stress. The following sections outline the most important findings from these experiments.

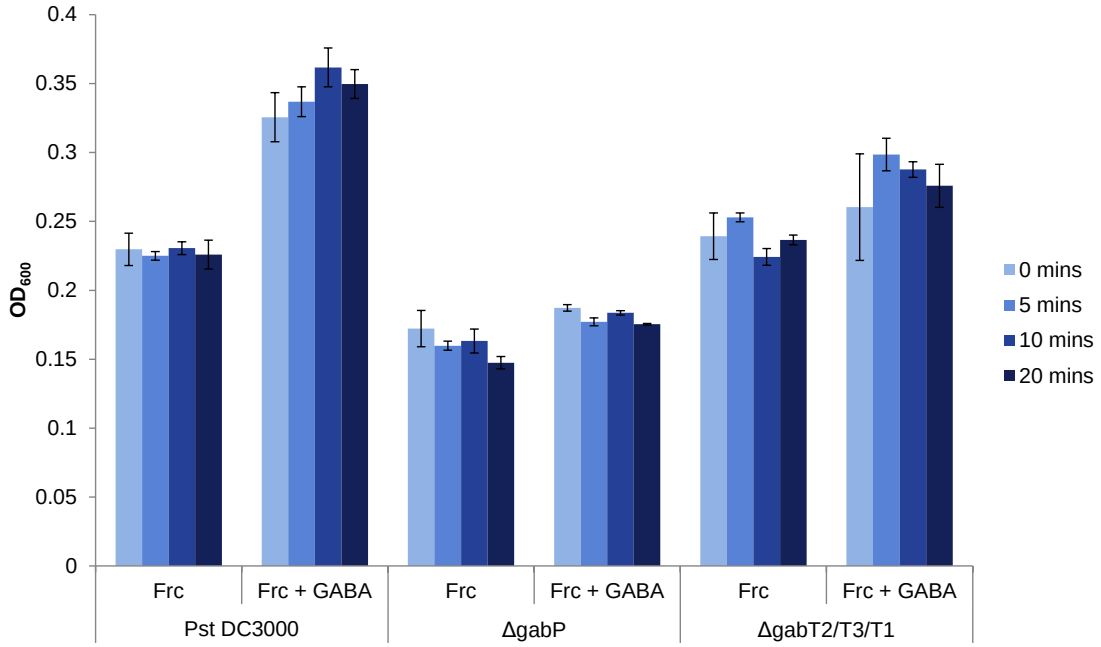

Figure 5.36: Heatshock treatments do not alter growth of Pst DC3000 (pBS63), Δ*gabP* (pBS63) or Δ*gabT2/T3/T1* (pBS63). Cells were incubated for 0, 5, 10 or 20 minutes at 42 degrees before the beginning of the experiment. Cells were then resuspended into either M9-fructose (Frc) or M9-fructose + 5 mM GABA (Frc + GABA). Optical density was then recorded over a 36 hour period. Error bars show standard deviation.

GABA metabolism is not involved in responses to oxygen limitation

Oxygen-limited conditions were created by wrapping the join of the lid and base of a 96-well plate with both micropore tape and parafilm to prevent as much gas diffusion as possible into the plate [303, 304]. Growth was not affect by a reduction in oxygen (Figure 5.37A), but there was a notable decrease in expression of virulence genes in the oxygen-limited condition (Figure 5.37B). The reduction in observed virulence gene expression was most likely mainly due a reduction in luminescence

as oxygen is one of the substrates involved in the luciferase light-emitting reaction [305], and thus it is most likely only an apparent reduction in virulence, though this requires experimental verification. The addition of GABA in the oxygen-limited condition did not alleviate this effect, nor did the absence of the GABA permease or transaminase genes.

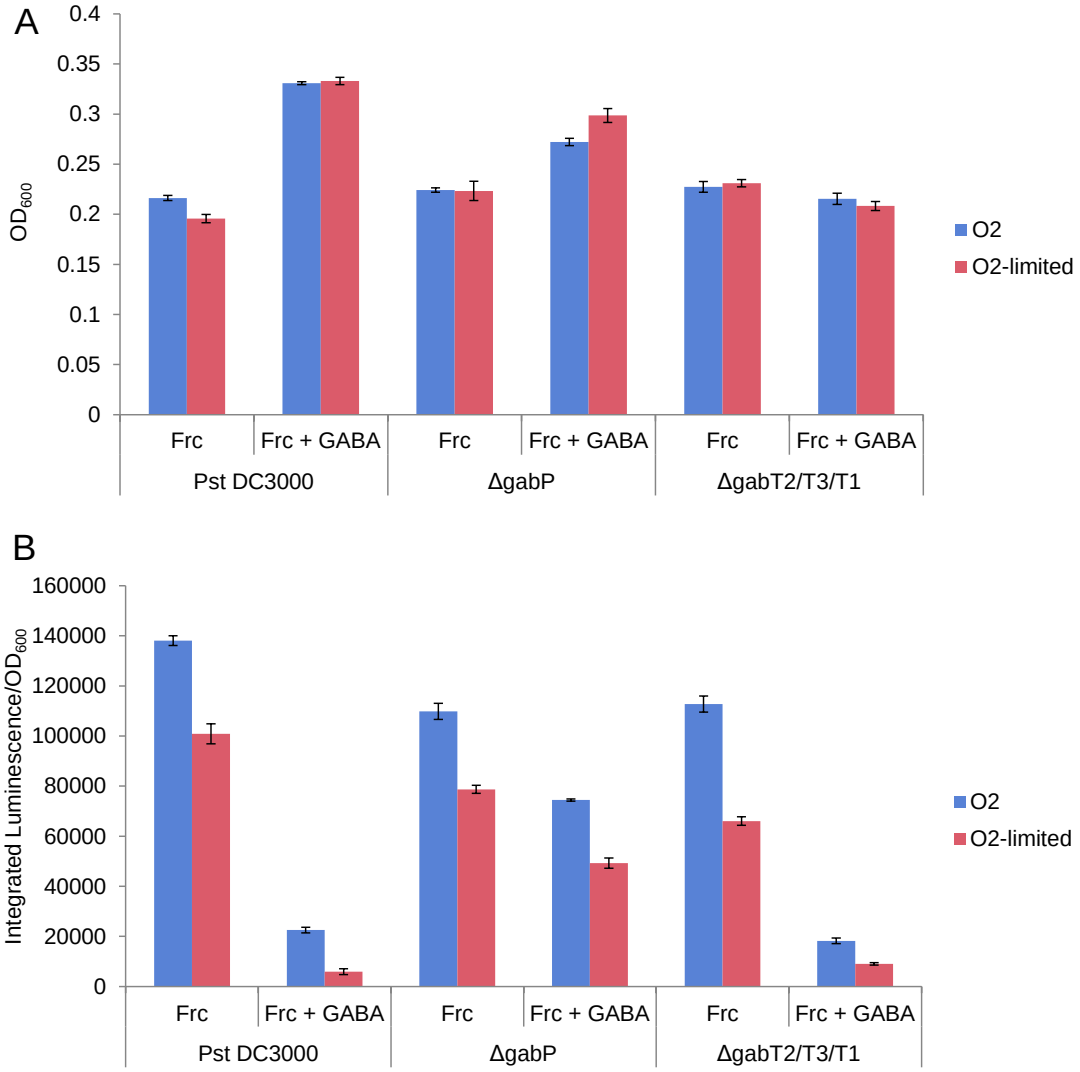

Figure 5.37: Growth and *hrpL* expression in Pst DC3000 (pBS63), Δ*gabP* (pBS63) and Δ*gabT2/T3/T1* (pBS63) in oxygen-unlimited and oxygen-limited conditions. Cells were incubated in either M9-fructose (Frc) or M9-fructose + 5 mM GABA (Frc + GABA) in 96 well plates which were wrapped with parafilm and micropore tape (oxygen limited conditions) or left unwrapped (oxygen unlimited conditions). Optical density (A) and luminescence (B) was then recorded over a 36 hour period. Luminescence was corrected for optical density and integrated over the 36 hour period. Error bars show standard deviation.

GABA metabolism may have a role in pH regulation

GABA has been shown to be involved in cytosolic pH regulation in several bacterial species [280, 302], and has been hypothesised to be involved in responses to

pH changes in pseudomonads [306]. In *E. coli*, both GAD activity and a glutamate:GABA antiporter have been shown to be required to survive low pH conditions [307]. Whilst Pst DC3000 is not predicted to have any GAD genes, and therefore cannot regulate intracellular pH levels by the H^+-consuming decarboxylation of glutamate to GABA, it was hypothesised that the levels of intracellular GABA may also contribute to this response. The wild type strain and GABA mutants were therefore tested across a range of pH conditions, from pH 4.5 to pH 9 to determine if GABA has a role in Pst DC3000 in pH regulation (Figure 5.38).

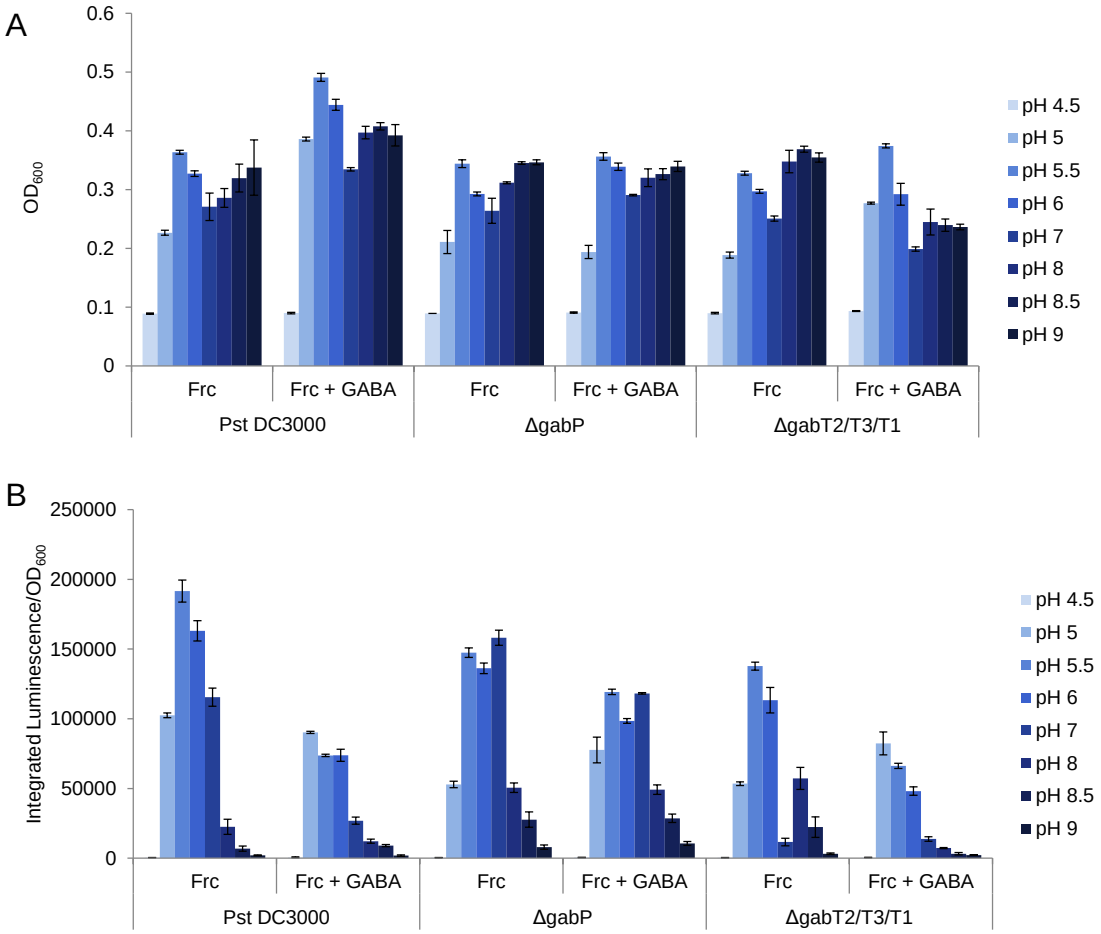

Figure 5.38: Growth and *hrpL* expression in Pst DC3000 (pBS63), Δ*gabP* (pBS63) and Δ*gabT2/T3/T1* (pBS63) across a range of pHs. Cells were incubated in M9-fructose or M9-fructose (Frc) + 5 mM GABA (Frc + GABA) which was adjusted to different pHs. Optical density (A) and luminescence (B) were recorded over 36 hours. Luminescence was corrected for optical density and integrated over the 36 hour period. Error bars show standard deviation.

All strains showed reduced growth at the lowest pH tested, pH 4.5, and were unable to express virulence genes under this condition. Interestingly, for all strains, the lowest growth apart from at pH 4.5 was at pH 7. It is possible that the addition of HCl and NaOH to increase or decrease acidity was the cause of this increase in growth, as it is possible chloride or sodium salts are a growth-limiting factor in M9 medium. Pst DC3000 exhibited increased growth, and decreased virulence gene ex-

pression, in the presence of GABA, but the patterns of growth and *hrpL* expression across the pH values was consistent with the no GABA treatment.

Δ*gabT2/T3/T1* was able to derive a small growth benefit from GABA at pH 5 and pH 5.5 but not at pHs higher than this. The lower pH appears to allow a higher tolerance of intracellular GABA (which is known to build up to high levels in this mutant strain). The higher pH values in combination with GABA have an inhibitory effect, and these results imply an interaction between intracellular GABA levels and pH regulation is occurring. In addition, virulence gene expression, which is normally strongly repressed in the presence of GABA in the wild type and Δ*gabT2/T3/T1*, is actually upregulated in Δ*gabT2/T3/T1* in the presence of GABA at pH 5.

GABA transaminase enzymes are sensitive to changes in temperature

The GABA mutants and wild type strain were also subject to heat-tolerance testing. The results are shown in Figure 5.39. A notable feature of the increased temperature (34 °C) condition was the lack of growth benefit derived from the presence of GABA in the wild type and Δ*gabP* strains when compared with growth at 28 °C. This effect was absent in the *gabT2/T3/T1* mutant as it can derive no significant growth benefit from GABA at either temperature. It is possible therefore that the GABA transaminases have an optimal catalytic temperature and at 34 °C they are not active enough to allow the strains to metabolise GABA to any great degree. It is likely that the enzymes of Pst DC3000 work optimally at the temperatures they usually encounter in their plant host (tomato plants will grow optimally between 18

°C and 25 °C, and very poorly above 35 °C).

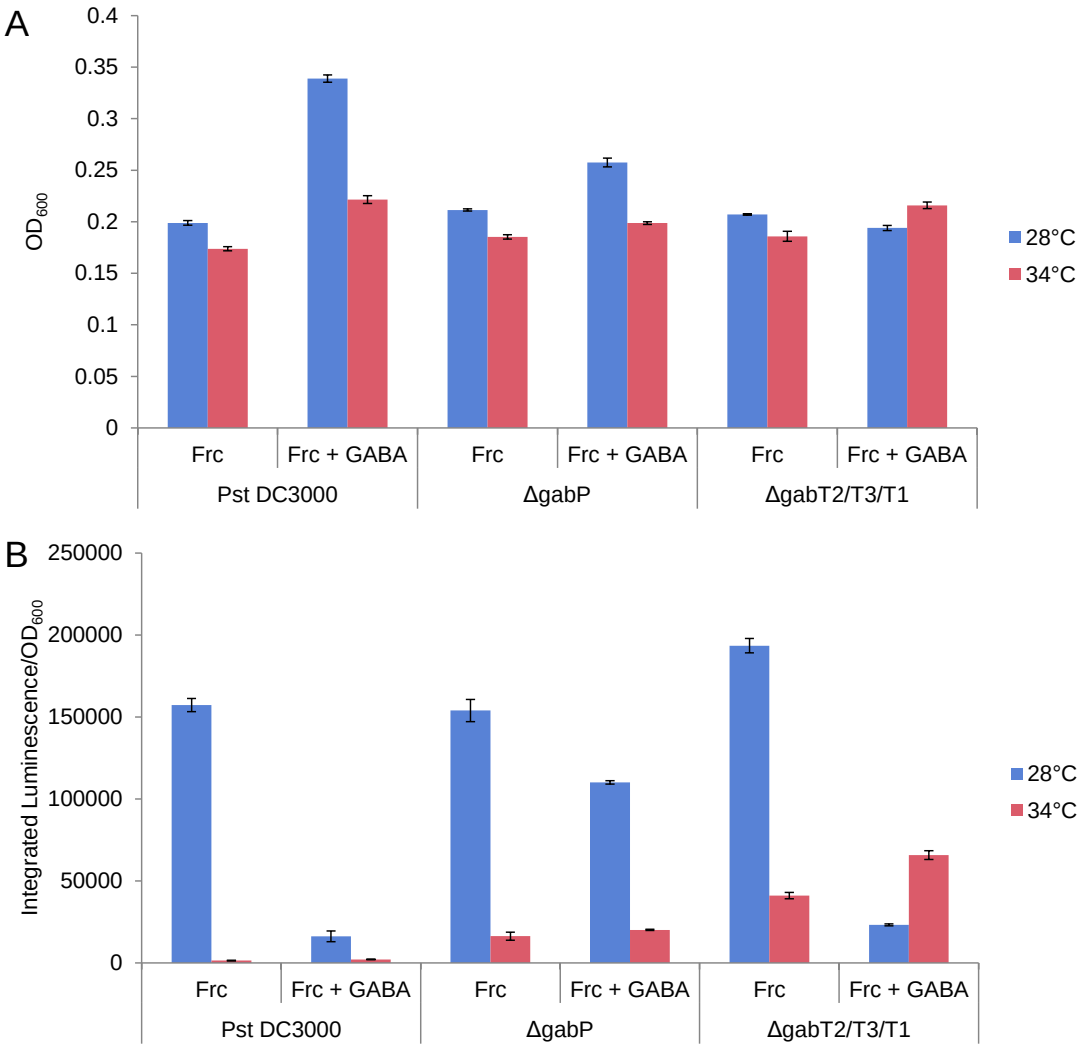

Figure 5.39: Growth and *hrpL* expression in Pst DC3000 (pBS63), Δ*gabP* (pBS63) and Δ*gabT2/T3/T1* (pBS63) at two temperatures. Cells were in grown in M9-fructose (Frc) or M9-fructose + 5 mM GABA (Frc + GABA) at 28 °C or 34 °C. Optical density (A) and luminescence (B) were recorded over 36 hours. Luminescence was corrected for optical density and integrated over the 36 hour period. Error bars show standard deviation.

Virulence gene expression was much reduced in all strains at the higher temperature. The T3SS of *P. syringae* has not previously been reported to be temperature regulated, but other gram-negative pathogens have been shown to regulate their virulence genes in response to temperature [308]. Interestingly, *hrpL* expression in

both Δ*gabP* and Δ*gabT2/T3/T1* was not inhibited to the same degree as in the wild type and Δ*gabT2/T3/T1* showed higher expression at 34 °C in the presence of GABA. This result, in conjunction with the responses of the strains to pH implies GABA may interact with the signalling pathway between stress detection systems and virulence gene expression. Indeed, bacteria have been shown to have similar regulatory responses to multiple different stresses, such as the stress response network of *E. coli*, regulated by the alternative sigma factor RpoS, which is upregulated in response to changes in osmolarity, pH, temperature and starvation [309]. As previously noted, RpoS is also known to regulate *gabP*, *gabT* and *gabD* expression in *E. coli* [257, 300] and an analogous system may operate in Pst DC3000.

Salt tolerance may be linked to the metabolism of GABA

The final stress condition to be tested was osmotic concentration. GABA is a known osmoprotectant [310] and so conditions which would confer osmotic stress were created using sodium chloride. In the absence of extracellular GABA additional salt was shown to increase the growth of all strains (Figure 5.40), though this effect was more pronounced in the wild type than in Δ*gabP* or Δ*gabT2/T3/T1*. When GABA was present in the medium, Δ*gabT2/T3/T1* was able to derive a growth benefit from it in the presence of 1 % NaCl, above the growth benefit conferred by NaCl in the absence of GABA.

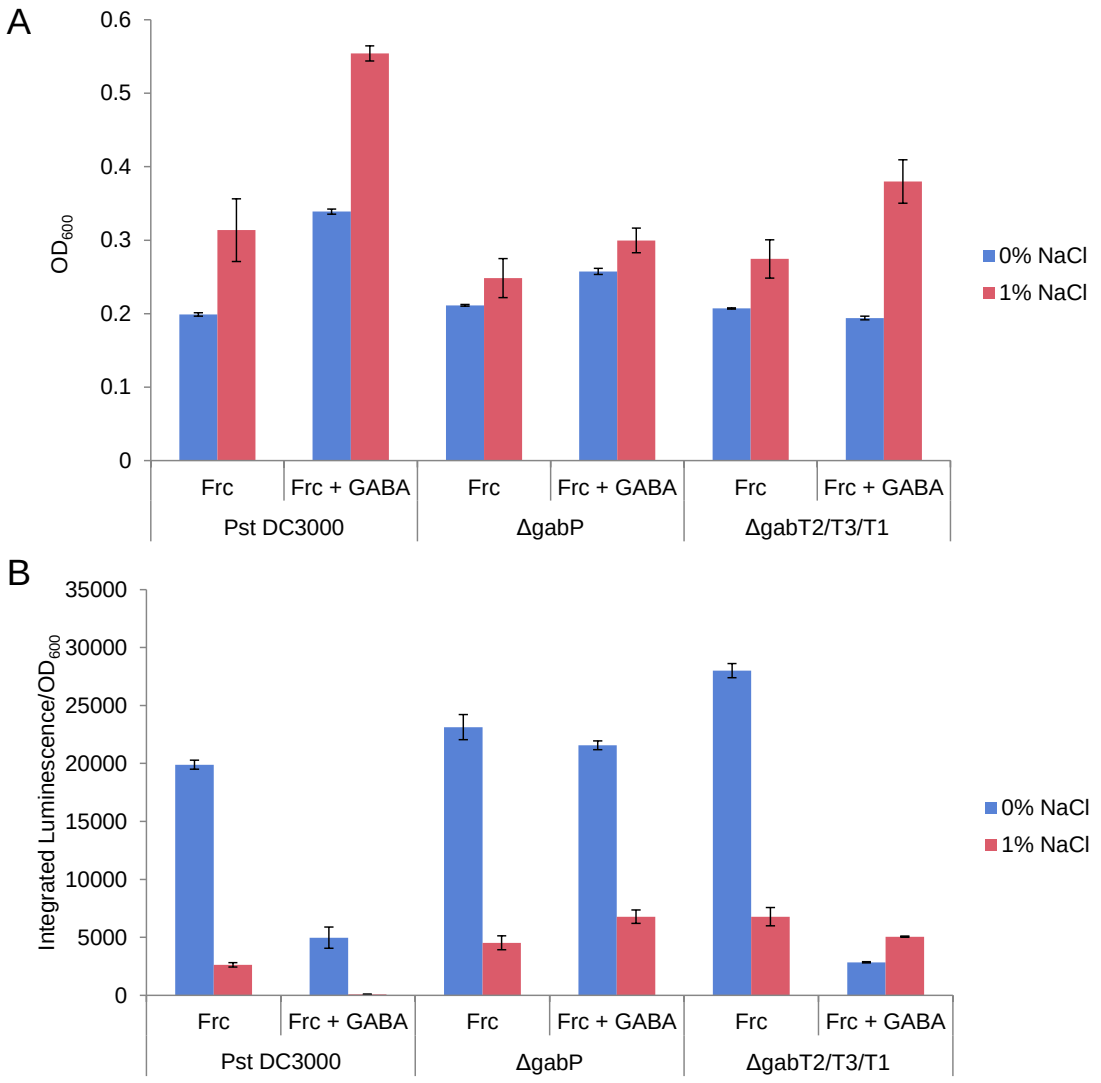

Figure 5.40: Growth and *hrpL* expression in Pst DC3000 (pBS63), Δ*gabP* (pBS63) and Δ*gabT2/T3/T1* (pBS63) under different osmotic conditions. Cells were grown in M9-fructose (Frc), M9-fructose + 5 mM GABA (Frc + GABA), M9-fructose + 1 % NaCl and M9-fructose + 5 mM GABA + 1 % NaCl. Optical density and luminescence were recorded over 36 hours. Luminescence was corrected for optical density and integrated over the 36 hour period. Error bars show standard deviation.

Virulence gene expression was repressed in the presence of extra salt in the wild type both with and without GABA. Δ*gabT2/T3/T1*, in a very similar way to the effects of increased temperature and low pH, showed no further *hrpL* repression in the presence of GABA with 1 % salt. This reinforces the hypothesis that GABA

may be acting at some point in a stress response regulatory cascade.

5.3 Discussion

This study has demonstrated an important role for GABA in the interaction of Pst DC3000 with its plant host. GABA has been shown to be depleted from the apoplastic environment, primarily via the action of a GABA permease (encoded by *gabP*) and then primarily metabolised via the action of three GABA transaminases (encoded by *gabT1*, *gabT2* and *gabT3*). Evidence for alternative, though less active, routes for GABA assimilation has been gathered by a novel 'unlabelling' technique. GABA causes a significant repression of virulence gene expression in Pst DC3000 and this repression was amplified in a triple GABA transaminase mutant. A *gabP* mutant was shown be less susceptible to virulence gene repression by GABA indicating that sufficient quantities of GABA must be inside the cell in order for repression to occur. GABA also appears to be involved in alleviation of stress, which may be of importance in the stressful host environment. The following sections outline the significance of this study.

5.3.1 GABA permease and GABA transaminase evolutionary histories

Phylogenetic analysis of GABA transaminase genes in *Pseudomonas* species revealed that all *Pseudomonas* strains for which genome sequences were available possess a putative *gabT2* gene. The conserved presence of the *gabT2* gene enforces the finding

by Park *et al* (2010) [88] that *gabT2* appears to be the most important of the GABA transaminase genes in Pst DC3000 as it is the only one of the three transaminase genes which can partially restore wild type GABA utilisation in a triple transaminase mutant.

The annotation of three *gab*T genes in all *P. syringae* strains and up to three *gabT* genes in several of the *P. fluorescens* and *P. chlororaphis* genomes suggests that three GABA transaminases may have been present in the last common ancestor of the *P. fluorescens* and *P. syringae* clades. The random nature of the presence or absence of *gabT1* and *gabT3* in the *P. fluorescens* clade also implies that the last common ancestor had all three GABA transaminases and these have been stochastically lost or retained. In addition, the finding of putative GABA permease genes in all *Pseudomonas* species, apart from *P. aeruginosa* and *P. mendocina* indicates that at least one GABA permease was present in the last common ancestor of the *Pseudomonas* genus.

Pst DC3000 is known to live in a GABA-rich environment and both this study and others have established GABA as a virulence inhibitor [71, 88]. It is therefore unsurprising that the assimilation of GABA is a priority, as it is an abundant carbon and nitrogen source. Rapid turnover of GABA, by the action of GABA transaminases, can also be explained by the negative effect this molecule has on virulence if left to build up intracellularly. What is more curious, however, is that three GABA transaminases are also predicted to be present in all *P. syringae* species, many of

which are not known to infect plant species which have high levels of GABA in their apoplastic compartments. However, several plants are known to upregulate GABA levels in response to stresses [7, 302], and as bacterial infection is a type of biotic stress, GABA may constitute part of the plants' defence response which must be rapidly dealt with by the invading pathogen, or alternatively may provide a important nutrient source for the pathogen.

5.3.2 Δ*gabP* and Δ*gabT2/T3/T1* are unaffected in their ability to grow in the host or to deplete nutrients from host apoplast, but demonstrate different utilisation profiles for several substrates

GABA is a major component of the tomato host apoplast [71]. It was therefore interesting that neither Δ*gabP* nor Δ*gabT2/T3/T1* were impaired in their ability to grow *in planta* or in extracted host apoplast, and in addition, were able to deplete all of the apoplastic components that Pst DC3000 can, including GABA. This appears to be due to Pst DC3000 having previously unidentified pathways for GABA assimilation and metabolism which are discussed in Section 5.3.3. However, unexpectedly, the GABA mutants showed different utilisation profiles to Pst DC3000 in response to several metabolites when tested using Biolog GN2 microarrays.

In particular, glutamate was metabolised to a greater degree in both Δ*gabP* and Δ*gabT2/T3/T1* than in Pst DC3000. It is unclear why this might be the case, but

the addition of glutamate to cells with unbalanced GABA metabolism may provide more optimal osmotic conditions for the cells: glutamate is known to increase in other bacterial species in response to osmotic stress [280]. This idea is explored further in Section 5.3.6.

Δ*gabT2/T3/T1* was shown to be unable to metabolise 2-oxoglutarate. This implies that 2-oxoglutarate can only be converted to glutamate by the action of GABA transaminases in Pst DC3000 and therefore that, in Pst DC3000, 2-oxoglutarate is an amino group acceptor for GABA transaminase enzymes. In addition, the deletion of GABA transaminase genes, whilst creating large intracellular pools of GABA as shown in Section 5.2.4 also appears to limit the intracellular pool of glutamate, as shown in Section 5.2.16. Section 5.3.5 explores the possibility that glutamate abundances are involved in environmental sensing and the regulation of virulence genes.

5.3.3 Pst DC3000 possesses previously unknown pathways for GABA assimilation and metabolism

The finding that both Δ*gabP* and Δ*gabT2/T3/T1* were able to grow using GABA as a nitrogen source led to several lines of investigation to determine the mechanism by which this was achieved. The unlabelling experiments (Section 5.2.4) provided the answer: Pst DC3000 has an alternative assimilatory pathway for GABA and an alternative means by which GABA can be metabolised other than by the three currently identified GABA transaminases. Both of these mechanisms are less effi-

cient than their known counterparts, thus providing sufficient nitrogen for growth in the presence of an alternative carbon source, but insufficient carbon for discernible growth after 36 hours.

In terms of GABA transport, several other GABA transporters have been described in *Agrobacterium tumefaciens* and *Rhizobium leguminosarum* [259, 260, 311], which are distinct from the *gabP* lineage of GABA transporters. These are shown in Table 5.3 along with their homologues in Pst DC3000. These present possible ways by which Pst DC3000 may transport GABA at a low level, and knock-out mutagenesis of these genes in the Δ*gabP* mutant background should give an indication of whether or not these genes are involved in GABA assimilation.

Gene	Species	Gene in Pst DC3000	Pst DC3000 annotation
gtsABCD	*Rhizobium leguminosarum*	PSPTO_2667/6/5/4	spermidine/putrescine ABC transporter, ATP-binding protein
braDEFG	*Rhizobium leguminosarum*	PSPTO_4918/7/6/5	high-affinity branched-chain amino acid ABC transporter, ATP-binding protein
atu2422	*Agrobacterium tumefaciens*	PSPTO_4919	high affinity branched-chain amino acid ABC transporter, periplasmic amino acid-binding protein

Table 5.3: GABA transporters in plant-dwelling gram-negative bacteria and their homologues in Pst DC3000

The alternative GABA transporter appears to be immediately active, based on the GABA assimilation profiles in Section 5.2.4, and growth profiles in Section 5.2.2, however, the same unlabelling experiment shows that the alternative GABA metabolic pathway takes a longer time to be induced as GABA assimilation begins later in the Δ*gabT2/T3/T1* strain. Interestingly, in Δ*gabT2/T3/T1* GABA is assimilated in to the TCA cycle, which is evidenced by the similarity of unlabelling pat-

terns to Pst DC3000, though at a later time point. It is therefore likely that GABA is being converted to succinic-semialdehyde and acting as an amino-group donor, as it does by the action of the GABA transaminase genes, but by an enzyme which has a low level affinity for GABA. There are multiple other transaminases in Pst DC3000, but a potential gene to investigate for the function of GABA metabolism is *daT* (PSPTO_2136), which is predicted to encode a 2,4-diaminobutyrate 4-transaminase (which catalyses the conversion of 2,4-diaminobutanoate and 2-oxoglutarate to aspartate 4-semialdehyde and glutamate), and which is related to the *gabT* genes.

5.3.4 Unlabelling experiments reveal the activity of certain metabolic pathways

In addition to revealing that Pst DC3000 must have alternative proteins for the transport and catabolism of GABA, the unlabelling experiments were also able to shed light on the activity of several metabolic pathways. In Pst DC3000, the distribution of unlabelled carbon throughout the protein-based amino acids gave an indication as to the direction and magnitude of several key fluxes. The absence of significant amounts of unlabelled carbon in histidine, serine, glycine, phenylalanine and tyrosine in the Glc + GABA treatment demonstrates that there is neither a gluconeogenic flux from pyruvate to phosphoenolpyruvate (PEP) nor is there an appreciable flux from oxaloacetate to PEP (though the slight increase in unlabelled carbon in phenylalanine and tyrosine hints at a very small flux). This is consistent with the observation in Section 4.2.6 (see Figure 4.17) that a low level of flux exists under glucose-fed conditions from oxaloacetate to PEP in Pst DC3000. The

small increase in unlabelled carbon observed in glycine, but not in serine, may be explained by the uptake of unlabelled CO_2 into the amino acid by the action of glycine synthase, the percentage of which would be increasing as unlabelled GABA is metabolised via the TCA cycle.

In the Glc + GABA treatment, in Pst DC3000 cells (Figure 5.12), the percentage of label (around 80 %) remaining in amino acids derived from pyruvate (alanine, valine and leucine) can be explained by fluxes of roughly the same size from PEP to pyruvate and from malate or oxaloacetate to pyruvate (it can be inferred from phenylalanine and tyrosine that the labelling of PEP is around 96 % and the labelling of oxaloacetate can be deduced from aspartate to be around 55 %). Metabolic flux analysis of Pst DC3000 cells in the presence of glucose (Section 4.2.6) showed both of these fluxes were active, with fluxes of 0.54 from PEP to pyruvate and 0.88 from malate to pyruate, providing evidence that an unlabelling approach can be used to determine if pathways are active. The differences between the flux values for these reactions from the unlabelling and MFA studies may be due to the inclusion of GABA, which may alter metabolic fluxes more generally.

The unlabelling strategy thus presents a novel way to map the fate of substrates, and to some degree the resulting fluxes, where ^{13}C substrates are not commercially available.

5.3.5 The role of GABA in C:N sensing and implications for virulence

As discussed in Chapter 3, there is strong evidence for Pst DC3000 cells changing their virulence gene expression in response to changing intracellular metabolite abundances, specifically in response to glutamate or associated metabolites. The abundance of GABA relative to glutamate in Δ*gabT2/T3/T1* cells appeared to be a causal factor in the increased virulence gene repression experienced by this strain. However, it is unclear if this is due to disruption of an intracellular ratio sensing mechanism (for example, the abundance of GABA relative to glutamate) or if the increase of GABA alone, or an unmeasured byproduct, causes the repression. This result adds weight to the discovery in Chapter 3 that significant intracellular changes occur in metabolite abundances under different environmental conditions and characterisation of possible sensing mechanisms and their metabolite targets is of great importance. As discussed previously, the two-component systems NtrB-NtrC and CbrA-CbrB, implicated in nitrogen and carbon sensing respectively and known to regulate virulence genes in other bacterial species, are a possible starting point in this line of investigation. The hypothesis that Pst DC3000 cells may be regulating virulence genes in response to their intracellular carbon:nitrogen ratios is examined in more depth in Section 6.3.

5.3.6 The role of GABA in stress tolerance and implications for virulence

The host apoplast has been described as a stressful environment for invading bacterial cells, specifically with regard to water potential and oxidative stress [10, 312, 313]. As GABA is highly abundant in this environment, and as GABA is a well established osmolyte in plants [251], in addition to GABA being reported to act as an osmolyte in some bacterial species [306], the ability of the GABA mutants to tolerate stresses in the presence and absence of GABA was tested. A strong correlation was found in the alleviation of virulence gene and growth inhibition in Δ*gabT2/T3/T1* in the presence of GABA and an abiotic stress. Δ*gabT2/T3/T1* has been shown in this study to have high levels of intracellular GABA under the M9-fructose + 5 mM GABA test conditions, and thus is can be concluded that the excess GABA is interacting in some way with Pst DC3000's response to stressful environments. In *P. aeruginosa* and *P. fluorescens*, a master regulator protein, RpoS, is responsible for the coordinated response to high or low temperature, hyperosmolarity and acidic pH [314, 315]. In *E. coli*, RpoS is known to activate the GABA operon, specifically *gabT*. Whilst this relationship has not been established in *Pseudomonas* species, it would be a interesting avenue to pursue to fully understand the interaction between GABA and stress responses.

5.3.7 Summary

The aim of this chapter was to gain a better understanding of how the most abundant metabolite in the host apoplast influences the virulence of Pst DC3000. GABA is assimilated by Pst DC3000 cells incubated in apoplastic extracts and it causes repression of virulence gene expression, an effect which is amplified by increasing concentrations of GABA. Pst DC3000 primarily imports GABA via a GABA permease, encoded by *gabP*, but at least one other transport mechanism for GABA exists, which brings GABA into Pst DC3000 cells less rapidly than GabP. GABA is usually metabolised by GABA transaminase enzymes, three of which have been identified in Pst DC3000. When the genes encoding these enzymes are deleted, Pst DC3000 is still able to grow in the presence of GABA, but to a much reduced level. This demonstrated that GABA can be catabolised by an alternative, as yet unidentified route. Rapid turnover of GABA appears to be of high importance to Pst DC3000, and it is likely that this is due to the repressive effect this molecule has on the expression of T3SS genes. Phylogenetic analysis suggests that *P. syringae* strains all appear to have numerous genes involved in GABA metabolism, implying rapid metabolism of GABA may be required to evade host defences more broadly or to tolerate a stressful host environment. This study has also shown a link between intracellular GABA abundance and stress tolerance, where excess intracellular GABA alleviates growth repression and virulence gene repression by the stressor. GABA is therefore a highly significant metabolite at the tomato-Pst DC3000 metabolic interface, and a possible target for manipulation of host defence responses.

Chapter 6

General Discussion

This study has demonstrated an intimate interaction between metabolism and virulence gene expression in the plant pathogen *Pseudomonas syringae* pv. tomato DC3000 (Pst DC3000). Metabolic characterisation of the apoplastic environment provided the foundation for understanding how Pst DC3000 cells respond to the host environment. Apoplastic metabolites were shown to have differing effects on the expression of virulence genes and in particular, the abundant apoplastic metabolic GABA requires rapid metabolic turnover to avoid virulence gene repression. Both intracellular metabolite pools and central carbon fluxes were shown to be altered in Pst DC3000 cells exposed to conditions that stimulate virulence gene expression. These experiments have provided several important advances in our understanding of Pst DC3000-tomato metabolic interactions and have highlighted new areas for future research.

6.1 Profiling the ecological niche of Pst DC3000: the limitations of apoplast extracts for understanding the *in planta* bacterial habitat

Extracting apoplastic fluid from plant tissues has typically been used to study the *in planta* environment that pathogenic bacteria occupy [71, 75]. In this study it has led to the detection and relative quantification of sugars and organic acids, and the apoplast was found to be particularly rich in amino acids. This analysis subsequently allowed depletion and virulence gene expression analyses to be undertaken and these have provided valuable insights into how Pst DC3000 responds to its host environment.

However, whilst apoplast extracts can be informative about many features of the apoplastic compartment, several results from this and other studies have emphasised some of the shortcomings of the technique. First, the composition of the apoplast has been shown to change in response to various biotic and abiotic stresses, and will even change composition with day-night cycles [8, 73, 75, 316]. Apoplastic extractions, however, only provide static information about a single point in time. In this study, the apoplast extracts were able to inform on the metabolites found in healthy apoplast and which metabolites Pst DC3000 depletes from a healthy apoplast sam-

ple, but not on how the apoplast might change in response to Pst DC3000 in real time.

Second, iron was not present at detectable levels in the tomato apoplast extracts, which was unusual as iron had previously been shown to be present at detectable levels in sugar beet leaf apoplast [70], had been identified in tomato xylem fluid [142], and Pst DC3000 requires iron for the expression of virulence genes [155]. This implies the apoplast extract technique is not completely suited to the identification of all metal ions. If iron ions are tightly bound to the plant cell walls, it is possible that the same is true of other metal ions. Pst DC3000 has been shown to downregulate genes associated with iron acquisition [103] and siderophore mutants of Pst DC3000 are still capable of pathogenesis [317]. These lines of evidence point to the apoplast being an iron-rich environment, and further efforts should be made to measure the abundance of this metal and others which may be bound to plant cell walls.

Third, virulence gene expression in apoplastic fluid is around 20-fold lower than in fructose-based minimal medium. A similar result has been noted by Rico *et al* (2008) [71] and Xiao *et al* (1992) [152]. One of the possible explanations provided by Rico *et al* (2008) [71] for this discrepancy was the extraction method changing the osmolarity of the environment. The observed reduction in virulence gene expression in response to excess sodium chloride in Section 5.2.19 adds weight to this hypothesis. In addition, a recent study by Stauber *et al* (2012) [80] showed that differential

virulence gene expression may be regulated in response to cell density. Nutrients which caused slower growth, such as fructose, caused high levels of virulence gene induction, whilst those that caused more rapid growth, such as organic acids were typically more repressive [80]. In this study, tomato leaf apoplast extract caused rapid and high levels of growth in Pst DC3000, whereas growth in fructose-based minimal media was much slower.

Interestingly, upon inoculation into the plant host Pst DC3000 cells show a delay before beginning to divide, though still express their virulence genes (Prof. John Mansfield, personal communication), which was not observed in growth assays conducted in extracted apoplastic fluid. This indicates either that Pst DC3000 is not converting assimilated nutrients into products for growth as a result of a plant signal that is not present in apoplast extracts, or that nutrients in the apoplast are spatially structured and that this means they are assimilated more slowly, resulting in slower growth. There is significant evidence that upon entry into the apoplast, Pst DC3000 cells form colonies [318], and do not move freely as they will in liquid apoplast extracts. This, in combination with spacial structuring of apoplastic nutrients, may result in lower growth rates than observed *in vitro*, and thus higher virulence gene expression. *In planta* metabolite and ion visualisation techniques have been developed [78, 319] which may allow full *in planta* characterisation of the apoplast and the metabolic interactions between Pst DC3000 cells and this compartment to become a reality in the near future.

6.2 Prospects for metabolic flux analysis of Pst DC3000 *in planta*

One of the aims of this study was to lay the ground-work for metabolic flux analysis of Pst DC3000 cells within host plants in order to more fully understand the adaptation to the plant environment. This study has successfully characterised the fluxes of Pst DC3000 in glucose and fructose-based media, which allows comparisons with published flux maps of *Pseudomonas* strains, however, a more relevant setting in which to quantify fluxes would be during infection of the plant host. This is now particularly pertinent as this study has shown there to be significant metabolic changes in Pst DC3000 cells incubated in *hrp* gene inducing environments. Establishing and testing a metabolic model in a minimal medium is the first step towards this goal and the following considerations will have to be addressed to move the system *in planta*.

Whilst it is possible to monitor the depletion of multiple carbon substrates within a complex environment, as shown by this study (Section 3.2.2), the mathematical modelling involved in the uptake of potentially more than 24 carbon substrates would be rather more difficult. The establishment of isotopic and metabolic steady state would also present a further challenge, particularly in choosing how to label the bacterial cells within such a nutrient-rich environment and when to harvest cells for analysis. Section 5.2.4 supplies some evidence that an unlabelling approach might prove suitable, with the bacterial cells fully labelled as they entered the plant. The

reduction in the abundance of labelled carbon could then be monitored over time with dynamic MFA. A further challenge would be the distinguishing of bacterial metabolites from plant metabolites. One approach to this could be the isolation of a specific bacterial protein from the bacteria-infected plant tissues, such as the GFP method developed by Shaikh *et al* (2008) [213]. However, the extraction of bacterial soluble metabolites, which this study has shown are required for full resolution of fluxes, would not be possible using a protein-based method. There will be significant hurdles, therefore, in characterising metabolic fluxes in Pst DC3000 *in planta*, but if possible, will be a highly significant step forward in the understanding of plant-pathogen interactions.

6.3 Are altered metabolite profiles a symptom or a cause of virulence gene expression?

The sensing of carbon:nitrogen ratios and nitrogen limitation is common to many organisms as a way to optimise growth and development in changing environments [154, 320–322]. The metabolites 2-oxoglutarate and glutamine are frequently implicated in this processes: *Salmonella typhimurium* uses internal glutamine abundance to sense nitrogen limitation (low glutamine levels are perceived as indicating a nitrogen-limited environment) [154] and cyanobacteria have been shown to use internal 2-oxoglutarate to monitor their 'nitrogen status', where excess nitrogen produces an increase in the 2-oxoglutarate pool [153]. The tomato apoplast has been assumed to be a nitrogen-limited environment for Pst DC3000 as nitrogen-limited

conditions *in vitro* cause virulence gene expression [71]. Thus, if Pst DC3000 was responding to a nitrogen-limited environment in the same way as *S. typhimurium* or cyanobacteria, differences in glutamine and 2-oxoglutarate levels would be expected.

However, in this study, the metabolite which most obviously showed a correlation with virulence gene expression changes was glutamate. Glutamine levels often, but not always, reflected glutamate levels, and 2-oxoglutarate abundances stayed consistent throughout treatment conditions. Is it possible in Pst DC3000 that glutamate instead provides the required signal? In *P. putida* the NtrB-NtrC two-component system regulates a number of operons that encode genes involved in nitrogen assimilation in an RpoN-dependent manner [168]. The Ntr system is controlled by a P_{II} protein, encoded by *glnK*, and *glnK* is upregulated under nitrogen limiting conditions [168]. The expression of the NADP-glutamate dehydrogenase encoding gene, *gdhA* (glutamate dehydrogenase catalyses the conversion of glutamate to 2-oxoglutarate), is controlled by NtrC: NtrC directly represses *gdhA* transcription under nitrogen limitation in *P. putida* [168]. In *P. putida*, inactivity of glutamate dehydrogenase, and therefore a potential excess of glutamate, is the result of perceived nitrogen limitation. However, currently *gdhA* is not know to be present in the genome of Pst DC3000, though a different glutamate dehydrogenase (NAD-specific) is encoded. If a similar system operates in *P. syringae* strains, then high levels of glutamate produced by Pst DC3000 in apoplast extracts and fructose minimal media would be consistent with the apoplast and *hrp*-inducing minimal media being perceived as nitrogen-limited environments by Pst DC3000.

One way to determine if levels of intracellular glutamate are causing changes in virulence gene expression in Pst DC3000 would be to engineer inducible downregulation of glutamate dehydrogenase genes, or the upregulation of other genes involved in glutamate synthesis, and to monitor the virulence gene expression in these strains in response to apoplastic extracts or fructose minimal medium. Monitoring the expression of virulence genes in response to extracellular GABA may also give an indication if GABA accumulation reduces virulence gene expression via this mechanism.

However, glutamate levels, and indeed other metabolite abudances may be a 'symptom' of virulence gene expression, rather than a 'cause'. Both NtrB-NtrC and the related CbrA-CbrB proteins, a carbon regulatory system which is thought to interact with NtrB-NtrC in *P. aeruginosa* [150], have been implicated in virulence across a number of bacterial species [169–171, 323]. Notably, the *hrpL*-regulators HrpR and HrpS show high levels of similarity (60 % identity [50]) to the NtrB-NtrC two-component system. It would be interesting to test whether HrpR and HrpS do function in the same way as the NtrB/C-CbrA/B system and whether the NtrB/C-CbrA/B system itself is involved in Pst DC3000 virulence. In addition, as the NtrB/C-CbrA/B system is known to regulate many *Pseudomonas* metabolic operons [168, 324], determining whether alterations in *ntrB/C-cbrA/B* expression cause changes in metabolic fluxes in Pst DC3000 may provide an explanation as to the signficant changes observed in the metabolic flux analysis of Pst DC3000 incubated in fructose and glucose minimal media.

6.4 Applications of findings from this study for disease control

This study and others have emphasised the importance of the environment for the expression of virulence genes in Pst DC3000 and other plant pathogenic bacteria [50]. The apoplastic environment presents an interesting possibility for the engineering of increased plant resistance to bacterial pathogens as this is the primary plant:pathogen interface. GABA was shown to repress virulence gene expression in Pst DC3000 and the GABA-overexpressing tobacco plants (GADΔC1) used in Section 5.2.10 showed reduced HR symptoms upon inoculation with Pst DC3000 in comparison with $\Delta gabP$ (which shows limited virulence gene repression in response to GABA). It would be interesting to engineer Pst DC300's host plant, tomato, to overproduce GABA to determine if this is equally successful in the repression of virulence genes. Other virulence gene-repressive substrates identified in this study may also be worth investigating. Threonine, in particular, was one of the most repressive metabolites tested, and as Pst DC3000 cannot metabolise this amino acid, it may be an interesting target for overexpression in tomato plants.

Virulence genes in Pst DC3000 are induced by several substrates known to upregulate virulence gene expression in other phytopathogenic bacteria, such as fructose and mannitol. An interesting extension of this study would be to characterise virulence gene expression in species of *Erwinia*, *Ralstonia* and *Xanthomonas*, and additional *P. syringae* strains, in response to apoplastic metabolites as well as mon-

itoring metabolite abundances under *hrp*-inducing conditions.

6.5 Conclusions

This study has provided some interesting prospects for future research initiatives. First, the ground-work has been laid for characterising metabolic fluxes in the important plant pathogen Pst DC3000 within its host environment and the identification of altered fluxes under virulence gene inducing conditions has given this a strong rationale. Second, the mechanism by which Pst DC3000 cells monitor their intracellular metabolite pools merits further investigation, as these have also been shown to change in response to virulence gene inducing and repressing conditions, with the NtrB/C-CbrA/B system a likely candidate. Finally, a more detailed understanding of the composition of the apoplastic compartment, in terms of temporal dynamics and spacial structuring of nutrients, will provide an enhanced understanding of the metabolic context for virulence in Pst DC3000.

Bibliography

[1] Garber ED (1960) The host as a growth medium. *Annals of the New York Academy of Sciences* 88:1187–1194.

[2] Gupta KJ, et al. (2013) The form of nitrogen nutrition affects resistance against *Pseudomonas syringae* pv. phasolicola in tobacco. *Journal of Experimental Botany* 64:553–568.

[3] Rico A, McCraw SL, Preston GM (2011) The metabolic interface between *Pseudomonas syringae* and plant cells. *Current Opinion in Microbiology* 14:31–38.

[4] Olea F, et al. (2004) Up-regulation and localisation of asparagine synthetase in tomato leaves infected by the bacterial pathogen *Pseudomonas syringae*. *Plant & Cell Physiology* 45:770–780.

[5] Georgieva I, Edreva A, Rodeva R, Sotirova V, Stoimenova E (2000) Metabolic changes in tomato fruits and seeds after viral, bacterial and fungal infections. *Acta Physiologiae Plantarum* 22:281–284.

[6] Allwood JW, Clarke A, Goodacre R, Mur LA (2010) Dual metabolomics: a

novel approach to understanding plant-pathogen interactions. *Phytochemistry* 71:590–597.

[7] Ward JL, et al. (2010) The metabolic transition during disease following infection of *Arabidopsis thaliana* by *Pseudomonas syringae* pv. tomato. *The Plant Journal* 63:443–457.

[8] Lopez-Gresa MP, et al. (2010) Metabolic response of tomato leaves upon different plant-pathogen interactions. *Phytochemical Analysis* 21:89–94.

[9] Thilmony R, Underwood W, He SY (2006) Genome-wide transcriptional analysis of the *Arabidopsis thaliana* interaction with the plant pathogen *Pseudomonas syringae* pv. tomato dc3000 and the human pathogen *Escherichia coli* O157:H7. *The Plant Journal* 46:34–53.

[10] Hernandez-Morales A, et al. (2009) Transcriptional profile of *Pseudomonas syringae* pv. phaseolicola NPS3121 in response to tissue extracts from a susceptible *Phaseolus vulgaris* l. cultivar. *BMC Microbiology* 9:257–73.

[11] Rohmer L, Hocquet D, Miller SI (2011) Are pathogenic bacteria just looking for food? Metabolism and microbial pathogenesis. *Trends in Microbiology* 19:341–348.

[12] Allwood JW, Ellis DI, Goodacre R (2008) Metabolomic technologies and their application to the study of plants and plant-host interactions. *Physiologia Plantarum* 132:117–135.

[13] Mulet M, Lalucat J, Garca-Valds E (2010) DNA sequence-based analysis of the *Pseudomonas* species. *Environmental Microbiology* 12:1513–1530.

[14] Loper JE, et al. (2012) Comparative genomics of plant-associated *Pseudomonas* spp.: Insights into diversity and inheritance of traits involved in multitrophic interactions. *PLoS Genet* 8:e1002784.

[15] Spiers A, Buckling A, Rainey PB (2000) The causes of *Pseudomonas* diversity. *Microbiology* 146:2345–2350.

[16] Strange RN (2005) Plant disease: a threat to global food security. *Annual Review of Phytopathology* 43:83–116.

[17] Sawada H, Suzuki F, Matsuda I, Saitou N (1999) Phylogenetic analysis of *Pseudomonas syringae* pathovar suggests the horizontal gene transfer of *argK* and the evolutionary stability of *hrp* gene cluster. *Journal of Molecular Evolution* 49:627–644.

[18] Scortichini M, Marcelletti S, Ferrante P, Petriccione M, Firrao G (2012) *Pseudomonas syringae* pv. actinidiae: a re-emerging, multi-faceted pandemic pathogen. *Molecular Plant Pathology* 13:631–640.

[19] Green S, et al. (2010) Comparative genome analysis provides insighrs into the evolution and adaptation of *Pseudomonas syringae* pv. aesculi on *Aesculus hippocastanum*. *PLoSONE* 5:e10224.

[20] Sarkar SF, Gordon JS, Martin GB, Guttman DS (2006) Comparative genomics of host-specific virulence in *Pseudomonas syringae*. *Genetics* 174:1041–1056.

[21] Preston GM (2000) *Pseudomonas syringae* pv. tomato: the right pathogen, of the right plant, at the right time. *Molecular Plant Pathology* 1:263–275.

[22] Morris CE, et al. (2008) The life history of the plant pathogen *Pseudomonas syringae* is linked to the water cycle. *The ISME Journal* 2:321–334.

[23] Katagiri F, Thilmony R, He SY (2002) The *Arabidopsis thaliana-Pseudomonas syringae* interaction. *The Arabidopsis Book* 1:e0039.

[24] Jones JDG, Dangl JL (2006) The plant immune system. *Nature* 444:323–329.

[25] Gurian-Sherman D, Lindow SE (1993) Bacterial ice nucleation: significance and molecular basis. *The FASEB Journal* 7:1338–1343.

[26] Marco ML, Legac J, Lindow SE (2005) *Pseudomonas syringae* genes induced during colonisation of leaf surfaces. *Environmental Microbiology* 7:1379–1391.

[27] Pinzon A, Rodriguez-R LM, Gonzlez A, Bernal A, Restrepo S (2011) Targeted metabolic reconstruction: a novel approach for the characterization of plant–pathogen interactions. *Briefings in Bioinformatics* 12:151–162.

[28] Cai R, et al. (2011) The plant pathogen *Pseudomonas syringae* pv. tomato is genetically monomorphic and under strong selection to evade tomato immunity. *PLoS Pathogens* 7:e1002130.

[29] Whalen MC, Innes RW, Bent AF, Staskawicz BJ (1991) Identification of *Pseudomonas syringae* pathogens of *Arabidopsis* and a bacterial locus determining avirulence on both *Arabidopsis* and soybean. *The Plant Cell* 3:49–59.

[30] Buell C, et al. (2003) The complete genome sequence of the *Arabidopsis* and tomato pathogen *Pseudomonas syringae* pv. tomato DC3000. *Proceedings of the National Academy of Sciences* 100:10181–10186.

[31] Gorke B, Stulke J (2008) Carbon catabolite repression in bacteria: many ways to make the most out of nutrients. *Nature Reviews Microbiology* 6:613–624.

[32] Rico A, Jones R, Preston GM (2009) Adaptation to the plant apoplast by plant pathogenic bacteria. *Plant Pathogenic Bacteria: Genomics and Molecular Biology* pp 63–89.

[33] Gimenez-Ibanez S, Rathjen JP (2010) The case for the defense: plants versus *Pseudomonas syringae*. *Microbes and Infection* 12:428–437.

[34] Zipfel C (2009) Early molecular events in PAMP-triggered immunity. *Current Opinion in Plant Biology* 12:414–420.

[35] Zipfel C, et al. (2004) Bacterial disease resistance in *Arabidopsis* through flagellin perception. *Nature* 428:764–767.

[36] Schwessinger B, Zipfel C (2008) News from the frontline: recent insights into pamp-triggered immunity in plants. *Current Opinion in Plant Biology* 11:389–395.

[37] Tsuda K, Sato M, Glazebrook J, Cohen JD, Katagiri F (2008) Interplay between MAMP-triggered and SA-mediated defense responses. *The Plant Journal* 53:763–775.

[38] Wei HL, Collmer A (2012) Multiple lessons from the multiple functions of a regulator of type III secretion system assembly in the plant pathogen *Pseudomonas syringae*. *Molecular Microbiology* 85:195–200.

[39] Oh HS, Park DH, Collmer A (2010) Components of the *Pseudomonas syringae*

type III secretion system can suppress and may elicit plant innate immunity. *Molecular Plant-Microbe Interactions* 23:727–739.

[40] Tang X, Xiao Y, Zhou JM (2006) Regulation of the type III secretion systen in phphytopathogen bacteria. *Molecular Plant-Microbe Interactions* 19:1159–1166.

[41] Tampakaki AP, et al. (2010) Playing the "harp": Evolution of our understanding of *hrp/hrc* genes. *Phytopathology* 48:347–370.

[42] Cunnac S, et al. (2011) Genetic disassembly and combinatorial reassembly identify a minimal functional repertoire of type III effectors in *Pseudomonas syringae*. *Proceedings of the National Academy of Sciences* 108:2975–2980.

[43] Block A, Alfano JR (2011) Plant targets for *Pseudomonas syringae* type III effectors: virulence targets or guarded decoys? *Current Opinion in Microbiology* 14:39–46.

[44] Kazmierczak MJ, Wiedmann M, Boor KJ (2005) Alternative sigma factors and their role in bacterial virulence. *Microbiology and Molecular Biology Reviews* 69:527–543.

[45] MacLean D, Studholme DJ (2010) A Boolean model of the *Pseudomonas syringae hrp* regulon predicts a tightly regulated system. *PLoSONE* 5:e9101.

[46] Ortiz-Martin I, Thwaites R, Macho AP, Mansfield JW, Beuzon CR (2010) Positive regulation of the Hrp type III secretion system in *Pseudomonas syringae* pv. phaseolicola. *Molecular Plant-Microbe Interactions* 23:665–685.

[47] Maurtani M, et al. (2008) Gac two-component system in *Pseudomonas syringae* pv. tabaci is regquired for viruelence but not for hypersensitive reaction. *Molecular Genetics and Genomics* 279:313–322.

[48] Chatterjee A, Cui Y, Collmer A, Alfano JR, Chatterjee AK (2003) GacA, the response regulator of a two-component system, acts as a master regulator in *Pseudomonas syringae* pv. tomato DC3000 by controlling regulatory RNA transcriptional activators, and alternative sigma factors. *Molecular Plant-Microbe Interactions* 16:1106–1117.

[49] Ichinose Y, Taguchi F, Mukaihara T (2013) Pathogenic and virulence factors of *Pseudomonas syringae*. *Journal of General Plant Pathology* 79:285–296.

[50] Brencic A, Winans SC (2005) Detection of ,and response, to signals involved in host-microbe interactions by plant-associated bacteria. *Microbiology and Molecular Biology Reviews* 69:155–194.

[51] Wei W, et al. (2000) The gene coding for the Hrp pilus structural protein is required for type III secretion of Hrp and Avr pprotein in *Pseudomonas syringae* pv. tomato. *Proceedings of the National Academy of Sciences* 97:2247–2252.

[52] Bretz J, Losada L, Lisboa K, Hutcheson SW (2002) Lon protease functions as a negative regulator of type III protein secretion in *Pseudomonas syringae*. *Molecular Microbiology* 45:397–409.

[53] Yang HJ, Lee JS, Cha JY, Baik HS (2011) Negative regulation of pathogenesis in *Pseudomonas syringae* pv. tabaci 11528 by ATP-dependent Lon protease. *Molecules and Cells* 32:317–323.

[54] Ferreira AO, et al. (2006) Whole-genome expression profiling defines the *hrpL* regulon of *Pseudomonas syringae* pv. tomato DC3000, allows *de novo* reconstruction of the Hrp cis element, and identifies novel coregulated genes. *Molecular Plant-Microbe Interactions* 19:1167–1179.

[55] Uppalapati SR, et al. (2005) The phytotoxin coronatine and methyl jasmonate impact multiple phytohormone pathways in tomato. *The Plant Journal* 42:201–217.

[56] Brooks DM, Bender CL, Kunkel BN (2005) The *Pseudomonas syringae* phytotoxin coronatine promotes virulence by overcoming salicylic acid-dependent defences in *Arabidopsis thaliana*. *Molecular Plant Pathology* 6:629–639.

[57] Zheng XY, et al. (2012) Coronatine promotes *Pseudomonas syringae* virulence in plants by activating a signalling cascade that inhibits salicylic acid accumulation. *Cell Host & Microbe* 11:587–596.

[58] Kenyon J, Turner JG (1990) Physiological changes in *Nicotiana tabacum* leaves during development of chlorosis caused by coronatine. *Physiological and Molecular Plant Pathology* 37:463–477.

[59] Sreedharan A, Penaloza-Vazquez A, Kunkel BN, Bender CL (2006) CorR regulates muliple components of virulence in *Pseudomonas syringae* pv. tomato DC3000. *Molecular Plant-Microbe Interactions* 19:768–779.

[60] Keith RC, Keith LMW, Hernandez-Guzman G, Uppalapati SR, Bender CL (2003) Alginate gene expression by *Pseudomonas syringae* pv. tomato DC3000 in host and non-host plants. *Microbiology* 149:1127–1138.

[61] Willis DK, Holmstadt JJ, Kinscherf TG (2001) Genetic evidence that loss of virulence associated with *gacS* or *gacA* mutations in *Pseudomonas syringae* B728a does not result from effects on alginate production. *Applied and Environmental Microbiology* 67:1400–1403.

[62] Mutka AM, Fawley S, Tsao T, Kunkel BN (2013) Auxin promotes susceptibility to *Pseudomonas syringae* via a mechanism independent of suppression of salicylic acid-mediated defences. *The Plant Journal* 74:746–754.

[63] Chen Z, et al. (2007) *Pseudomonas syringae* type III effector AvrRpt2 alters *Arabidopsis thaliana* auxin physiology. *Proceedings of the National Academy of Sciences* 104:20131–20136.

[64] Flor HH (1971) Current status of the gene-for-gene concept. *Annual Review of Phytopathology* 9:275–296.

[65] Deslandes L, et al. (2003) Physical interaction between RRs1-R, a protein conferring resistance to bacterial wilt, and PopP2, a type III effector targeted to the plant nucleus. *Proceedings of the National Academy of Sciences* 100:8024–8029.

[66] Van der Biezen EA, Jones JDG (1998) Plant disease-resistance proteins and the gene-for-gene concept. *Trends in Biochemical Sciences* 23:454–456.

[67] van der Hoorn RAL, Kamoun S (2008) From guard to decoy: a new model for perception of plant pathogen effectors. *The Plant Cell* 20:2009–2017.

[68] Dangl JL, Jones JDG (2001) Plant pathogens and integrated defence responses to infection. *Nature* 411:826–833.

[69] Collier SM, Moffett P (2009) NB-LRRs work a "bait and switch" on pathogens. *Trends in Plant Science* 14:521–529.

[70] Lopez-Millan AF, Morales F, Abadia A, Abadia J (2000) Effects of iron deficiency on the composition of the leaf apoplastic fluid and xylem sap in sugar beet. Implications for iron and carbon transport. *Plant Physiology* 124:873–884.

[71] Rico A, Preston G (2008) *Pseudomonas syringae* pv. tomato DC3000 uses constitutive and apoplast-induced nutrient assimilation pathways to catabolize nutrients that are abundant in the tomato apoplast. *Molecular Plant-Microbe Interactions* 21:269–282.

[72] Grignon C, Sentenac H (1991) pH and ionic conditions in the apoplast. *Annual Review of Plant Physiology and Plant Molecular Biology* 42:103–128.

[73] Jia W, Davies WJ (2007) Modification of leaf apoplastic pH in relation to stomatal sensitivity to root-sourced abscicis acid signals. *Plant Physiology* 143:68–77.

[74] Almeida DPF, Huber DJ (1999) Apoplastic pH and inorganic ion levels in tomato fruit: A potential means for regulation of cell wall metabolism during ripening. *Physiologia Plantarum* 105:506–512.

[75] Solomon PS, Oliver RP (2001) The nitrogen content of the tomato leaf apoplast increases during infection by *Cladosporium fulvum*. *Planta* 213:241–249.

[76] Li XZ, Starratt AN, Cuppels DA (1998) Identification of tomato leaf factors that activate toxin gene expression in *Pseudomonas syringae* pv. tomato DC3000. *Phytopathology* 88:1094–1100.

[77] Fones H, Preston GM (2012) The impact of transition metals on bacterial plant disease. *FEMS Microbiology Reviews* 37:495–519.

[78] Moore KL, et al. (2014) Combined nano SIMS and synchrotron X-ray fluorescence reveal distinct cell-cell and subcellular distribution patterns of trace elements in rice tissues. *New Phytologist* 201:104–115.

[79] Huynh T, Dahlbeck D, Staskawicz B (1989) Bacterial blight of soybean: regulation of a pathogen gene determining host cultivar specificity. *Science* 245:1374.

[80] Stauber JL, Loginicheva E, Schechter LM (2012) Carbon source and cell density-dependent regulation of type III secretion system gene expression in *Pseudomonas syringae* pathovar tomato DC3000. *Research in Microbiology* 163:531–539.

[81] Rahme LG, Mindrinos MN, Panopoulos NJ (1992) Plant and environmental sensory signals control the expression of *hrp* genes in *Pseudomonas syringae* pv. phaseolicola. *Journal of Bacteriology* 174:3499–3507.

[82] Mole BM, Baltrus DA, Dangl JL, Grant SR (2007) Global virulence regulation networks in phytopathogenic bacteria. *Trends in Microbiology* 15:363–371.

[83] Lan L, Deng X, Zhou J, Tang X (2006) Genome-wide gene expression analysis of *Pseudomonas syringae* pv. tomato DC3000 reveals overlapping and distinct

pathways regulated by *hrpL* and *hrpRS*. *Molecular Plant-Microbe Interactions* 19:976–987.

[84] Guo Y, Figueiredo F, Jones J, Wang N (2011) HrpG and HrpX play global roles in coordinating different virulence traits of *Xanthomonas axonopodis* pv. citri. *Molecular Plant-Microbe Interactions* 24:649–661.

[85] Jones R (2009) Ph.D. thesis (University of Oxford).

[86] Mithani A, Hein J, Preston GM (2011) Comparative analysis of metabolic networks provides insight into the evolution of plant pathogenic and non-pathogenic lifestyles in *Pseudomonas*. *Molecular Biology and Evolution* 28:483–499.

[87] Bouche N, Fromm H (2004) GABA in plants: just a metabolite? *Trends in Plant Science* 9:110–115.

[88] Park D, et al. (2010) Mutations in γ-aminobutyric acid (GABA) transaminase genes in plants or *Pseudomonas syringae* reduce bacterial virulence. *The Plant Journal* 64:318–330.

[89] Caspi R, et al. (2012) The MetaCyc database of metabolic pathways and enzymes and the BioCyc collection of pathway/genome databases. *Nucleic Acids Research* 40:742–753.

[90] Moran NA (2002) Microbial minimalism: gene reduction in bacterial pathogens. *Cell* 108:583–586.

[91] Truman W, de Zabala MT, Grant M (2006) Type III effectors orchestrate a

complex interplay between transcriptional networks to modify basal defence responses during pathogenesis and resistance. *The Plant Journal* 46:14–33.

[92] Perez-Garcia A, et al. (1998) Light-dependent changes of tomato glutamine synthetase in response to *Pseudomonas syringae* infection or phosphinothricin treatment. *Physiologia Plantarum* 102:377–384.

[93] Jones AME, et al. (2004) Specific changes in the *Arabidopsis* proteome in response to bacterial challenge: differentiating basal and R-gene mediated resistance. *Phytochemistry* 65:1805–1816.

[94] Jones AME, Thomas V, Bennett MH, Mansfield JW, Grant M (2006) Modifications to the arabidopsis defense proteome occur prior to significant transcriptional change in response to inoculation with *Pseudomonas syringae*. *Plant Physiology* 142:1603–1620.

[95] Parker J, et al. (2013) Quantitative proteomics of tomato defense against *Pseudomonas syringae* infection. *Proteomics* 13:1934–1946.

[96] Carrari F, et al. (2006) Integrated analysis of metabolite and transcript levels reveals the metabolic shifts that underlie tomato fruit development and highlight regulatory aspects of metabolic network behaviour. *Plant Physiology* 142:1380–1396.

[97] Maeda H, Dudareva N (2012) The shikimate pathway and aromatic amino acid biosynthesis in plants. *Annual Review of Plant Biology* 63:73–105.

[98] Berger S, Sinha AK, Roitsch T (2007) Plant physiology meets phytopathology: plant primary metabolism and plant-pathogen interactions. *Journal of*

Experimental Botany 58:4019–4026.

[99] Lopez-Gresa MP, et al. (2011) Identification of defence metabolites in tomato plants infected by the bacterial pathogen *Pseudomonas syringae*. *Environmental and Experimental Botany* 74:216–228.

[100] Zacares, L. Lopez-Gresa MP, Fayos J, Primo J, Belles JM, Conejero V (2007) Induction of p-coumaroyldopamine and feruloyldopamine, two novel metabolites, in tomato by the bacterial pathogen *Pseudomonas syringae*. *Molecular Plant-Microbe Interactions* 20:1439–1448.

[101] Rio-Alvarez I, et al. (2013) Light regulates motility, attachment and viruelnce in the plant pathogen *Pseudomonas syringae* pv. tomato DC3000. *Environmental Microbiology* DOI: 10.1111/1462-2920.12240.

[102] Hoffland E, Jeger MJ, van Beusichem ML (2000) Effect of nitrohen supply rate on disease resistance in tomato depends on the pathogen. *Plant and Soil* 218:239–247.

[103] Yu X, et al. (2013) Transcriptional responses of *Pseudomonas syringae* to growth in epiphytic versus apoplastic leaf sites. *Proceedings of the National Academy of Sciences* 110:425–434.

[104] Fiehn O (2002) Metabolomics - the link between genotypes and phenotypes. *Plant Molecular Biology* 48:155–171.

[105] Zamboni N, Fendt S, Rühl M, Sauer U (2009) ^{13}C-based metabolic flux analysis. *Nature Protocols* 4:878–892.

[106] Ratcliffe R, Shachar-Hill Y (2006) Measuring multiple fluxes through plant metabolic networks. *The Plant Journal* 45:490–511.

[107] Silby M, et al. (2009) Genomic and genetic analyses of diversity and plant interactions of *Pseudomonas fluorescens*. *Genome Biology* 10:51.

[108] Jackson RW, Preston GM, Rainey PB (2005) Genetic characterisation of *Pseudomonas fluorescens* SBW25 *rsp* gene expression in the phytosphere and *in vitro*. *Journal of Bacteriology* 187:8477–8488.

[109] Sambrook J, Russell D (2001) *Molecular cloning: a laboratory manual.* (Cold Spring Harbor Laboratory Press).

[110] Winsor G, et al. (2011) *Pseudomonas* genome database: improved comparative analysis and population genomics capability for *Pseudomonas* genomes. *Nucleic Acids Research* 39:596–600.

[111] Yuan J, Reed A, Chen F, Stewart C (2006) Statistical analysis of real-time PCR data. *BMC Bioinformatics* 7:85.

[112] Vandesompele J, et al. (2002) Accurate normalization of real-time quantitative RT-PCR data by geometric averaging of multiple internal control genes. *Genome Biology* 3:1–12.

[113] Katoh K, Standley D (2013) MAFFT multiple sequence alignment software Version 7: improvements in performance and usability. *Molecular Biology and Evolution* 30:772–780.

[114] Suyama M, Torrents D, Bork P (2006) PAL2NAL: robust conversion of protein

sequence alignments into the corresponding codon alignments. *Nucleic Acids Research* 34:609–612.

[115] Stamatakis A (2006) RAxML-VI-HPC: maximum likelihood-based phylogenetic analyses with thousands of taxa and mixed models. *Bioinformatics* 22:2688–2690.

[116] Pavlidis P, Noble W (2003) Matrix2png: A utility for visualising matrix data. *Bioinformatics* 19:295–296.

[117] Lisec J, Schauer N, Kopka J, Willmitzer L, Fernie A (2006) Gas chromatography mass spectrometry–based metabolite profiling in plants. *Nature Protocols* 1:387–396.

[118] Lommen A (2009) Metalign: interface-driven, versatile metabolomics tool for hyphenated full-scan mass spectrometry data preprocessing. *Analytical Chemistry* 81:3079–3086.

[119] Antoniewicz M, Kelleher J, Stephanopoulos G (2007) Accurate assessment of amino acid mass isotopomer distributions for metabolic flux analysis. *Analytical Chemistry* 79:7554–7559.

[120] Masakapalli SK (2011) Ph.D. thesis (University of Oxford).

[121] Wahl S, Dauner M, Wiechert W (2003) New tools for mass isotopomer data evaluation in ^{13}C flux analysis: mass isotope correction, data consistency checking, and precursor relationships. *Biotechnology and Bioengineering* 85:259–268.

[122] Dauner M, Sauer U (2001) Stoichiometric growth model for riboflavin-producing *Bacillus subtilis*. *Biotechnology and Bioengineering* 76:132–143.

[123] Hara A, Radin N (1978) Lipid extraction of tissues with a low-toxicity solvent. *Analytical Biochemistry* 90:420–426.

[124] Kidambi S, Sundin G, Palmer D, Chakrabarty A, Bender C (1995) Copper as a signal for alginate synthesis in *Pseudomonas syringae* pv. syringae. *Applied and Environmental Microbiology* 61:2172–2179.

[125] Read R, Costerton J (1987) Purification and characterization of adhesive exopolysaccharides from *Pseudomonas putida* and *Pseudomonas fluorescens*. *Canadian Journal of Microbiology* 33:1080–1090.

[126] Zamze S, Smith A, Hignett R (1985) Composition of lipopolysaccharide from strains of *Pseudomonas syringae* pv. morsprunorum of differing host specificity and virulence. *Journal of General Microbiology* 131:1941–1950.

[127] Sohn S, Kim T, Park J, Lee S (2010) *In silico* genome-scale metabolic analysis of *Pseudomonas putida* KT2440 for polyhydroxyalkanoate synthesis, degradation of aromatics and anaerobic survival. *Biotechnology Journal* 5:739–750.

[128] Heilmann H (1972) On the peptidoglycan of the cell walls of *Pseudomonas aeruginosa*. *European Journal of Biochemistry* 31:456–463.

[129] Wiechert W (2001) ^{13}C metabolic flux analysis. *Metabolic Engineering* 3:195–206.

[130] Fischer E, Sauer U (2003) Metabolic flux profiling of *Escherichia coli* mutants

in central carbon metabolism using GC-MS. *European Journal of Biochemistry* 270:880–891.

[131] Feng X, Tang YJ (2011) Evaluation of isotope discrimination in ^{13}C-based metabolic flux analysis. *Analytical Biochemistry* 417:295–297.

[132] Wiechert W, Siefke C, de Graaf A, Marx A (2000) Bidirectional reaction steps in metabolic networks: II. Flux estimation and statistical analysis. *Biotechnology and Bioengineering* 55:118–135.

[133] Masakapalli SK, et al. (2010) Subcellular flux analysis of central metabolism in a heterotrophic *Arabidopsis* cell suspention using steady-state stable isotope labeling. *Plant Physiology* 152:602–619.

[134] Lohaus G, Pennewiss K, Sattelmacher B, Hussmann M, Muehling KH (2001) Is the infiltration-centrifugation technique appropriate for the isolation of apoplastic fluid? A critical evaluation with different plant species. *Physiologia Plantarum* 111:457–465.

[135] Husted S, Schjoerring JK (1995) Apoplastic pH and ammonium concentration in leaves of *Brassica napus* L. *Plant Physiology* 109:1453–1460.

[136] Ruan YL, Patrick JW, Brady CJ (1996) The composition of apoplast fluid recovered from intact developing tomato fruit. *Functional Plant Biology* 23:9–13.

[137] Joosten MHAJ, Hendrickx LJM, De Wit PJGM (1990) Carbohydrate composition of apoplastis fluids isolated from tomato leaves inoculated with virulent

or avirulent races of *Cladosporium fulvum* (syn. *Fulvia fulva*). *Netherlands Journal of Plant Pathology* 96:103–112.

[138] Baker CJ, et al. (2010) Effect of viroid infection on the dynamics of phenolic metabolites in the apoplast of tomato leaves. *Physiological and Molecular Plant Pathology* 74:214–220.

[139] Klann EM, Chetelat RT, Bennett AB (1993) Expression of acid invertase gene controls sugar composition in tomato (*Lycopersicon*) fruit. *Plant Physiology* 103:863–870.

[140] Senden MHMN, Van Der Meer AJGM, Limborgh J, Wolterbeek HT (1992) Analysis of major tomato xylem organic aicds and PITC-derivatives of amino acids by RP-HPLC and UV detection. *Plant and Soil* 142:81–89.

[141] Bialczyk J, Lechowski Z, Dziga D (2004) Composition of the xylem sap of tomato seedlings cultivated on media with HCO_3 - and nitrogen source as NO_3 - or NH_4+. *Plant and Soil* 263:265–272.

[142] White MC (1981) Metal complexation in xylem fluid: 1. Chemical composition of tomato and soybean stem. *Plant Physiology* 67:292–300.

[143] Perez-Garcia A, Canovas FM, Gallardo F, Hirel B, de Vicente A (1995) Differential expression of glutamine synthetase isoforms in tomato detached leaflets infected with *Pseudomonas syringae* pv. tomato. *Molecular Plant-Microbe Interactions* 8:96–103.

[144] Moreno R, Martnez-Gomariz M, Yuste L, Gil C, Rojo F (2009) The *Pseudomonas putida* Crc global regulator controls the hierarchical assimilation of

amino acids in a complete medium: Evidence from proteomic and genomic analyses. *Proteomics* 9:2910–2928.

[145] Rojo F (2010) Carbon catabolite repression in *Pseudomonas*: optimizing metabolic versatility and interactions with the environment. *FEMS Microbiology Reviews* 34:658–684.

[146] Filiatrault MJ, et al. (2013) CrcZ and CrcX regulate carbon source utilization in *Pseudomonas syringae* pathovar tomato strain DC3000. *RNA Biology* 10:245–255.

[147] Zhang XX, Rainey PB (2008) Dual involvement of CbrAB and NtrBC in the regulation of histidine utilisation in *Pseudomonas fluorescens* SBW25. *Genetics* 178:185–195.

[148] Hervas AB, Conosa I, Santero E (2008) Transcriptional analysis of *Pseudomonas putida* in response to nitrogen availability. *Journal of Bacteriology* 190:416–420.

[149] Abdou L, Chou HT, Hass D, Lu CD (2011) Promoter recognition and activation by the global response regulator CbrB in *Pseudomonas aeruginosa*. *Journal of Bacteriology* 193:2784–2792.

[150] Nishijyo T, Hass D, Itoh Y (2001) The CbrA-CbrB two-component regulatory system controls the utilisation of multiple carbon and nitrogen ssource in *Pseudomonas aeruginosa*. *Molecular Microbiology* 40:917–931.

[151] Boch J, et al. (2002) Identification of *Pseudomonas syringae* pv. tomato genes induced during infection of *Arabidopsis thaliana*. *Molecular Microbi-*

ology 44:73–88.

[152] Xiao Y, Lu Y, Heu S, Hutcheson SW (1992) Organisation and environmental regulation of the *Pseudomonas syringae* pv. syringae 61 *hrp* cluster. *Journal of Bacteriology* 174:1734–1741.

[153] Muro-Pastor MI, Reyes JC, Florencio FJ (2001) Cyanobacteria perceive nitrogen status by sensing intracellular 2-oxoglutarate levels. *The Journal of Biological Chemistry* 276:38320–38328.

[154] Ikeda TP, Shauger AE, Kustu S (1996) *Salmonella typhimurium* apparently perceives external nitrogen limitation as internal glutamine limitation. *Journal of Molecular Biology* 259:589–607.

[155] Kim BJ, et al. (2009) Effect of iron concentration on the growth rate of *Pseudomonas syringae* and the expression of virulence factors in *hrp*-inducing minimal medium. *Applied and Environmental Microbiology* 75:2720–2726.

[156] Sattelmacher B (2001) The apoplast and its significance for plant mineral nutrition. *New Phytologist* 149:167–192.

[157] Hu P, Leighton T, Ishkhanova G, Kustu S (1999) Sensing of nitrogen limitation by *Bacillus subtilis*: comparison to enteric bacteria. *Journal of Bacteriology* 181:5042–5050.

[158] Preston GM, Bertrand N, Rainey PB (2001) Type III secretion in plant growth-promoting *Pseudomonas fluorescens* SBW25. *Molecular Microbiology* 41:999–1014.

[159] Morales G, Linares JF, Beloso A, Martinez J, Rojo F (2004) The *Pseudomonas putida* Crc global regulator controls the expression of genes from several chromosomal catabolite pathways for aromatic compounds. *Journal of Bacteriology* 186:1337–1344.

[160] Linares JF, et al. (2010) The global regulator Crc modultes metabolism, susceptibility to antibiotics and virulence in *Pseudomonas aeruginosa*. *Environmental Microbiology* 12:3196–3212.

[161] Frimmersdorf E, Horatzek S, Pelnikevich A, Wiehlmann L, Schomburg D (2010) How *Pseudomonas aeruginosa* adapts to various eenvironment: a metabolomic approach. *Environmental Microbiology* 12:1734–1747.

[162] Tempest DW, Meers JL (1970) Influence of environment on the content and composition of microbial free amino acid pools. *Journal of General Microbiology* 64:171–185.

[163] Clark VL, Peterson DE, Bernlohr RW (1972) Changes in free amino acid production and intracellular amino acid pools of *Bacillus licheniformis* as a function of culture age and growth media. *Journal of Bacteriology* 112:715–725.

[164] Whatmore AM, Chudek JA, Reed RH (1990) The effects of osmotic upshock on the intracellular solute pools of *Bacillus subtilis*. *Journal of General Microbiology* 136:2527–2535.

[165] Hua SST, Tsai VY, Lichens GM, Noma AT (1982) Accumulation of amino acids in *Rhizobium* sp. strain WR1001 in response to sodium chloride salinity.

Applied and Environmental Microbiology 44:135–140.

[166] Guedon E, Serrir P, Ehrlich SD, Renault P, Delorme C (2001) Pleotropic transcriptional repressor CodY senses the intracellular pool of branched-chain amino acids in *Lactococcus lactis*. *Molecular Microbiology* 40:1227–1239.

[167] van Schaik W, et al. (2013) The global regulator CodY regulates toxin gene expression in *Bacillus anthracis* and is required for full virulence. *Infection and Immunity* 81:4437–4445.

[168] Hervas AB, Canosa I, Santero E (2010) Regulation of glutamate dehydrogenase expression in *Pseudomonas putida* results from its direct repression under nitrogen-limiting conditions. *Molecular Microbiology* 78:305–319.

[169] Rietsch A, Wolfgang MC, Mekalanos JJ (2004) Effect of metabolic imbalance on expression of type III secretion genes in *Pseudomonas aeruginosa*. *Infection and Immunity* 72:1383–1390.

[170] Yeung AT, Bains M, Hancock RE (2011) The sensor kinase CbrS is a global regulator that modulates metabolism, virulence, and antibiotic resistance in *Pseudomons aeruginosa*. *Journal of Bacteriology* 193:918–931.

[171] Gallarato LA, et al. (2013) Exopolyphophatase of *Pseudomonas aeruginosa* is essential for the production of virulence factors and its expression is controlled by NtrC and PhoB, acting at two interspaced promoters. *Microbiology* 160:406–417.

[172] Warner JB, Lolkema JS (2003) CcpA-dependent carbon catabolite repression in bacteria. *Microbiology and Molecular Biology Reviews* 67:475–490.

[173] Barbier T, Nicolas C, Letesson JJ (2011) *Brucella* adaptation and survival at the crossroad of metabolism and virulence. *FEBS Letters* 585:2929–2934.

[174] Chavarria M, Fuhrer T, Sauer U, Pflger-Grau K, de Lorenzo V (2013) Cra regulates the cross-talk between the two branches of the phosphoenolpyruvate:phosphotransferase system of *Pseudomonas putida*. *Environmental Microbiology* 15:121–132.

[175] Pfluger-Grau K, Chavarria M, de Lorenzo V (2011) The interplay of the EIIA(Ntr) component of the nitrogen-related phosphotransferase (PTS(Ntr)) of *Pseudomonas putida* with pyruvate dehydrogenase. *Biochimica et Biophysica Acta* 1810:995–1005.

[176] Commichau FM, Forchhammer K, Stulke J (2006) Regulatory links between carbon and nitrogen metabolism. *Current Opinion in Microbiology* 9:167–172.

[177] Chavarra M, Kleijn RJ, Sauer U, Pflger-Grau K, de Lorenzo V (2012) Regulatory tasks of the phosphoenolpyruvate-phosphotransferase system of *Pseudomonas putida* in central carbon metabolism. *mBio* 3:e00028–12.

[178] Deutscher J, Herro R, Bourand A, Mijakovic I, Poncet S (2005) P-Ser-Hpr - a link between carbon metabolism and the virulence of some pathogenic bacteria. *Biochimica et Biophysica Acta* 1754:118–125.

[179] Sauer U, Zamboni N (2008) From biomarkers to integrated network responses. *Nature Biotechnology* 26:1090–1092.

[180] Haverkorn van Rijsewijk BRB, Nanchen A, Nallet S, Kleijn RJ, Sau (2011) Large-scale ^{13}C-flux analysis reveals distinct transcriptional control of respi-

ratory and fermentative metabolism in *Escherichia coli*. *Molecular Sys* 7:477.

[181] Fernie AR, Geigenberger P, Stitt M (2005) Flux an important, but neglected, component of functional genomics. *Current Opinion in Plant Biology* 8:174–182.

[182] Sauer U (2006) Metabolic networks in motion: ^{13}C-based flux analysis. *Molecular Systems Biology* 2:62.

[183] Beste DJV, McFadden J (2010) System-level strategies for studying the metabolism of *Mycobacterium tuberculosis*. *Molecular Systems Biology* 6:2363–2372.

[184] der Werf MJV, Overkamp KM, Muilwijk B, Coulier L, Hankemeier T (2007) Microbial metabolomics: Toward a platform with full metabolome coverage. *Analytical Biochemistry* 370:17–25.

[185] Reaves ML, Rabinowitz JD (2011) Metabolomics in systems microbiology. *Current Opinion in Biotechnology* 22:17–25.

[186] Heinemann M, Sauer U (2010) Systems biology of microbial metabolism. *Current Opinion in Microbiology* 13:337–343.

[187] Kruger NJ, Masakapalli SK, Ratcliffe RG (2012) Strategies for investigating the plant metabolic network with steady-state metabolic flux analysis: lessons from an *Arabidopsis* cell culture and other systems. *Journal of Experimental Botany* 63:2309–2323.

[188] Fuhrer T, Fischer E, Sauer U (2005) Experimental identification and quantifi-

cation of glucose metabolism in seven bacterial species. *Journal of Bacteriology* 187:1581–1590.

[189] Rohwer JM (2012) Kinetic modelling of plant metabolic pathways. *Journal of Experimental Botany* 63:2275–2292.

[190] Kruger NJ, Ratcliffe RG (2012) Pathways and fluxes: exploring the plant metabolic network. *Journal of Experimental Botany* 63:2243–2246.

[191] Orth JD, Thiele I, Palsson BO (2010) What is flux balance analysis? *Nature Biotechnology* 28:245–248.

[192] Lee DS, et al. (2009) Comparative genome-scale metabolic reconstruction and flux balance analysis of multiple *Staphylococcus aureus* genomes identify novel antimicrobial drug targets. *Journal of Bacteriology* 191:4015–4024.

[193] Chaganti SB, Kim DH, Lalman JA (2011) Flux balance analysis of mixed anaerobic microbial communities: Effects of linoleic acid (LA) and pH on biohydrogen production. *International Journal of Hydrogen Energy* 36:14141–14152.

[194] Golomysova A, Gomelsky M, Ivanov PS (2010) Flux balance analysis of photoheterotrophic growth of purple nonsulfur bacteria relevant to biohydrogen production. *International Journal of Hydrogen Energy* 35:12751–12760.

[195] Jain R, Srivastava R (2009) Metabolic investigation of host/pathogen interaction using MS2-infected *Escherichia coli*. *BMC Systems Biology* 3:121.

[196] Chen X, Shachar-Hill Y (2012) Insights into metabolic efficiency from flux analysis. *Journal of Experimental Botany* 63:2343–2351.

[197] Schuetz R, Kuepfer L, Sauer U (2007) Systematic evaluation of objective functions for predicting intracellular fluxes in *Escherichia coli*. *Molecular Systems Biology* 3:119.

[198] Williams TCR, et al. (2010) A genome-scale metabolic model acaccurate predicts fluxes in central carbon metabolism under stress conditions. *Plant Physiology* 154:311–323.

[199] Cheung CY, et al. (2013) A method for accounting for maintenance costs in flux balance analysis improves the prediction of plant cell metabolic phenotypes under stress conditions. *The Plant Journal* 75:1050–1061.

[200] Zamboni N, et al. (2005) Transient expression and flux changes during a shift from high to low riboflavin production in continuous cultures of bacillus subtilis. *Biotechnology and Bioengineering* 89:219–232.

[201] Zamboni N, et al. (2004) The *Bacillus subtilis yqjI* gene encodes the NADP+-dependent 6-P-gluconate dehydrogenase in the pentose phosphate pathway. *Journal of Bacteriology* 186:4528–4534.

[202] Fischer E, Sauer U (2005) Large-scale in vivo flux analysis shows rigidity and suboptimal performance of *Bacillus subtilis* metabolism. *Nature Genetics* 37:636–640.

[203] Noh K, Wiechert W (2006) Experimental design principles for isotopically instationary ^{13}C labeling experiments. *Biotechnology and Bioengineering*

94:234–251.

[204] Zamboni N (2011) ^{13}C metabolic flux analysis in complex systems. *Current Opinion in Biotechnology* 22:103–108.

[205] Liu L, et al. (2012) Phosphoketolase pathway for xylose catabolism in *Clostridium acetobutylicum* revealed by ^{13}C metabolic flux analysis. *Journal of Bacteriology* 194:5413–5422.

[206] Hartel T, et al. (2012) Characterization of central carbon metabolism of *Streptococcus pneumoniae* by isotopologue profiling. *Journal of Biological Chemistry* 287:4260–4274.

[207] Fischer E, Sauer U (2003) A novel metabolic cycle catalyzes glucose oxidation and anaplerosis in hungry *Escherichia coli*. *Journal of Biological Chemistry* 278:46446–46451.

[208] Beste DJV, et al. (2011) ^{13}C metabolic flux analysis identifies an unusual route for pyruvate dissimilation in mycobacteria which requires isocitrate lyase and carbon dioxide fixation. *PLoS Pathogens* 7:e1002091.

[209] Tannler S, et al. (2008) CcpN controls central carbon fluxes in *Bacillus subtilis*. *Journal of Bacteriology* 190:6178–6187.

[210] Zamboni N, Sauer U (2009) Novel biological insights through metabolomics and ^{13}C-flux analysis. *Current Opinion in Microbiology* 12:553–558.

[211] Ruhl M, Hardt WD, Sauer U (2011) Subpopulation-specific metabolic pathway usage in mixed cultures as revealed by reporter protein-based ^{13}C analysis.

Applied and Environmental Microbiology 77:1816–1821.

[212] Roling WF, Ferrer M, Golyshin PN (2010) Systems approaches to microbial communities and their functioning. *Current Opinion in Biotechnology* 21:532–538.

[213] Shaikh AS, Tang YJ, Mukhopadhyay A, Keasling JD (2008) Isotopomer distributions in amino acids from a highly expressed protein as a proxy for those from total protein. *Analytical Chemistry* 80:886–890.

[214] Kruger NJ, Huddleston JE, Le Lay P, Brown ND, Ratcliffe R (2007) Network flux analysis: impact of ^{13}C-substrates on metabolism in *Arabidopsis thaliana* cell suspension cultures. *Phytochemistry* 68:2176–2188.

[215] Wiechert W (2007) The thermodynamic meaning of metabolic exchange fluxes. *Biophysical Journal* 93:2255–2264.

[216] Fischer E, Zamboni N, Sauer U (2004) High-throughput metabolic flux analysis based on gas chromatography-mass spectrometry derived ^{13}C constraints. *Analytical Biochemistry* 325:308–316.

[217] Chen X, Alonso AP, Allen DK, Reed JL, Shachar-Hill Y (2011) Synergy between ^{13}C-metabolic flux analysis and flux balance analysis for understanding metabolic adaption to anaerobiosis in *E. coli*. *Metabolic Engineering* 13:38–48.

[218] Masakapalli SK, Kruger NJ, Ratcliffe RG (2013) The metabolic flux phenotype of heterotrophic *Arabidopsis* cells reveals a complex response to changes in nitrogen supply. *The Plant Journal* 74:569–582.

[219] Tang YJ, et al. (2009) Advances in analysis of microbial metabolic fluxes via ^{13}C isotopic labeling. *Mass Spectrometry Reviews* 28:362–375.

[220] Pramanik J, Keasling JD (1998) Effect of *Escherichia coli* biomass composition on central metabolic fluxes predicted by a stoichiometric model. *Biotechnology and Bioengineering* 60:230–238.

[221] Antoniewicz MR, Kelleher JK, Stephanopoulos G (2006) Determination of confidence intervals of metabolic fluxes estimated from stable isotope measurements. *Metabolic Engineering* 8:324–337.

[222] Williams TCR, et al. (2008) Metabolic network fluxes in heterotrophic *Arabidopsis* cells: stability of the flux distribution under different oxygenation conditions. *Plant Physiology* 148:704–718.

[223] Leighty RW, Antoniewicz MR (2012) Parallel labeling experiments with [U-^{13}C]glucose validate *E. coli* metabolic network model for ^{13}C metabolic flux analysis. *Metabolic Engineering* 14:533–541.

[224] del Castillo T, et al. (2007) Convergent peripheral pathways catalyze initial glucose catabolism in *Pseudomonas putida*: Genomic and flux analysis. *Journal of Bacteriology* 189:5142–5152.

[225] Wang ZJ, et al. (2012) Metabolic flux analysis of the central carbon metabolism of the industrial vitamin B12 producing strain *Pseudomonas denitrificans* using ^{13}C-labeled glucose. *Journal of the Taiwan Institute of Chemical Engineers* 43:181–187.

[226] Conway T (1992) The Entner-Doudoroff pathway: history, physiology and molecular biology. *FEMS Microbiology Reviews* 103:1–28.

[227] Sauer U, Eikmanns BJ (2005) The PEP:pyruvate:oxaloacetate node as the switch point for carbon flux distribution in bacteria. *FEMS Microbiology Reviews* 29:765–794.

[228] Kleijn RJ, van Winden WA, van Gulik WM, Heijnen JJ (2005) Revisiting the ^{13}C-label distribution of the non-oxidative branch of the pentose phosphate pathway based upon kinetic and genetic evidence. *FEBS Journal* 272:4970–4982.

[229] Wierckx N, Ruijssenaars HJ, de Winde JH, Schmid A, Blank LM (2009) Metabolic flux analysis of a phenol producing mutant of *Pseudomonas putida* S12: Verification and complementation of hypotheses derived from transcriptomics. *Journal of Biotechnology* 143:124–129.

[230] Chung JCS, Rzhepishevska O, Ramstedt M, Welch M (2013) Type III secretion system expression in oxygen-limited *Pseudomonas aeruginosa* cultures is stimulated by isocitrate lyase activity. *Open Biology* 3:120131.

[231] Kochanowski K, et al. (2013) Functioning of a metabolic flux sensor in *Escherichia coli*. *Proceedings of the National Academy of Sciences* 110:1130–1135.

[232] Shimada T, Yamamoto K, Ishihama A (2011) Novel members of the Cra regulon involved in carbon metabolism in *Escherichia coli*. *Journal of Bacteriology* 193:649–659.

[233] Sonnleitner E, et al. (2012) Novel targets of the CbrAB/Crc carbon catabolite control system revealed by transcript abundance in *Pseudomonas aeruginosa*. *PLoS ONE* 7:e44637.

[234] Dong YH, Zhang XF, Zhang LH (2013) The global regulator Crc plays a multifaceted role in modulation of type III secretion system in *Pseudomonas aeruginosa*. *Microbiology Open* 2:161–172.

[235] Tunio SA, et al. (2010) The moonlighting protein fructose-1, 6-bisphosphate aldolase of *Neisseria meningitidis*: surface localization and role in host cell adhesion. *Molecular Microbiology* 76:605–615.

[236] Pancholi V, Chhatwal GS (2003) Housekeeping enzymes as virulence factors for pathogens. *International Journal of Medical Microbiology* 293:391–401.

[237] Eisenreich W, Dandekar T, Heesemann J, Goebel W (2010) Carbon metabolism of intracellular bacterial pathogens and possible links to virulence. *Nature Reviews Microbiology* 8:401–412.

[238] Lindsey TL, Hagins JM, Sokol PA, Silo-Suh LA (2008) Virulence determinants from a cystic fibrosis isolate of *Pseudomonas aeruginosa* include isocitrate lyase. *Microbiology* 154:1616–1627.

[239] Hagins JM, Scoffield JA, Suh SJ, Silo-Suh L (2010) Influence of RpoN on isocitrate lyase activity in *Pseudomonas aeruginosa*. *Microbiology* 156:1201–1210.

[240] Hendrickson EL, Guevera P, Ausubel FM (2000) The alternative sigma factor RpoN is required for *hrp* activity in *Pseudomonas syringae* pv. maculicola and

acts at the level of *hrpL* transcription. *Journal of Bacteriology* 182:3508–3516.

[241] Mellgren EM, Kloek AP, Kunkel BN (2009) Mqo, a tricarboxylic acid cycle enzyme, is required for virulence of *Pseudomonas syringae* pv. tomato strain DC3000 on *Arabidopsis thaliana*. *Journal of Bacteriology* 191:3132–3141.

[242] Fell DA (2005) Enzymes, metabolites and fluxes. *Journal of Experimental Botany* 56:267–272.

[243] Akihiro T, et al. (2008) Biochemical mechanism on GABA accumulation during fruit development in tomato. *Plant and Cell Physiology* 49:1378–1389.

[244] Niegemann E, Schulz, A. amd Bartsch K (1993) Molecular organisation of the *Escherichia coli gab* cluster: nucleotide sequence of the structural genes *gabD* and *gabP* and expression of the GABA permease gene. *Archives of Microbiology* 160:454–460.

[245] Roberts MR (2007) Does GABA act as a signal in plants? *Plant Signalling and Behaviour* 2:408–409.

[246] Shelp BJ, Bown AW, Faure D (2006) Extracellular γ-aminobutyrate mediates communication between plants and other organisms. *Plant Physiology* 142:1350–1352.

[247] Planamente S, et al. (2012) Structural basis for selective GABA binding in bacterial pathogens. *Molecular Microbiology* 86:1085–1099.

[248] Dagorn A, et al. (2013) Gamma-aminobutyric acid acts as a specific virulence regulator in *Pseudomonas aeruginosa*. *Microbiology* 159:339–351.

[249] Sanacora G, et al. (2004) Subtype-specific alterations of gamma-aminobutyric acid and glutamate inpatients with major depression. *Archives of General Psychiatry* 61:705–713.

[250] Shelp BJ, Allan W, Faure D (2009) *Signalling and communication in plants* eds Baluska F, J. V (Springer).

[251] Fait A, Fromm H, Walter D, Galili G, Fernie AR (2008) Highway or byway: the metabolic role of the GABA-shunt in plants. *Trends in Plant Science* 13:14–19.

[252] Prell J, Boesten B, Poole P, Priefer UB (2002) The *Rhizobium leguminosarum* bv. viciae VF39 γ-aminobutyrate (GABA) aminotransferase gene (*gabT*) is induced by GABA and highly expressed in bacteroids. *Microbiology* 148:615–623.

[253] Zhu L, et al. (2010) Structure and regulation of the *gab* gene cluster, involved in the γ-aminobutyric acid shunt, are controlled by a σ^{54} factor in *Bacillus thuringiensis*. *Journal of Bacteriology* 192:346–355.

[254] Jack DL, Paulsen IT, Saier MH (2000) The amino acid/polyamine/organocation (APC) superfamily of transporters specific for amino acids, polyamines and organocations. *Microbiology* 146:1797–1814.

[255] Brechtel CE, Hu L, King SC (1996) Substrate specificity of the *Escherichia coli* 4-aminobutyrate carrier encoded by *gabP*. *Journal of Biological Chemistry* 271:783–788.

[256] Ferson AE, Wray, Jr LV, Fisher SH (1996) Expression of the *Bacillus subtilis gabP* gene is regulated independently in response to nitrogen and amino acid availability. *Molecular Microbiology* 22:693–701.

[257] Vijayakumar SRV, Kirchhof MG, Patten CL, Schellhorn HE (2004) RpoS-regulated genes of *Escherichia coli* identified by random *lacZ* fusion mutagenesis. *Journal of Bacteriology* 186:8499–8507.

[258] Kumar S, Punekar NS (1997) The metabolism of 4-aminobutyrate (GABA) in fungi. *Mycological Research* 101:403–409.

[259] Planamente S, et al. (2010) A conserved mechanism of GABA binding and antagonism is revealed by structure-function analysis of the periplasmic binding protein Atu2422 in *Agrobacterium tumefaciens*. *Journal of Biological Chemistry* 285:30294–30303.

[260] Hosie AHF, Allaway D, Galloway CS, Dunsby HA, Poole PS (2002) *Rhizobium leguminosarum* has a second general amino acid permease with unusually broad substrate specificity and high similarity to branched-chain amino acid transporters (Bra/ LIV) of the ABC family. *Journal of Bacteriology* 184:4071–4080.

[261] Ma D, et al. (2012) Structure and mechanism of a glutamate-GABA antiporter. *Nature* 483:632–636.

[262] Shelp BJ, et al. (2012) Hypothesis/review: Contribution of putrescine to 4-aminobutyrate (GABA) production in response to abiotic stress. *Plant Science* 194:130–135.

[263] Shah P, Swiatlo E (2008) A multifaceted role for polyamines in bacterial pathogens. *Molecular Microbiology* 68:4–16.

[264] Kurihara S, et al. (2005) A novel putrescine utilization pathway involves gamma-glutamylated intermediates of *Escherichia coli* K-12. *Journal of Biological Chemistry* 280:4602–4608.

[265] Shelp BJ, Mullen RT, Waller JC (2012) Compartmentation of GABA metabolism raises intriguing questions. *Trends in Plant Science* 17:57–59.

[266] Michaeli S, et al. (2011) A mitochondrial GABA permease connects the GABA shunt and the TCA cycle, and is essential for normal carbon metabolism. *The Plant Journal* 67:485–498.

[267] Maitre M (1997) The gamma-hydroxybutyrate signalling system in brain: organisation and functional implications. *Progress in Neurobiology* 51:337–361.

[268] Breitkreuz KE, et al. (2003) A novel gamma-hydroxybutyrate dehydrogenase: identification and expression of an *Arabidopsis* cDNA and potential role under oxygen deficiency. *The Journal of Biological Chemistry* 278:41552–41556.

[269] Prell J, Bourds A, Karunakaran R, Lopez-Gomez M, Poole P (2009) Pathway of γ-aminobutyrate metabolism in *Rhizobium leguminosarum* 3841 and its role in symbiosis. *Journal of Bacteriology* 191:2177–2186.

[270] Schneider BL, et al. (2002) The *Escherichia coli* gabDTPC operon: Specific γ-aminobutyrate catabolism and nonspecific induction. *Journal of Bacteriology* 184:6976–6986.

[271] Seifi HS, et al. (2013) Concurrent overactivation of the cytosolic glutamine synthetase and the GABA shunt in the ABA-deficient sitiens mutant of tomato leads to resistance against *Botrytis cinerea*. *New Phytologist* 199:490–504.

[272] Huang T, Jander G, de Vos M (2011) Non-protein amino acids in plant defense against insect herbivores: Representative cases and opportunities for further functional analysis. *Phytochemistry* 72:1531–1537.

[273] MacGregor KB, Shelp BJ, Peiris S, Bown AW (2003) Overexpression of glutamate decarboxylase in transgenic tobacco plants deters feeding by phytophagous insect larvae. *Journal of Chemical Ecology* 29:2177–2182.

[274] Palanivelu R, Brass L, Edlund AF, Preuss D (2003) Pollen tube growth and guidance is regulated by POP2, an *Arabidopsis* gene that controls uppercaseGABA levels. *Cell* 114:47–59.

[275] Xing SG, Jun YB, Hau ZW, Liang LY (2007) High accumulation of γ-aminobutyric acid induced by salt stress though stimulating the activity of diamine oxidases in *Gycine max* (l.) merr. roots. *Plant Physiology and Biochemistry* 45:560–566.

[276] Renault H, et al. (2010) The *Arabidopsis pop2-1* mutant reveals the involvement of GABA transaminase in salt stress tolerance. *BMC Plant Biology* 10:20.

[277] Beuve N, et al. (2004) Putative role of gamma-aminobutyric acid (GABA) as a long-distance signal in up-regulation of nitrate uptake in *Brassica napus*. *Plant, Cell & Environment* 27:1035–1046.

[278] Barbosa JM, Singh NK, Cherry JH, Locy RD (2010) Nitrate uptake and utilization is modulated by exogenous gamma-aminobutyric acid in *Arabidopsis thaliana* seedlings. *Plant Physiology and Biochemistry* 48:443–450.

[279] Shelp BJ, et al. (2012) Strategies and tools for studying the metabolism and function of γ-aminobutyrate in plants. II. integrated analysis. *Botany* 90:781–793.

[280] Feehily C, Karatzas K (2013) Role of glutamate metabolism in bacterial responses towards acid and other stresses. *Journal of Applied Microbiology* 114:11–24.

[281] Li H, Qiu T, Huang G, Cao Y (2010) Production of gamma-aminobutyric acid by *Lactobacillus brevis* NCL912 using fed-batch fermentation. *Microbial Cell Factories* 9:85–91.

[282] Cotter PD, Gahan CG, Hill C (2001) A glutamate decarboxylase system protects *Listeria monocytogenes* in gastric fluid. *Molecular Microbiology* 40:465–475.

[283] Gut H, et al. (2006) *Escherichia coli* acid resistance: pH-sensing, activation by chloride and autoinhibition in GadB. *EMBO Journal* 25:2643–2651.

[284] Tian J, Bryk R, Itoh M, Suematsu M, Nathan C (2005) Variant tricarboxylic acid cycle in mycobacterium tuberculosis: identification of α-ketoglutarate decarboxylase. *Proceedings of the National Academy of Sciences* 102:10670–10675.

[285] Feehily C, O'Byrne CP, Karatzas KAG (2013) Functional γ-aminobutyrate shunt in *Listeria monocytogenes*: role in acid tolerance and succinate biosynthesis. *Applied and Environmental Microbiology* 79:74–80.

[286] Ogawa J, et al. (2011) A novel L-isoleucine metabolism in *Bacillus thuringiensis* generating (2S,3R,4S)-4-hydroxyisoleucine, a potential insulinotropic and anti-obseity amino acid. *Applied Microbiological Biotechnology* 89:1929–1938.

[287] Vadyvaloo V, Jarrett C, Sturdevant DE, Sebbane F, Hinnebusch BJ (2010) Transit through the flea vector induces a pretransmission innate immunity resistance phenotype in *Yersinia pestis*. *PLoS Pathogens* 6:e1000783.

[288] Zhou L, Wang J, Zhang LH (2007) Modulation of bacterial type III secretion system by a spermidine transporter dependent signaling pathway. *PLoS ONE* 2:e1291.

[289] Bearson BL, Lee IS, Casey TA (2009) *Escherichia coli* O157:H7 glutamate- and arginine-dependent acid-resistance systems protect against oxidative stress during extreme acid challenge. *Micrbiology* 155:805–812.

[290] Chevrot R, et al. (2006) GABA controls the level of quorum-sensing signal in *Agrobacterium tumefaciens*. *Proceedings of the National Academy of Sciences* 103:7460–7464.

[291] Haudecoeur E, et al. (2008) Proline antagonises GABA-induced quenching of quorum-sensing in *Agrobacterium tumefaciens*. *Proceedings of the National Academy of Sciences* 106:14587–14592.

[292] Planamente S, Morera S, Faure D (2013) *In planta* fitness-cost of the Atu4232-regulon encoding for a selective GABA-binding sensor in *Agrobacterium*. *Communicative and Integrative Biology* 6:e23692.

[293] Yuan ZC, Haudecoeur E, Faure D, Kerr KF, Nester EW (2008) Comparative transcriptome analysis of *Agrobacterium tumefaciens* in response to plant signal salicylic acid, indole-3-acetic acid and γ-amino butyric acid reveals signalling cross-talk and *Agrobacterium*-plant co-evolution. *Cellular Microbiology* 10:2339–2354.

[294] Ramos-Gonzalez MI, Campos MJ, Ramos JL (2005) Analysis of *Pseudomonas putida* KT2440 gene expression in the maize rhizosphere: *In vitro* expression technology capture and identification of root-activated promoters. *Journal of Bacteriology* 187:4033–4041.

[295] Wilkinson SG (1983) Composition and structure of lipopolysaccharides from *Pseudomonas aeruginosa*. *Clinical Infectious Diseases* 5:941–949.

[296] Ma D, Lu P, Shi Y (2013) Substrate selectivity of the acid-activated glutamate/γ-aminobutyric acid (GABA) antiporter GadC from *Escherichia coli*. *Journal of Biological Chemistry* 288:15148–15153.

[297] McLean DM, et al. (2003) Overexpression of glutamate decarboxylase in transgenic tobacco plants confers resistance to the northern root-knot nematode. *Molecular Breeding* 11:277–285.

[298] Ramos LS, et al. (2013) The fire blight pathogen *Erwinia amylovora* requires the *rpoN* gene for pathogenicity in apple. *Molecular Plant Pathology* 14:838–

843.

[299] Hendrickson EL, et al. (2000) Virulence of the phytopathogen *Pseudomonas syringae* pv. maculicola is *rpoN* dependent. *Journal of Bacteriology* 182:3498–3507.

[300] Metzner M, Germer J, Hengge R (2004) Multiple stress signal integration in the regulation of the complex S-dependent csiD-ygaF-gabDTP operon in *Escherichia coli*. *Molecular Microbiology* 51:799–811.

[301] Dong T, Yu R, Schellhorn H (2011) Antagonistic regulation of motility and transcriptome expression by RpoN and RpoS in *Escherichia coli*. *Molecular Microbiology* 79:375–386.

[302] Karatzas KAG, Brennan O, O'Byrne CP (2010) Intracellular accumulation of high levels of γ-aminobutyrate by *Listeria monocytogenes* 10403S in response to low pH: uncoupling of γ-aminobutyrate synthesis from efflux in a chemically defined medium. *Applied and Environmental Microbiology* 76:3529–3537.

[303] Cramton SE, Ulrich M, Gotz F, Doring G (2001) Anaerobic conditions induce expression of polysaccharide intercellular adhesin in *Staphylococcus aureus* and *Staphylococcus epidermidis*. *Infection and Immunity* 69:4079–4085.

[304] Pimm TP, et al. (2000) The strigent response of *Mycobacterium tuberculosis* is required for long-term survival. *Journal of Bacteriology* 182:4889–4898.

[305] Winson MK, et al. (1998) Engineering the *luxCDABE* genes from *Photorhabdus luminescens* to provide a bioluminescent reporter for constitutive and pro-

moter probe plasmids and mini-Tn5 constructs. *FEMS Microbiology Letters* 163:193–202.

[306] Mountford DO, Pybus V (1992) Regulatory influences on the production of gamma-aminobutyric acid by a marine pseudomonad. *Applied and Environmental Microbiology* 58:237–242.

[307] Castanie-Cornet MP, Penfound TA, Smith D, Elliott JF, Foster JW (1999) Control of acid resistance in *Escherichia coli*. *Journal of Bacteriology* 181:3525–3535.

[308] Konkel ME, Tilly K (2000) Temperature-regulated expression of bacterial virulence genes. *Microbes and Infection* 2:157–166.

[309] Hengge-Aronis R (2002) Recent insignts into the general stress response regulatory network in *Escherichia coli*. *Journal of Molecular Microbiology and Biotechnology* 4:341–346.

[310] Mazzucotelli E, Tartari A, Cattivelli L, Forlani G (2006) Metabolism of gamma-aminobutyric acid during cold acclimation and freezing and its relationship to frost tolerance in barley and wheat. *Journal of Experimental Botany* 57:3755–3766.

[311] White JP, Prell J, Ramachandran VK, Poole PS (2008) Characterisation of a γ-aminobutyric acid transport system of *Rhizobium leguminosarum* bv. viciae 3841. *Journal of Bacteriology* 191:1547–1555.

[312] Wright CA, Beattie GA (2004) *Pseudomonas syringae* pv. tomato cells encounter inhibitory levels of water stress during the hypersensitive response

of *Arabidopsis thaliana*. *Proceedings of the National Academy of Sciences* 101:3269–3274.

[313] Bolwell PP, Page A, Pislewska M, Wojtasek P (2001) Pathogenic infection and the oxidative defences in plant apoplast. *Protoplasma* 217:20–32.

[314] Jorgensen F, et al. (1999) RpoS-dependent stress tolerance in *Pseudomonas aeruginosa*. *Microbiology* 145:835–844.

[315] Stockwell VO, Loper JE (2005) The sigma factor RpoS is required for stress tolerance and enenvironment fitness of *Pseudomonas fluorescens* pf-5. *Microbiology* 151:3001–3009.

[316] Starrach N, Mayer WE (1989) Changes in the apoplastic pH and K+ concentrations in the *Phaseolus* pulvinus *in situ* in relation to rhythmic leaf movements. *Journal of Experimental Botany* 40:865–873.

[317] Jones AM, Wildermuth MC (2011) The phytopathogen *Pseudomonas syringae* pv. tomato DC3000 has three high-affinity iron-scavenging systems functional under iron limitation conditions but dispensable for pathogenesis. *Journal of Bacteriology* 193:2767–2775.

[318] Badel JL, Carkowski AO, Deng WD, Collmer A (2002) A gene in the *Pseudomonas syringae* pv. tomato Hrp pathogenicity island conserved effector locus, *hopPtoA1*, contributes to efficient formation of bacterial colonies *in planta* and is duplicated elsewhere in the genome. *Molecular Plant-Microbe Interactions* 15:1014–1024.

[319] Li B, et al. (2013) Visualising metabolite distribution and enzymative conversion in plant tissues by desorption electrospray ionisation mass spectrometry imaging. *The Plant Journal* 74:1059–1071.

[320] Zheng ZL (2009) Carbon and nitrogen nutrient balance signalling in plants. *Plant Signalling and Behaviour* 4:584–591.

[321] Sang Y, Sun W, Yang Z (2012) Signalling mmechanism integrating carbon and nitrogen utilisation in plants. *Frontiers in Biology* 7:548–556.

[322] Forchhammer K (2006) Global carbon/nitrogen control by p_ii signal transduction in cyanobacteria: from signals to targets. *FEMS Microbiology Reviews* 28:319–333.

[323] Dorrell N, et al. (1999) Investigation into the role of the response regulatory ntrc in the metabolism and virulence of *Brucella suis*. *Microbial Pathogenesis* 27:1–11.

[324] Li W, Lu CD (2007) Regulation of carbon and nitrogen utilisation by CbrAB and NtrBC two-component systems in *Pseudomonas aeruginosa*. *Journal of Bacteriology* 189:5413–5420.

Appendices

Appendix A

Appendix

A.1 Biolog GN2 MicroPlate Substrates

Pyruvic Acid Methyl Ester	Glycogen	Tween 40	Tween 80
N-Acetyl-D-Galactosamine	Adonitol	L-Arabinose	D-Saccharide
N-Acetyl-D-Glucosamine	D-Mannitol	D-Mannose	D-Melibiose
Succinic Acid Mono-Methyl-Ester	Cis-Aconitic Acid	Acetic Acid	Dextrin
p-Hydroxy Phenylacetic Acid	D-Psicose	D-Arabitol	Itaconic Acid
D,L-α-Glycerol Phosphate	Malonic Acid	Propionic Acid	Quinic Acid
β-Methyl-D-Glucoside	2-Aminoethanol	2,3-Butanediol	Glycerol
γ-Hydroxybutyric Acid	D-Cellobiose	i-Erythritol	D-Fructose
α-D-Glucose	L-Fructose	D-Galactose	Gentiobiose
D-Glucosaminic Acid	α-D-Lactose	Lactulose	Maltose
β-Hydroxybutyric Acid	D-Raffinose	L-Rhamnose	D-Sorbitol
D-Galactonic Acid Lactone	D-Trehalose	Turanose	Xylitol
D-Galacturonic Acid	Formic Acid	Sucrose	Citric Acid
α-Hydroxybutyric Acid	m-Inositol	D-Glucuronic Acid	D-Gluconic Acid
α-Keto Butyric Acid	α-Keto Valeric Acid	D,L-Lactic Acid	Sebacic Acid
α-Keto Glutaric Acid	Succinic Acid	Bromosuccinic Acid	Succinamic Acid
Glucuronamide	L-Alaninamide	D-Alanine	L-Alanine
L-Alanylglycine	L-Asparagine	L-Aspartic Acid	L-Glutamic Acid
Glycyl-L-Aspartic Acid	Hydroxy-L-Proline	L-Histidine	L-Leucine
Glycyl-L-Glutamic Acid	L-Ornithine	L-Phenylalanine	L-Proline
L-Pyroglutamic Acid	D-Serine	L-Serine	L-Threonine
γ-Amino Butyric Acid	D,L-Carnitine	Urocanic Acid	Inosine
D-Glucose-6-Phosphate	Thymidine	Phenyethylamine	Putrescine
α-D-Glucose-1-Phosphate	Uridine	α-Cyclodextrin	Water

A.2 Principal component analysis: flux value scaling comparisons

(N)=600, Variables (K)=28 (X=28, Y=0)

Pst DC3000 fructose pH 5.5

A	R2X	R2X(cum)	Eigenvalues	Q2	Limit	Q2(cum)	Significance	Iterations
0	Cent.							
1	0.224	0.224	6.28	0.164	0.0361	0.164	R1	12
2	0.0964	0.321	2.7	-0.00242	0.0373	0.162	R2	96
3	0.0876	0.408	2.45	0.0455	0.0386	0.2	R1	28

Table A.1: Pst DC3000 fructose pH 5.5 fluxes scaled to unit variance

A	R2X	R2X(cum)	Eigenvalues	Q2	Limit	Q2(cum)	Significance	Iterations
0	Cent.							
1	0.222	0.222	6.23	0.161	0.0361	0.161	R1	18
2	0.104	0.326	2.91	0.00597	0.0373	0.166	R2	115
3	0.0966	0.423	2.71	0.0475	0.0386	0.205	R1	36

Table A.2: Pst DC3000 fructose pH 5.5 fluxes pareto scaled

A	R2X	R2X(cum)	Eigenvalues	Q2	Limit	Q2(cum)	Significance	Iterations
0	Cent.							
1	0.218	0.218	6.11	0.143	0.0361	0.143	R1	29
2	0.141	0.359	3.94	-0.03	0.0373	0.117	NS	39

Table A.3: Pst DC3000 fructose pH 5.5 fluxes mean centered

Pst DC3000 glucose pH 7

A	R2X	R2X(cum)	Eigenvalues	Q2	Limit	Q2(cum)	Significance	Iterations
0	Cent.							
1	0.263	0.263	7.35	0.219	0.0361	0.219	R1	11
2	0.0951	0.358	2.66	0.053	0.0373	0.26	R1	36

Table A.4: Pst DC3000 glucose pH 7 fluxes scaled to unit variance

A	R2X	R2X(cum)	Eigenvalues	Q2	Limit	Q2(cum)	Significance	Iterations
0	Cent.							
1	0.247	0.247	6.91	0.201	0.0361	0.201	R1	17
2	0.105	0.352	2.94	-0.0842	0.0373	0.134	NS	47

Table A.5: Pst DC3000 glucose fluxes pareto scaled

A	R2X	R2X(cum)	Eigenvalues	Q2	Limit	Q2(cum)	Significance	Iterations
0	Cent.							
1	0.229	0.229	6.43	-0.136	0.0361	-0.1	R2	68
2	0.201	0.431	5.63	0.09	0.0373	-0.001	R1	42
3	0.153	0.584	4.29	-0.0549	0.0386	-0.056	R2	11
4	0.067	0.651	1.87	0.0394	0.0401	-0.0144	R2	42
5	0.0523	0.703	1.46	0.0704	0.0416	0.057	R1	15

Table A.6: Pst DC3000 glucose pH 7 fluxes mean centered

Pfl SBW25 fructose pH 5.5

A	R2X	R2X(cum)	Eigenvalues	Q2	Limit	Q2(cum)	Significance	Iterations
0	Cent.							
1	0.301	0.301	8.44	0.254	0.0361	0.254	R1	10
2	0.0891	0.39	2.5	0.014	0.0373	0.265	R2	47
3	0.0687	0.459	1.92	0.0235	0.0386	0.282	R2	40

Table A.7: Pfl SBW25 fructose pH 5.5 fluxes scaled to unit variance

A	R2X	R2X(cum)	Eigenvalues	Q2	Limit	Q2(cum)	Significance	Iterations
0	Cent.							
1	0.26	0.26	7.29	0.211	0.0361	0.211	R1	22
2	0.145	0.406	4.07	0.0292	0.0373	0.234	NS	18

Table A.8: Pfl SBW25 fructose pH 5.5 fluxes pareto scaled

A	R2X	R2X(cum)	Eigenvalues	Q2	Limit	Q2(cum)	Significance	Iterations
0	Cent.							
1	0.275	0.275	7.7	-0.0382	0.0361	-0.0382	NS	14
2	0.2	0.475	5.61	0.219	0.0373	0.189	R1	20

Table A.9: Pfl SBW25 fructose pH 5.5 fluxes mean centered

Pfl SBW25 glucose pH 7

A	R2X	R2X(cum)	Eigenvalues	Q2	Limit	Q2(cum)	Significance	Iterations
0	Cent.							
1	0.248	0.248	6.93	0.195	0.0361	0.195	R1	12
2	0.112	0.36	3.14	0.0962	0.0373	0.273	R1	21

Table A.10: Pfl SBW25 glucose pH 7 fluxes scaled to unit variance

A	R2X	R2X(cum)	Eigenvalues	Q2	Limit	Q2(cum)	Significance	Iterations
0	Cent.							
1	0.224	0.224	6.27	0.123	0.0361	0.123	R1	24
2	0.136	0.359	3.79	-0.0732	0.0373	0.0592	R2	27
3	0.0967	0.456	2.71	0.0747	0.0386	0.129	R1	34

Table A.11: Pfl SBW25 glucose pH 7 fluxes pareto scaled

A	R2X	R2X(cum)	Eigenvalues	Q2	Limit	Q2(cum)	Significance	Iterations
0	Cent.							
1	0.416	0.416	11.7	-0.0624	0.0361	-0.0624	NS	9
2	0.135	0.551	3.78	0.14	0.0373	0.0858	R1	23

Table A.12: Pfl SBW25 glucose pH 7 fluxes mean centered

A.3 Metabolic network model

Pathway	Reaction name	Reactant 1	Reactant 2	Product 1	Product 2
Glycolysis	gly1	F6P		G6P	
		ABCDEF		ABCDEF	
	gly2	F6P		F16P	
		ABCDEF		ABCDEF	
	gly3	F16P		TP	TP
		ABCDEF		DEF	CBA
	gly4	TP		PEP	
		ABC		ABC	
	gly5	PEP		PYR	
		ABC		ABC	
Pentose-phosphate	ppp0	G6P		PG	
		ABCDEF		ABCDEF	
	ppp1	PG		P5P	CO2
		ABCDEF		BCDEF	A
	ppp2a	P5P		TP	TKC2
		ABCDE		CDE	AB
	ppp2b	E4P	TKC2	F6P	
		abcd	AB	ABabcd	
	ppp2c	P5P	TKC2	S7P	
		abcde	AB	ABabcde	
	ppp3a	S7P		E4P	TAC3
		ABCDEFG		DEFG	ABC
	ppp3b	TP	TAC3	F6P	
		abc	ABC	ABCabc	
Entner-doudoroff	edp1	PG		KDPG	
		ABCDEF		ABCDEF	
	edp2	KDPG		PYR	TP
		ABCDEF		ABC	DEF
TCA Cycle	tca1	PYR		CO2	AcCoA
		ABC		A	BC
	tca2	AcCoA	OAA	CIT	
		AB	abcd	ABbcda	
	tca2b	CIT		ICIT	
		ABCDEF		EDCBAF	
	tca3	ICIT		AKG	CO2
		ABCDEF		ABCDE	F
	tca4	AKG		SUC	CO2
		ABCDE		BCDE	A
	tca5	SUC		FUM	
		ABCD		ABCD	
	tca6	FUM		MAL	
		ABCD		ABCD	
	tca7	FUM		MAL	
		ABCD		DCBA	
	tca8	MAL		OAA	
		ABCD		ABCD	
Glyoxylate shunt	gox1	ICIT		SUC	GOX
		ABCDEF		FCDE	AB
	gox2	GOX	AcCoA	MAL	
		AB	ab	ABba	

Pathway	**Reaction**	**Reactant 1**	**Reactant 2**	**Product 1**	**Product 2**
Recycling	ana1	MAL		CO2	PYR
		ABCD		D	ABC
	ana2	PYR	CO2	OAA	
		ABC	D	ABCD	
	ana3	OAA		PEP	CO2
		ABCD		ABC	D
Macromolecular	g6pOUT	G6P		WALL	
		ABCDEF		ABCDEF	
	f6pOUT	F6P		F6Peff	
		ABCDEF		ABCDEF	
	s7pOUT	S7P		S7Peff	
		ABCDEFG		ABCDEFG	
	co2	CO2		CO2eff	
		A		A	
	rna	P5P		RNA	
		ABCDE		ABCDE	
	rnaOUT	RNA		RNAout	
		ABCDE		ABCDE	
	tpOUT	TP		TPeff	
		ABC		ABC	
	lipidOUT	AcCoA		AcCoAeff	
		AB		AB	
Amino acids	glu	AKG		GLU	
		ABCDE		ABCDE	
	gluOUT	GLU		GLUeff	
		ABCDE		ABCDE	
	asp	OAA		ASP	
		ABCD		ABCD	
	aspOUT	ASP		ASPeff	
		ABCD		ABCD	
	arg	AKG	CO2	ARG	
		ABCDE	a	ABCDEa	
	argOUT	ARG		ARGeff	
		ABCDEF		ABCDEF	
	asp_arg	ASP		FUM	
		ABCD		ABCD	
	ser	TP		SER	
		ABC		ABC	
	cys	SEReff		CYS	
		ABC		ABC	
	cysOUT	CYS		CYSeff	
		ABC		ABC	
	gly	SER		GLY	CX
		ABC		AB	C
	glyb	THR		GLY	AcCoA
		ABCD		AB	CD
	glyc	GLY		CO2	CX
		AB		A	B
	glyOUT	GLY		GLYeff	
		AB		AB	
	cxeff	CX		CXeff	
		A		A	

Pathway	Reaction	Reactant 1	Reactant 2	Product 1	Product 2
Amino acids(cont.)	ala	PYR		ALA	
		ABC		ABC	
	alaOUT	ALA		ALAeff	
		ABC		ABC	
	leu1	PYR	PYR	ISOVAL	CO2
		ABC	abc	abBCc	A
	leu2	ISOVAL	AcCoA	LEU	CO2
		ABCDE	ab	abBCDE	A
	leuOUT	LEU		LEUeff	
		ABCDEF		ABCDEF	
	val	ISOVAL		VAL	
		ABCDE		ABCDE	
	valOUT	VAL		VALeff	
		ABCDE		ABCDE	
	met	ASP	CX	MET	
		ABCD	a	ABCDa	
	metOUT	MET		METeff	
		ABCDE		ABCDE	
	thr	ASP		THR	
		ABCD		ABCD	
	thrOUT	THR		THReff	
		ABCD		ABCD	
	ile	PYR	THR	ILE	CO2
		ABC	abcd	abBcdC	A
	ileOUT	ILE		ILEeff	
		ABCDEF		ABCDEF	
	aro1	E4P	PEP	ARO	
		ABCD	abc	abcABCD	
	aro2	E4P	PEP	ARO	
		ABCD	abc	abDCBAc	
	phe_tyr	ARO	PEP	PHE_TYR	CO2
		ABCDEFG	abc	abcBCDEFG	A
	pheOUT	PHE_TYR		PHE_TYReff	
		ABCDEFGHI		ABCDEFGHI	
	pro	GLU		PRO	
		ABCDE		ABCDE	
	proOUT	PRO		PROeff	
		ABCDE		ABCDE	
	lys	ASP	PYR	LYS	CO2
		ABCD	abc	ABCDcb	a
	lys1	ASP	PYR	LYS	CO2
		ABCD	abc	abcDCB	A
	lysOUT	LYS		LYSeff	
		ABCDEF		ABCDEF	
	his	P5P	CX	HIS	
		ABCDE	a	aEDCBA	
	hisOUT	HIS		HISeff	
		ABCDEF		ABCDEF	

Pathway	Reaction	Reactant 1	Reactant 2	Product 1	Product 2
Amino acids(cont.)	trp2ca	P5P		PEP	CCa
		ABCDE		CDE	AB
	trpaOUT	CCa		CCaeff	
		AB		AB	
	trp2cb	PEP		CO2	CCb
		ABC		A	BC
	trpbOUT	CCb		CCbeff	
		AB		AB	
	ser_trpcOUT	SER		SEReff	
		ABC		ABC	
	trpdOUT	E4P		E4Peff	
		ABCD		ABCD	

Table A.13: Carbon atom transitions in Pst DC3000 and Pfl SBW25

A.4 *Pseudomonas* species strain abbreviations

Abbreviation	Species	Abbreviation	Species
Pae	*P. aeruginosa*	Ppr	*P. protogens*
Pbr	*P. brassicacearum*	Pps	*P. psychrotolerans*
Pch	*P. choloraphis*	Ppu	*P. putida*
Pen	*P. entomophila*	Ppy	*P. psychrophila*
Pex	*P. extremaustralis*	Psa	*P. savastanoi*
Pfl	*P. fluorescens*	Psp	*Pseudomonas* species (unnamed)
Pfr	*P. fragi*	Pst	*P. stutzeri*
Pfu	*P. fulva*	Psx	*P. synxantha*
Pfv	*P. fuscovaginae*	Psy	*P. syringae*
Pme	*P. mendocina*	Pto	*P. tolaasii*
Pmo	*P. monteilii*	Pvi	*P. viriflava*
Ppd	*P. pseudoalcaligenes*		

Table A.14: *Pseudomonas* strain abbreviations used in Figures 5.1, 5.2 and 5.3. The *P. mendocina* clade also includes *P. alcaliphila* and *P. pseudomalcaligenes*.